



Diurnal regulation of folate homeostasis controls DNA methylation in *Arabidopsis*

Valentin Hankofer

Vollständiger Abdruck der von der TUM School of Life Sciences der Technischen Universität
München zur Erlangung eines

Doktors der Naturwissenschaften (Dr. rer. nat.)

genehmigten Dissertation.

Vorsitz: Prof. Dr. Kay H. Schneitz

Prüfer der Dissertation:

1. Prof. Dr. Jörg Durner
2. Prof. Dr. Frank Johannes

Die Dissertation wurde am 19.10.2023 bei der Technischen Universität München eingereicht
und durch die TUM School of Life Sciences am 08.02.2024 angenommen.

Summary

In recent years, epigenetic regulation in plants has received great attention, particularly in the context of heritable phenotypic variation that leads to enhanced plant fitness. A growing body of studies highlights the importance of chromatin modifications including DNA methylation for increased tolerance against abiotic and biotic stressors. However, the pathways that convey epigenetic changes in response to environmental signals are often not fully understood, especially when epigenetic regulation converges with other cellular processes such as metabolism. It is therefore of great interest to understand how epigenetic regulation together with metabolism, which is a hallmark of phenotypic adaptation to the growth regime, contributes to plant – environment interactions.

This work investigated how environment-dependent changes in folate-mediated one-carbon metabolism (FOCM) affect DNA methylation in *Arabidopsis thaliana*. Previous studies have shown that the METHYLENETETRAHYDROFOLATEDEHYDROGENASE1 (MTHFD1)-dependent folate metabolism controls DNA methylation through an unknown mechanism that affects the remethylation of homocysteine (Hcy) to methionine. Accordingly, *mthfd1-1* mutant plants exhibit accumulation of Hcy and S-adenosylhomocysteine (SAH), as well as genome-wide losses of DNA methylation. SAH, Hcy and methionine are part of the activated methyl cycle (AMC) in the cytosol that gives rise to S-adenosylmethionine (SAM), the universal methyl group donor for transmethylation reactions. Epigenetic changes in *mthfd1-1* are most likely a direct consequence of SAH accumulation, as SAH is a competitive inhibitor of SAM-dependent methyltransferases such as DNA and histone methyltransferases.

Here, a knockout mutant of *10-FORMYLTETRAHYDROFOLATE SYNTHETASE (THFS)* in the *mthfd1-1* genetic background was identified, that restored genome-wide DNA methylation patterns and complemented the impaired folate metabolism, specifically Hcy remethylation to methionine. Furthermore, changes in the light regime were shown to define the *mthfd1-1* phenotype: while 16 h of light inflicted strong defects, growth at 10 h of light was permissive. Strikingly, not only the length of the photoperiod but also daytime affected Hcy remethylation in *mthfd1-1*: concentrations of SAH and Hcy increased during the day and declined at night. The route of isotopic labeled methyl groups for methylation reactions on DNA was traced, whereby changes in the flux of methyl groups that oscillate with day and night cycles were observed. Thereby, the role of formate as an important one-carbon source for daytime-specific Hcy remethylation could be emphasized. In summary, sensitivity and fidelity of DNA methylation pathways to environment-dependent changes in folate-mediated one-carbon metabolism suggests a novel mechanism for epigenetic regulation.

Zusammenfassung

In den letzten Jahren wurde der epigenetischen Regulierung in Pflanzen große Aufmerksamkeit geschenkt, besonders im Hinblick auf vererbare phänotypische Variationen, die zu einer erhöhten Fitness der Pflanzen beitragen. Eine wachsende Zahl von Studien unterstreicht die Bedeutung von Chromatinmodifikationen, einschließlich DNA-Methylierung, für eine erhöhte Toleranz gegenüber abiotischen und biotischen Stressfaktoren. Jedoch sind die Wege, über die epigenetische Veränderungen als Reaktion auf Umweltsignale vermittelt werden, oftmals nicht vollständig aufgeschlüsselt, speziell wenn die epigenetischen Mechanismen mit anderen adaptiven Prozessen wie dem Stoffwechsel konvergieren. Es ist daher von großem Interesse zu verstehen, wie die epigenetische Regulierung gemeinsam mit dem Stoffwechsel, einem typischen Kennzeichen der phänotypischen Umwelanpassung, zu den Wechselwirkungen zwischen Pflanze und Umwelt beitragen.

In dieser Arbeit wurden umweltabhängige Veränderungen im Folatstoffwechsel und deren Einfluss auf die DNA-Methylierung in *Arabidopsis thaliana* untersucht. Frühere Studien konnten zeigen, dass der METHYLENETETRAHYDROFOLATEDEHYDROGENASE1 (MTHFD1)-abhängige Folatstoffwechsel DNA-Methylierung durch einen unbekanntem Mechanismus steuert, der die Remethylierung von Homocystein (Hcy) zu Methionin beeinflusst. Dementsprechend weisen *mthfd1-1* Mutanten eine Erhöhung von Hcy und S-Adenosylhomocystein (SAH) sowie genomweite Reduktion von DNA-Methylierung auf. SAH, Hcy und Methionin sind Teil des aktivierten Methylzyklus im Zytosol, der zur Synthese von S-Adosylmethionin (SAM), dem universellen Methylgruppendonor für Transmethylierungen führt. Epigenetische Veränderungen in *mthfd1-1* sind höchstwahrscheinlich eine Konsequenz der Akkumulation von SAH, da SAH ein kompetitiver Inhibitor von SAM-abhängigen Methyltransferasen, einschließlich DNA- und Histon-Methyltransferasen ist.

In der vorliegenden Arbeit wurde eine Knockout-Mutante der 10-FORMYLTETRAHYDROFOLATE SYNTHETASE (THFS) in der *mthfd1-1* Mutante identifiziert, die genomweite DNA-Methylierungsmuster und den defekten Folatstoffwechsel, insbesondere die Remethylierung von Hcy zu Methionin wiederherstellt. Darüber hinaus konnte gezeigt werden, dass Veränderungen der Lichtverhältnisse den Phänotyp von *mthfd1-1* beeinflussen. Während 16-stündiges Wachstum im Licht zu starken Defekten führte, wurden diese bei 10-stündigem Wachstum im Licht aufgehoben. Auffallend war dabei, dass nicht nur die Länge der Photoperiode, sondern auch die Tageszeit die Remethylierung von Hcy in *mthfd1-1* bestimmte: tagsüber stiegen die Konzentrationen von SAH und Hcy, während sie nachts wieder sanken. Die Route von isotopenmarkierten Methylgruppen für DNA-Methylierung

wurde nachverfolgt, wobei Veränderungen im Fluss der Methylgruppen beobachtet wurden, die mit Tag- und Nachtzyklen oszillierten. Dadurch konnte die Rolle von Formiat als wichtige Kohlenstoff-Quelle für die tageszeitspezifische Remethylierung von Hcy hervorgehoben werden. Zusammenfassend lässt sich sagen, dass die Empfindlichkeit und Genauigkeit von DNA-Methylierungswegen in Abhängigkeit von umweltbedingten Veränderungen im Folatstoffwechsel einen neuen Mechanismus der epigenetischen Regulierung darstellt.

Scientific Contributions

Publications related to this work

Hankofer V, Poschet G, Ghirardo A, Obermaier L, Barthel G, Lange B, Weber B, Suresh Kumar J, Gross I, Schäffner A, Rychlik M, Schnitzler JP, Hell R, Wirtz M, Durner J, Groth M. Diurnal regulation of folate homeostasis controls DNA methylation in *Arabidopsis*. Manuscript in preparation.

Auge GA, **Hankofer V**, Groth M, Antoniou-Kourouniotti R, Ratikainen II, Lampei C. Plant environmental memory: Implications, mechanisms and opportunities for plant scientists and beyond. *AoB PLANTS*, DOI: <https://doi.org/10.1093/aobpla/plad032>

Other publications

Bugaeva W, Könnel A, Peter J, Mees J, **Hankofer V**, Schick C, Schmidt A, Banguela-Castillo A, Philippar K. FAX1 and FAX3 proteins in the inner envelope of plastids can complement each other for fatty acid transport. *The Plant Journal*, submitted June 2022. Under Revision, preprint available: DOI: <https://doi.org/10.1101/2023.02.09.527856>

Oral Presentations related to this work

Nov. 24th 2022

Diurnal regulation of folate homeostasis controls DNA methylation in *Arabidopsis*. 6th Munich Epigenetics Spotlight Meeting, Munich, Germany. Selected from abstract.

Jun. 21 – 25th 2021

Diurnal regulation of folate-mediated one-carbon homeostasis ensures gene silencing by DNA methylation in *Arabidopsis*. 31st International Conference on *Arabidopsis* Research (ICAR), virtual. Symposium 'Plant Memory: Environmental Information Integration Within and Across Generations'. Selected from abstract.

Mar. 1st 2021

Silence at night: diurnal regulation of folate metabolism controls DNA methylation in *Arabidopsis*. Virtual joint epigenetics seminar between Riken Japan and Helmholtz Munich. Invited speaker.

Poster Presentations related to this work

Aug. 27 – 30th 2022

Hankofer V, Poschet G, Ghirardo A, Obermaier L, Barthel G, Lange B, Weber B, Suresh Kumar J, Gross I, Rychlik M, Schnitzler JP, Hell R, Wirtz M, Durner J, Groth M. Diurnal regulation of folate homeostasis controls DNA methylation in *Arabidopsis*. 15th EMBL Conference: Transcription and chromatin, Heidelberg, Germany. Selected from abstract.

Oct. 10 – 12th 2019

Hankofer V, Barthel G, Wirtz M, Hell R, Díaz de la Garza R, Durner J, Groth M. Light-dependent regulation of one-carbon metabolism controls DNA methylation. 5th Munich International Chromatin Symposium: Chromatin Dynamics, Biomedical Center, LMU Munich, Germany. Selected from abstract.

Jul. 10 – 12th 2019

Hankofer V, Barthel G, Wirtz M, Hell R, Díaz de la Garza R, Durner J, Groth M. Folate metabolism links epigenetic regulation to redox homeostasis. The 14th Plant Oxygen Group Conference 2019, Munich, Germany. Selected from abstract.

Table of contents

Table of Figures	V
Table of Supplementary Figures.....	VI
List of Tables.....	VII
List of Supplementary Tables	VII
Abbreviations	VIII
1 Introduction	1
1.1 Plant growth is defined by the environment	1
1.2 Epigenetic regulation through DNA methylation and active demethylation in plants	1
1.2.1 <i>De novo</i> and maintenance of DNA methylation	2
1.2.2 Active DNA demethylation.....	5
1.3 DNA methylation has several molecular functions.....	5
1.4 Metabolic regulation of epigenetic mechanisms	6
1.4.1 Folate structure and <i>de novo</i> synthesis in <i>Arabidopsis</i>	7
1.4.2 Folate-mediated one-carbon: a central player for plant metabolism.....	10
1.4.3 One-carbon metabolism controls DNA methylation	14
1.4.4 MTHFD1 is required for proper DNA methylation in <i>Arabidopsis</i>	15
1.4.5 Plant phenotypes are plastic and adaptive to changing environments.....	15
1.5 Aims of this study	16
2 Results.....	17
2.1 MTHFD1 and THFS are regulators of folate metabolism	17
2.1.1 The <i>mthfd1-1</i> phenotype is complemented by mutation of <i>THFS</i>	17
2.1.2 DNA methylation patterns are restored in <i>mthfd1-1 x thfs</i>	20
2.1.3 THFS is part of the cytosolic folate metabolism	21
2.1.4 Targeted mutation of <i>THFS</i> by CRISPR-Cas9 rescues <i>mthfd1-1</i>	22
2.1.5 <i>thfs</i> complements other mutant alleles of <i>MTHFD1</i>	25
2.1.6 Transition from vegetative to reproductive growth is delayed in <i>mthfd1-1</i>	26
2.1.7 Growth of <i>mthfd1-1</i> is retarded under LD but normal under SD conditions	29

2.2	Deregulation of circadian clock components correlates with altered expression of genes from the cytosolic one-carbon metabolism	31
2.2.1	Accumulation of Hcy and SAH show diurnal patterns in <i>mthfd1-1</i> under LD....	33
2.2.2	5-formyl-THF strongly accumulates in <i>mthfd1-1</i>	35
2.2.3	One-carbon metabolism is not impaired in <i>mthfd1-1</i> under SD growth	37
2.2.4	Application of 5-formyl-THF inhibits root growth in <i>mthfd1-1</i> x <i>thfs</i>	39
2.2.5	Methionine salvage cycle and <i>de novo</i> synthesis are impaired in <i>mthfd1-1</i> under LD and SD conditions.....	41
2.2.6	Mutation of <i>MTHFD1</i> affects cellular amino acid biosynthesis under LD and SD conditions.....	45
2.2.7	Energy metabolism is not affected in <i>mthfd1-1</i>	47
2.2.8	The glutathione redox balance is not affected in <i>mthfd1-1</i>	49
2.2.9	Enzymes of the cytosolic folate metabolism regulate one-carbon dynamics....	51
2.2.10	MTHFD1 and THFS activities are reduced in their mutant backgrounds.....	52
2.2.11	Cellular activity of SHMT is not reduced in <i>mthfd1-1</i> but slightly increased in the <i>thfs</i> mutant background.....	53
2.2.12	SHMT activity is reduced under SD and probably less affected by 5-formyl-THF than anticipated	55
2.3	Tracing the routes of one-carbon using stable isotope labeling	56
2.3.1	Formate-derived one-carbon is found in glycine	60
2.3.2	Formate and glycine derived one-carbon is equally incorporated into serine between genotypes	62
2.3.3	Formate is a major one-carbon source for methionine synthesis.....	66
2.3.4	Formate is a major source of one-carbon for DNA methylation	68
3	Discussion.....	70
3.1	The universal methyl group donor SAM is just not universal.....	70
3.2	A stable metabolome ensures a functional epigenome.....	71
3.3	Supply of one-carbon methylation reactions: when and where is it coming from? ..	73
3.3.1	Formate is an important but neglected source of one-carbon.....	74
3.3.2	Glycine and serine interconversion is an additional source of one-carbon.....	75

3.3.3	Distribution and compartmentalization of folate metabolism controls one-carbon partitioning.....	77
3.4	Energy and redox metabolism are not affected in <i>methfd1-1</i>	80
3.5	Either both or none: MTHFD1 and THFS control DNA methylation	80
3.6	Conclusions and future perspective.....	83
4	Material and Methods.....	85
4.1	Material	85
4.1.1	Chemicals	85
4.1.2	Media	85
4.1.3	Vectors.....	86
4.1.4	Bacterial strains.....	86
4.1.5	Primers used in this study	86
4.2	Methods	88
4.2.1	Plant material	88
4.2.2	Plant growth and harvest.....	89
4.2.3	Transformation of <i>Escherichia coli</i> cells.....	89
4.2.4	Transformation of <i>Agrobacterium tumefaciens</i> cells	89
4.2.5	Transformation of <i>Arabidopsis</i> with <i>Agrobacterium tumefaciens</i> cells	90
4.2.6	Isolation of genomic DNA from plant material.....	90
4.2.7	Polymerase chain reaction, restriction enzyme digestion, agarose gel electrophoresis, PCR gel extraction and Sanger sequencing	91
4.2.8	<i>SDC_{pro}-GFP</i> expression analyses.....	91
4.2.9	Subcellular localization of THFS.....	92
4.2.10	CRISPR-Cas9-mediated mutation of <i>THFS</i>	92
4.2.11	Whole genome bisulfite sequencing	93
4.2.12	Gene expression analyses	94
4.2.13	Enzymatic activity analyses.....	94
4.2.14	Folate quantification	96
4.2.15	Analyses of DNA methylation level.....	96

4.2.16	Quantification of thiols, amino acids, and adenosine nucleotides	97
4.2.17	roGFP measurement.....	97
4.2.18	Isotopic labeling analyses	97
4.2.19	Automated plant phenotyping.....	99
4.2.20	Root growth analysis.....	100
4.2.21	Computational analysis and tools.....	100
	Supplementary Figures	101
	Supplementary Tables.....	112
	References.....	119
	Acknowledgment.....	137

Table of Figures

Figure 1.	DNA methylation pathways in <i>Arabidopsis</i>	4
Figure 2.	DNA methylation is controlled by the supply of SAM and removal of SAH.	7
Figure 3.	Structure of THF and its derivates.	8
Figure 4.	Folate <i>de novo</i> biosynthesis in plants.	10
Figure 5.	Folate-mediated one-carbon metabolism spans cellular compartments and provides one-carbon for biosynthetic pathways in <i>Arabidopsis</i>	14
Figure 6.	Mutation of <i>THFS</i> complements the <i>methfd1-1</i> phenotype.	20
Figure 7.	CHG methylation is restored in <i>methfd1-1 x thfs</i>	21
Figure 8.	<i>THFS</i> is localized in the cytosol.	22
Figure 9.	Targeted mutation of <i>THFS</i> via CRISPR-Cas9 suppresses the <i>methfd1-1</i> phenotype.	25
Figure 10.	Mutation of <i>THFS</i> complements <i>methfd1-3</i>	26
Figure 11.	Photoperiodic control of flowering is impaired in <i>methfd1-1</i> under LD conditions.	28
Figure 12.	The <i>methfd1-1</i> phenotype is suppressed under short day growth conditions.	30
Figure 13.	Diurnal expression of clock and one-carbon genes is altered in <i>methfd1-1</i>	32
Figure 14.	Impaired methyl cycle in <i>methfd1-1</i> leads to diurnal <i>SDC</i> expression under LD conditions.	34
Figure 15.	Impaired folate cycle in <i>methfd1-1</i> leads to accumulation of 5-formyl-THF under LD conditions.	36
Figure 16.	One-carbon metabolites are not altered in <i>methfd1-1</i> under SD conditions.	38
Figure 17.	Exogenous supply of 5-formyl-THF inhibits root growth but does not affect DNA methylation in <i>methfd1-1 x thfs</i>	40
Figure 18.	Metabolic pathways of methionine formation in <i>Arabidopsis</i>	42
Figure 19.	Methionine biosynthesis is impaired in <i>methfd1-1</i> under LD and SD conditions.	43
Figure 20.	Methionine salvaging is impaired in <i>methfd1-1</i> under LD and SD conditions.	45
Figure 21.	Amino acid biosynthesis in <i>Arabidopsis</i>	46
Figure 22.	Glutamate and proline biosynthesis are partially impaired in <i>methfd1-1</i>	47
Figure 23.	ATP formation is not impaired in <i>methfd1-1</i>	48

Figure 24.	Reduction of NADPH does not impair the glutathione redox balance in <i>methfd1-1</i>	50
Figure 25.	Mutation of <i>MTHFD1</i> and <i>THFS</i> lead to reduced enzyme activities.	53
Figure 26.	SHMT activity is elevated in <i>thfs</i> and <i>methfd1-1 x thfs</i>	54
Figure 27.	SHMT activity is reduced under SD conditions but increased by addition of 5- formyl-THF.	56
Figure 28.	Reconstructing the route of one-carbon via isotope labeling.	60
Figure 29.	Formate incorporation into glycine is day time dependent.	62
Figure 30.	Formate and glycine are both incorporated into serine.	64
Figure 31.	One-carbon flow through the GDC-SHMT complex is not reduced in <i>methfd1-1</i>	65
Figure 32.	Formate is a major one-carbon source for Hcy remethylation.	67
Figure 33.	Formate is a main source for cytosine methylation and thymine synthesis.	68
Figure 34.	<i>MTHFD1</i> and <i>THFS</i> regulate the flow of one-carbon.	82
Figure 35.	Diurnal regulation and supply of one-carbon control DNA methylation.	83

Table of Supplementary Figures

Supplementary Figure 1.	Plant <i>MTHFD1</i> and <i>THFS</i> genes share conserved sequences with mammalian <i>MTHFD1</i> which combines both gene functions.	102
Supplementary Figure 2.	<i>THFS</i> is localized in the cytosol.	102
Supplementary Figure 3.	Biosynthesis of aromatic amino acids is not impaired in <i>methfd1-1</i>	103
Supplementary Figure 4.	<i>methfd1-1</i> shows accumulation of alanine and valine during the day under LD growth.	104
Supplementary Figure 5.	Biosynthesis of arginine, glutamine and histidine are mostly unaffected in <i>methfd1-1</i>	105
Supplementary Figure 6.	Chloroplastic and mitochondrial fractions of protein extracts for enzyme activity measurements.	106
Supplementary Figure 7.	SHMT activity was measured via the formation of 5-methyl-THF.	107
Supplementary Figure 8.	TIC chromatograms of free amino acids from plant extract and standard mix.	108
Supplementary Figure 9.	TIC chromatograms of nucleobases from plant extract and standard mix.	109

Supplementary Figure 10. Mass spectra of free amino acids glycine, methionine, and serine.	110
Supplementary Figure 11. Mass spectra of nucleobases adenine, 5-methylcytosine and thymine.....	111

List of Tables

Table 1. List of primers used for genotyping.....	86
Table 2. List of primers and oligonucleotides used for CRISPR-Cas9-mediated mutation of <i>THFS</i>	87
Table 3. List of primers used for generating the THFS-GFP fusion construct.	87
Table 4. List of primers used for RT-qPCR.....	88
Table 5. Primers used for McrBC-qPCR.....	88

List of Supplementary Tables

Supplementary Table 1. Adjusted <i>P</i> values corresponding to Figures 11, 13 and 14.....	112
Supplementary Table 2. Adjusted <i>P</i> values corresponding to Figure 14.....	112
Supplementary Table 3. Adjusted <i>P</i> values corresponding to Figure 15.	113
Supplementary Table 4. Adjusted <i>P</i> values corresponding to Figure 16.	113
Supplementary Table 5. Adjusted <i>P</i> values corresponding to Figures 19 and 20.....	114
Supplementary Table 6. Adjusted <i>P</i> values corresponding to Figure 19 and 20.	114
Supplementary Table 7. Adjusted <i>P</i> values corresponding to Figure 22.	115
Supplementary Table 8. Adjusted <i>P</i> values corresponding to Figures 23 and 24.....	115
Supplementary Table 9. Adjusted <i>P</i> values corresponding to Figures 25, 26 and 27.....	116
Supplementary Table 10. Adjusted <i>P</i> values corresponding to Figures 29 and 32.....	116
Supplementary Table 11. Adjusted <i>P</i> values corresponding to Figures 30 and 31.....	117
Supplementary Table 12. Adjusted <i>P</i> values corresponding to Supplementary Figures 3 and 4.....	117
Supplementary Table 13. Adjusted <i>P</i> values corresponding to Supplementary Figure 5. ...	118
Supplementary Table 14. Preliminary control reactions of MTHFR and SHMT.	118

Abbreviations

5mC	5-methylcytosine
μl	microliter
μM	micromolar
AMC	activated methyl cycle
ATP	adenosine triphosphate
BSTFA	(N,O-Bis-(trimethylsilyl)-trifluoroacetamid) containing 1 % TMCS (trimethylchlorosilane)
cm	centimeter
Col-0	<i>Arabidopsis thaliana</i> ecotype Columbia
CTAB	cetyltrimethylammonium bromide
DMR	differentially methylated region
DMSO	dimethyl sulfoxide
DNA	deoxyribonucleic acid
dNTP	deoxynucleotide triphosphate
DTT	dithiothreitol
E_{GSH}	glutathione redox balance
fM	femtomolar
FOCM	folate-mediated one-carbon metabolism
GFP	green fluorescent protein
h	hour(s)
Hcy	homocysteine
K_m	Michaelis constant
LD	long day
M	molar
MES	2-(N-morpholino)ethanesulfonic acid
MI	Methylation Index
min	minute(s)
ml	milliliter
mm	millimeter
mM	millimolar
MOPS	3-(N-morpholino)propanesulfonic acid
mRNA	messenger RNA
ms	millisecond(s)
MS	Murashige and Skoog medium
MTBSTFA	(N-tert-Butyldimethylsilyl-N-methyltrifluoroacetamide) containing 1% TMCS (trimethylchlorosilane)
NAD ⁺ /NADH	nicotinamide adenine dinucleotide
NADP ⁺ /NADPH	nicotinamide adenine dinucleotide phosphate
nt	nucleotide
ON	overnight
PLP	pyridoxal-5-phosphate
rcf	relative centrifugal force
RdDM	RNA-directed DNA methylation
RFP	red fluorescent protein

RNA	ribonucleic acid
roGFP	reduction-oxidation sensitive green fluorescent protein
ROS	reactive oxygen species
rpm	revolutions per minute
RT	room temperature
s	second(s)
SAH	S-adenosylhomocysteine
SAM	S-adenosylmethionine
s.d.	standard deviation
SD	short day
sgRNA	single guide RNA
siRNA	small interfering RNA
TCA	Citric acid cycle
TE	transposable element
Tris	2-Amino-2-(hydroxymethyl)propane-1,3-diol
WGBS	whole genome bisulfite sequencing
% (v/v)	percent volume fraction
% (w/v)	percent weight fraction

1 Introduction

1.1 Plant growth is defined by the environment

Plants are sessile organisms that permanently reside at their germination sites. And due to their sessile life, plants must adapt to an ever-changing growth environment. This is achieved by sophisticated molecular mechanisms for the perception of environmental signals and the subsequent adaptation to ensure survival and reproductive success. A variety of stimuli encompasses the natural growth environment that is diurnally and seasonally changing and extends to abiotic and biotic stressors. Climate change is expected to increase the frequency of extreme weather events ranging from floods and water logging to drought and high temperatures. This will drastically affect agricultural production which is vulnerable to mischievous growth regimes (Lesk *et al*, 2022). For instance, global yields of wheat, rice, maize and soybean, four major crops responsible for two-thirds of human caloric intake are estimated to decrease with increasing temperatures (Zhao *et al*, 2017). It is therefore of great interest and importance to understand and improve stress tolerance in plants through targeted breeding approaches. The acute sensing mechanisms that plants employ to survive the range of adverse environments are well-studied (Lamers *et al*, 2020). However, most stresses are recurring or chronic and might even amplify in future. Interestingly, plants have developed responses to mitigate repeated stress of the same kind they were exposed to before. This phenomenon termed stress memory allows plants for stress adaptation in a prepared or primed state through rapid changes in gene expression. Chromatin accessibility for gene transcription is controlled by epigenetic modifications which comprise post-translational modifications of histones and DNA methylation among others (Lämke & Bäurle, 2017; Auge *et al*, 2023). Epigenetic phenomena are stable but principally reversible and potentially heritable which makes them a strong candidate for rapid and recurring adaptation to environmental stress through stress memory (Vriet *et al*, 2015; Lämke & Bäurle, 2017; Auge *et al*, 2023). Yet, the identification of stress-responsive pathways and targets of epigenetic regulation remains challenging (Auge *et al*, 2023).

1.2 Epigenetic regulation through DNA methylation and active demethylation in plants

In the past two decades the number of studies focusing on epigenetic regulation increased steadily (Eriksson *et al*, 2020). And with growing interest, the definition of what epigenetic regulation is became ambiguous (Berger *et al*, 2009; Heard & Martienssen, 2014; Henikoff &

Greally, 2016). Nevertheless, it is generally accepted that epigenetic regulation addresses the perpetuation of gene expression and function across cell divisions without alterations of the DNA sequence (Henikoff & Greally, 2016). This perpetuation depends on chromatin structure conferred by histone modifications as well as DNA methylation. DNA methylation is a self-evident candidate for the transmission of epigenetic information. In contrast to DNA-associated proteins such as histones, DNA methylation remains intact and covalently bound to the DNA during replication (Henikoff & Greally, 2016). For that reason, this study mainly focused on DNA methylation, an epigenetic mark that is established through methylation of cytosines at position 5 resulting in 5-methylcytosine (5mC). DNA methylation does not only depend on the establishment but also on the maintenance, and active removal of cytosine methylation. Plants have evolved distinct pathways and enzymes that catalyze these activities at specific sequences and genomic regions of DNA (Du *et al*, 2015; Zhang *et al*, 2018). DNA methylation is found in three sequence contexts: in symmetrical sequences CG and CHG (H corresponds to A, T or C) and the asymmetrical sequence CHH (Law & Jacobsen, 2010; Du *et al*, 2015).

1.2.1 *De novo* and maintenance of DNA methylation

In plants, sequence-independent *de novo* DNA methylation is established via the RNA-directed DNA methylation (RdDM) pathway which requires small interfering RNAs (siRNAs) (**Figure 1 A**) (Law & Jacobsen, 2010; Pikaard *et al*, 2012; Matzke & Mosher, 2014; Zhang *et al*, 2018). siRNA formation starts through POLYMERASE IV (POL IV) mediated transcription of RNA, followed by duplication of transcripts by RNA-DEPENDENT RNA POLYMERASE 2 (RDRP2, also known as RDR2) giving rise to double-stranded RNA (dsRNA) which is subsequently cleaved into siRNAs by DICER-LIKE PROTEIN 3 (DCL3). POL IV recruitment to target loci is accomplished by SAWADEE HOMEODOMAIN HOMOLOGUE 1 (SHH1) which binds methylated histone H3 lysine 9 (H3K9me2) (Zhang *et al*, 2013; Law *et al*, 2013). SNF2 DOMAIN-CONTAINING PROTEIN CLASSY 1 (CLSY1) is an interaction partner of SHH1 and essential for POL IV catalyzed siRNAs synthesis (Smith *et al*, 2007; Zhang *et al*, 2018; Zhou *et al*, 2018; Zhou *et al*, 2022). Next, ARGONAUTE 4 (AGO4) proteins are loaded with 24 nucleotide (nt) siRNAs to bind complementary scaffold RNAs produced by POL V (Zhang *et al*, 2018). Here, AGO is interacting with the DNA methyltransferase DOMAINS REARRANGED METHYLASE 2 (DRM2) which catalyzes *de novo* DNA methylation. Scaffold RNAs are thought to be retained on the chromatin through RRP6-LIKE 1 (RRP6L1) (Zhang *et al*, 2014). Association of POL V with chromatin depends on the chromatin remodeler DDR complex, which interacts with SUPPRESSOR OF VARIATION 3-9 HOMOLOGUE PROTEIN 2 (SUVH2) and SUVH9, two histone methyltransferase family proteins devoid of

methyltransferase activity (Johnson *et al*, 2014; Liu *et al*, 2014; Zhang *et al*, 2018). Pre-existing DNA methylation is recognized by the SET and RING finger-associated (SRA) domains of SUVH2 and SUVH9 – a mechanism that is required for genome-wide POL V recruitment (Johnson *et al*, 2014).

In contrast to *de novo* DNA methylation, maintenance depends on the cytosine sequence contexts that are targeted by different pathways. DNA methyltransferase METHYLTRANSFERASE 1 (MET1) catalyzes cytosine methylation independently of histone methylation in the CG context (**Figure 1 B**). However, MET1 depends on VARIANT IN METHYLATION (VIM) proteins, ubiquitin E3 ligases that also contain a SRA domain for binding hemimethylated DNA after DNA replication – a process that leads to methylation of unmodified cytosines in the daughter strands (Du *et al*, 2015; Zhang *et al*, 2018). Non-CG methylation is maintained by the activities of DNA methyltransferases CHROMOMETHYLASE 3 (CMT3) and to a lesser extent by CMT2 and depends on histone methylation (**Figure 1 C**) (Lindroth *et al*, 2001; Stroud *et al*, 2014; Zhang *et al*, 2018). Histone methyltransferases SUVH4 (also known as KRYPTONITE, KYP), SUVH5 and SUVH6 are responsible for the catalyzation of H3K9 methylation (Jackson *et al*, 2002; Malagnac *et al*, 2002; Jackson *et al*, 2004; Ebbs & Bender, 2006; Bernatavichute *et al*, 2008; Stroud *et al*, 2013; Zhang *et al*, 2018). CMT3 and CMT2 share similar bromo-adjacent homology (BAH) and chromodomains for binding H3K9me2 and catalyze non-CG methylation (Du *et al*, 2012; Du *et al*, 2015). SUVH4, SUVH5 and SUVH6 in turn bind non-CG sequences via their SRA domains and implement H3K9 methylation (Du *et al*, 2015; Zhang *et al*, 2018). This mechanism constitutes a reinforcing loop that requires no further mediators or adaptors (Du *et al*, 2015). CHH methylation is additionally maintained by DRM2 through the RdDM pathway (Zemach *et al*, 2013).

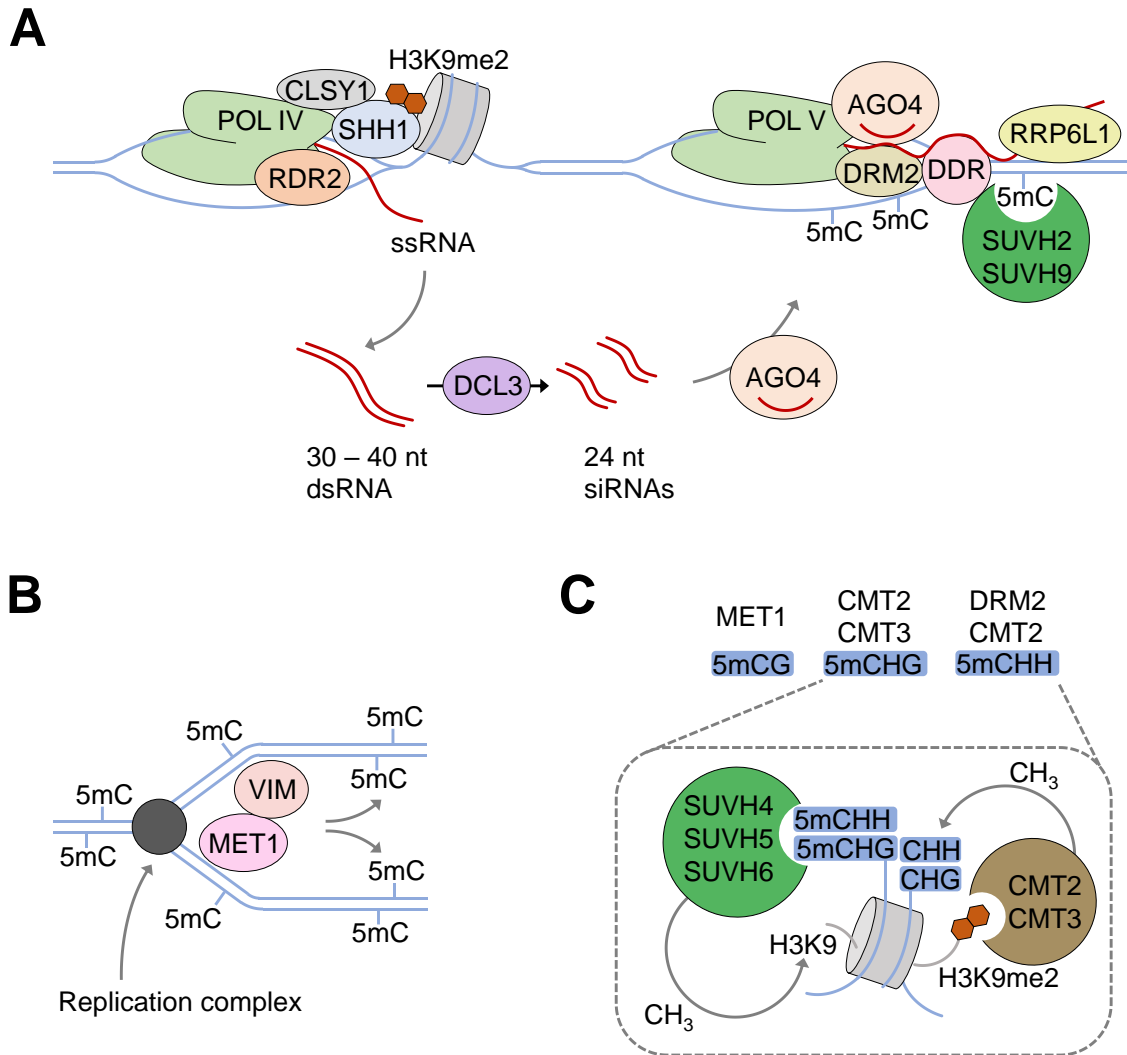


Figure 1. DNA methylation pathways in *Arabidopsis*.

DRM2-mediated *de novo* DNA methylation via the RNA-directed DNA methylation pathway (A) as well as DNA methylation maintenance pathways (B, C) catalyze sequence-specific methylation of cytosines. POL IV: POLYMERASE IV, RDR2: RNA-DEPENDENT RNA POLYMERASE 2, DCL3: DICER-LIKE PROTEIN 3, SHH1: SAWADEE HOMEODOMAIN HOMOLOGUE 1, CLSY1: SNF2 DOMAIN CONTAINING PROTEIN CLASSY 1, AGO4: ARGONAUTE 4, POL V: POLYMERASE V, DRM2: DOMAINS REARRANGED METHYLASE 2, RRP6L1: RRP6-LIKE 1, DDR: DDR complex containing DEFECTIVE IN RNA-DIRECTED DNA METHYLATION 1 (DRD1), DEFECTIVE IN MERISTEM SILENCING 3 and RDM1, SUVH2, 4, 5, 6, 9: SUPPRESSOR OF VARIATION 3-9 HOMOLOGUE PROTEIN 2, 4, 5, 6, 9, MET1: METHYLTRANSFERASE 1, VIM: VARIANT IN METHYLATION, CMT2, 3: CHROMOMETHYLASE 2, 3, 5mC: 5-methylcytosine, CG, CHG, CHH: 5-methylcytosine sequence context with H = A, C, T, H3K9: histone H3 lysine 9, H3K9me2: methylated histone H3 lysine 9. Adapted figure (Du *et al*, 2015; Zhang *et al*, 2018).

1.2.2 Active DNA demethylation

In *Arabidopsis*, DNA demethylation is catalyzed by four bifunctional 5mC DNA glycosylases, namely REPRESSOR OF SILENCING 1 (ROS1), TRANSCRIPTIONAL ACTIVATOR DEMETER (DME), DEMETER-LIKE PROTEIN 2 (DML2) and DML3 that initiate DNA demethylation through a base excision repair pathway in all cytosine sequence contexts (Gong *et al*, 2002; Gehring *et al*, 2006; Ortega-Galisteo *et al*, 2008; Zhang *et al*, 2018). These enzymes commence DNA demethylation through hydrolysis of glycosylic bonds between the 5-methylcytosine and the deoxyribose, followed by base excision as well as elimination reactions that result in a gap and eventually generation of a 3' OH group needed to be filled by DNA polymerase and ligase enzymes (Martínez-Macías *et al*, 2012; Lee *et al*, 2014; Li *et al*, 2015; Zhang *et al*, 2018).

1.3 DNA methylation has several molecular functions

DNA methylation is an epigenetic modification that, together with histone modifications and non-histone proteins, characterize chromatin structure and DNA accessibility (Zhang *et al*, 2018). In doing so, DNA methylation functions in the regulation of gene expression, silencing of transposable elements (TEs, transposons), as well as plant development through genome imprinting or mediating responses to environmental signals including abiotic and biotic stresses as initially mentioned (Zhang *et al*, 2018).

In *Arabidopsis*, approximately 5 % of genes are methylated in their promotor regions (Zhang *et al*, 2018). Promotor DNA methylation usually inhibits gene transcription as it represses binding of transcription activators. Alternatively, cytosine methylation can act indirectly on gene expression by recruiting proteins to chromatin that transcriptionally repress genes without affecting DNA methylation levels (Ichino *et al*, 2021). Yet, recent reports also unraveled DNA methylation interacting proteins that recruit enhancers of gene expression negating the silencing effect of proximal TE insertions (Harris *et al*, 2018). Accordingly, DNA demethylation can secure gene expression by preventing the spreading of DNA methylation from nearby TEs into promotor regions (Tang *et al*, 2016). Genome-wide analysis of DNA methylation in triple mutants of DNA demethylases *ros1 dml2 dml3 (rda)* uncovered loci at intergenic regions and TEs, where pathways of active DNA demethylation and methylation converge (Penterman *et al*, 2007). Active demethylation is therefore considered a protective measure to secure gene activity from detrimental DNA methylation spreading from proximal loci (Penterman *et al*, 2007; Williams *et al*, 2022). Gene body methylation is observed in exons of one third of transcribed genes and only occurs in the CG context (Lister *et al*, 2008; Du *et al*, 2015). Although it was

proposed that gene body methylation might regulate splicing and transcriptional elongation, the overall functions remain elusive (Choi *et al*, 2020). TEs are mobile, dynamic, and repetitive nucleotide sequences that can potentially induce DNA rearrangement. DNA methylation safeguards genome integrity and stability by promoting the packaging of genomic regions that contain TEs, enforcing a transcriptionally silent state (Fedoroff, 2012). In *Arabidopsis*, TE silencing in the pericentromeric heterochromatin and TE-containing euchromatin is facilitated by dense methylation in all sequence contexts (Zhang *et al*, 2018). Another function of DNA methylation termed genomic imprinting describes the establishment of parent-specific allele expression patterns after fertilization (Sato & Köhler, 2022). Differential gene expression in progeny results from epigenetic mechanisms including DNA demethylation during male and female gametogenesis causing alleles to be either maternally or paternally silenced (Köhler & Weinhofer-Molisch, 2010; Gehring, 2013; Sato & Köhler, 2022).

A growing number of studies showed that changes in epigenetic regulation can enhance resilience of plants against recurring abiotic and biotic stresses (Auge *et al*, 2023). For instance, active DNA demethylation of TEs inside the regulatory region of *TNL RESISTANCE METHYLATED GENE1 (RMG1)* by ROS1 confers basal resistance against the pathogenic bacterium *Pseudomonas syringae* (Halter *et al*, 2021). Furthermore, it was shown that recurring hyperosmotic stress over multiple generations led to changes in DNA methylation patterns that correlated with increased survival (Wibowo *et al*, 2016; Auge *et al*, 2023). Whereas a stress-free generation would cause the loss of transgenerational stress memory and the resetting of DNA methylation patterns (Wibowo *et al*, 2016; Auge *et al*, 2023).

1.4 Metabolic regulation of epigenetic mechanisms

Although several distinct pathways employing different DNA methyltransferases for spatio-temporal and sequence specific DNA methylation were characterized, they share one common feature: they are dependent on S-adenosylmethionine (SAM), a universal donor of methyl groups for transmethylation reactions. In the biochemical reaction of DNA methylation, methyl groups are transferred from SAM to position 5 of cytosine via the activity of DNA methyltransferases generating 5-methylcytosine and the byproduct S-adenosylhomocysteine (SAH). Albeit targeting of DNA methyltransferases to specific genomic regions is regulated by specialized pathways, DNA methyltransferases can be intrinsically regulated (Lyko, 2018). One of these intrinsic regulatory mechanisms of DNA methyltransferase activity is the supply of SAM and removal of SAH (**Figure 2**). Removal of SAH is particularly important as it inhibits DNA methyltransferases competitively (Cantoni, 1975; Moffatt & Weretilnyk, 2001; Rahikainen

et al, 2018). The ratio between SAM and SAH was introduced as the Methylation Index (MI), a measure for the cellular methylation potential and status (La Haba & Cantoni, 1959; Moffatt *et al*, 2002; Groth *et al*, 2016).

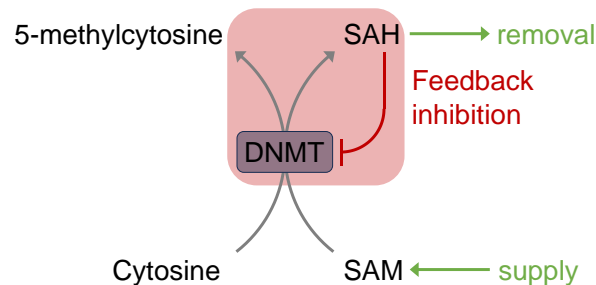


Figure 2. DNA methylation is controlled by the supply of SAM and removal of SAH.
DNMT: DNA methyltransferase, SAM: S-adenosylmethionine, SAH: S-adenosylhomocysteine.

SAM is synthesized in the cytosolic activated methyl cycle (AMC, also known as methionine cycle) and universally provides one-carbon in the form of methyl groups for transmethylation reactions (Roje, 2006). SAM formation and SAH removal are intimately linked to folate-mediated one-carbon metabolism (FOCM), the source of one-carbon for the AMC. Although SAM and SAH are important components defining DNA methylation performance, they are sometimes overlooked in the pathways mediating and implementing DNA methylation. Therefore, it must be emphasized that there are additional metabolic pathways that can influence epigenetic mechanisms but which were not further addressed in this work (Lu & Thompson, 2012; Nieborak & Schneider, 2018; Lindermayr *et al*, 2020; Lu *et al*, 2023).

1.4.1 Folate structure and *de novo* synthesis in *Arabidopsis*

Folate is the generic term for tetrahydrofolate (THF) and derivatives of it. THF comprises three moieties: a pterin ring, *para*-aminobenzoate (*p*ABA) and a mono- or polyglutamate tail (**Figure 3 A**) (Gorelova *et al*, 2017a). Oxidized forms of THF are dihydrofolate (DHF) and folic acid (FA) which require reduction to become biologically active. One-carbon substitutes of various oxidation states can be transferred to THF at positions N5 and N10 resulting in derivatives of THF: 5-methyl-THF, 5,10-methylene-THF, 5,10-methenyl-THF, 5-formyl-THF and 10-formyl-THF (**Figure 3 B**). Depending on the type of one-carbon substitute, folates have different biological and metabolic functions. Additionally, the number of glutamate residues in the

glutamate tail affects folate compartmentalization and availability as substrates for enzyme-catalyzed reactions (Gorelova *et al*, 2017a).

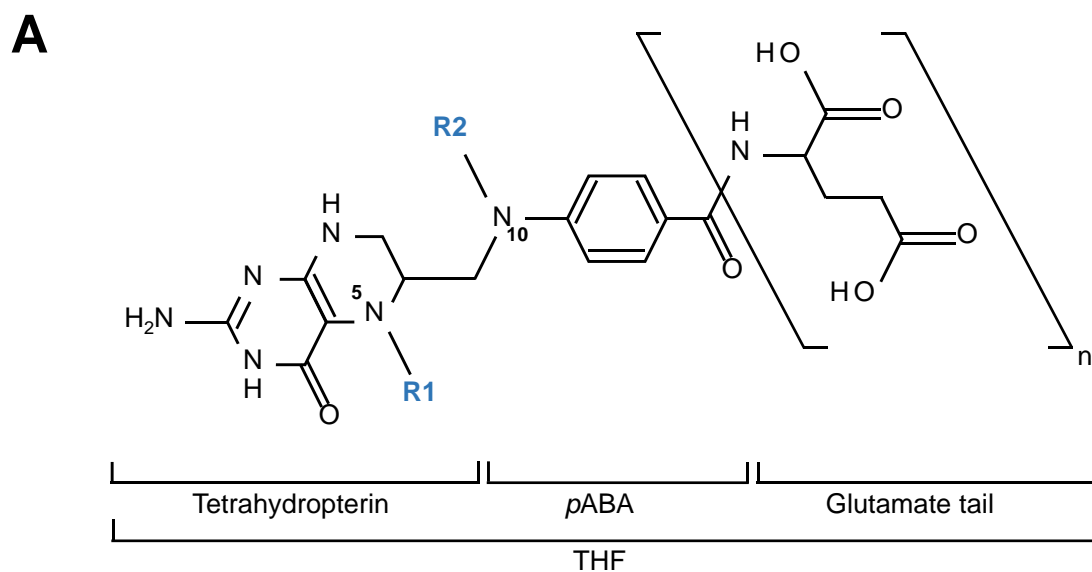


Figure 3. Structure of THF and its derivatives.

(A) Chemical structure of THF with positions of one-carbon substituents R1 and R2. (B) Possible one-carbon groups attached to nitrogen at position 5 and 10. *pABA*: *para*-aminobenzoate, THF: tetrahydrofolate. Adapted figure (Gorelova *et al*, 2017a).

Plants, bacteria and fungi share the ability for *de novo* folate synthesis (Gorelova *et al*, 2017a; Gorelova *et al*, 2019; Kolton *et al*, 2022). In plants, folate biosynthesis is divided between chloroplasts, mitochondria and the cytosol, where the synthesis of pterin starts with the conversion of guanosine triphosphate (GTP) into dihydroneopterin triphosphate (DHN-P₃) and formate (Kolton *et al*, 2022). This first committed step in pterin biosynthesis is catalyzed

Introduction

by GTP CYCLOHYDROLASE-1 (GCH1) (**Figure 4 Enzyme 1**) (Basset *et al*, 2002), an enzyme that has been proposed to be a rate-limiting step in folate synthesis (Hossain *et al*, 2004). After the dual dephosphorylation of dihydroneopterin, the formation of the pterin moiety is catalyzed by DIHYDRONEOPTERINE ALDOLASE (DHNA) (**Figure 4 Enzyme 2**), which cleaves the lateral side chain of dihydroneopterin resulting in 6-hydroxymethyldihydropterine (HMDHP) (Goyer *et al*, 2004; Gorelova *et al*, 2017a). The second moiety of THF, *p*ABA, is synthesized from chorismate in plastids. First, chorismate and glutamine are converted to aminodeoxychorismate (ADC) and glutamate by AMINODEOXYCHORISMATE SYNTHASE (ADCS) (**Figure 4 Enzyme 3**) (Basset *et al*, 2004a). In the following step, ADC is converted to *p*ABA by AMINODEOXYCHORISMATE LYASE (ADCL) (**Figure 4 Enzyme 4**) (Basset *et al*, 2004b). Although *p*ABA is produced in plastids, reversible conversion of *p*ABA to its β -D-glucopyranosyl ester (*p*ABA-Glc) has been described in the cytosol (Quinlivan *et al*, 2003). It was proposed that *p*ABA, a hydrophobic and weak acid, can distribute freely within cellular compartments while esterification to *p*ABA-Glc may abolish this characteristic and instead yield a storage form of *p*ABA (Quinlivan *et al*, 2003). The final steps of THF synthesis in the mitochondria begin with pyrophosphorylation of HMDHP and coupling with *p*ABA resulting in the formation of dihydropteroate (DHP) which is catalyzed by a bifunctional enzyme harboring HMDHP PYROPHOSPHOKINASE (HPPK) and DIHYDROPTEROATE SYNTHASE (DHPS) activities (**Figure 4 Enzymes 5 & 6**) (Rébeillé *et al*, 1997; Gorelova *et al*, 2017a). The DHPS domain was shown to be feedback-inhibited by DHF and THF monoglutamate which indicated that DHPS might act as a potential target for regulation of folate synthesis (Mouillon *et al*, 2002). Next, DHF is formed by addition of a glutamate residue to the *p*ABA moiety of DHP by DIHYDROFOLATE SYNTHETASE (DHFS) (**Figure 4 Enzyme 7**) before DHF is reduced to THF by DIHYDROFOLATE REDUCTASE (DHFR), a bifunctional enzyme coupled to THYMIDYLATE SYNTHASE (TS) (**Figure 4 Enzyme 8**) (Gorelova *et al*, 2017a; Gorelova *et al*, 2017b). In the last step, a polyglutamate tail is added to THF by FOLYLPOLYGLUTAMATE SYNTHETASE (FPGS), of which three isoforms exist in the cytosol, mitochondria and plastids (**Figure 4 Enzyme 9**) (Ravanel *et al*, 2001; Gorelova *et al*, 2017a). Polyglutamylation is thought to be another point of regulation since the length of the polyglutamate tail affects compartmentalization of folates and efficacy for folate-dependent enzymes (Shane, 1989; Appling, 1991; Gorelova *et al*, 2017a). However, the polyglutamate tail is not static and can be shortened or completely removed by the endo- and exopeptidase activity of vacuolar γ -GLUTAMYL HYDROLASE (GGH) (Orsomando *et al*, 2005; Akhtar *et al*, 2010; Hanson & Gregory, 2011).

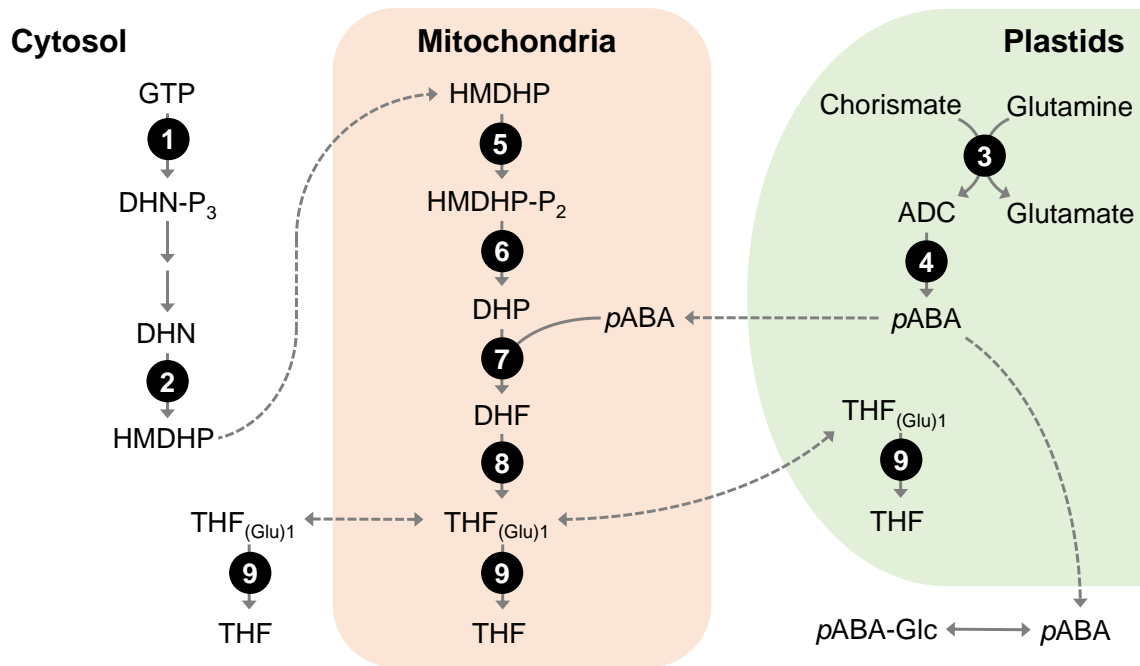


Figure 4. Folate *de novo* biosynthesis in plants.

Folate *de novo* synthesis in the cytosol, mitochondria, and plastids. GTP: guanosine triphosphate; DHN-P₃: dihydroneopterin triphosphate, DHN: dihydroneopterin, HMDHP: 6-hydroxymethyldihydropterin, HMDHP-P₂: 6-hydroxymethyldihydropterin pyrophosphate, DHP: dihydropteroate, DHF: dihydrofolate, THF and THF_{(Glu)1} are abbreviations for poly- and monoglutamylated tetrahydrofolate, respectively. ADC: aminodeoxychorismate, *p*ABA: *para*-aminobenzoic acid, *p*ABA-Glc: β -D-glucopyranosyl ester of *para*-aminobenzoic acid. (1) GTP CYCLOHYDROLASE-1 (GCH1) (2) DIHYDRONEOPTERINE ALDOLASE (DHNA) (3) AMINODEOXYCHORISMATE SYNTHASE (ADCS) (4) AMINODEOXYCHORISMATE LYASE (ADCL) (5) 6-HYDROXYMETHYLDIHYDROPTERIN PYROPHOSPHOKINASE (HPPK) (6) DIHYDROPTEROATE SYNTHASE (DHPS) (7) DIHYDROFOLATE SYNTHETASE (DHFS) (8) DIHYDROFOLATE REDUCTASE (DHFR) (9) FOLYLPOLYGLUTAMATE SYNTHETASE (FPGS). Adapted figure (Gorelova *et al*, 2017a).

1.4.2 Folate-mediated one-carbon: a central player for plant metabolism

THF and its derivatives play a central role as cofactors for one-carbon transfer reactions. Depending on the one-carbon substitute at positions N5 or N10 of THF (**Figure 3 B**), folates take part in various metabolic pathways including the biosynthesis of nucleotides, formyl-methionyl-tRNA, pantothenate as well as amino acid metabolism (Gorelova *et al*, 2017a; Lindermayr *et al*, 2020). As mentioned before, folate-mediated one-carbon is pivotal for the synthesis of SAM, which acts as the precursor and substrate for the synthesis of polyamines and the plant hormone ethylene besides its function in DNA methylation (Roje, 2006). Like folate biosynthesis, FOCM spreads across the cytosol, mitochondria and plastids and orchestrates the conversion of the different folate species (**Figure 5**). In plants, one-carbon can enter the FOCM through the activity of SERINE HYDROXYMETHYLTRANSFERASE

Introduction

(SHMT), an enzyme with 7 isoforms localized to mitochondria (SHM1 & SHM2), chloroplasts (SHM3), the cytosol (SHM4 & SHM5) and nucleus (SHM6 & SHM7) (**Figure 5 Enzyme 1**) (Turner *et al*, 1992; Besson *et al*, 1993; Rebeille *et al*, 1994; Neuburger *et al*, 1996; Zhang *et al*, 2010; Huang *et al*, 2016; Ruszkowski *et al*, 2018; Nogués *et al*, 2022). SHMTs are pyridoxal-5-phosphate (PLP)-dependent enzymes with multiple catalytic activities. Yet, the main function is the reversible conversion of serine and THF into glycine and 5,10-methylene-THF. The direction from serine to glycine provides one-carbon for the formation of 5,10-methylene-THF, a central hub for many folate-dependent biosynthetic pathways and the interconversion to other folates. Thymidylate synthesis in mitochondria and the cytosol depends on 5,10-methylene-THF and is catalyzed by TS which occurs as a bifunctional enzyme with DHFR that also mediates the penultimate step of THF synthesis (**Figure 4 Enzyme 8**). METHYLENETETRAHYDROFOLATE REDUCTASE (MTHFR) catalyzes the reduction of 5,10-methylene-THF to 5-methyl-THF (**Figure 5 Enzyme 2**) (Roje *et al*, 1999; Roje *et al*, 2002a). 5-methyl-THF in turn provides one-carbon for the remethylation of homocysteine (Hcy) to methionine in the AMC which is mediated by METHIONINE SYNTHASE (MS), with two isoforms MS1 and MS2 located in the cytosol and an additional one, MS3 in chloroplasts (**Figure 5 Enzyme 3**) (Ravanel *et al*, 2004; Sauter *et al*, 2013). S-ADENOSYLMETHIONINE SYNTHETASE (SAMS) is the only enzyme that synthesizes SAM from ATP and methionine with 4 isoforms located in the nucleus and cytosol (**Figure 5 Enzyme 4**) (Roje, 2006; Sekula *et al*, 2020). SAM is a hallmark of the AMC which ensures the cellular capacity for transmethylation reactions that are catalyzed by a broad range of methyltransferases (**Figure 5 Enzyme 5**) (Rahikainen *et al*, 2018). The byproduct of transmethylation, SAH, is removed by S-ADENOSYLHOMOCYSTEINE HYDROLASE (SAHH) to mitigate its adverse effect on methyltransferases (**Figure 5 Enzyme 6**) (Cantoni, 1975; Moffatt & Weretilnyk, 2001). As described above, Hcy is formed via the activity of SAHH and remethylated to methionine, completing the AMC.

Besides 5-methyl-THF, 5,10-methylene-THF is converted to 5,10-methenyl-THF through the reversible dehydrogenase activity of the bifunctional enzyme METHYLENETETRAHYDROFOLATEDEHYDROGENASE (MTHFD) which is found in the cytosol, mitochondria, and plastids (**Figure 5 Enzyme 7a**). In the presence of glycine, 5,10-methenyl-THF can be converted to 5-formyl-THF through another catalytic activity of SHMT (**Figure 5 Enzyme 1**). 5-formyl-THF is the only folate species that is not used as a one-carbon donor and is thought to act as a storage form of folates that is reintroduced into the mitochondrial FOCM via 5-FORMYLTETRAHYDROFOLATE CYCLOLIGASE (5-FCL) (**Figure 5 Enzyme 11**) (Roje *et al*, 2002b). The reversible cycloligase activity of MTHFD converts 5,10-

Introduction

methenyl-THF to 10-formyl-THF, a folate cofactor that provides one-carbon for two transformylation steps in the *de novo* synthesis of purines (**Figure 5 Enzyme 7b**) (Boldt & Zrenner, 2003; Zrenner *et al*, 2006). 10-formyl-THF is also generated from formate and ATP through 10-FORMYLTETRAHYDROFOLATE SYNTHETASE (THFS), which catalyzes the reversible reaction that is assumed to be restricted to the cytosol (**Figure 5 Enzyme 8**) (Gorelova *et al*, 2019). However, previous studies raised the possibility for mitochondrial and chloroplastic activity of THFS which needs further investigation (Kirk *et al*, 1994; Gorelova *et al*, 2017a). In mitochondria, instead of THFS a 10-FORMYLTETRAHYDROFOLATE DEFORMYLASE (10-FDF) was described to irreversibly metabolize 10-formyl-THF to formate and THF (**Figure 5 Enzyme 10**) (Collakova *et al*, 2008). Besides SHMT, the mitochondrial GLYCINE DECARBOXYLASE COMPLEX (GDC) plays an important role in the conversion of glycine and THF to CO₂, NH₃ and 5,10-methylene-THF (**Figure 5 Enzyme 12**). Together with another molecule of glycine, 5,10-methylene-THF is then used to synthesize serine and THF through the mitochondrial SHMT, a reaction that is thermodynamically unfavored as the main reaction is in the serine to glycine direction. Additionally, 5,10-methylene-THF donates one-carbon for the synthesis of pantothenate, a precursor of coenzyme A and the acyl-carrier protein, both important for central and secondary metabolism (Coxon *et al*, 2005). As already mentioned, isoforms of FPGS are found in the cytosol, mitochondria and plastids and catalyze the addition of polyglutamate tails to folates (**Figure 5 Enzyme 9**) (Ravanel *et al*, 2001; Mehrshahi *et al*, 2010). Polyglutamylation increases enzyme affinity, subcellular compartmentation and stability and is therefore regarded as an important regulatory feature of folate homeostasis (Gorelova *et al*, 2017a).

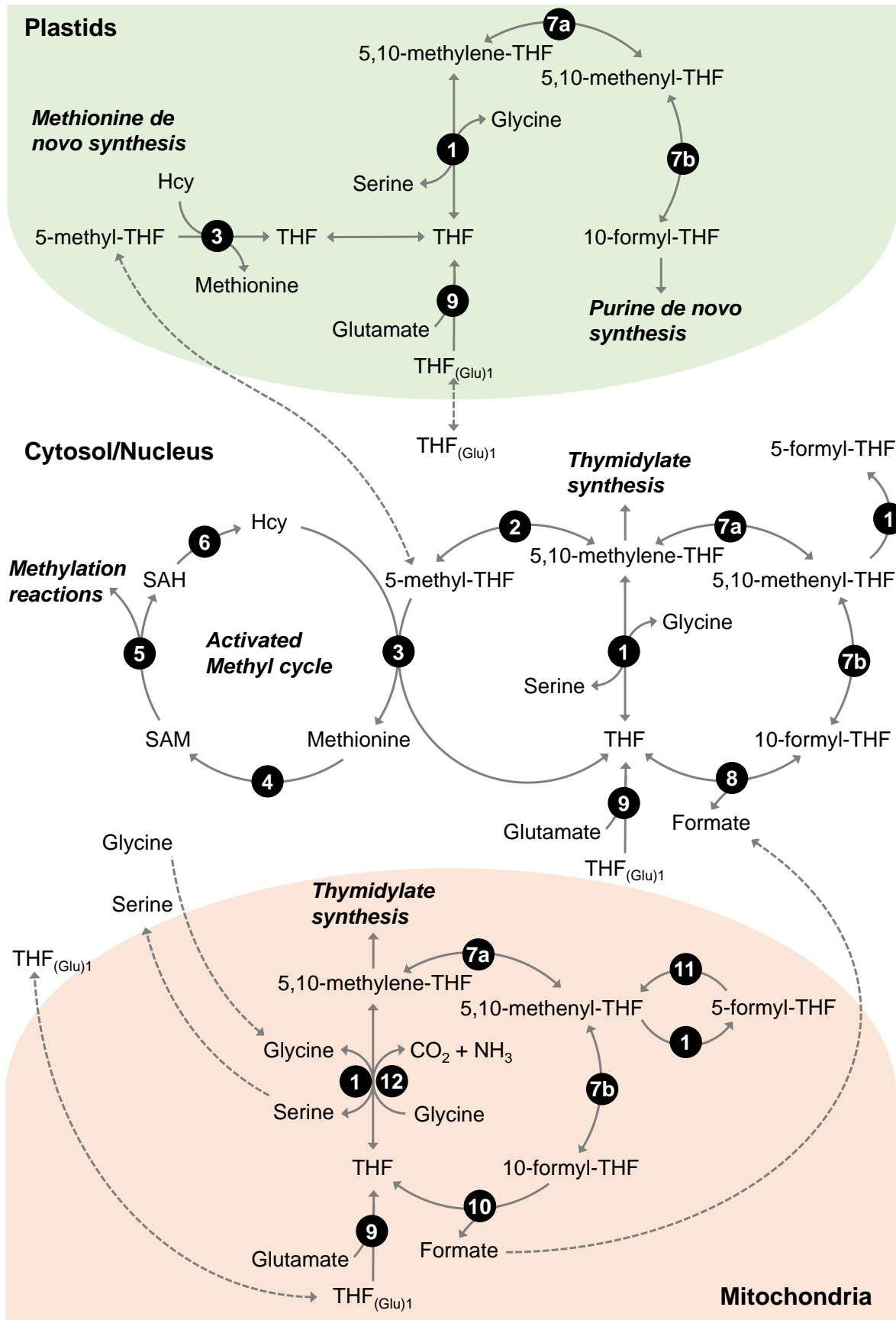


Figure 5. Folate-mediated one-carbon metabolism spans cellular compartments and provides one-carbon for biosynthetic pathways in *Arabidopsis*.

Folate metabolism provides one-carbon for various biochemical reactions and biosynthetic pathways including methionine, purine, and thymidylate *de novo* synthesis. Additionally, SAM is a methyl group donor for methylation reactions including cytosine and H3K9 methylation. (1) SERINE HYDROXYMETHYLTRANSFERASE (SHMT), (2) METHYLENETETRAHYDROFOLATE REDUCTASE (MTHFR), (3) METHIONINE SYNTHASE (MS), (4) S-ADENOSYLMETHIONINE SYNTHETASE (SAMS), (5) methyltransferases including DNA and histone methyltransferases, (6) S-ADENOSYLHOMOCYSTEINE HYDROLASE (SAHH), (7a) METHYLENETETRAHYDROFOLATE DEHYDROGENASE & (7b) METHENYLTETRAHYDROFOLATE CYCLOHYDROLASE (MTHFD), (8) 10-FORMYLTETRAHYDROFOLATE SYNTHETASE (THFS), (9) FOLYLPOLYGLUTAMATE SYNTHETASE (FPGS), (10) 10-FORMYLTETRAHYDROFOLATE DEFORMYLASE (10-FDF), (11) 5-FORMYLTETRAHYDROFOLATE CYCLOLIGASE (5-FCL), (12) GLYCINE DECARBOXYLASE COMPLEX (GDC), THF and THF_(Glu)1 are abbreviations for poly- and monoglutamylated tetrahydrofolate, respectively. Adapted figure (Gorelova *et al*, 2017a; Lindermayr *et al*, 2020).

1.4.3 One-carbon metabolism controls DNA methylation

The existence of similarly structured, parallel one-carbon cycles in the cytosol, mitochondria and plastids is intriguing yet plausible as it allows for metabolic flexibility and specialization towards the one-carbon transfer reactions they support. However, there are examples showing that this specialization can also be disadvantageous, particularly in the context of cytosolic one-carbon metabolism that is indispensable for DNA methylation. As such, mutation of *SAHH1* was shown to increase SAH concentrations and reduce the MI resulting in DNA hypomethylation, a reduction of DNA methylation levels (Rocha *et al*, 2005; Ouyang *et al*, 2012; Huang *et al*, 2019). Decreased levels of DNA methylation in the CHG and CHH context as well as diminished H3K9me2 were found in mutant plants of *SAMS3*, one of the isoforms of SAM synthetases that localizes in the cytosol and nucleus (Meng *et al*, 2018). Furthermore, a mutant of the catalytically inactive *SHM7* isoform of *SHMT* with altered DNA methylation was characterized (Huang *et al*, 2016). Interestingly, *SHM7* mutants exhibited DNA methylation reduction in roots and an increase in shoots through an unknown mechanism highlighting a tissue-specific defect (Huang *et al*, 2016). Furthermore, it could be shown that FPGS1-mediated glutamylation of folates is essential for DNA and histone methylation as *fpgs1* mutants also displayed SAH and Hcy accumulation together with genome-wide reduction of DNA methylation and derepression of gene silencing (Zhou *et al*, 2013). Importantly, similar effects were also observed in mammals. Humans are devoid of folate *de novo* synthesis and predominantly obtain folates from a plant-based diet. Folate deficiency is primarily caused by insufficient dietary intake and can lead to severe health issues such as neural tube defects (Smithells *et al*, 1976; Czeizel & Dudás, 1992). Exemplarily, it was demonstrated that the maternal diet during conception affects the establishment of DNA methylation in children (Dominguez-Salas *et al*, 2014). Intriguingly, the causal link in this study was the seasonal

environment-dependent diet of rural women in Gambia that resulted in different season-specific concentrations of substrates and cofactors necessary for one-carbon metabolism (Dominguez-Salas *et al*, 2014). These examples show that metabolic enzymes are factors required for DNA methylation and highlight the importance of concerted action between methylation pathways and one-carbon metabolism to safeguard genome stability.

1.4.4 MTHFD1 is required for proper DNA methylation in *Arabidopsis*

This work is based on another metabolic enzyme that influences DNA methylation in *Arabidopsis*. In a previous study, it was shown that cytosolic MTHFD1-dependent folate metabolism controls repressive DNA methylation through an unknown mechanism that affects remethylation of Hcy to methionine (**Figure 5**) (Groth *et al*, 2016). EMS-induced mutation of *MTHFD1*, hereafter named *mthfd1-1*, led to a predicted substitution of a conserved arginine by glutamine in the nicotinamide adenine dinucleotide phosphate (NADPH/NADP⁺) binding motif which led to reduced growth, genome-wide loss of DNA methylation and release of TE silencing. Changes in DNA methylation were most likely the result of SAH accumulation and the successive reduction of the MI. DNA methylation was decreased in all sequence contexts of cytosine, but particularly in CHG and CHH along with reduction in H3K9me₂ (Groth *et al*, 2016). Despite the dependence of non-CG methylation and H3K9me₂, the defect was also found in CG methylation, however, to a lesser extent. This indicated that the reduced MI affected all methylation reactions mediated by DNA methyltransferases. 5-methyl-THF which provides one-carbon for Hcy remethylation was not reduced in *mthfd1-1* and both methionine and SAM were even increased compared to wild type. Seemingly, MTHFD1 is a regulator of folate homeostasis and vital for accurate DNA methylation as well as TE repression but in contrast to mutants of *SAHH* or *SAMS* it is not part of the AMC but acts upstream of Hcy remethylation.

1.4.5 Plant phenotypes are plastic and adaptive to changing environments

Analysis of within-species genetic variation in plants grown along longitudinal climates is frequently used to describe and interpret adaptation to local microenvironments - often in search for climate adaptive loci (Koornneef *et al*, 2004; Hancock *et al*, 2011). Genetic diversity is thus considered to contribute to local acclimatization of plant accessions to differences in the growth environment (Takou *et al*, 2019). Genetic variation has also been linked to epigenetic changes between *Arabidopsis* accessions from different geographic locations (Schmitz *et al*, 2013; Dubin *et al*, 2015; Kawakatsu *et al*, 2016). These findings supported the idea of plant environmental responses associated with epigenetic variation (Kawakatsu *et al*,

2016; Dubin *et al*, 2015). However, an aspect that is not considered or addressed by sequencing analyses of genetic and epigenetic variation are metabolic states and their dynamics as well as the conclusions drawn for adaptive phenotypic plasticity (Weizmann *et al*, 2023). Photosynthesis and the complex metabolic network that it fuels are tightly regulated and rapidly adjusted upon environmental changes. In recent years, a growing number of studies integrates accession-specific metabolic phenotypes to predict environment-dependent phenotypic plasticity (Kleessen *et al*, 2012; Tong *et al*, 2023; Weizmann *et al*, 2023). Although incorporation of metabolic phenotypes for predictions of beneficial adaptive traits has been successful, it remains poorly understood which factors arise and influence a metabolic network under certain conditions (Hashemi *et al*, 2023). These factors comprise kinetic properties of catalytic enzymes, the rate of metabolic reactions or metabolic concentrations among others (Hashemi *et al*, 2023). As such, resolving the network and regulation of folate-mediated one-carbon metabolism together with genetic and epigenetic information could help predict phenotypic plasticity in plants.

1.5 Aims of this study

While biochemical reactions and pathways of folates were deciphered throughout the past 70 years, the knowledge about the regulation of one-carbon dynamics as well as its impact and crosstalk with epigenetic regulation remains sparse. Indeed, there are studies showing that epigenetic mechanisms, especially DNA methylation are controlled by one-carbon metabolism. Here, most insights were obtained from genetic screens that aimed to identify gene silencing mechanisms (Lindermayr *et al*, 2020). Nonetheless, the underlying mechanisms are often ambiguous. In addition, the plant metabolism itself is highly adaptive to environmental changes and as photoautotrophic organisms, plant development and responses to the growth environment are fueled by metabolites produced through photosynthesis (Lindermayr *et al*, 2020). Therefore, this study aimed to unravel the link between folate-mediated one-carbon homeostasis and DNA methylation in *Arabidopsis*. Here, it was hypothesized that genome integrity and stability are synergistically preserved by DNA methylation and one-carbon metabolism via several means. First, folates are essential for nucleotide synthesis, the basic building blocks of DNA. Second, folates provide SAM for DNA and histone methylation which are important for TE silencing. Third, the metabolome is dynamic and depends on the growth environment, especially on light for photosynthesis and thus has the potential to convey environmentally induced changes in the epigenome. The *mthfd1-1* mutant was utilized to address these points in *Arabidopsis* and to answer the simplified question of how one-carbon is regulated and provided for DNA methylation.

2 Results

2.1 MTHFD1 and THFS are regulators of folate metabolism

Folate metabolism is similarly organized between mammals (Tibbetts & Appling, 2010; Martha S. Field *et al*), plants (Hanson *et al*, 2000; Hanson & Roje, 2001; Gorelova *et al*, 2017a) and yeast (McNeil *et al*, 1996; Hjortmo *et al*, 2008). Accordingly, more than 30 years ago, MTHFD catalyzed enzyme activities were found in mammals (Hum *et al*, 1988; Peri *et al*, 1989; Christensen *et al*, 2005), plants (Kirk *et al*, 1995; Chen *et al*, 1999), and yeast (Appling & Rabinowitz, 1985; Yang & MacKenzie, 1993; West *et al*, 1993; West *et al*, 1996) throughout the nucleus and cytosol, mitochondria and additionally in plastids in plants. However, there are significant differences in the respective function and structure of MTHFD isoforms between the compartments. Most strikingly, the cytosolic MTHFD dehydrogenase and cyclohydrolase as well as THFS synthetase activities are combined in one trifunctional MTHFD1 enzyme (also termed C1 tetrahydrofolate synthase) in mammals (Ducker & Rabinowitz, 2017) and yeast (Appling & Rabinowitz, 1985; Chen *et al*, 1999), while in plants MTHFD dehydrogenase and cyclohydrolase activities are separated from THFS synthetase activity, also in their coding sequences (**Supplementary Figure 1**) (Kirk *et al*, 1994; Kirk *et al*, 1995; Gorelova *et al*, 2019). In *Arabidopsis thaliana*, THFS is the entry point for formate-derived one-carbon into the cytosolic folate cycle and together with MTHFD1 it jointly constitutes a formate-dependent pathway. As described before, *mthfd1-1* showed reduced DNA methylation, potentially linking formate metabolism to epigenetic regulation. Because both enzymes are structurally independent from each other, *THFS* might be active and unaffected by mutation of *mthfd1-1*. Therefore, the roles of *THFS* and *MTHFD1* in this pathway that seemingly controls one-carbon for DNA methylation were resolved.

2.1.1 The *mthfd1-1* phenotype is complemented by mutation of *THFS*

In search of a modifying effect on the phenotype of *mthfd1-1*, the *mthfd1-1* mutant harboring the methylation sensitive reporter *SDC_{pro}-GFP* was crossed with a T-DNA insertion mutant of *THFS* (SALK_067510, hereafter termed *thfs*). The *SDC_{pro}-GFP* reporter is based on the *SUPPRESSOR OF DRM1 DRM2 CMT3 (SDC)* locus that is silenced by CHG and CHH methylation of tandem repeats within the promotor region (Henderson & Jacobsen, 2008; Moissiard *et al*, 2012; Groth *et al*, 2016; Liu *et al*, 2020). Consequently, GFP was expressed in *mthfd1-1* due to genome-wide loss of DNA methylation (**Figure 6 B, D**) (Groth *et al*, 2016). Surprisingly, mutation of *THFS* did not result in a similar phenotype (**Figure 6 B, D**). Although *THFS* is located in the same metabolic pathway as *MTHFD1*, *thfs* mutant plants did not show

Results

delayed flowering and dwarfism (**Figure 6 A, C**) nor induction of *SDC_{pro}-GFP* expression like *methfd1-1* as previously reported by Groth *et al* (2016) (**Figure 6 B, D**). Crossing both mutant plants even suppressed the *methfd1-1* phenotype in the *methfd1-1* x *thfs* double mutant. Astonishingly, while *methfd1-1* displayed drastic phenotypic changes, impairment of the formate-dependent route of one-carbon in its entirety resulted in wild type-like growth in the *methfd1-1* x *thfs* double mutant (**Figure 6**).

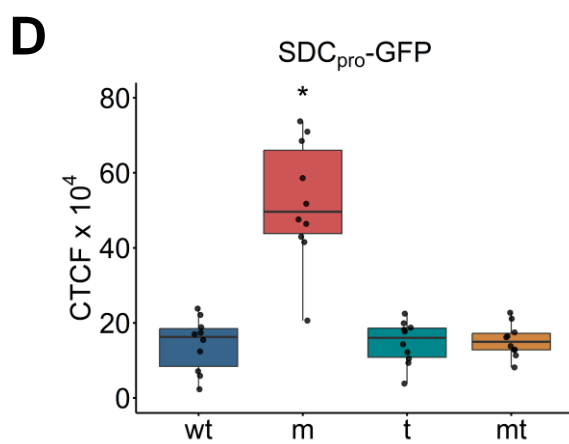
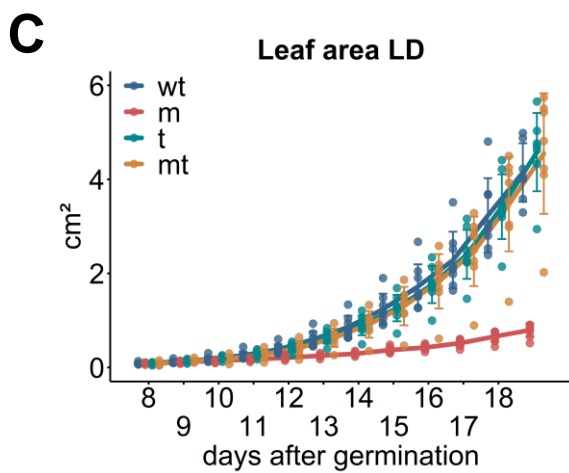
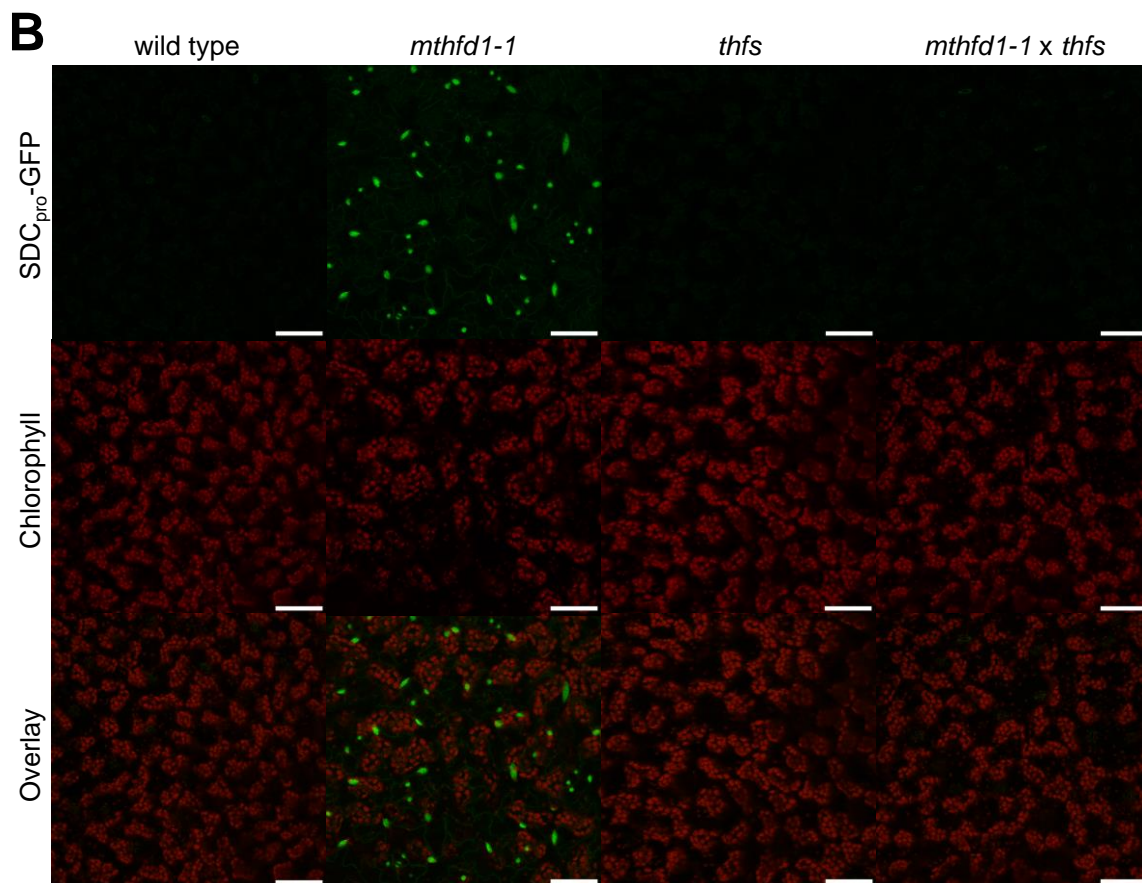
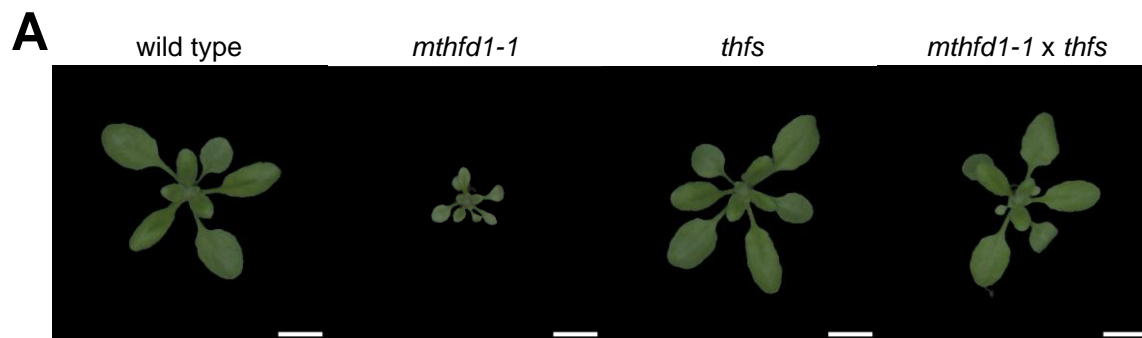


Figure 6. Mutation of *THFS* complements the *mthfd1-1* phenotype.

(A) Pictures of 3-week-old LD grown wild type (wt), *mthfd1-1* (m), *thfs* (t) and *mthfd1-1* x *thfs* (mt) plants from automated phenotyping. Scale bars = 1 cm. (B) Maximum projections along the z axis of subcellular expression of *SDC_{pro}-GFP* in cell nuclei acquired from confocal microscopy of the ventral side of leaves. Scale bars = 50 μ m (C) Leaf area quantification of plant pictures from automated phenotyping between 8 and 18 days after germination. Mean values \pm s.d. ($n = 7-8$) are shown. (D) Corrected Total Cellular Fluorescence (CTCF) of *SDC_{pro}-GFP* from maximum projections. Mean values \pm s.d. ($n = 10$) are shown. Asterisks represent statistical differences between genotypes (One-way ANOVA followed by post-hoc Tukey test, $P < 0.05$).

2.1.2 DNA methylation patterns are restored in *mthfd1-1* x *thfs*

In order to see if DNA methylation was restored in the double mutant *mthfd1-1* x *thfs*, global DNA methylation levels were analyzed at single-nucleotide resolution by whole genome bisulfite sequencing (WGBS) and compared to wild type, *mthfd1-1* and *thfs* plants. Groth *et al* (2016) have previously calculated differentially methylated regions (DMRs) with decreased DNA methylation in *mthfd1-1* and mutants of DNA methyltransferases compared to wild type reference hypo-DMRs. These defined DMRs were used to assess DNA methylation pathway specific patterns in *mthfd1-1* x *thfs*. Among the cytosine sequence contexts, CMT2-dependent CHG methylation was most affected in *mthfd1-1* (Groth *et al*, 2016). A heat map of hierarchically clustered CHG hypo-DMRs displayed wild type-like DNA methylation levels in *thfs* and *mthfd1-1* x *thfs* (**Figure 7**). These sequencing results validated the initial results obtained from the expression analysis of DNA methylation sensitive *SDC_{pro}-GFP* (**Figure 6 B, D**) and confirmed complementation of DNA methylation in the double mutant *mthfd1-1* x *thfs* for CHG methylation.

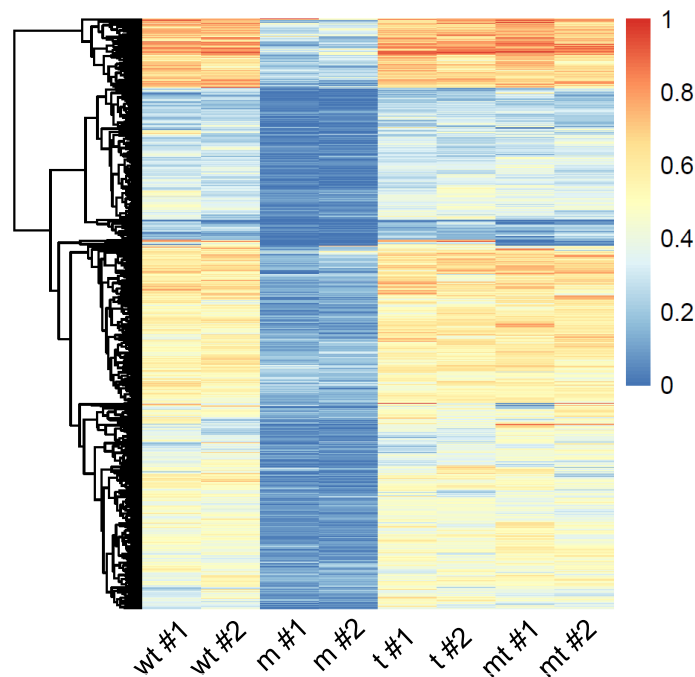


Figure 7. CHG methylation is restored in *mthfd1-1 x thfs*.

DNA methylation at *mthfd1-1* CHG hypo-DMRs in 3-week-old wild type (wt), *mthfd1-1* (m), *thfs* (t), *mthfd1-1 x thfs* (mt) plants grown under LD conditions. Two replicates (#1, #2) per genotype were analyzed by whole genome bisulfite sequencing.

2.1.3 THFS is part of the cytosolic folate metabolism

Previous studies measured THFS activity in the cytosol and mitochondria (Kirk *et al*, 1994). Therefore, it became generally accepted that THFS is not restricted to one compartment but shares isoforms in the cytosol, mitochondria and plastids with enzyme activity that is sequential and tightly linked to that of MTHFD and SHMT (Gorelova *et al*, 2017a; Lindermayr *et al*, 2020). Yet, latest studies predicted that *THFS* is likely a single copy gene with a single functional formate-tetrahydrofolate ligase domain confined to the cytosol (Gorelova *et al*, 2019). To confirm the cytosolic localization, the expression of GFP-tagged full length THFS was analyzed through *in vivo* confocal microscopy (**Figure 8**). Under the control of its native promotor, THFS localization was verified exclusively in the cytosolic cell periphery. Additionally, THFS-GFP expression was analyzed in maximum projections compared to wild type ecotype Col-0 to detect potential artificial fluorescence signals (**Supplementary Figure 2**). Using the public subcellular localization database for *Arabidopsis* proteins (SUBA5), the localization of THFS was predominantly predicted in the cytosol (Hooper *et al*, 2017; Hooper *et al*, 2022). These results strongly supported that THFS operates within the cytosolic FOCM, the compartment where MTHFD1 was reported to be mainly localized and that harbors the AMC responsible for

SAM synthesis (Groth *et al*, 2016). In combination with the mutational approach of *mthfd1-1* complementation (**Figure 6**), *thfs* was shown to control a cytosolic mechanism that interfered with Hcy remethylation.

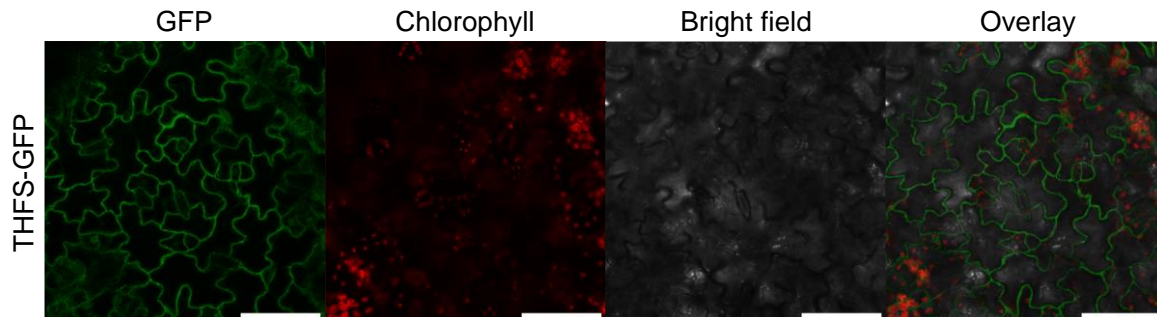


Figure 8. THFS is localized in the cytosol.

Images of THFS-GFP subcellular localization from confocal microscopy of the ventral side of leaves. Scale bars = 50 μ m.

2.1.4 Targeted mutation of *THFS* by CRISPR-Cas9 rescues *mthfd1-1*

To verify the complementing effect of *THFS* inactivation on the *mthfd1-1* phenotype, CRISPR-Cas9 based mutagenesis was used to target exons 2 and 3 of *THFS* (**Supplementary Figure 1 B**). Sequences, where single guide RNAs (sgRNAs) guided endonucleases were targeted are indicated along the position of T-DNA insertion of *thfs* (SALK_067510) (**Supplementary Figure 1 B**). After a multiplex construct containing sgRNAs and CRISPR-Cas9 endonuclease was transformed into the *mthfd1-1* genetic background, positive transformants were selected by red fluorescent protein (RFP) expression in seed coats. Thereby, mutant alleles of *THFS* were identified such as the complemented line *thfs-20*, which showed suppression of *SDC_{pro}-GFP* expression (**Figure 9 C, D**). Mutation of *THFS* in *thfs-20* was confirmed using Sanger sequencing, whereas sequencing of *thfs-23*, a *mthfd1-1* mutant that was not complemented in growth or *SDC_{pro}-GFP* expression (**Figure 9 A, B, C, D**), was attested for wild type *THFS* alleles. Again, WGBS was used to measure DNA methylation levels in all cytosine sequence contexts (**Figure 9 E**). Since DNA methylation patterns of the *mthfd1-1* mutant background were already extensively examined (Groth *et al*, 2016), low coverage sequencing with approximately 2X coverage for each cytosine was used to survey the global DNA methylation levels. Similar to recovery of DNA methylation in *mthfd1-1* x *thfs*, cytosine methylation was restored in all sequence contexts in the complemented CRISPR-Cas9 line *thfs-20* compared

Results

to *thfs-23* (**Figure 9 E**). Thus, *thfs-20* showed about 25 %, 7 % and 2 % cytosine methylation for the CG, CHG and CHH sequence contexts, respectively, while they were reduced to 15 %, 2.5 % and 1.2 % in *thfs-23*. Hence, the methylation levels in *thfs-20* were approximately at wild type DNA methylation levels of 25 %, 8 %, and 4 % for CG, CHG, and CHH, respectively (Groth *et al*, 2016).

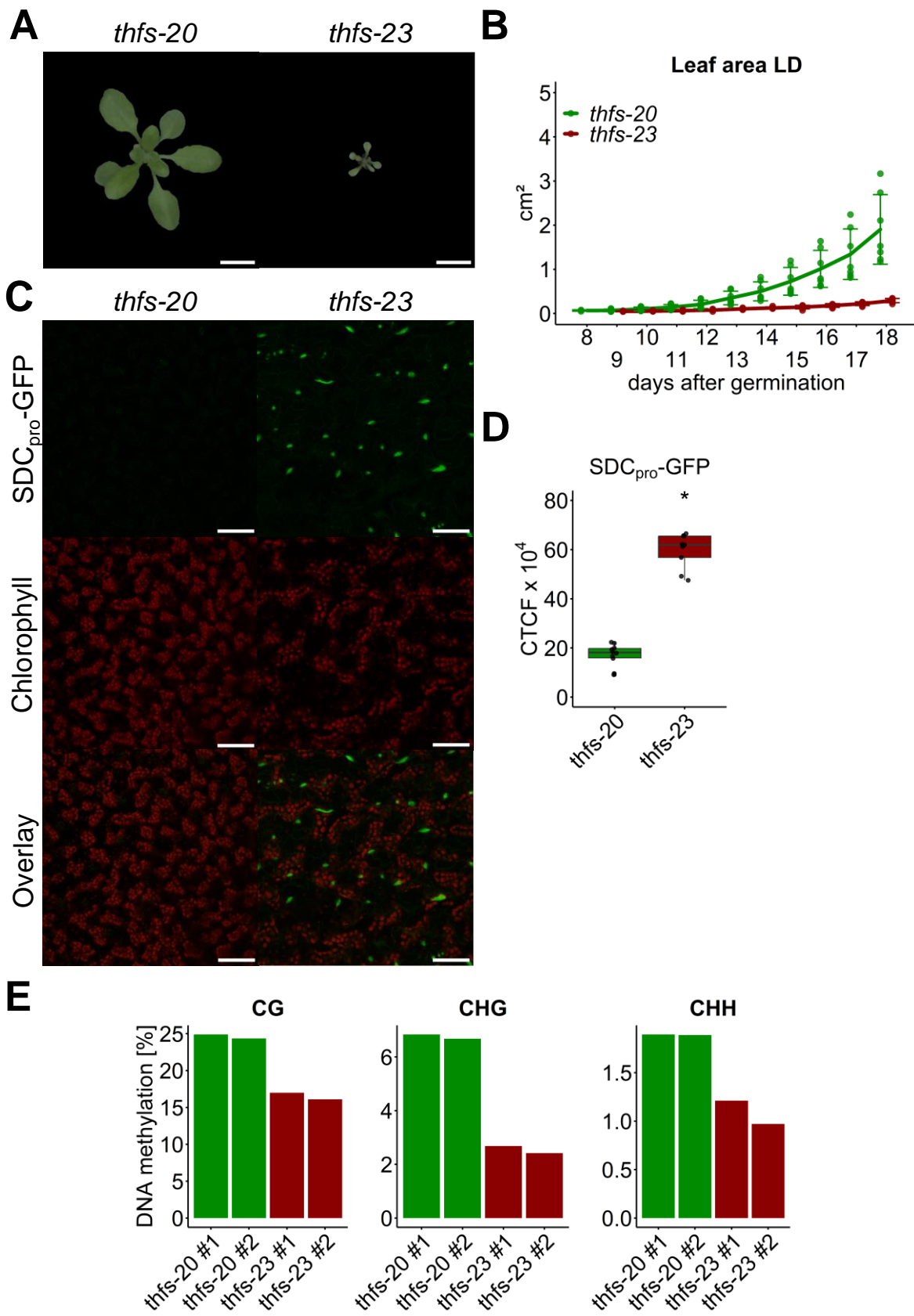


Figure 9. Targeted mutation of *THFS* via CRISPR-Cas9 suppresses the *mthfd1-1* phenotype.

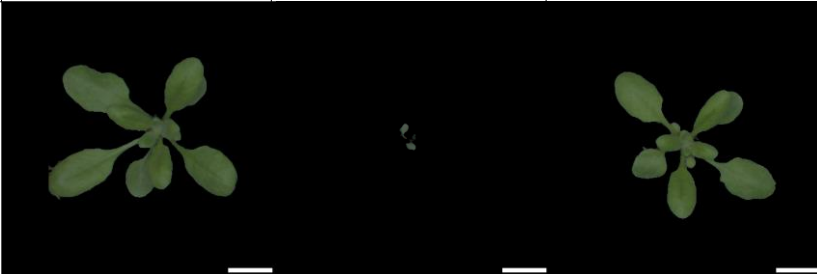
(A) Pictures of 3-week-old LD grown *thfs-20* and *thfs-23* plants from automated phenotyping. Scale bars = 1 cm. (B). Leaf area quantification of plant pictures from automated phenotyping between 8 and 18 days after germination. Mean values \pm s.d. ($n = 7$) are shown. (C) Maximum projections along the z axis of the subcellular expression of *SDC_{pro}-GFP* in cell nuclei acquired from confocal microscopy. Scale bars = 50 μ m. (D) Corrected Total Cellular Fluorescence (CTCF) of *SDC_{pro}-GFP* quantified from maximum projections. Mean values \pm s.d. ($n = 10$) are shown. Asterisks represent statistical differences between genotypes (Student's *t*-test, $P < 0.05$) (E) Genome-wide DNA methylation for all cytosine sequence contexts (H = A, C, T). Two replicates (#1, #2) per genotype were analyzed by whole genome bisulfite sequencing.

2.1.5 *thfs* complements other mutant alleles of *MTHFD1*

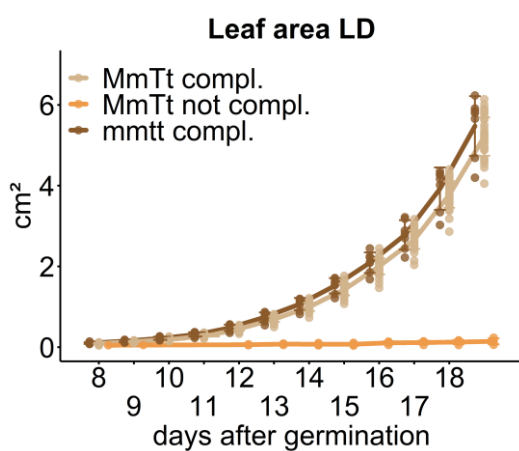
To test if mutation of *THFS* also complements defective phenotypes of other *MTHFD1* alleles, *thfs* was crossed with the T-DNA insertion mutant *mthfd1-3* (SALK_015165), a line where it was previously not possible to recover a homozygous mutant due to strong growth defects (Groth *et al*, 2016). The position of the T-DNA insertion in *mthfd1-3* is indicated together with the EMS-generated mutagenesis in *mthfd1-1* (**Supplementary Figure 1 C**). A double homozygous line *mthfd1-3* x *thfs* (mmtt) was compared to a segregating double heterozygous line *MTHFD1/mthfd1-3* x *THFS/thfs* (MmTt), to retrieve gene variants of individuals that were complemented or had a homozygous *mthfd1-3* allele that did not show complementation. Segregation analysis of the double heterozygous line *MTHFD1/mthfd1-3* x *THFS/thfs* (MmTt) was carried out using automated phenotyping and resulted in offspring individuals with complemented wild type and non-complemented phenotypes in a proportion of 10:1, respectively (**Figure 10 A, B**). All offspring individuals of the double homozygous *mthfd1-3* x *thfs* (mmtt) mutant had a wild type phenotype, illustrating that mutation of *THFS* also complemented other *MTHFD1* alleles (**Figure 10 A**). A separate experiment was used to assess relative DNA methylation levels of *MTHFD1/mthfd1-3* x *THFS/thfs* (MmTt) and *mthfd1-3* x *thfs* (mmtt) offsprings using McrBC-qPCR (**Figure 10 C**). Offspring individuals with MmTt and mmtt genotype showed a complemented wild type phenotype and Col-0 DNA methylation levels while non-complemented, homozygous *mthfd1-3* mutant plants with heterozygous *thfs* alleles showed reduced relative DNA methylation levels (**Figure 10 C**). These results unexpectedly showed that the cytosolic formate-dependent pathway was dispensable for DNA methylation while its elimination was also sufficient to complement the *mthfd1-1* phenotype.

A

parent genotype F2	<i>MTHFD1/mthfd1-3</i> x <i>THFS/thfs</i> (MmTt)		<i>mthfd1-3</i> x <i>thfs</i> (mmtt)
offspring phenotype F3	complemented	not complemented	complemented
offspring individuals F3	36	4	7



B



C

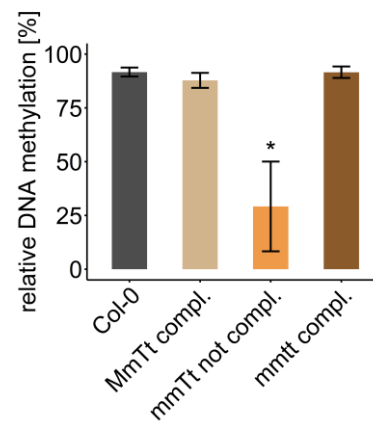


Figure 10. Mutation of *THFS* complements *mthfd1-3*.

(A) Segregation analyses of LD grown heterozygous *MTHFD1/mthfd1-3* x *THFS/thfs* (MmTt) and homozygous *mthfd1-3* x *thfs* (mmtt) parental F2 mutant lines led to complemented and non-complemented F3 offsprings. Scale bars = 1 cm (B) Leaf area quantification of plant pictures from automated phenotyping between 8 and 18 days after germination. Mean values \pm s.d. calculated from the number of offspring individuals from (A). (C) Relative DNA methylation levels in complemented and non-complemented mutant lines compared to wild type Col-0 analyzed via McrBC-qPCR. Mean values \pm s.d. from individuals of Col-0 ($n = 2$), MmTt compl. ($n = 4$), mmtt not compl. ($n = 5$) and mmtt compl. ($n = 5$) are shown. Asterisks represent statistical differences between genotypes (One-way ANOVA followed by post-hoc Tukey test, $P < 0.05$).

2.1.6 Transition from vegetative to reproductive growth is delayed in *mthfd1-1*

Although all plants in this study, wild type and mutant lines, were grown under same temperature and light conditions, *mthfd1-1* plants did not only show reduced growth but also exhibited delayed development, specifically in flower formation. After 5 weeks of growth under long day (LD) conditions, *mthfd1-1* plants started to form first flower buds while wild type, *thfs*

Results

and *mthfd1-1* x *thfs* plants had already transitioned to reproductive growth and formed inflorescences (**Figure 11 A**). Prolonged vegetative growth of 5 weeks led to an increase in leaf numbers when first flowers emerged in *mthfd1-1* compared to a shorter vegetative growth period of 3 weeks in the other genotypes corresponding to lower leaf numbers (**Figure 11 B**). *Arabidopsis thaliana* is a long day plant, meaning that long day growth conditions induce the expression of the *FLOWERING LOCUS T (FT)* gene, a mobile florigen that conveys seasonal flowering to ensure maximal reproductive success during the long days of summer (Andrés & Coupland, 2012; Song *et al*, 2015). Under LD conditions, photoperiodic expression of *FT* peaks around dusk and is mainly controlled by the transcriptional activator *CONSTANS (CO)*. *CO* in turn is positively regulated by the photo-induced FLAVIN-BINDING, KELCH REPEAT, F-BOX 1 (*FKF1*)-*GIGANTEA (GI)* complex which accumulates late in the afternoon and degrades repressors of *CO* (Andrés & Coupland, 2012; Song *et al*, 2015). Therefore, RT-qPCR was used to analyze the diurnal expression of *GI*, *FKF1* and *FT* (**Figure 11 C, D, E**, respectively). Interestingly, reduced expression of all genes could be detected in *mthfd1-1* when they were expected to peak (Turck *et al*, 2008; Song *et al*, 2015). Apparently, deregulation of genes required for photoperiod-dependent development led to delayed growth of *mthfd1-1* plants. Reduction of *FT*, but not *FKF1* and *GI* expression in *thfs* and *mthfd1-1* x *thfs* was potentially caused by other regulatory mechanisms of *FT* regulation (Song *et al*, 2015). However, these did not delay the transition from vegetative to reproductive growth (**Figure 11 A, B**).

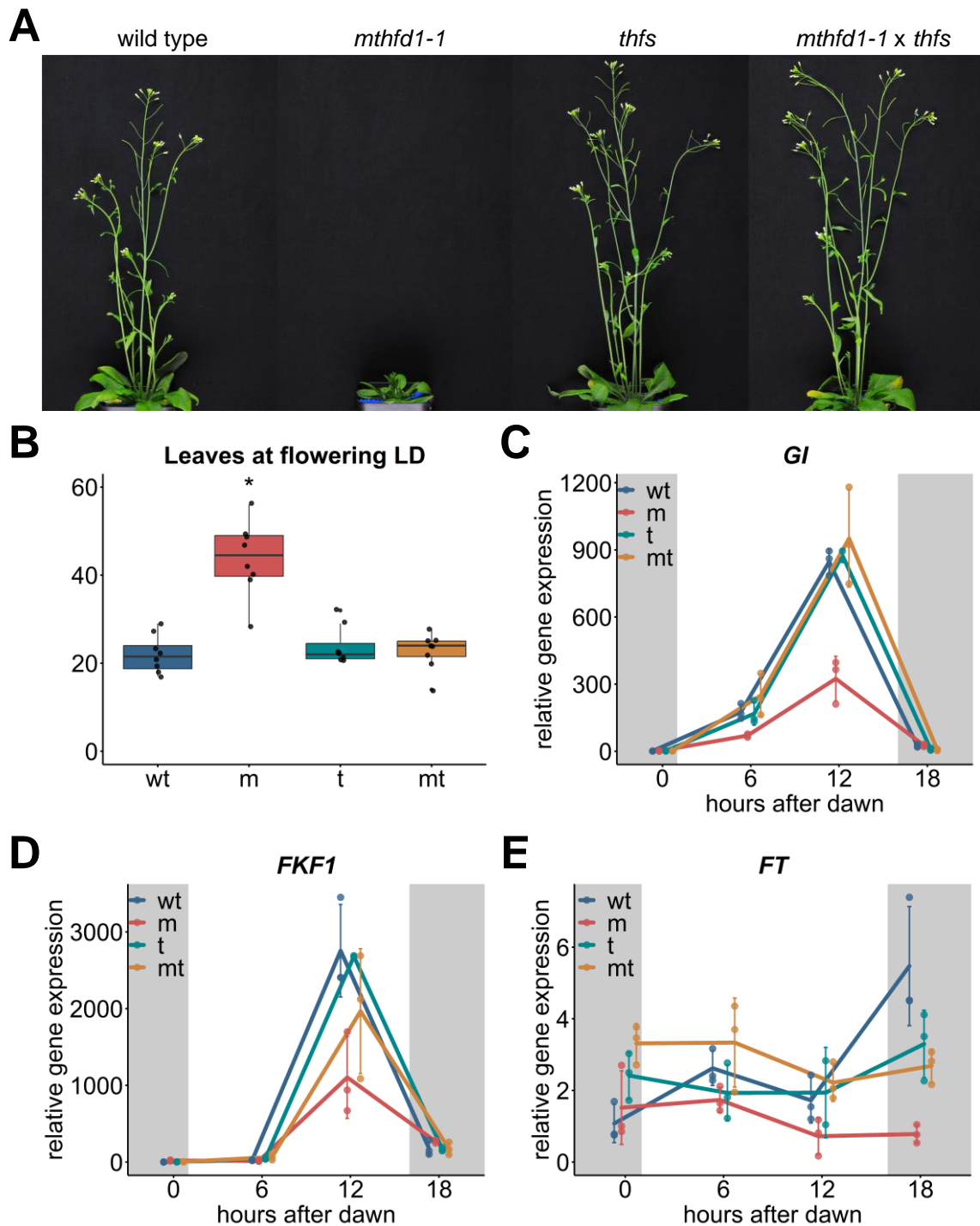


Figure 11. Photoperiodic control of flowering is impaired in *mthfd1-1* under LD conditions.

(A) Pictures of 5-week-old LD grown wild type (wt), *mthfd1-1* (m), *thfs* (t) and *mthfd1-1 x thfs* (mt) plants. (B) Leaf numbers after first flowers emerged. For wt, t and mt leaves were counted after 3.5 weeks, for m after 5 weeks of growth. Mean values \pm s.d. ($n = 8$) are shown. Asterisks represent statistical differences between genotypes (One-way ANOVA followed by post-hoc Tukey test, $P < 0.05$). Diurnal expression of *GI* (C) *FKF1* (D) and *FT* (E) in rosette leaves of 3-week-old wt, m, t, mt plants harvested at 0, 6, 12, 18 hours after dawn using RT-qPCR, normalized to *PP2A* transcript levels. Mean values \pm s.d. ($n = 3$) are shown. Adjusted P values indicating statistical differences between genotypes at each

timepoint (One-way ANOVA followed by post-hoc Tukey test, $P < 0.05$) can be found in **Supplementary Table 1**.

2.1.7 Growth of *mtbfd1-1* is retarded under LD but normal under SD conditions

GI, *FKF1*, *CO* and *FT* are part of a regulatory pathway that promotes flowering specifically under LD conditions and that is controlled by the length of the photoperiod and the circadian clock (Andrés & Coupland, 2012). Since *mtbfd1-1* showed delayed flowering under LD similar to mutants of this regulatory pathway such as *gi*, the mutant of *GI* (Koorneef *et al*, 1991; Andrés & Coupland, 2012), *mtbfd1-1* plants were grown under short day (SD) conditions to test if shortening the length of the photoperiod alters the phenotype. Interestingly, when grown under SD conditions *mtbfd1-1* growth defects were almost entirely complemented (**Figure 12 A, B**) compared to LD conditions (**Figure 6 A, C**). As mentioned before, the *mtbfd1-1* mutant allele led to increased expression of transposable elements (TEs) (Groth *et al*, 2016). Therefore, to assess the photoperiodic impact on gene silencing, *mtbfd1-1* was grown under SD conditions for 4 weeks along wild type, *thfs* and *mtbfd1-1* x *thfs* plants. Subsequently, batches were halved: one half was shifted to LD conditions for 24 hours starting at dawn while the second half kept growing under SD conditions. Afterwards SD and SD to LD shifted plants were analyzed for relative gene expression of TEs *SADHU3*, *ATCOPIA28* (Quesneville, 2020; Rangwala & Richards, 2010) and the *SDC* locus (Henderson & Jacobsen, 2008) (**Figure 12 C**). Under SD conditions, expression levels of *SADHU3* and *SDC* were higher in *mtbfd1-1* compared to wild type, *thfs* and the *mtbfd1-1* x *thfs* complementation line, emphasizing that the *mtbfd1-1* phenotype was not completely suppressed under SD growth (**Figure 12 C**). However, shifting the plants from SD to LD led to even stronger induction of *SADHU3*, *ATCOPIA28* and *SDC* expression in *mtbfd1-1*, significantly higher than expression under SD conditions. Meanwhile, TE expression in the double mutant *mtbfd1-1* x *thfs* remained wild type-like with or without the shift to LD, further confirming the complementation of the *mtbfd1-1* phenotype through mutation of *THFS*. These results implied that the *mtbfd1-1* phenotype was photoperiod dependent.

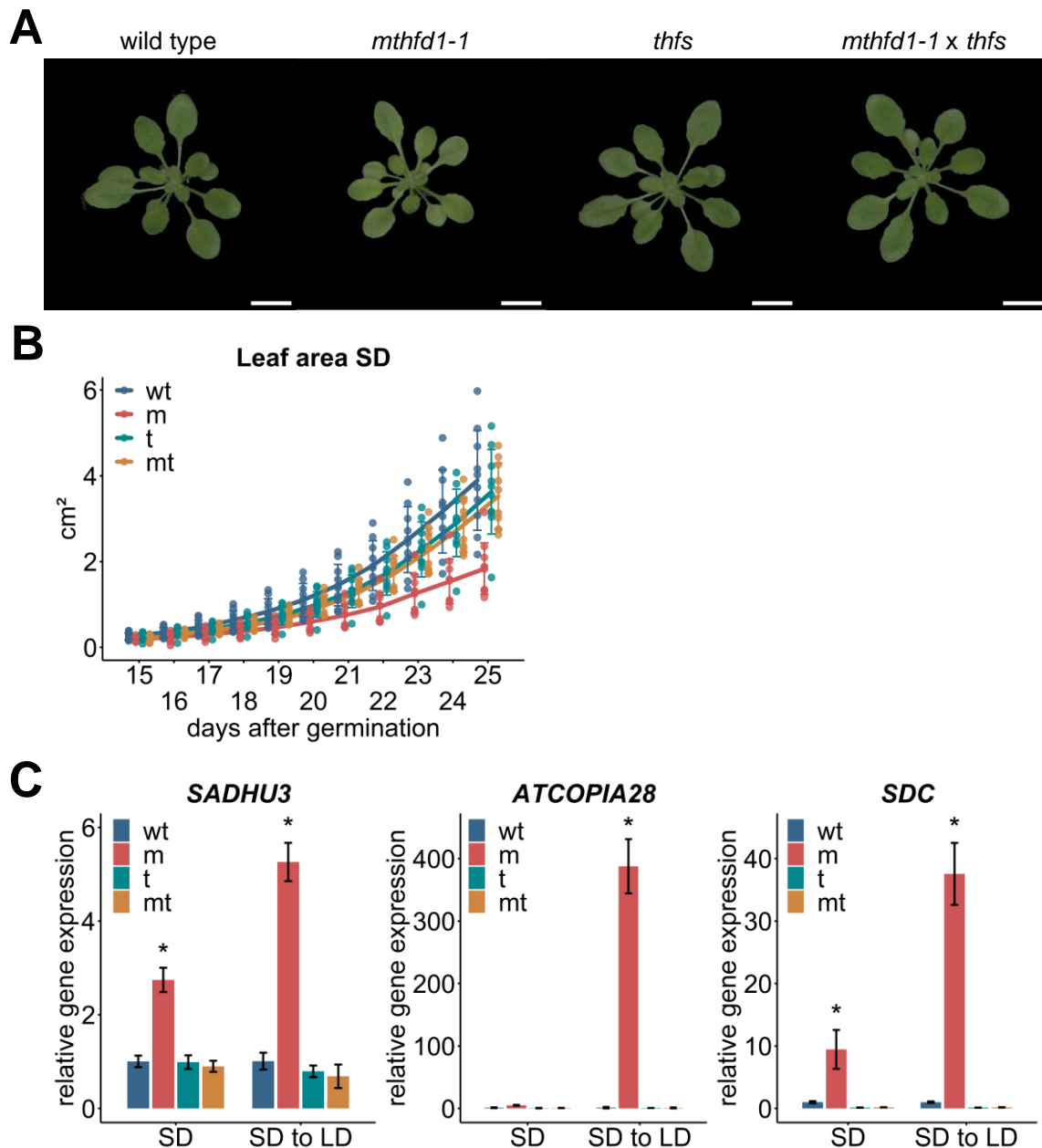


Figure 12. The *mthfd1-1* phenotype is suppressed under short day growth conditions.

(A) Pictures of 4-week-old wild type (wt), *mthfd1-1* (m), *thfs* (t) and *mthfd1-1 x thfs* (mt) plants from automated phenotyping grown under SD conditions. (B) Leaf area quantification of plant pictures from automated phenotyping between 15 and 25 days after germination. Mean values \pm s.d. ($n = 10$) are shown. (C) Relative expression of *SADHU3*, *ATCOPIA28* and *SDC* in rosette leaves of 4-week-old wt, m, t and mt plants harvested at dawn using RT-qPCR and normalized to *PP2A* transcript levels. Plants were shifted from SD to LD conditions for 24 h and compared to plants grown under SD conditions as control. Mean values \pm s.d. ($n = 3$) are shown. Asterisks represent statistical differences between genotypes for each growth condition (SD, SD to LD) (One-way ANOVA followed by post-hoc Tukey test, $P < 0.05$).

2.2 Deregulation of circadian clock components correlates with altered expression of genes from the cytosolic one-carbon metabolism

Since plants are sessile, phototrophic organisms, their metabolic status and partitioning must be synchronized to light – dark cycles to provide substrates for practically all biological reactions. The circadian clock is a biological timekeeper that governs these rhythmic changes and regulates genetic, metabolic, physiological and behavioral processes accordingly (Nakamichi, 2020). The core of this clock is made up of transcriptional and translational feedback loops of morning-phased and evening-expressed genes called the morning and evening complex, respectively (Greenham & McClung, 2015). However, a growing number of studies highlighted that the clock itself is regulated by feedback modulation of cellular processes such as metabolism (Sanchez & Kay, 2016; Cervela-Cardona *et al*, 2021). *GI*, which showed reduced expression in *mthfd1-1* (**Figure 11 C**) is known to control clock function and photoperiodic flowering (Park *et al*, 1999; Nakamichi, 2020) indicating that the misbalance in one-carbon metabolism in *mthfd1-1* might affect clock-regulation or vice versa. *CIRCADIAN CLOCK ASSOCIATED 1* (*CCA1*) encodes a morning-phased transcription factor at dawn that represses the evening-expressed gene *GI* and activates its own repressor *PSEUDO-RESPONSE REGULATOR 5* (*PRR5*) (Greenham & McClung, 2015; Sanchez *et al*, 2020). Diurnal expression levels of *CCA1* and *PRR5* were analyzed using RT-qPCR to examine if these core components and ultimately the circadian clock were deregulated in *mthfd1-1*. Indeed, *PRR5* which is predicted to peak in the afternoon showed higher expression in *mthfd1-1* compared to wild type leading to repression of *CCA1* at dawn (**Figure 13 A**) (Greenham & McClung, 2015). Expression levels of *MTHFD1*, *THFS*, *SHM4* and *SAHH1* were investigated to assess the effect of clock deregulation on the cytosolic one-carbon metabolism (**Figure 13 B**). Interestingly, *MTHFD1* expression was uniform in all genotypes with an increase in expression at dawn and a decrease at dusk. Although *MTHFD1* showed diurnal expression, clock deregulation in *mthfd1-1* did not affect its expression pattern. As expected, *THFS* showed very low expression in the *thfs* mutant background while expression was slightly higher at 6 hours after dawn in wild type compared to *mthfd1-1* (**Figure 13 B**). Low expression of *THFS* in the *thfs* background indicated a null mutant due to post-transcriptional degradation caused by the mutation. Although, expression of both *SHM4* and *SAHH1* was increased in *mthfd1-1*, both genes did not show diurnal patterns in any of the genotypes. However, since both genes are involved in cytosolic one-carbon metabolism, increased product formation of *SHM4* and *SAHH1* catalyzed reactions was expected.

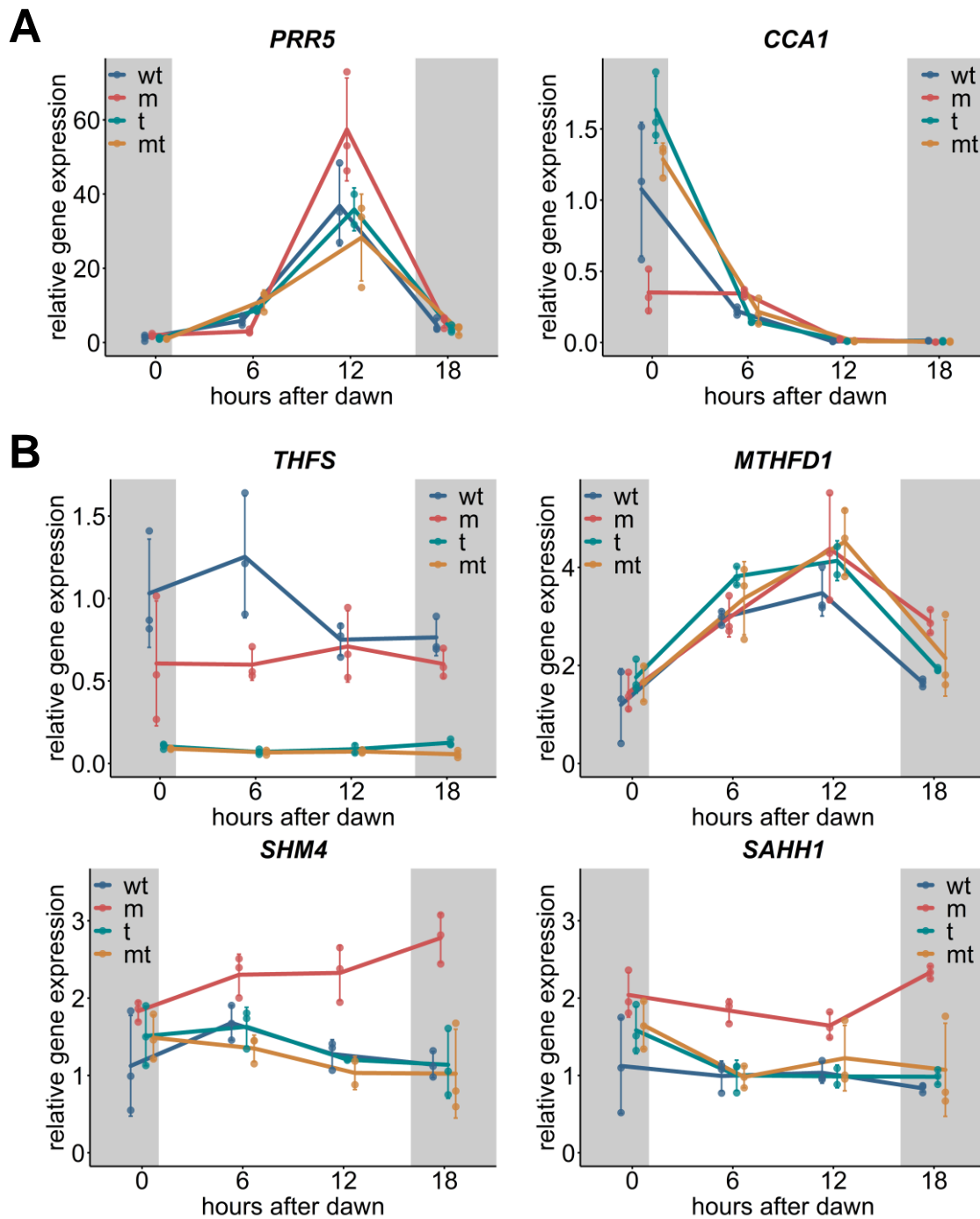


Figure 13. Diurnal expression of clock and one-carbon genes is altered in *mthfd1-1*.

Relative expression of clock genes *PRR5* and *CCA1* (A) and genes of the cytosolic one-carbon metabolism *THFS*, *MTHFD1*, *SHM4* and *SAHH1* (B) in rosette leaves of 3-week-old wild type (wt), *mthfd1-1* (m), *thfs* (t), *mthfd1-1* × *thfs* (mt) plants harvested at 0, 6, 12 and 18 hours after dawn using RT-qPCR and normalized to *PP2A* transcript levels. Mean values ± s.d. ($n = 3$) are shown. Adjusted P values indicating statistical differences between genotypes at each timepoint (One-way ANOVA followed by post-hoc Tukey test, $P < 0.05$) can be found in **Supplementary Table 1**.

2.2.1 Accumulation of Hcy and SAH show diurnal patterns in *methfd1-1* under LD

To test if diurnal changes in gene expression resembled metabolic changes, metabolites of the cytosolic AMC were measured to assess the effect of *methfd1-1* and *thfs* mutation on one-carbon homeostasis. Strong accumulation of SAH and Hcy was observed in *methfd1-1* compared to the other genotypes including the complemented double mutant *methfd1-1 x thfs*, with highest levels of both metabolites at 6 and 12 hours after dawn, respectively (**Figure 14 A**). Additionally, a diurnal pattern of metabolite levels was observed: concentrations of SAH and Hcy rose at dawn and declined at dusk, further indicating a daytime dependence of the defective *methfd1-1* phenotype. SAM and methionine concentrations showed a similar pattern in wild type, *thfs* and *methfd1-1 x thfs* plants with increasing levels at dawn and decreasing levels at dusk, with slightly higher SAM concentrations in *methfd1-1 x thfs* throughout the day (**Figure 14 A**). In contrast to *methfd1-1 x thfs*, SAM and methionine levels were reduced in *methfd1-1* during the day but showed a steady increase into the night surpassing concentrations found in the other genotypes. An overlapping increase of SAM and decrease of SAH in *methfd1-1* at dusk indicated abolition of SAH inhibition of DNA methyltransferases during the night. This was illustrated by reduction in the Methylation Index (MI = SAM/SAH) in *methfd1-1* during the day that increased at dusk until the end of the night (**Figure 14 B**). To investigate if the reduced MI resembled changes in diurnal DNA methylation levels, expression of *SDC*, a target for DNA methylation was analyzed (**Figure 14 C**) (Henderson & Jacobsen, 2008). *SDC* expression correlated positively with SAH and Hcy levels and negatively with the MI in *methfd1-1* and showed a similar diurnal pattern as SAH with increasing transcript levels at dawn that decreased at dusk. In wild type, *thfs* and the double mutant *methfd1-1 x thfs*, *SDC* expression remained low during the 24 h of the day. These results highlighted that impaired Hcy remethylation in *methfd1-1* showed daytime specific dynamics with low levels of SAH and Hcy at night when the light was off and increasing levels during the light period of the day.

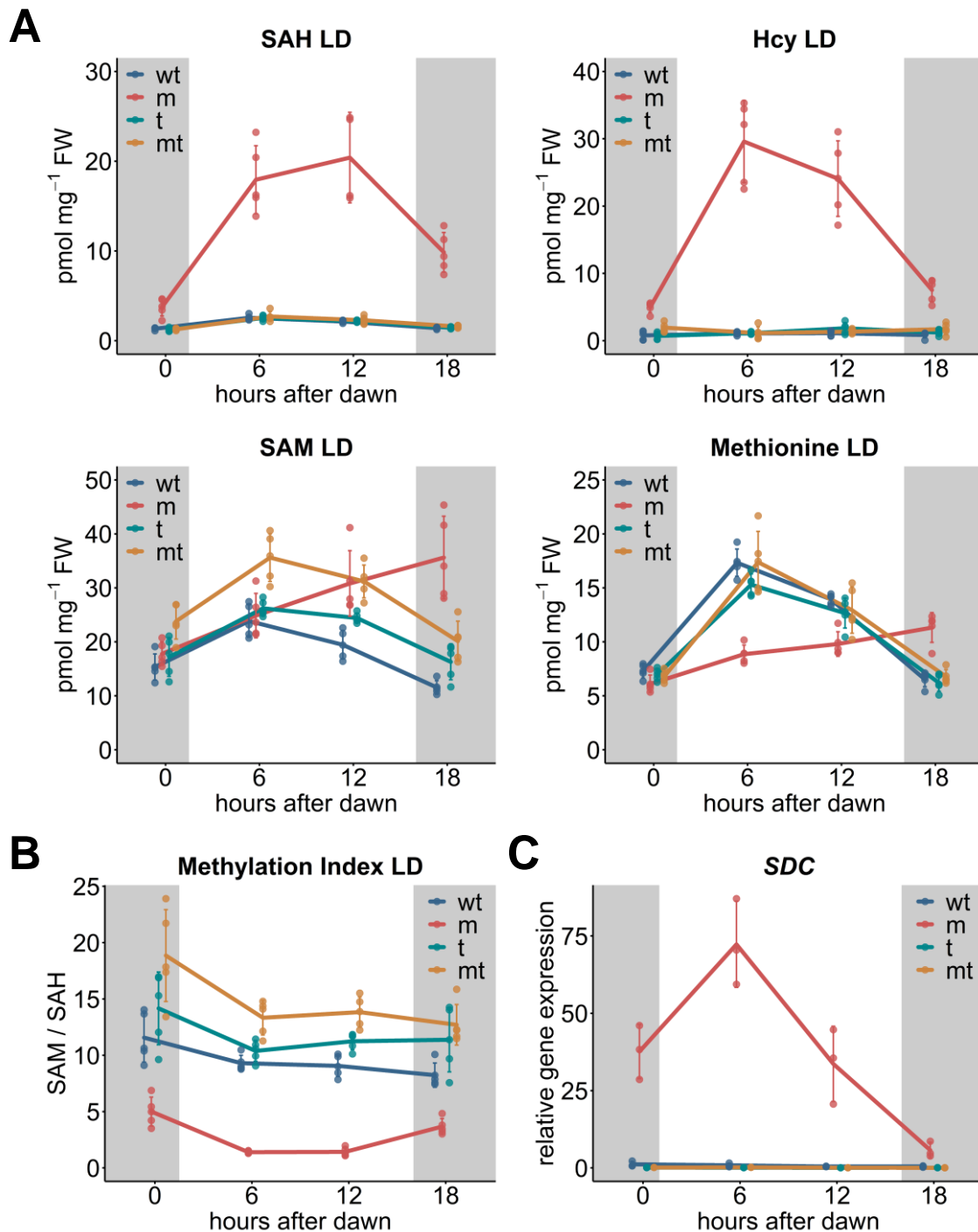


Figure 14. Impaired methyl cycle in *methfd1-1* leads to diurnal *SDC* expression under LD conditions.

Steady-state levels of SAH, Hcy, SAM and methionine (A) and Methylation Index (MI) (B) in leaves of 3-week-old wild type (wt), *methfd1-1* (m), *thfs* (t) and *methfd1-1* × *thfs* (mt) plants harvested at 0, 6, 12 and 18 hours after dawn. (C) Relative expression of *SDC* in rosette leaves of 3-week-old plants using RT-qPCR and normalization to *PP2A* transcript levels. Mean values ± s.d. for metabolites and the MI ($n = 5$) and *SDC* expression ($n = 3$) are shown. Adjusted P values indicating statistical differences between genotypes at each timepoint (One-way ANOVA followed by post-hoc Tukey test, $P < 0.05$) can be found in **Supplementary Table 2** for metabolites and the MI and **Supplementary Table 1** for *SDC* expression.

2.2.2 5-formyl-THF strongly accumulates in *mthfd1-1*

After investigation of the AMC, concentrations of folate cycle metabolites were analyzed (**Figure 15 A, B**). Serine is introduced into the folate cycle as one-carbon source via the activity of SHMTs (Mouillon *et al*, 1999), which use serine and THF to produce 5,10-methylene-THF and the byproduct glycine. Serine and glycine showed similar diurnal patterns as SAM and methionine in all genotypes (**Figure 15 A**). However, serine levels were significantly higher in *mthfd1-1* at all timepoints compared to wild type, *thfs* and the complemented *mthfd1-1 x thfs* double mutant while glycine levels did not differ between genotypes. Accumulation of serine in *mthfd1-1* indicated obstructed incorporation of serine derived one-carbon as substitute of folates. Therefore, the different folate species that act as cofactors accepting and providing one-carbon were analyzed. THF accumulated strongly at 12 hours after dawn in *mthfd1-1* while concentrations in *thfs* and *mthfd1-1 x thfs* were wild type-like (**Figure 15 B**). There were no apparent differences in the diurnal concentrations of 10-formyl-FA between *mthfd1-1*, wild type and *thfs* (**Figure 15 B**). In *mthfd1-1 x thfs* however, there was a slight decrease compared to the other genotypes most probably caused by reduced activities of MTHFD1 and THFS, as both enzymes lead to the formation of 10-formyl-THF (**Figure 5**), which is part of the pool measured in its oxidized form 10-formyl-FA. 5-methyl-THF concentrations were similar between all genotypes except for *thfs* at 12 hours after dawn, when 5-methyl-THF was slightly reduced. Additionally, 5-methyl-THF was higher in *thfs* and *mthfd1-1 x thfs* at night, indicating that formation or accumulation of 5-methyl-THF was daytime dependent in these genotypes (**Figure 15 B**). Concentrations of 5-formyl-THF showed diurnal patterns in wild type, *thfs* and *mthfd1-1 x thfs* with decreased levels after dawn during the light period that increased at night. In *mthfd1-1*, 5-formyl-THF strongly accumulated during the course of the day without showing a diurnal pattern (**Figure 15 B**). This was surprising as 5-formyl-THF is the only folate species in plants that does not serve as a cofactor donating one-carbon but was proposed to act as a stable storage form of folates (Gorelova *et al*, 2017a). As mentioned before, 5-formyl-THF acts as an inhibitor of various enzymes that is formed from 5,10-methenyl-THF by SHMT in the presence of glycine (Goyer *et al*, 2005). One of the many targets of 5-formyl-THF inhibition are SHMTs themselves (Goyer *et al*, 2005; Li *et al*, 2021), thus indicating that accumulation of 5-formyl-THF in *mthfd1-1* might have caused inhibition of SHMTs, specifically the cytosolic isoform SHM4.

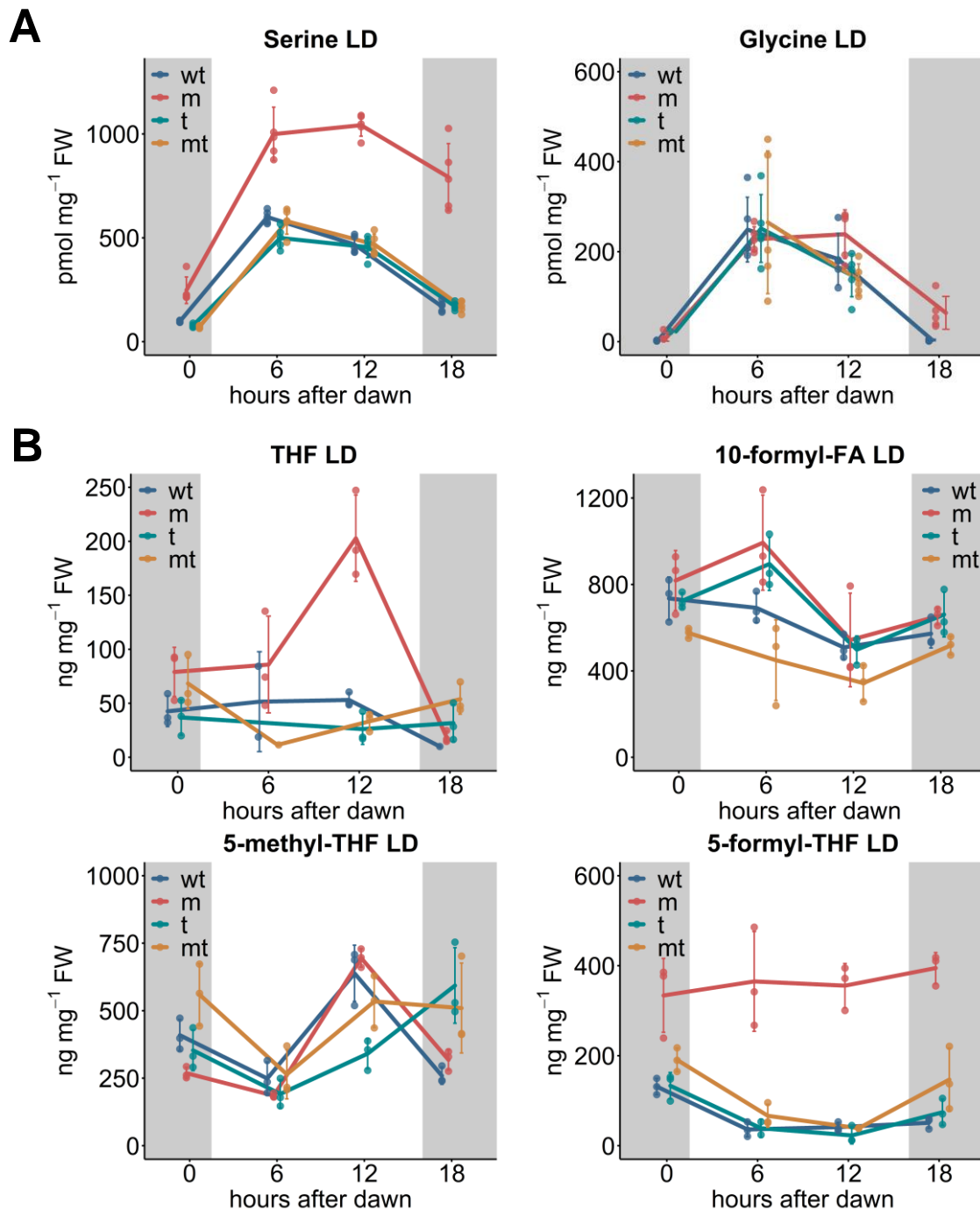


Figure 15. Impaired folate cycle in *mthfd1-1* leads to accumulation of 5-formyl-THF under LD conditions.

Steady-state levels of serine and glycine (A) as well as THF, 10-formyl-FA, 5-methyl-THF and 5-formyl-THF (B) in leaves of 3-week-old LD grown wild type (wt), *mthfd1-1* (m), *thfs* (t) and *mthfd1-1* x *thfs* (mt) plants harvested at 0, 6, 12 and 18 hours after dawn. Mean values \pm s.d. for folates ($n = 3$) as well as serine and glycine ($n = 5$) are shown. Adjusted P values indicating statistical differences between genotypes at each timepoint (One-way ANOVA followed by post-hoc Tukey test, $P < 0.05$) can be found in **Supplementary Table 3**.

2.2.3 One-carbon metabolism is not impaired in *mthfd1-1* under SD growth

As shown before, the *mthfd1-1* phenotype was at least partially suppressed when plants were grown under SD conditions (**Figure 12 A, B**). This was confirmed by a reduced expression of *SADHU3*, *ATCOPIA28* and *SDC* under SD conditions and a strong derepression of these genes when plants were shifted from SD to LD conditions (**Figure 12 C**). This was an indication that Hcy remethylation was restored in *mthfd1-1* when plants were grown under SD conditions. To verify this, cellular levels of methyl and folate cycle metabolites were analyzed from SD grown wild type, *mthfd1-1*, *thfs* and *mthfd1-1 x thfs* plants (**Figure 16**). Compared to metabolite levels in LD grown plants (**Figure 14 & Figure 15**), *mthfd1-1* did not show significant accumulation of SAH or Hcy compared to wild type or the other genotypes (**Figure 16 A**). Furthermore, SAM and methionine levels in *mthfd1-1* exhibited the same diurnal pattern as the other genotypes, with highest levels at 6 hours after dawn, during the light period (**Figure 16 A**). Although serine was slightly increased in *mthfd1-1* at 6 and 12 hours after dawn, levels dropped to wild type concentrations until 18 hours after dawn pointing to almost complete metabolization of serine (**Figure 16 B**). Glycine concentrations showed a diurnal pattern in all genotypes with a strong increase after dawn that gradually decreased after dusk. Interestingly, glycine levels were higher in *mthfd1-1* at the beginning of the dark period but reached wild type levels at 18 hours after dawn (**Figure 16 B**). Growth of *mthfd1-1* under SD had a similar effect on folates which showed wild type levels at 6 and 18 hours after dawn, especially for THF and 5-formyl-THF (**Figure 16 C**). 10-formyl-FA concentrations were still reduced in *mthfd1-1 x thfs* compared to wild type, *mthfd1-1* and *thfs*, most likely owing to the mutations in *MTHFD1* and *THFS* leading to reduced formation of 10-formyl-FA, the oxidized form of 10-formyl-THF, independently of day length (**Figure 16 C**). 5-methyl-THF levels were uniform in all genotypes except for *mthfd1-1 x thfs* which showed increased concentrations at 6 and 18 hours after dawn.

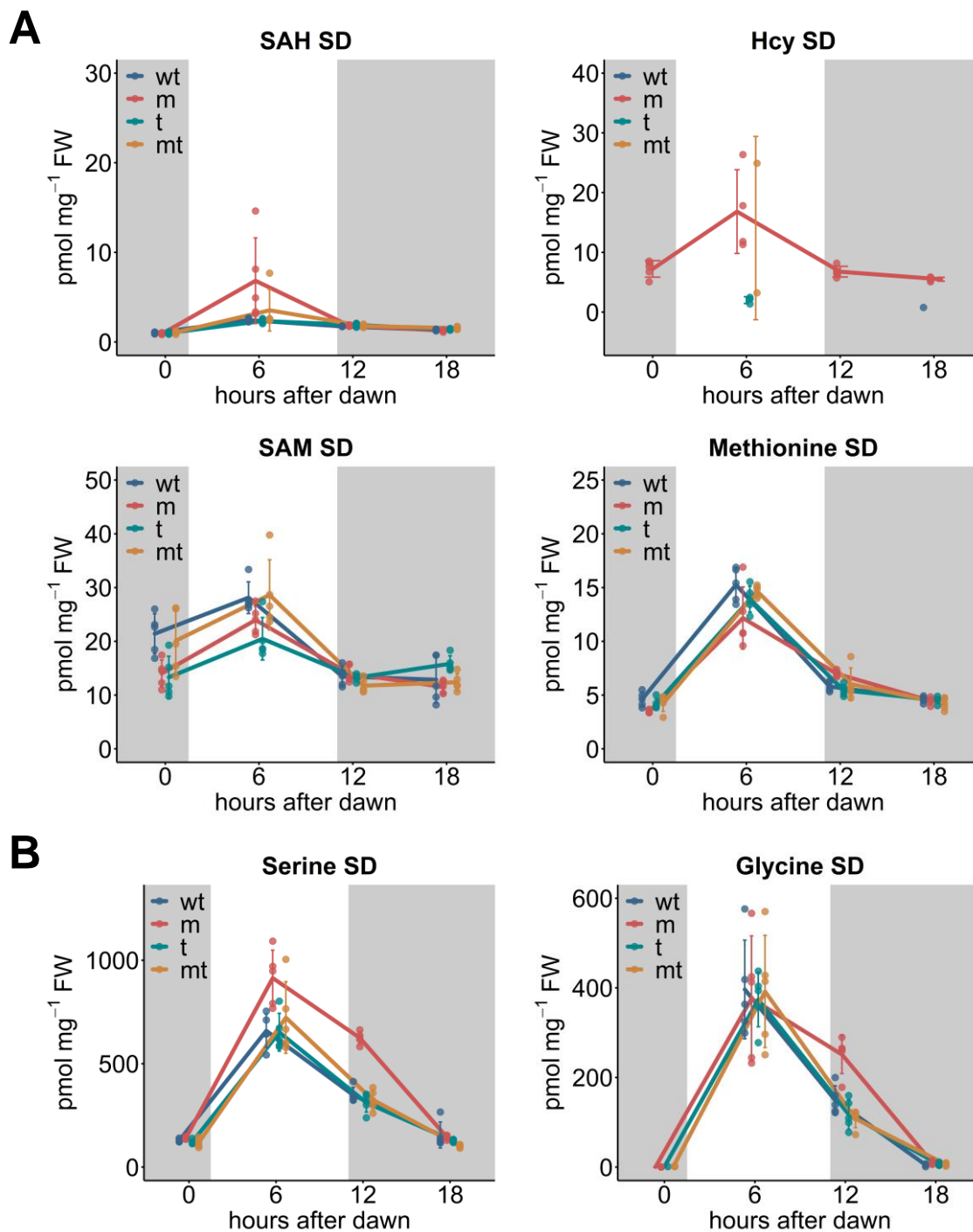


Figure 16. One-carbon metabolites are not altered in *mthfd1-1* under SD conditions.

Steady-state levels of SAH, Hcy, SAM, methionine (A), serine, glycine (B) and THF, 10-formyl-FA, 5-methyl-THF and 5-formyl-THF (C) in leaves of 4-week-old SD grown wild type (wt), *mthfd1-1* (m), *thfs* (t) and *mthfd1-1* × *thfs* (mt) plants harvested at 0, 6, 12 and 18 hours after dawn. Mean values ± s.d. for methyl cycle metabolites ($n = 5$) and folates ($n = 3$) are shown. Adjusted P values indicating statistical differences between genotypes at each timepoint (One-way ANOVA followed by post-hoc Tukey test, $P < 0.05$) can be found in **Supplementary Table 4**.

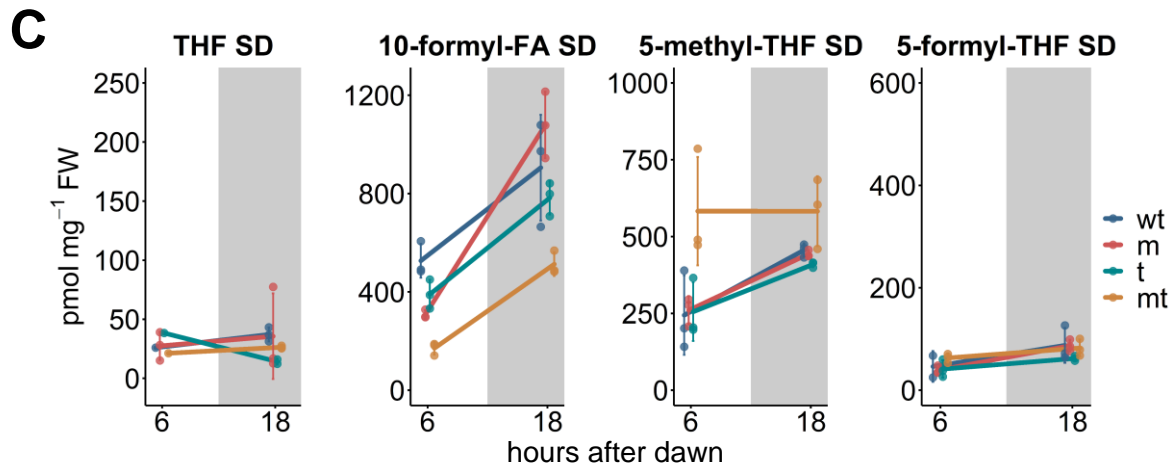


Figure 16. continued.

2.2.4 Application of 5-formyl-THF inhibits root growth in *methfd1-1* x *thfs*

In a next step, it was assessed if external application of 5-formyl-THF was sufficient to deteriorate the *methfd1-1* phenotype or to reintroduce the *methfd1-1* phenotype in the complemented *methfd1-1* x *thfs* double mutant. For this purpose, wild type, *methfd1-1*, *thfs* and *methfd1-1* x *thfs* plants were grown on solidified media plates supplied with 500 μ M 5-formyl-THF, 500 μ M 5-methyl-THF and 25 μ M sulfanilamide, an inhibitor of folate synthesis (**Figure 17**). Indeed, exogenous application of 5-formyl-THF led to reduced root growth in *methfd1-1* and *methfd1-1* x *thfs* compared to mock-treated control plants. In contrast, 5-methyl-THF did not influence root growth, while addition of sulfanilamide led to reduction in root length in all genotypes (**Figure 17 A**). Collectively, these results suggested that 5-formyl-THF might act as a regulating metabolite of one-carbon metabolism that strongly affects growth of plants that harbor impaired activity of MTHFD1. However, previous results showed that exogenous application of 5-formyl-THF to *methfd1-1* did not additionally reduce DNA methylation levels (Groth *et al*, 2016). Again, low coverage WGBS sequencing with 2X coverage on average was used to clarify if 5-formyl-THF led to reduced DNA methylation levels in *methfd1-1* x *thfs* or if its action was restricted to impair root growth without affecting methylation reactions. In line with previous reports from *methfd1-1*, exogenous 5-formyl-THF supply did not influence DNA methylation in *thfs* or *methfd1-1* x *thfs* and did also not reintroduce hypomethylation in one of the cytosine methylation contexts in the complemented double mutant (**Figure 17 B**).

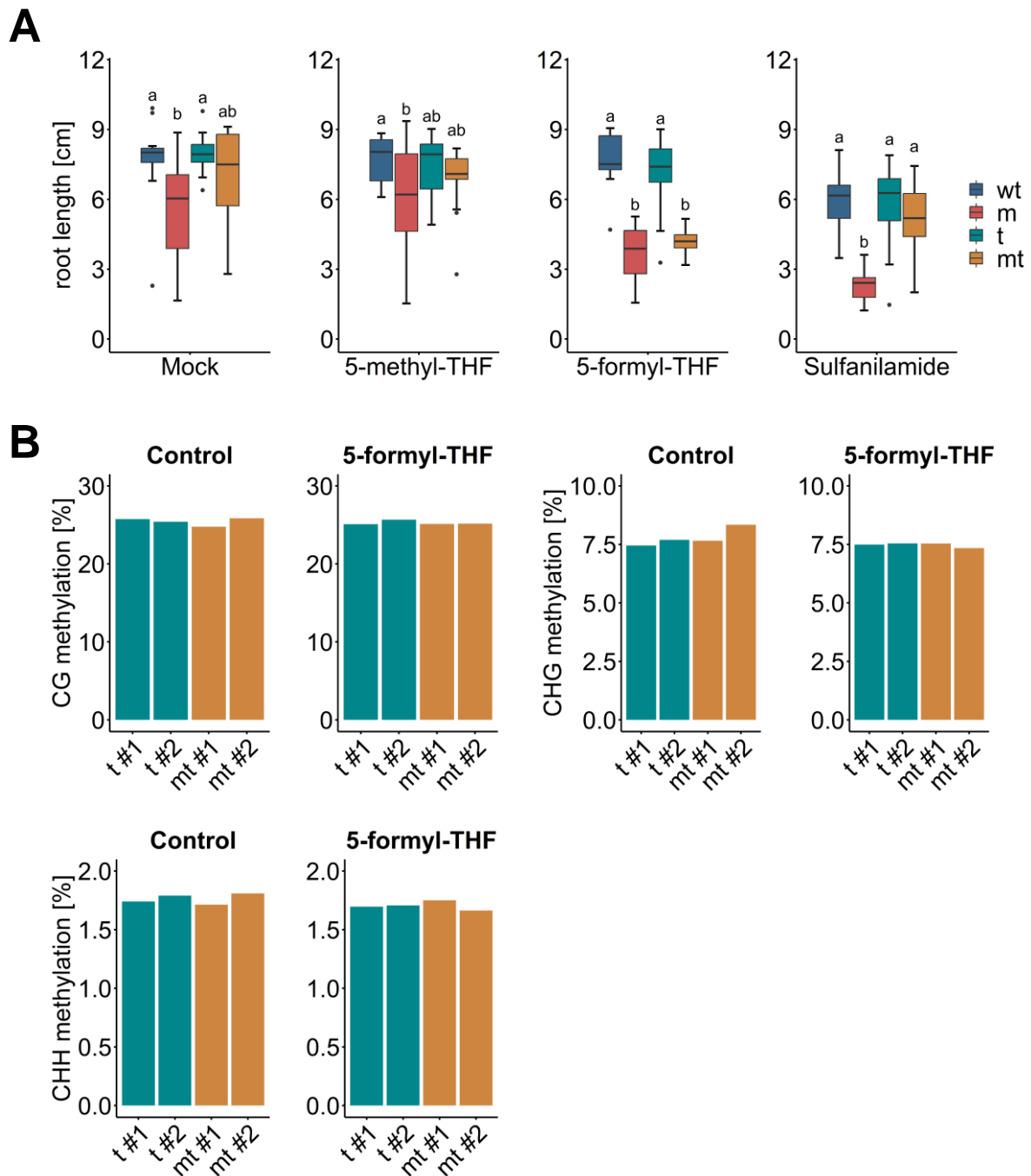


Figure 17. Exogenous supply of 5-formyl-THF inhibits root growth but does not affect DNA methylation in *methf1-1 x thfs*.

(A) Root lengths of 2-week-old LD grown wild type (wt), *methf1-1* (m), *thfs* (t) and *methf1-1 x thfs* (mt) plants grown on full-strength MS media plates supplied with 500 μ M 5-methyl-THF, 500 μ M 5-formyl-THF or 25 μ M sulfanilamide were compared to mock-treated plants. Mean values \pm s.d. ($n = 15$) are shown. Lowercase letters represent statistical differences between genotypes for each supplement (One-way ANOVA followed by post-hoc Tukey test, $P < 0.05$). (B) Genome-wide DNA methylation levels for all cytosine sequence contexts (H = A, C, T). Two replicates (#1, #2) per genotype (t, mt) were analyzed by whole genome bisulfite sequencing.

2.2.5 Methionine salvage cycle and *de novo* synthesis are impaired in *methfd1-1* under LD and SD conditions

Strong diurnal increase of Hcy, while levels of 5-methyl-THF remained wild type-like raised the question if other pathways of methionine formation that might complement the defects of Hcy remethylation were also impaired in *methfd1-1* under LD conditions. For this, metabolites of methionine *de novo* biosynthesis and the methionine salvage pathway were analyzed. Methionine is synthesized from Citric acid cycle derived aspartate in a series of reactions that also lead to the formation of the essential amino acids lysine, threonine and isoleucine (**Figure 18**) (Kirma *et al*, 2012). The synthesis of methionine starts with CYSTATHIONINE γ -SYNTHASE-(CGS)-mediated formation of cystathionine from cysteine and O-phosphohomoserine (HserP) (**Figure 18 Enzyme 1**). Thereafter, Hcy is formed from cystathionine and further processed to methionine via MS using the one-carbon donor 5-methyl-THF (**Figure 18 Enzyme 3**). THREONINE SYNTHETASE (TS) uses HserP for the synthesis of threonine, which is also a substrate for isoleucine formation (**Figure 18 Enzyme 2**). SAM allosterically activates TS (Mas-Droux *et al*, 2006; Jander & Joshi, 2009), but leads to translational arrest of CGS (Onouchi *et al*, 2005; Jander & Joshi, 2009; Onoue *et al*, 2011). It was suggested that regulation at this branch-point by SAM might play an important role in plant metabolite partitioning (Amir *et al*, 2002; Jander & Joshi, 2009). SAM is also utilized for polyamine and ethylene synthesis, reactions that produce 5-methylthioadenosine (MTA) as a byproduct (Sauter *et al*, 2013). MTA is then recycled via the Methionine salvage pathway to methionine in the cytosol (**Figure 18**) (Sauter *et al*, 2013; Watanabe *et al*, 2021). Therefore, diurnal concentrations of aspartate and its derived amino acids lysine, threonine and isoleucine along cysteine as well as MTA were measured in wild type, *methfd1-1*, *thfs* and *methfd1-1 x thfs* plants grown under LD and SD conditions (**Figure 19 & Figure 20**). Interestingly, under LD conditions aspartate was slightly decreased in *methfd1-1* at 6 and 12 hours after dawn during the day and increased to wild type levels at night (**Figure 19**). Under SD conditions, aspartate levels were uniform between genotypes and overall increased compared to LD growth. Asparagine was also invariable between genotypes and timepoints for LD and SD growth. Lysine was slightly decreased at 6 hours after dawn in *methfd1-1* under LD but unaffected under SD conditions. Threonine showed strong elevation in *methfd1-1* under LD and SD conditions, especially at timepoints during the dark periods. In *methfd1-1*, isoleucine was mainly increased at 12 hours after dawn under LD but not under SD conditions. Cysteine levels were increased in the double mutant *methfd1-1 x thfs* at 6 hours after dawn compared to the other genotypes while concentrations were equal between genotypes during SD growth. Interestingly, MTA was increased throughout the day in *methfd1-1* under LD and SD conditions (**Figure 20**). In *thfs* and *methfd1-1 x thfs*, MTA was decreased compared to wild type under LD conditions. In contrast,

under SD growth MTA levels were increased compared to wild type during the light period. These results illustrated that impaired metabolism in *methfd1-1* was not restricted to FOCM but extended to the biosynthesis of the aspartate family of amino acids as well as the methionine scavenging pathway. Strikingly, threonine and MTA levels were increased in *methfd1-1* under both conditions, LD and SD. Restoration of the one-carbon metabolome in *methfd1-1* under SD growth (**Figure 16**) highlights that the pathways of threonine *de novo* synthesis and methionine scavenging are apparently not required for phenotypic complementation in *methfd1-1* as they persisted defectively under SD growth.

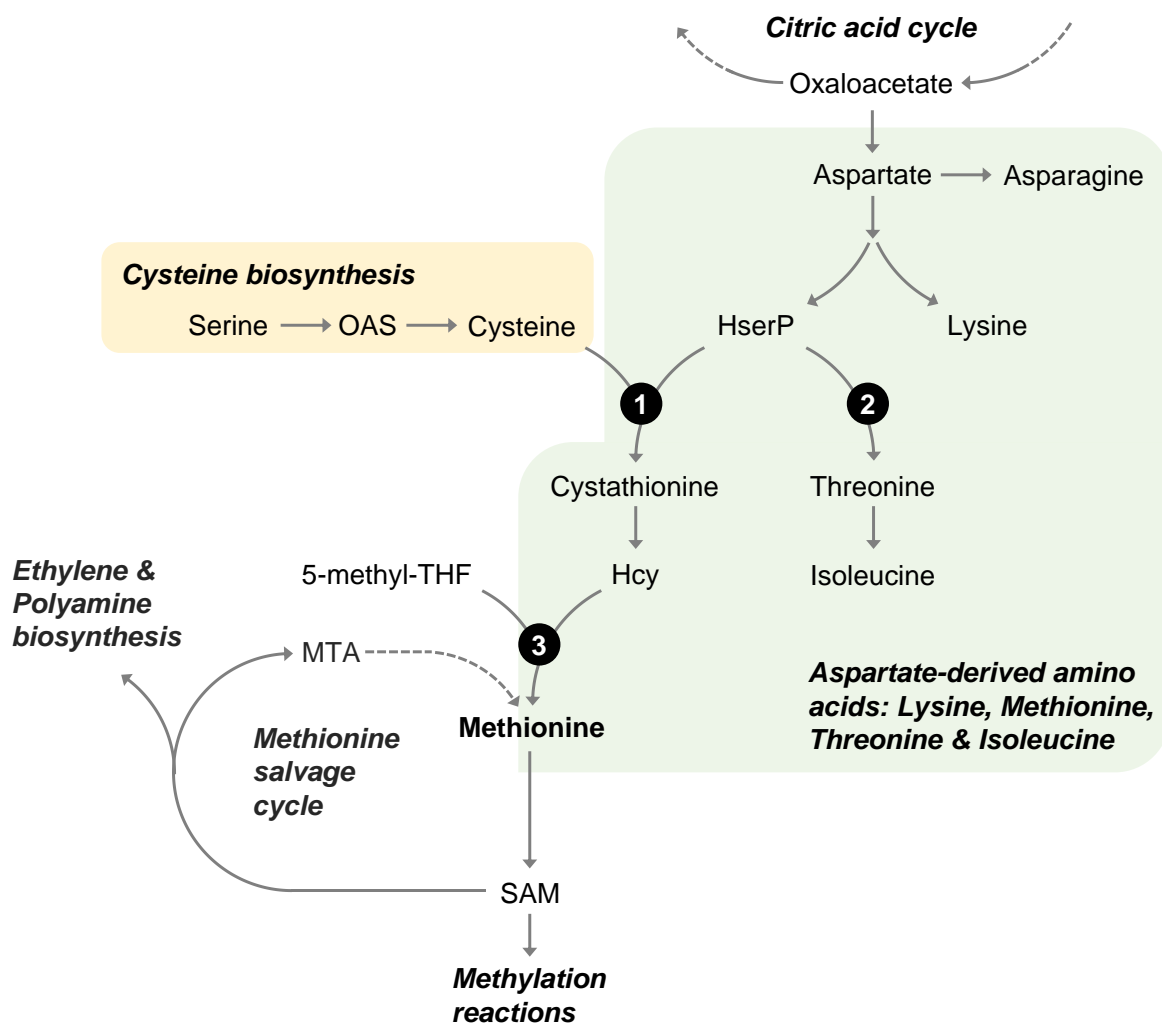


Figure 18. Metabolic pathways of methionine formation in *Arabidopsis*.

Methionine biosynthesis combines cysteine biosynthesis, the methionine salvage cycle and synthesis of the aspartate family of amino acid including asparagine, lysine, threonine, isoleucine among methionine. (1) CYSTATHIONINE γ -SYNTHASE (CGS), (2) THREONINE SYNTHASE (TS), (3) METHIONINE SYNTHASE (MS), OAS: O-acetylserine, HserP: O-phosphohomoserine, Hcy: homocysteine, MTA: 5-methylthioadenosine, SAM: S-adenosylmethionine.

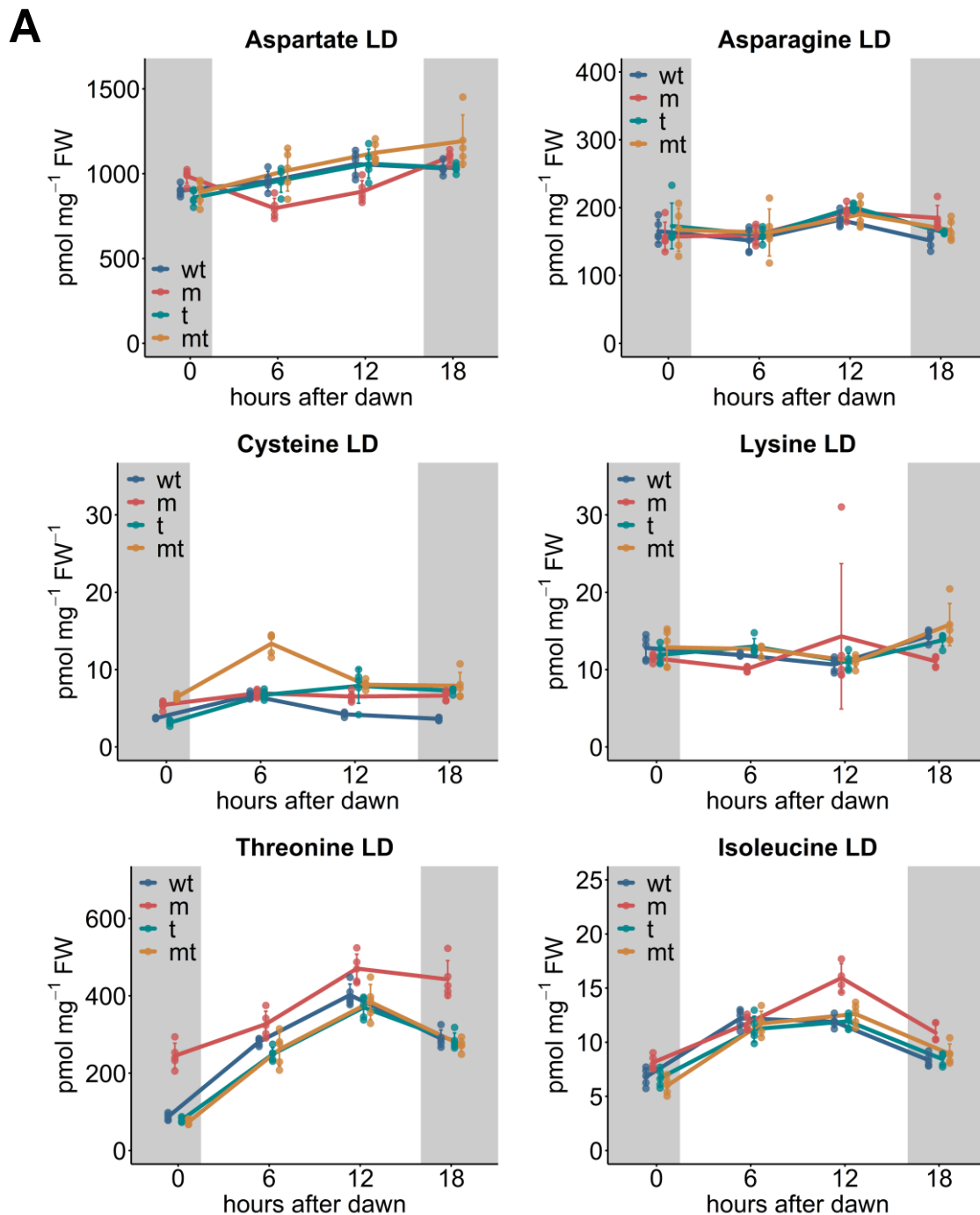


Figure 19. Methionine biosynthesis is impaired in *methfd1-1* under LD and SD conditions.

Steady-state levels of aspartate, asparagine, lysine, cysteine, threonine, and isoleucine in leaves of 3-week-old and 4-week-old wild type (wt), *methfd1-1* (m), *thfs* (t) and *methfd1-1* × *thfs* (mt) plants grown under LD (A) and SD (B) conditions, respectively. Plant material was harvested at 0, 6, 12 and 18 hours after dawn. Mean values ± s.d. ($n = 5$) are shown. Adjusted P values indicating statistical differences between genotypes at each timepoint (One-way ANOVA followed by post-hoc Tukey test, $P < 0.05$) can be found in **Supplementary Table 5** and **Supplementary Table 6**.

B

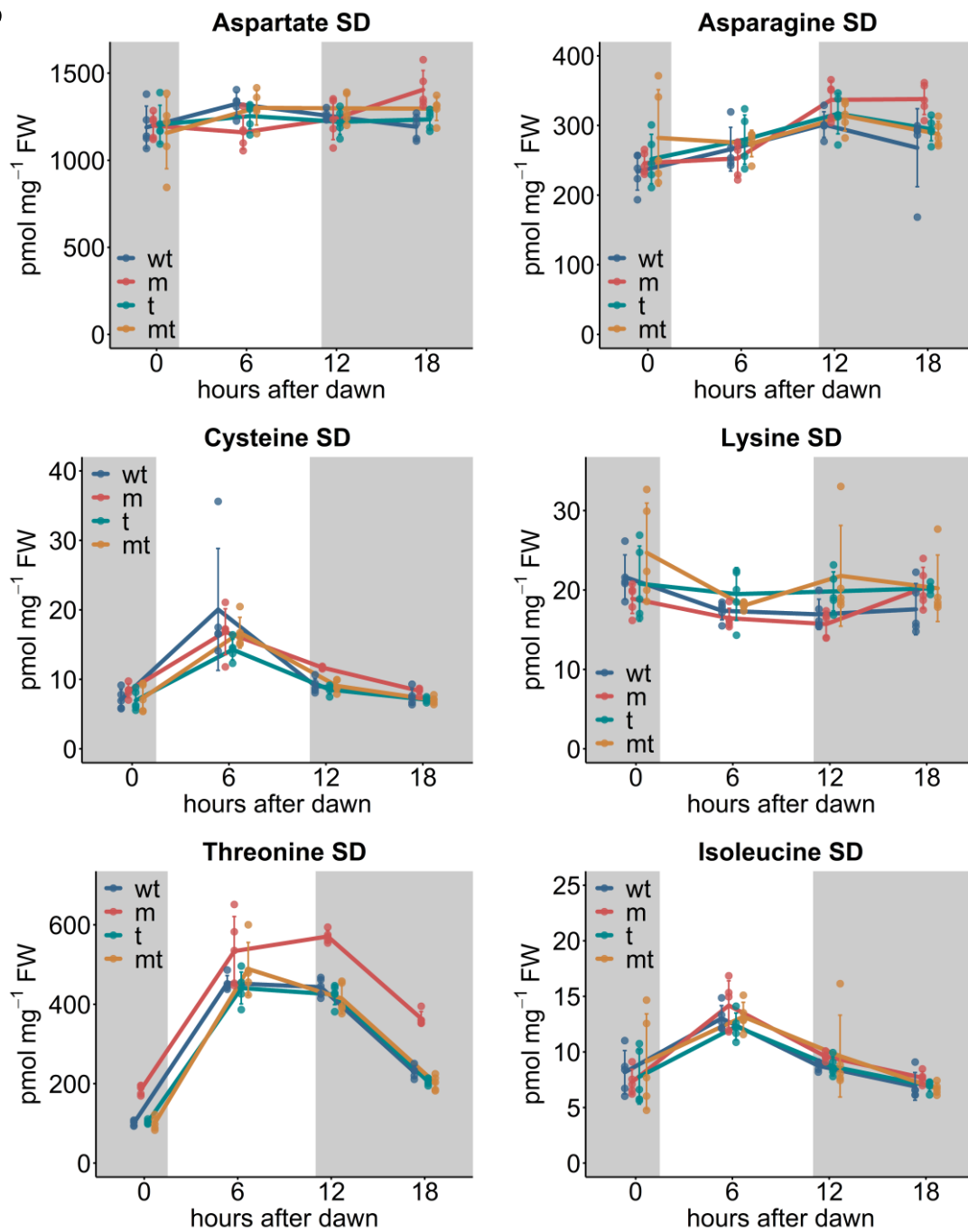


Figure 19. continued.

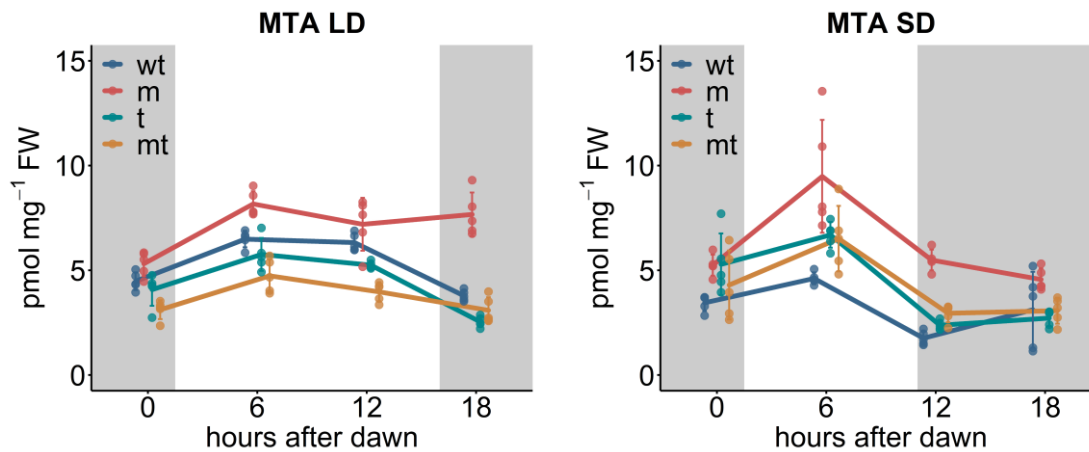


Figure 20. Methionine salvaging is impaired in *mthfd1-1* under LD and SD conditions.

Steady-state levels of MTA in leaves of 3-week-old and 4-week-old wild type (wt), *mthfd1-1* (m), *thfs* (t) and *mthfd1-1* × *thfs* (mt) plants grown under LD and SD conditions, respectively. Plant material was harvested at 0, 6, 12 and 18 hours after dawn. Mean values ± s.d. ($n = 5$) are shown. Adjusted P values indicating statistical differences between genotypes at each timepoint (One-way ANOVA followed by post-hoc Tukey test, $P < 0.05$) can be found in **Supplementary Table 5** and **Supplementary Table 6**.

2.2.6 Mutation of *MTHFD1* affects cellular amino acid biosynthesis under LD and SD conditions

Amino acid biosynthesis and catabolism are intimately linked to the central carbon metabolism (**Figure 21**). Carbon skeletons of amino acids are derived from intermediates of glycolysis and the Citric acid cycle and can be grouped according to their precursors: amino acids from the serine group cysteine and glycine, aromatic amino acids tryptophan, tyrosine and phenylalanine, amino acids from the pyruvate family alanine, leucine and valine, the glutamate family with arginine, glutamine, histidine and proline, as well as the aspartate family that was described above (**Figure 18** & **Figure 21**) (Trovato *et al*, 2021). To understand the extent of *mthfd1-1* and *thfs* mutations on the central carbon metabolism and the associated synthesis of other amino acids, steady-state levels of the residual amino acid groups were measured. Under LD growth, alanine and valine increased (**Supplementary Figure 4 A, C**), while concentrations of arginine decreased in *mthfd1-1* during the day (**Supplementary Figure 5 A**). Alanine and valine were restored to wild type level in *mthfd1-1* under SD conditions, while arginine was still reduced. Concentrations of leucine, glutamine and histidine were not affected under LD or SD growth (**Supplementary Figure 4** & **Supplementary Figure 5**). However, glutamate and proline from the glutamate family of amino acids showed altered concentrations in *mthfd1-1* under LD and SD growth (**Figure 22**). Glutamate is the substrate for glutamylation of folates which is important for folate stability, compartmentalization and efficacy for folate-dependent enzymes (Mehrshahi *et al*, 2010). As described previously, sequential conjugation

of glutamate residues to the *pABA* moiety of folates through γ -peptide linkage is catalyzed via FPGS (Mehrshahi *et al*, 2010). In *mthfd1-1* glutamate levels were reduced compared to the other genotypes during the light periods under LD and SD conditions (**Figure 22 A**). Interestingly, the glutamate level recovered after dusk in SD grown *mthfd1-1* plants but remained low under LD. Although glutamate levels were reduced in *mthfd1-1* in the light period under SD, this did not affect the cytosolic one-carbon metabolism or Hcy remethylation (**Figure 16**). Proline is generally considered to be a hallmark of stress responses in plants. When grown under harmful regimes, plants accumulate proline to mitigate and adapt to unfavorable conditions (Mattioli *et al*, 2009). In *mthfd1-1*, proline strongly increased during the day under LD and SD conditions (**Figure 22 B**). Even after dusk, during the dark period, proline concentrations remained elevated until the end of the night. Increased concentrations of proline under LD and SD further confirmed that the *mthfd1-1* phenotype was only partially restored and still exhibited signs of physiological stress.

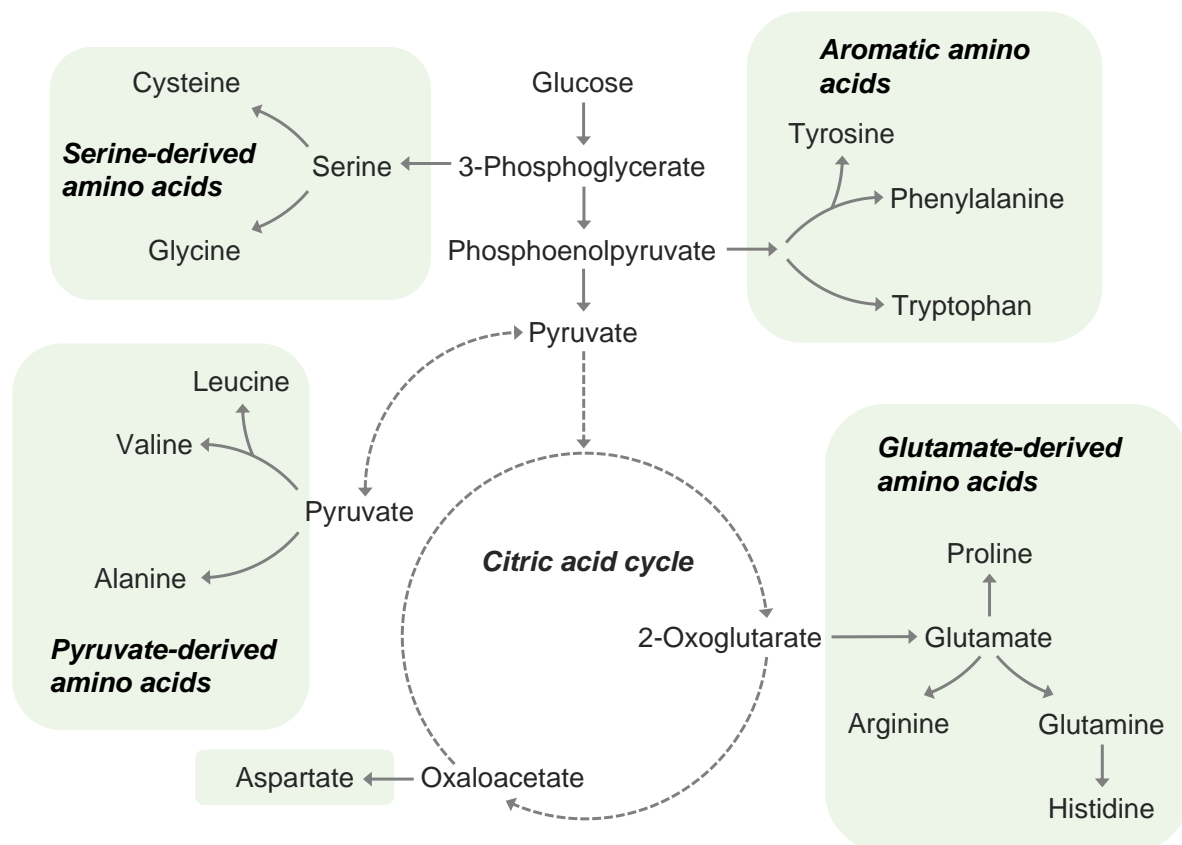


Figure 21. Amino acid biosynthesis in *Arabidopsis*.

Carbon skeletons of amino acids derive from 3-phosphoglycerate, phosphoenolpyruvate and pyruvate generated during glycolysis or from 2-oxoglutarate and oxalacetate formed in the Citric acid cycle. Adapted figure (Trovato *et al*, 2021).

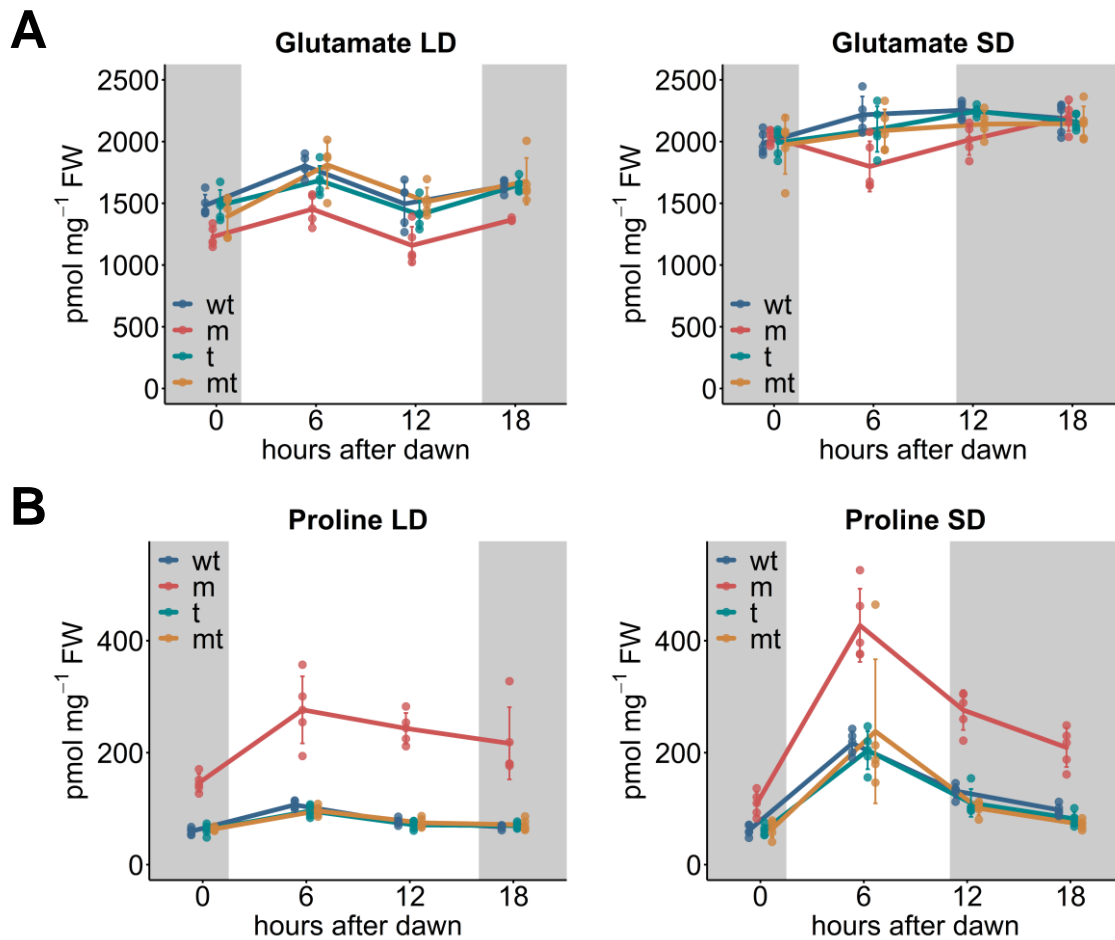


Figure 22. Glutamate and proline biosynthesis are partially impaired in *mthfd1-1*.

Steady-state levels of glutamate (A) and proline (B) in leaves of 3 and 4-week-old wild type (wt), *mthfd1-1* (m), *thfs* (t) and *mthfd1-1* × *thfs* (mt) plants grown under LD and SD conditions, respectively. Plant material was harvested at 0, 6, 12 and 18 hours after dawn. Mean values ± s.d. ($n = 5$) are shown. Adjusted P values indicating statistical differences between genotypes at each timepoint (One-way ANOVA followed by post-hoc Tukey test, $P < 0.05$) can be found in **Supplementary Table 7**.

2.2.7 Energy metabolism is not affected in *mthfd1-1*

As photoautotrophic organisms, plants can convert light into chemical energy and thereby produce organic compounds. Since this process is environment-dependent, precise spatio-temporal regulation is crucial for metabolic build-up and its allocation to fuel cellular activities (Cervela-Cardona *et al*, 2021). Adenosine triphosphate (ATP) is a common cofactor that provides energy for enzymatic reactions such as THFS-catalyzed formation of 10-formyl-THF from THF and formate, glutamylation of folates via FPGS as well as SAMS mediated formation of SAM from methionine and ATP. Formation of ATP in mitochondria by oxidative phosphorylation depends on reducing equivalents such as nicotinamide adenine dinucleotide

(NADH) which is generated in the Citric acid cycle (Fernie *et al*, 2004; Braun, 2020). Interestingly, NADH showed reduced levels in *methfd1-1 x thfs* compared to the other genotypes under LD conditions (**Figure 23 A**). Under SD growth, NADH levels were increased in *methfd1-1* throughout the day compared to lower levels in wild type, intermediate levels in *methfd1-1 x thfs* and high levels in *thfs* that were gradually decreasing during the course of the day (**Figure 23 B**). However, these diurnal fluctuations of NADH did not affect ATP levels between genotypes under LD and SD conditions except for a slight increase of ATP in *methfd1-1 x thfs* under LD growth (**Figure 23 A, B**). ATP concentrations showed a daytime-dependent pattern with increasing levels after dawn that decreased after dusk during the dark period. Additionally, uniform concentrations of ATP among genotypes indicated that purine *de novo* synthesis was mostly unaffected in wild type and the mutants *methfd1-1*, *thfs* and *methfd1-1 x thfs*.

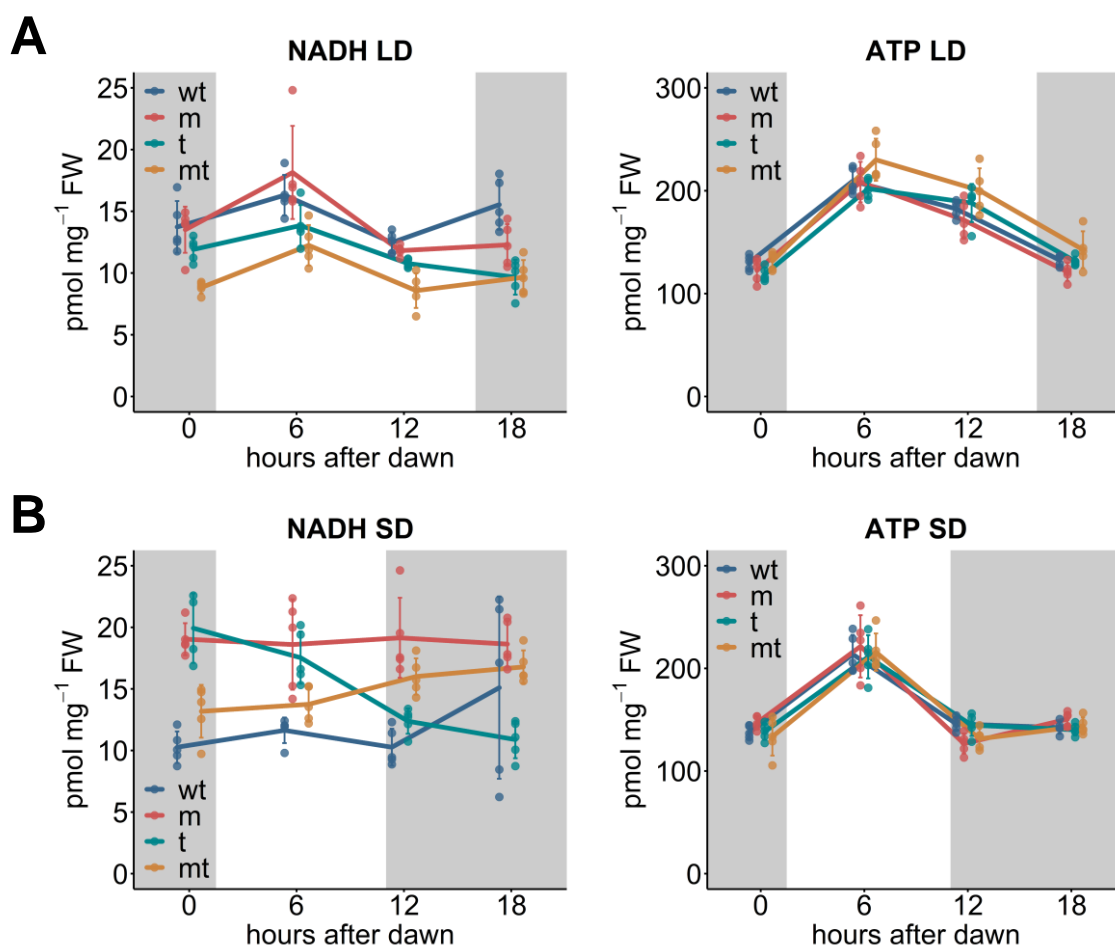


Figure 23. ATP formation is not impaired in *methfd1-1*.

Steady-state levels of NADH and ATP in leaves of 3-week-old LD (A) and 4-week-old SD grown (B) wild type (wt), *methfd1-1* (m), *thfs* (t) and *methfd1-1 x thfs* (mt) plants harvested at 0, 6, 12 and 18 hours after dawn. Mean values \pm s.d. ($n = 5$) are shown. Adjusted P values indicating statistical differences between

genotypes at each timepoint (One-way ANOVA followed by post-hoc Tukey test, $P < 0.05$) can be found in **Supplementary Table 8**.

2.2.8 The glutathione redox balance is not affected in *methfd1-1*

It has been proposed that MTHFD1-mediated formation of NADPH through its dehydrogenase activity could potentially contribute to the maintenance of redox balance in plants (Gorelova *et al*, 2017b; Farquharson, 2017). Mutation of the dehydrogenase activity of MTHFD1 in *methfd1-1* might therefore reduce NADPH levels resulting in redox imbalance. Mammalian studies highlighted that depletion of cytosolic or mitochondrial MTHFD activity led to decreased cellular ratios of NADPH/NADP⁺, reduced and oxidized glutathione (GSH/GSSG) as well as increased sensitivity to oxidative stress (Fan *et al*, 2014). GSSG regeneration to reduced GSH is NADPH-dependent and crucial for the glutathione-ascorbate cycle (Dorion *et al*, 2021). This cycle detoxifies hydrogen peroxide (H₂O₂), the most stable reactive oxygen species (ROS), a process which transiently changes the glutathione redox balance (E_{GSH}), a metric of oxidative stress (Meyer, 2008; Ugalde *et al*, 2020). Indeed, NADPH levels were reduced in *methfd1-1* compared to wild type, *thfs* and *methfd1-1 x thfs* under LD but not under SD conditions (**Figure 24 A, B**). Nevertheless, reduced glutathione (GSH) was not decreased in *methfd1-1* under LD conditions (**Figure 24 A**). Astonishingly, GSH concentrations were even increased in the mutant genotypes compared to wild type at 12 and 18 hours after dawn under LD but showed almost no differences under SD conditions (**Figure 24 A, B**). Especially the double mutant *methfd1-1 x thfs* showed increased levels of NADPH and GSH compared to wild type and *methfd1-1*. Since the double mutant harbors the same mutation of *MTHFD1* as the single mutant *methfd1-1*, reduction of NADPH was most likely not caused by impaired dehydrogenase activity of MTHFD1. This notion was confirmed by uniform NADPH levels between genotypes under SD conditions (**Figure 24 B**). Furthermore, reduction of NADPH in *methfd1-1* did not affect the GSH pool under LD growth. *In vivo* monitoring of cellular redox changes in wild type and *methfd1-1* was performed utilizing the redox-sensitive reporter GRX1-roGFP2 to confirm proper redox homeostasis in *methfd1-1* (Meyer *et al*, 2007; Ugalde *et al*, 2020). roGFP equilibrates with the E_{GSH} through GLUTAREDOXIN (GRX) which acts as a thiol-disulfide switch. This leads to roGFP excitation peaks at 410 nm and 480 nm depending on the redox state – the 410/480 nm ratio is therefore a powerful measure for changes in the redox balance (Ugalde *et al*, 2020). Although concentrations of GSH were increased in *methfd1-1*, no significant differences in the E_{GSH} were detected between wild type and *methfd1-1*, demonstrating that neither the redox state nor ROS scavenging were impaired in *methfd1-1* (**Figure 24 C, D**). Consistent with these

findings, no significant differences in the 410/480 nm ratio were detected between wild type and *mthfd1-1* upon addition of either 100 mM H₂O₂ (for complete oxidation of roGFP) or 20 mM dithiothreitol (DTT; for full reduction of roGFP) (**Figure 24 D**). These results could show that *MTHFD1* did not contribute substantially to the redox balance and that reduced levels of NADPH under LD conditions were likely caused by other processes.

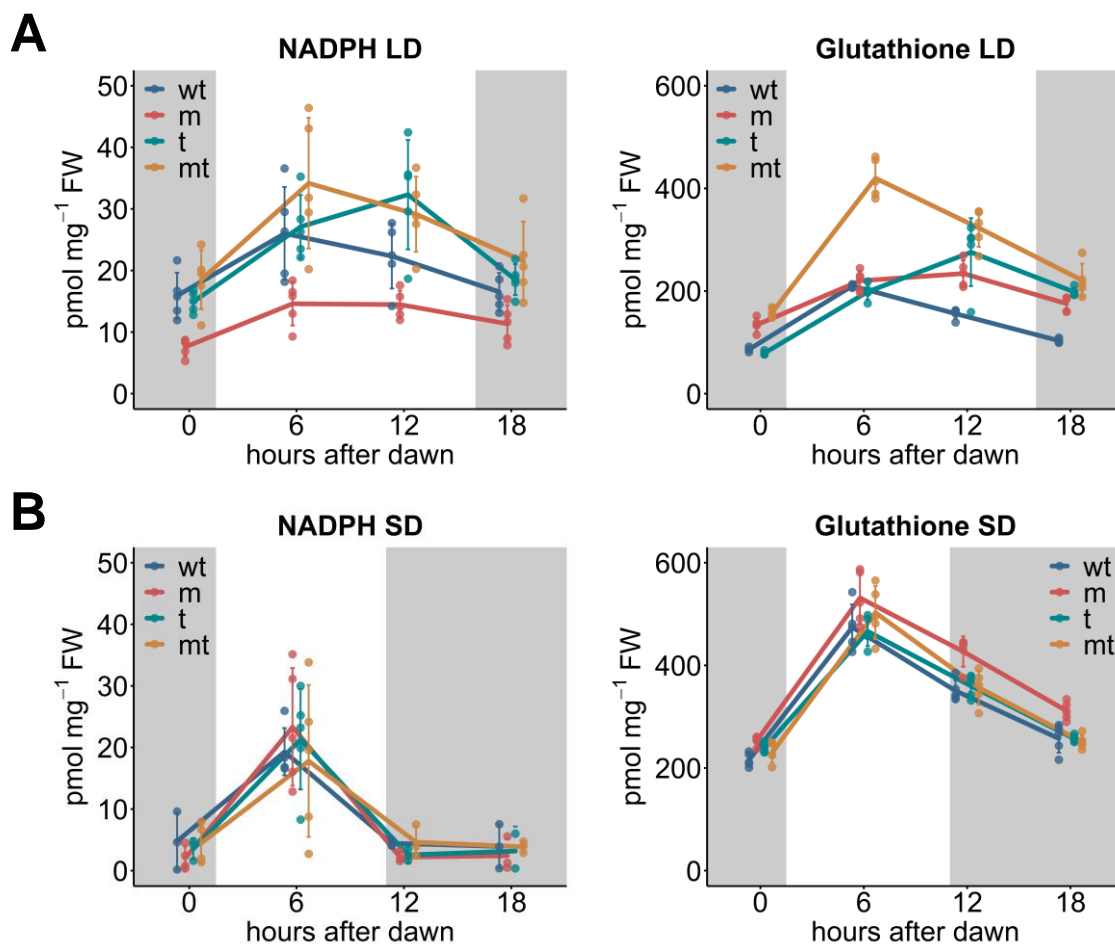


Figure 24. Reduction of NADPH does not impair the glutathione redox balance in *mthfd1-1*.

Steady-state levels of NADPH and reduced Glutathione in leaves of 3-week-old LD (A) and 4-week-old SD grown (B) wild type (wt), *mthfd1-1* (m), *thfs* (t) and *mthfd1-1* x *thfs* (mt) plants harvested at 0, 6, 12 and 18 hours after dawn. Mean values \pm s.d. ($n = 5$) are shown. Adjusted P values indicating statistical differences between genotypes at each timepoint (One-way ANOVA followed by post-hoc Tukey test, $P < 0.05$) can be found in **Supplementary Table 8**. (C) & (D) Redox-sensitive roGFP (GRX1-roGFP2) measurement of the glutathione redox balance (E_{GSH}) in 7-day-old wild type and *mthfd1-1* seedlings grown under LD conditions. (C) Normalized fluorescence of the 410/480 nm ratio measured for 4 hours before addition of 100 mM H₂O₂ and 20 mM DTT to fully oxidize and reduce the sensor, respectively. (D) Comparison of mean values of fully oxidized (H₂O₂) and reduced (DTT) measurements with imaging buffer as control. Mean values \pm s.d. ($n = 12$) are shown. No statistical differences between genotypes and treatments (H₂O₂ and DTT) were determined (Student's t -test, $P < 0.05$).

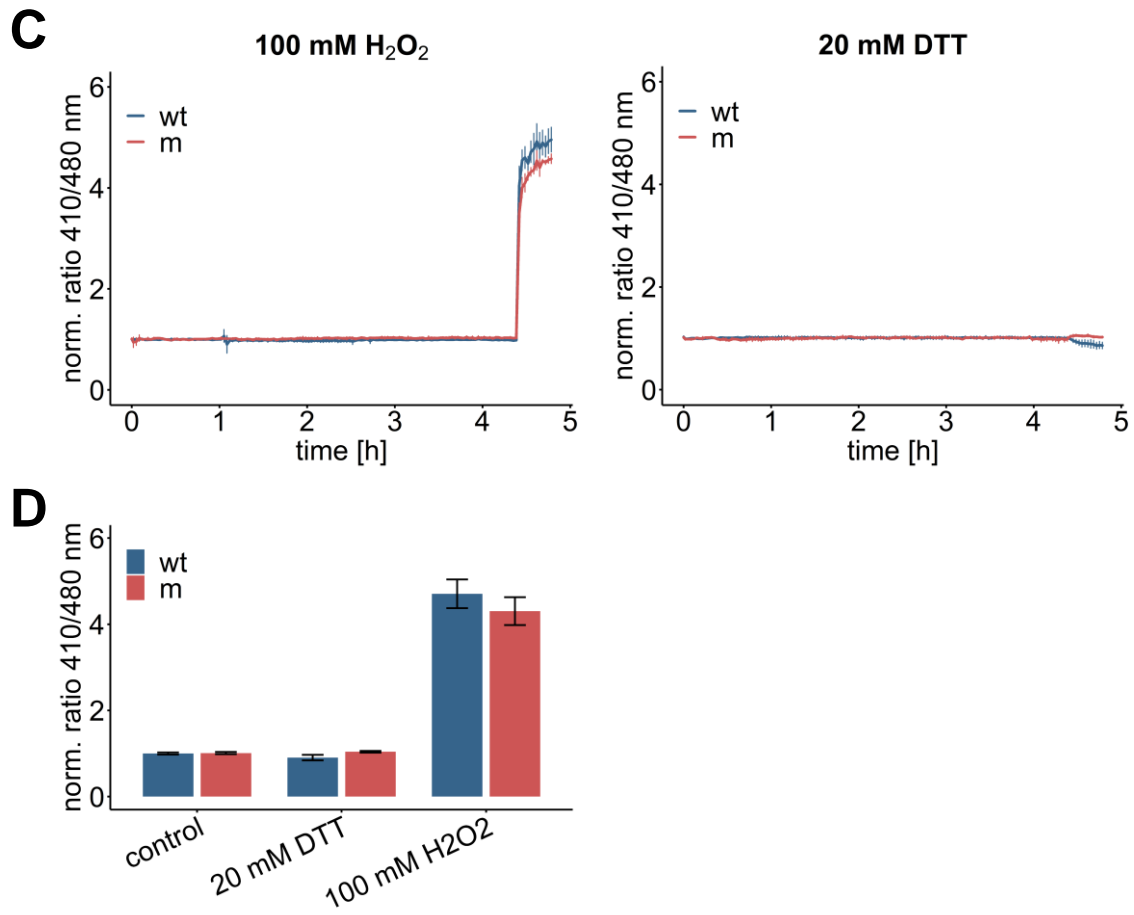


Figure 24. continued.

2.2.9 Enzymes of the cytosolic folate metabolism regulate one-carbon dynamics

This study strongly benefited from a wealth of studies that investigated the activities of MTHFD and SHMT isoforms throughout cellular compartments. As mentioned before, MTHFD catalyzed dehydrogenase and cyclohydrolase activities are found in the cytosol, nucleus, and organelles and together with SHMT they are responsible for the interconversion of the different one-carbon substituted folate species. While MTHFD activity is equally distributed in all compartments, SHMT shows ten- and twentyfold higher activities in mitochondria compared to plastids and the cytosol, respectively (Neuburger *et al*, 1996). The predominant localization of SHMT activity in mitochondria is linked to its function in photorespiration (Bauwe *et al*, 2010). Together with MTHFR and THFS, the cytosolic isoforms MTHFD1 and SHM4 are part of sequential one-carbon transfer reactions that lead to the formation of 5-methyl-THF, the substrate and prerequisite for Hcy remethylation. In the cytosol, serine and formate can serve

as sources for one-carbon for the biosynthesis of various folate species, especially 5,10-methylene-THF, a central hub for thymidylate, purine and 5-methyl-THF synthesis. To assess if 5-formyl-THF has a rate-limiting effect on one-carbon units through the FOCM (Goyer *et al*, 2005) that are independent of impaired Hcy remethylation, enzyme activities of these folate metabolic enzymes were measured. In order to preserve the cellular metabolome along the proteome in these activity measurements, and to include any effects of allosteric inhibition of enzyme activities through metabolic intermediates, a simple detergent-free extraction method was chosen to isolate soluble, cellular proteins. Two controls were used to determine and verify the cellular, soluble proteome in plant extracts. Activity of the mitochondrial marker enzyme SUCCINYL COA SYNTHETASE (SCS) was measured in samples extracted with the detergent-free extraction buffer from the experiments compared to samples isolated with an extraction buffer supplemented with a detergent. Extracts from both isolation methods displayed SCS activity, with higher levels in extracts isolated with the detergent, indicating that cytosolic and mitochondrial proteins were present in the extraction buffer from the enzyme activity measurements (**Supplementary Figure 6 A**). However, predominantly soluble proteins and not membrane proteins were isolated, as samples from detergent-free extraction did not show chlorophyll content (**Supplementary Figure 6 B**). Detergent-free isolation retained intact membranes and therefore integral proteins while organelles were disrupted releasing soluble proteins from mitochondria and chloroplasts (**Supplementary Figure 6 B**). Additionally, through this approach it should be tested, if activity of SHMT was able to complement the formate-dependent pathway which was impaired in *methfd1-1*, *thfs* and *methfd1-1 x thfs*.

2.2.10 MTHFD1 and THFS activities are reduced in their mutant backgrounds

First, activities of MTHFD1 and THFS were analyzed (**Figure 25 A, B**). Both enzymes showed reduced activities in their respective mutant backgrounds throughout the day (**Figure 25 A, B** left plots) and reduction of total daily activity (**Figure 25 A, B** right plots). These reduced activities are consistent with mutations in the genomic regions of *MTHFD1* and *THFS* and highlighted three things: first, mutation of *MTHFD1*, specifically the EMS-induced mutation of the NADPH /NADP⁺ binding motif which is needed for the dehydrogenase activity, led to strong induction of *methfd1-1* phenotype-associated metabolic deregulation. Second, other isoforms still contributed to total MTHFD activity, although their activities were not sufficient to complement *methfd1-1* and underlined the importance of cytosolic MTHFD1. Third, mutation of *THFS* led to reduced THFS activity which did not induce a similar phenotype as observed in *methfd1-1* although both enzymes are part of the same metabolic pathway.

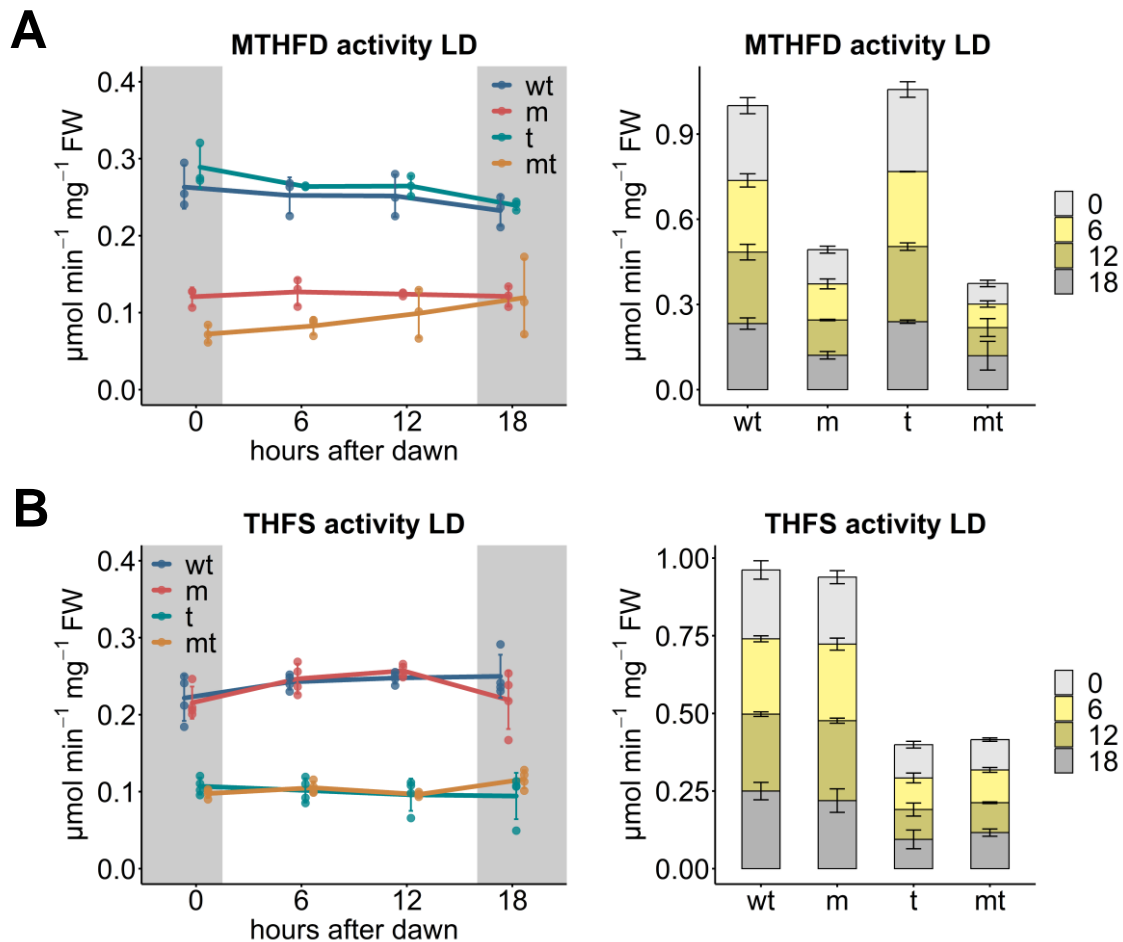


Figure 25. Mutation of *MTHFD1* and *THFS* lead to reduced enzyme activities.

MTHFD (A) and THFS (B) activities in 3-week-old rosettes of wild type (wt), *mthfd1-1* (m), *thfs* (t) and *mthfd1-1* × *thfs* (mt) plants grown under LD conditions and harvested at 0, 6, 12 and 18 hours after dawn. Plots on the left represent diurnal activities, plots on the right represent the total daily enzyme activities. Mean values ± s.d. for MTHFD ($n = 3$) and THFS ($n = 4$) are shown. Adjusted P values indicating statistical differences between genotypes at each timepoint (One-way ANOVA followed by post-hoc Tukey test, $P < 0.05$) can be found in **Supplementary Table 9**.

2.2.11 Cellular activity of SHMT is not reduced in *mthfd1-1* but slightly increased in the *thfs* mutant background

The combined activities of cellular SHMT isoforms from all compartments (SHM1, SHM2, SHM3 and SHM4, respectively) were measured throughout the daily light-dark cycle. If an increase in cellular 5-formyl-THF indeed influences SHMT activity, this approach would lead to reduced activity in *mthfd1-1* which showed a strong increase of 5-formyl-THF (**Figure 15**). Interestingly, there were no significant differences between genotypes and timepoints (**Figure 26 A**). Solely total SHMT activities in the *thfs* and *mthfd1-1* × *thfs* mutant plants were slightly higher compared to wild type and *mthfd1-1* (**Figure 26 A** right plot). Finally, the activity of

MTHFR, which provides 5-methyl-THF for Hcy remethylation was measured (**Figure 26 B**). Again, no significant differences could be observed between genotypes and timepoints, which was in line with mostly uniform concentrations of 5-methyl-THF between genotypes throughout the day under LD conditions (**Figure 15 B**).

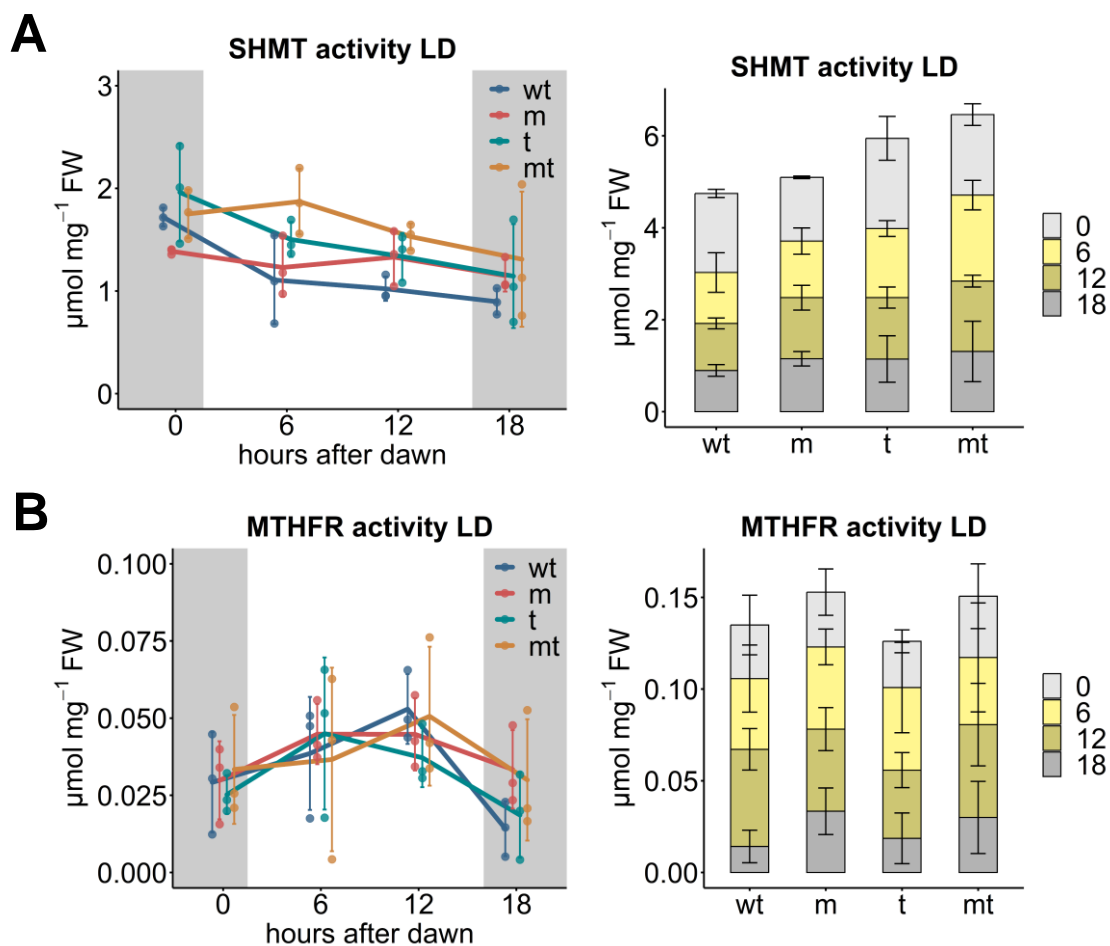


Figure 26. SHMT activity is elevated in *thfs* and *methfd1-1 x thfs*.

SHMT (A) and MTHFR (B) activities in 3-week-old rosettes of wild type (wt), *methfd1-1* (m), *thfs* (t) and *methfd1-1 x thfs* (mt) plants grown under LD conditions and harvested at 0, 6, 12 and 18 hours after dawn. 5,10-methylene-THF, the product of SHMT enzyme activity was chemically converted to 5-methyl-THF with NaBH₄ and measured using LC-MS (A). Synthesized 5-methyl-THF, the product of MTHFR was directly measured without the chemical conversion (B). Mean values ± s.d. (*n* = 3) are shown. Adjusted *P* values indicating statistical differences between genotypes at each timepoint (One-way ANOVA followed by post-hoc Tukey test, *P* < 0.05) can be found in **Supplementary Table 9**.

2.2.12 SHMT activity is reduced under SD and probably less affected by 5-formyl-THF than anticipated

The results obtained from SHMT activity measurements under LD growth were unforeseen. To get a richer picture, cellular SHMT activity was also measured in SD grown plants to ensure that the *methfd1-1* phenotype was not simply complemented by increased SHMT activity which could complement the formate-dependent pathway. However, this was not the case: the activities between all genotypes were uniform at 0 and 6 hours after dawn at the transition between the dark and light periods (**Figure 27 A**). Surprisingly, under SD growth SHMT enzyme activity was generally reduced compared to LD. For instance, under LD, mean activities were up to threefold increased in all mutant genotypes and the wild type compared to their SD grown counterparts at timepoints 0 and 6 hours after dawn.

To measure the influence of 5-formyl-THF on SHMT activity of LD grown plants, the protocol was adapted: extracts with cellular proteins were desalted before the enzyme reaction was started to exclude low molecular weight cofactors and substrates that could affect enzymatic performance. This guaranteed that only defined concentrations of the substrates serine and THF as well as the cofactor pyridoxal-5-phosphate (PLP) and different concentrations of the potential inhibitor 5-formyl-THF were present in the reaction buffer. Interestingly, increasing concentrations of 5-formyl-THF led to increased SHMT activity in all genotypes (**Figure 27 B**). Even more remarkable was the fact that the activity of SHMT in *thfs* and *methfd1-1 x thfs* was elevated compared to wild type and *methfd1-1* - similar to the daily total activities of non-desalted extracts before (**Figure 26 A** right plot). The enzyme activity measurements of SHMT were based on the chemical conversion of 5,10-methylene-THF, the product of SHMT enzyme activity to 5-methyl-THF using sodium borohydride (NaBH₄). 5-methyl-THF was then measured via LC-MS and compared to calibration curves of 5-methyl-THF (**Supplementary Figure 7 A, C**). To exclude the possibility that 5-formyl-THF was converted to 5-methyl-THF via NaBH₄, standards of 5-formyl-THF were treated with NaBH₄ and compared to untreated standards of the same concentration (**Supplementary Figure 7 B, D**). However, no differences were detected between treated and untreated standards, which meant that only the product from the SHMT-catalyzed reaction was measured (**Supplementary Figure 7 B, D**).

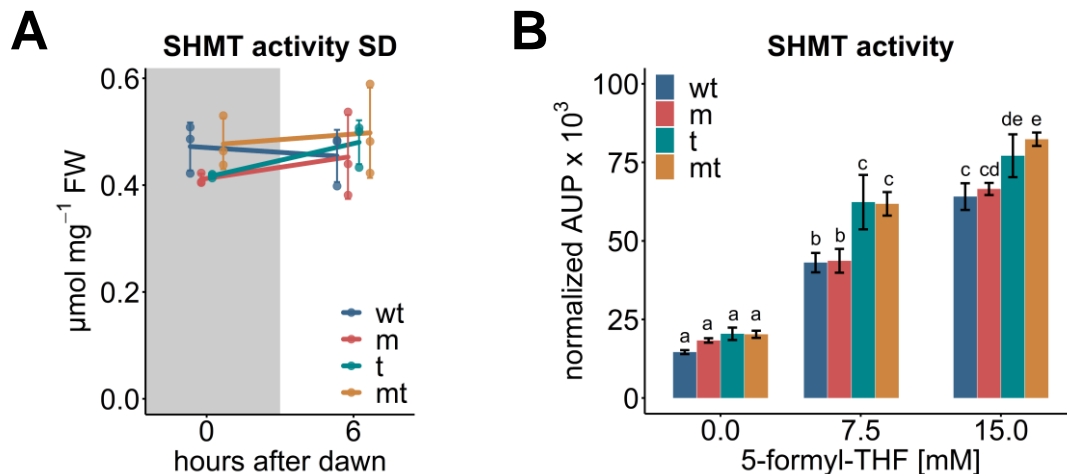


Figure 27. SHMT activity is reduced under SD conditions but increased by addition of 5-formyl-THF.

(A) SHMT activity in 4-week-old rosettes of wild type (wt), *mthfd1-1* (m), *thfs* (t) and *mthfd1-1* \times *thfs* (mt) plants grown under SD conditions and harvested at 0 and 6 hours after dawn. Mean values \pm s.d. ($n = 3$) are shown. Adjusted P values indicating statistical differences between genotypes at each timepoint (One-way ANOVA followed by post-hoc Tukey test, $P < 0.05$) can be found in **Supplementary Table 9**. (B) Desalted enzyme extracts were incubated with reaction buffers supplemented with 0, 7.5 or 15 mM 5-formyl-THF. Formation of 5-methyl-THF is indicated as normalized area under the peak (AUP). Mean values \pm s.d. ($n = 3$) are shown. Lowercase letters represent statistical differences between genotypes and supplements (Two-way ANOVA followed by post-hoc Tukey test, $P < 0.05$).

2.3 Tracing the routes of one-carbon using stable isotope labeling

Previous studies as well as this study used *in vitro* enzyme activity measurements for enzymes that catalyze the conversion of folates. These activities strongly depend on substrate concentrations, pH and other factors that are difficult to simulate *in vitro*. Also, steady-state concentrations of metabolites and intermediates of the FOCM and AMC are insufficient to illustrate pathway activity. Metabolite build-up is not only defined by production but also by consumption which emphasizes the need to understand the metabolite fluxes of a certain network (Jang *et al*, 2018). Stable isotope labeling with [α - ^{13}C] glycine and [^{13}C] formate was used as an approximation of *in vivo* one-carbon dynamics. This was achieved by analyzing label enrichment in various target compounds that depend on folate-mediated one-carbon for their biosynthesis. These targets included nucleobases adenine, thymine and 5-methylcytosine as well as the free amino acids glycine, methionine, and serine (**Figure 28 A**). Plants were grown in liquid cultures supplemented with labeled substrates in two setups: long-term label enrichment in nucleobases and short-term labeling of amino acids. These setups were replicated with non-labeled substrates to correct for naturally occurring isotopes. Long-

Results

term labeling for 1 week was used for analyses and comparison of label enrichment in the nucleotide synthesis pathways of adenine and thymine and methylation reactions of cytosine to 5-methylcytosine (**Figure 28 A**). Using this approach, the flow of one-carbon across the folate cycle and its pathway-dependent destination were determined under SD and LD conditions.

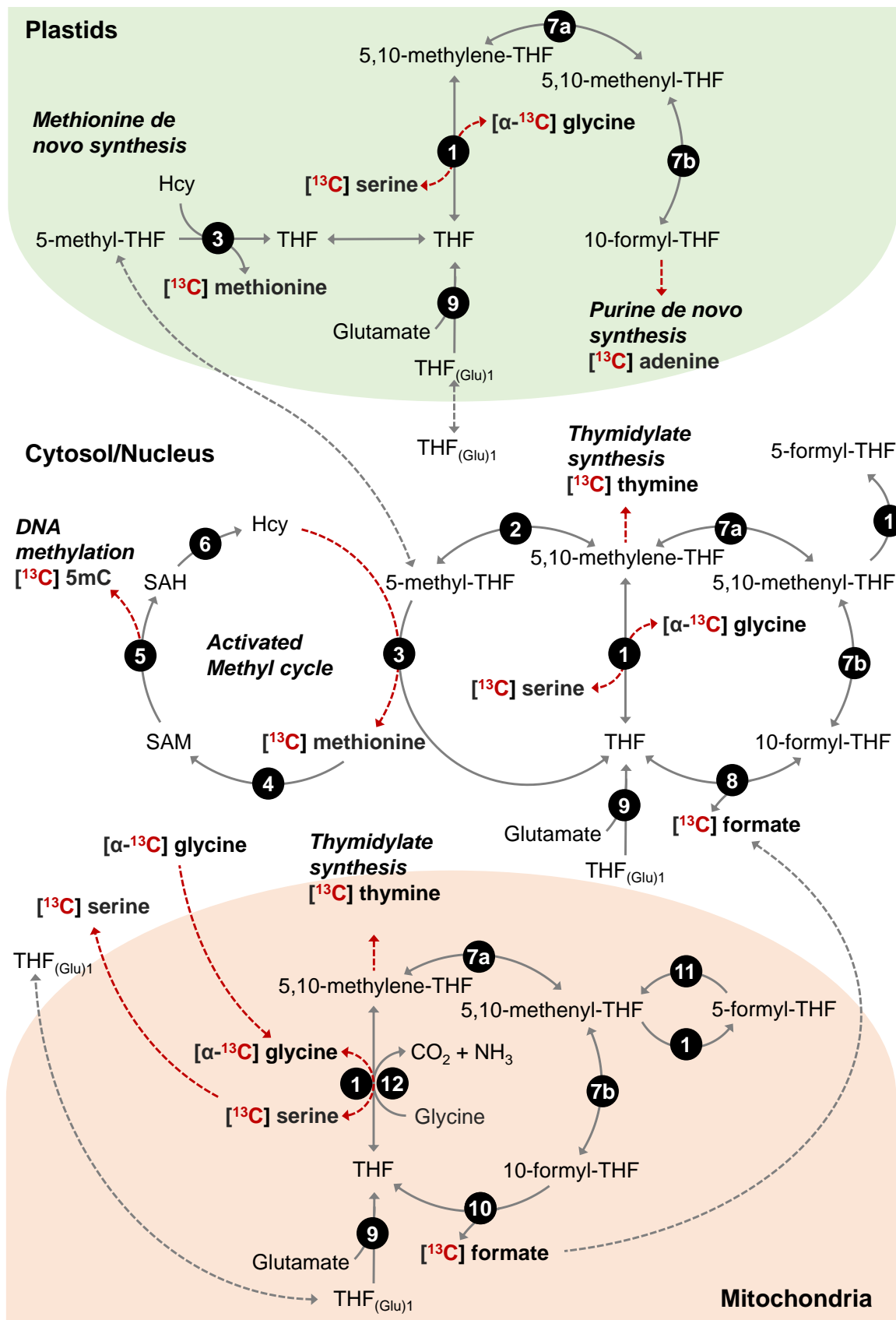
Short-term labeling in free amino acids was used to cover the diurnal flow of one-carbon through the interconversion of free amino acids glycine, methionine, and serine that are closely connected in FOCM. Glycine and serine are both substrates for catalytically active SHMTs with serine serving as one-carbon source for folate metabolism. Additionally, glycine that is produced during photorespiration is processed by GDC to 5,10-methylene-THF and incorporated into the folate pool in mitochondria. Interestingly, the formation of serine from glycine and formate via the 5,10-methylene-THF folate pool can lead to several isotopologues of serine, that share the same chemical formula and bonding arrangement but differ in their isotopic composition (**Figure 28 B**). Potentially, ^{13}C -enriched serine can be found as $[\alpha\text{-}^{13}\text{C}]$ serine, $[\beta\text{-}^{13}\text{C}]$ serine or $[\alpha\text{-}\beta\text{-}^{13}\text{C}]$ serine (**Figure 28 B**). However, using TD-GC-MS only serine with one or two ^{13}C atoms could be differentiated. This was not a problem as the exact positions and biochemical reactions that result in serine enriched with one ^{13}C ($[\alpha\text{-}^{13}\text{C}]$ serine, $[\beta\text{-}^{13}\text{C}]$ serine) or two ^{13}C ($[\alpha\text{-}\beta\text{-}^{13}\text{C}]$ serine) are well characterized (**Figure 28 B**) (Prabhu *et al*, 1996; Prabhu *et al*, 1998). Methionine was used as a measure of diurnal one-carbon flow towards the activated methyl cycle.

For short-term labeling, the addition of labeled substrates to plants was aligned to the start of the light or dark period (**Figure 28 C**). Thereafter, plant material was harvested after 4, 8, 16 and 24 hours after dawn or dusk, depending on when the substrates were added (**Figure 28 C**). Long-term labeled samples were harvested after 2 weeks of total growth at midday, 6 hours after dawn. After separation of free amino acids (**Supplementary Figure 8**) and nucleobases (**Supplementary Figure 9**) using gas chromatography, label enrichment was calculated from Selected Ion Monitoring (SIM) acquired mass spectra (**Supplementary Figure 10 & Supplementary Figure 11**). For instance, selected ions of serine had mass-to-charge ratios (m/z) of 390, 391, 392 and 393 (**Supplementary Figure 10 C**). A m/z of 390 corresponded to serine without any isotopic enrichment – neither naturally occurring nor derived from labeled substrates – and is therefore from here on denoted as M+0. A m/z of 391 indicates an increase in the mass of +1 due to a naturally occurring isotope or $[\alpha\text{-}^{13}\text{C}]$ glycine or $[\text{}^{13}\text{C}]$ formate-derived ^{13}C , hence denoted as M+1. In a similar manner, a m/z of 392 and 393 are denoted as M+2 and M+3, respectively. Fractions M+0, M+1, M+2 and M+3 encompassed the total abundance

Results

of a target compound. For further calculations, M+3 fractions were omitted since [α - ^{13}C] glycine or [^{13}C] formate-derived ^{13}C could only be enriched at two positions in serine, thus maximally M+2 (**Figure 28 B**). After correction for naturally occurring isotopes by subtraction of fractions obtained from samples supplied with non-labeled substrates, fractions were calculated as percentages of the total abundance of a target compound: $M+0 = M+0 / (M+0 + M+1 + M+2)$, $M+1 = M+1 / (M+0 + M+1 + M+2)$ and $M+2 = M+2 / (M+0 + M+1 + M+2)$.

A



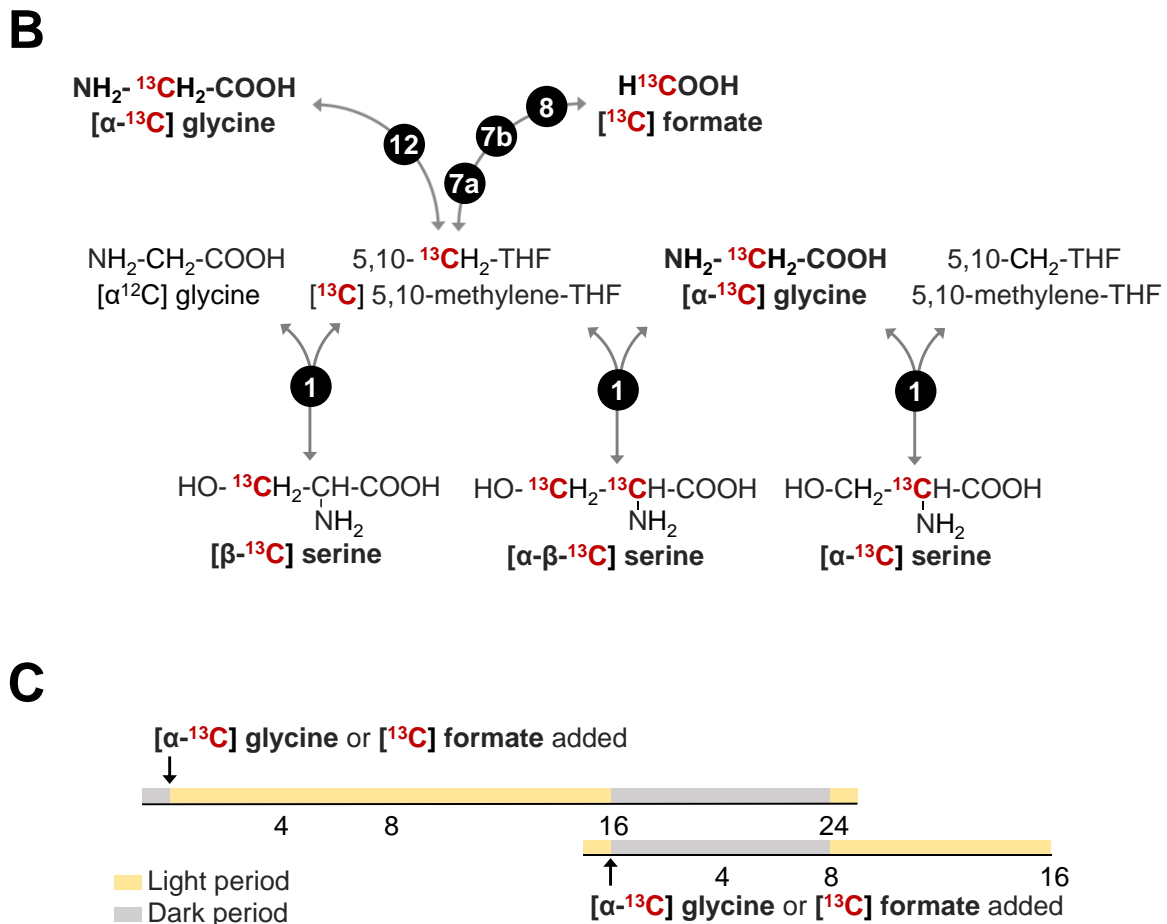


Figure 28. Reconstructing the route of one-carbon via isotope labeling.

(A) Possible routes and targets of $[\alpha\text{-}^{13}\text{C}]$ glycine and $[\text{}^{13}\text{C}]$ formate-derived ^{13}C . (B) Formation and conversion of $[\alpha\text{-}^{13}\text{C}]$ serine, $[\beta\text{-}^{13}\text{C}]$ serine and $[\alpha\text{-}\beta\text{-}^{13}\text{C}]$ serine. (C) Addition of labeling substrates $[\alpha\text{-}^{13}\text{C}]$ glycine and $[\text{}^{13}\text{C}]$ formate at the start of the day or night for short term labeling of amino acids. (1) SERINE HYDROXYMETHYLTRANSFERASE (SHMT), (2) METHYLENETETRAHYDROFOLATE REDUCTASE (MTHFR), (3) METHIONINE SYNTHASE (MS), (4) S-ADENOSYLMETHIONINE SYNTHETASE (SAMS), (5) methyltransferases including DNA and histone methyltransferases, (6) S-ADENOSYLMETHIONINE HYDROLASE (SAHH), (7a) METHYLENETETRAHYDROFOLATE DEHYDROGENASE & (7b) METHENYLTETRAHYDROFOLATE CYCLOHYDROLASE (MTHFD), (8) 10-FORMYLTETRAHYDROFOLATE SYNTHETASE (THFS), (9) FOLYLPOLYGLUTAMATE SYNTHETASE (FPGS), (10) 10-FORMYLTETRAHYDROFOLATE DEFORMYLASE (10-FDF), (11) 5-FORMYLTETRAHYDROFOLATE CYCLOLIGASE (5-FCL), (12) GLYCINE DECARBOXYLASE COMPLEX (GDC), THF and THF_(Glu)1 are abbreviations for poly- and monoglutamylated tetrahydrofolate, respectively. Adapted figure (Prabhu *et al*, 1996; Gorelova *et al*, 2017a; Lindermayr *et al*, 2020).

2.3.1 Formate-derived one-carbon is found in glycine

As donors of one-carbon substitutes for THF derivatives, glycine, serine, and formate are important intermediates of the cellular folate cycle. These intermediates are found throughout

Results

the cell and in addition take part in various folate-independent pathways. In preliminary experiments, stable isotope labeling with [α - β - β -D $_3$] serine did not result in significant label enrichment in one of the targets (data not shown). Therefore, [α - ^{13}C] glycine was chosen due to its high turnover through the GDC-SHMT complex in mitochondria that leads to the formation of [α - ^{13}C] serine, [β - ^{13}C] serine and [α - β - ^{13}C] serine which in turn can serve as one-carbon donors (**Figure 28 B**). [^{13}C] formate was used to analyze the flux of one-carbon through the cytosolic formate-dependent pathway harboring MTHFD1 and THFS. Additionally, most labeling studies predominantly focused on serine or glycine as primary one-carbon sources – formate was included to elucidate its role in one-carbon transfer towards DNA methylation reactions. [^{13}C] formate-derived one-carbon strongly accumulated in glycine, which was surprising (**Figure 29 A**). Through the activities of THFS, MTHFC and MTHFD, [^{13}C] 5,10-methylene-THF was produced from [^{13}C] formate which further transferred ^{13}C to serine resulting in SHMT-mediated formation of [β - ^{13}C] serine (**Figure 28 B**). Reversal of SHMT activity would simply transfer ^{13}C from serine back to 5,10-methylene-THF and thereby generate unlabeled glycine. Therefore, there must be another connection between formate and glycine that makes the transfer of one-carbon possible.

High [^{13}C] formate-derived label enrichment was found in all genotypes after 4 hours after dawn (**Figure 29 A** left plot), which steadily decreased into the dark period. When addition of [^{13}C] formate was aligned to the start of the night, only low levels of [^{13}C] enriched glycine could be detected after 4 and 8 hours after dawn (**Figure 29 A** right plot). After the transition from dark to the light period, ^{13}C -enriched glycine rose, making formate incorporation into glycine daytime dependent. [α - ^{13}C] glycine was measured to assess the consumption and integration into the metabolomes of all genotypes (**Figure 29 B**). Furthermore, it was taken as a measure for glycine turnover through the GDC-SHMT complex. Aligned to the start of the day, [α - ^{13}C] glycine levels decreased steadily in all genotypes with slightly higher levels in *methfd1-1* indicating less effective incorporation of glycine-derived one-carbon (**Figure 29 B** left plot). When [α - ^{13}C] glycine was added at the beginning of the dark period, ^{13}C was incorporated at lower rates in all genotypes at 4 and 8 hours after dusk in all genotypes compared to samples aligned to dawn, the start of the light period (**Figure 29 B**).

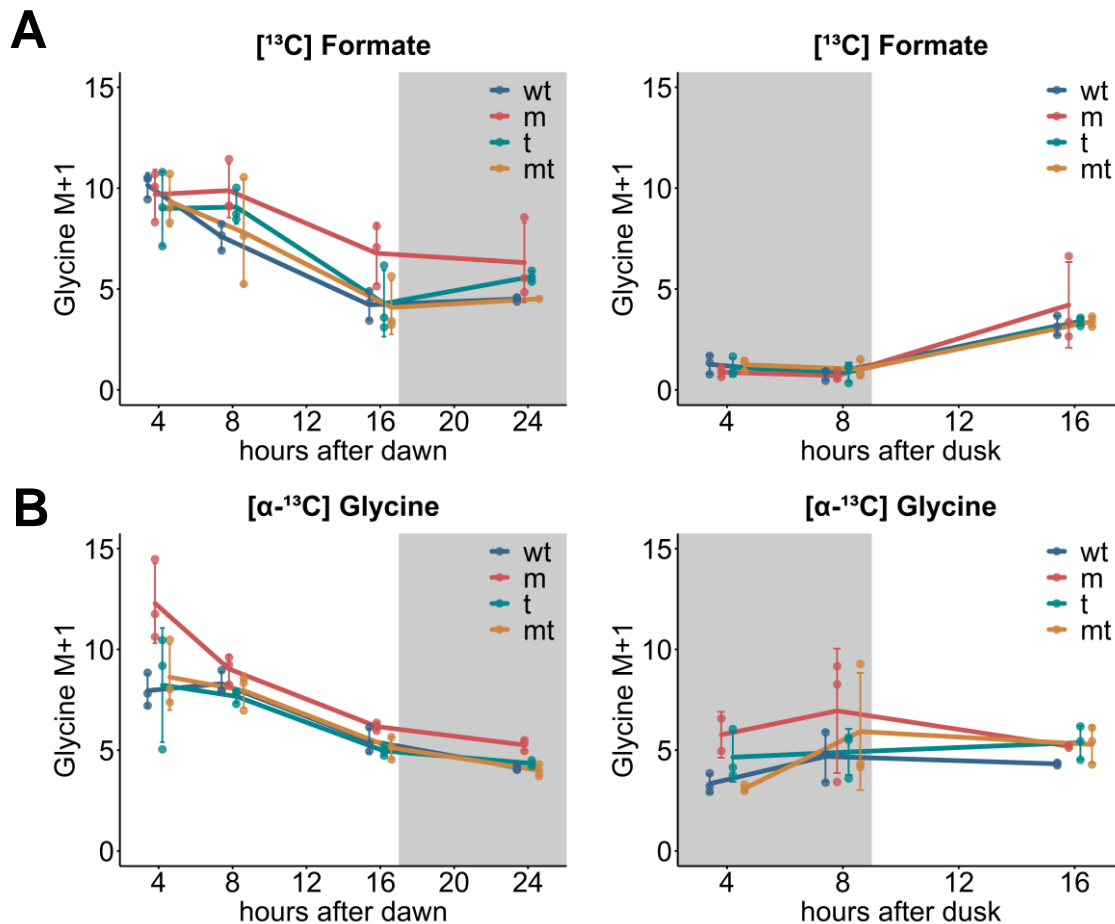


Figure 29. Formate incorporation into glycine is day time dependent.

^{13}C label enrichment in the M+1 fraction of glycine derived from ^{13}C formate (A) and $[\alpha\text{-}^{13}\text{C}]$ glycine (B). Labeled substrates were added aligned to the start of the light period and harvested after 4, 8, 16 and 24 hours after dawn (left plots) or aligned to the dark period with harvest points at 4, 8 and 16 hours after dusk (right plots). Mean values \pm s.d. ($n = 2\text{-}3$) are shown. Adjusted P values indicating statistical differences between genotypes at each timepoint (One-way ANOVA followed by post-hoc Tukey test, $P < 0.05$) can be found in **Supplementary Table 10**.

2.3.2 Formate and glycine derived one-carbon is equally incorporated into serine between genotypes

To test if glycine-to-serine conversion indeed happened as hypothesized before, ^{13}C formate and $[\alpha\text{-}^{13}\text{C}]$ glycine-derived label enrichment was measured in M+1 (**Figure 30**) and M+2 (**Figure 31**) fractions of serine, following the reactions described (**Figure 28 B**). Besides slightly higher label incorporation of ^{13}C into serine derived from both labeled substrates into M+1 and M+2 fractions in *methf1-1* at 16 hours after dawn, no differences between genotypes could be observed. Label enrichment into M+1 and M+2 fractions of serine was strong at 4

Results

hours after dawn for both labeling substrates (**Figure 30 & Figure 31** left plots). Afterwards, levels of labeled serine declined during the day and finally reached the lowest levels during the dark period at 20 and 24 hours after dawn. When [^{13}C] formate was added aligned to the dark period, label enrichment remained constant between the dark and light period in M+1 and M+2 fractions of serine (**Figure 30 A & Figure 31 A** right plots). In contrast, when [$\alpha\text{-}^{13}\text{C}$] glycine was added aligned to the dark period (**Figure 30 B & Figure 31 B** right plots), ^{13}C label was enriched in both fractions of serine at 4 and 8 hours after dusk and strongly declined at 16 hours after dusk. Formate-derived one-carbon would enter the folate cycle and pass the subsequent activities of MTHFC, MTHFD, SHMT and THFS (**Figure 28 A**). However, these results highlighted that serine formation originating from formate was daytime-dependent and that there must be a metabolic pathway that acts independently from THFS since THFS activity was reduced in *thfs* and *methfd1-1 x thfs* (**Figure 25 B**). Additionally, glycine-derived label enrichment in serine was uniform between genotypes - a fact that further demonstrated, that SHMT which catalyzed the reaction was not inhibited by 5-formyl-THF in *methfd1-1*.

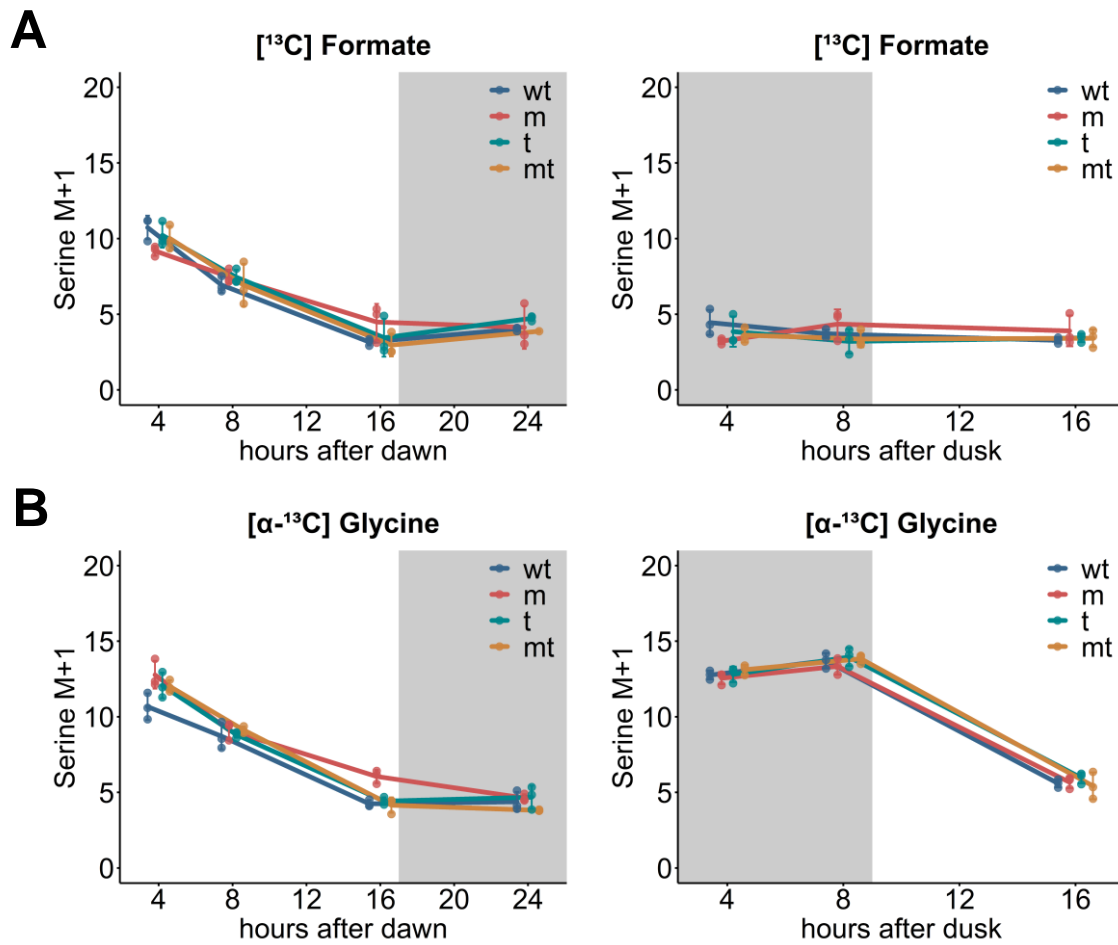


Figure 30. Formate and glycine are both incorporated into serine.

¹³C label enrichment in the M+1 fraction of serine derived from [¹³C] formate (A) and [α -¹³C] glycine (B). Labeled substrates were added aligned to the start of the light period and harvested after 4, 8, 16 and 24 hours after dawn (left plots) or aligned to the dark period with harvest points at 4, 8 and 16 hours after dusk (right plots). Mean values \pm s.d. ($n = 2-3$) are shown. Adjusted P values indicating statistical differences between genotypes at each timepoint (One-way ANOVA followed by post-hoc Tukey test, $P < 0.05$) can be found in **Supplementary Figure 11**.

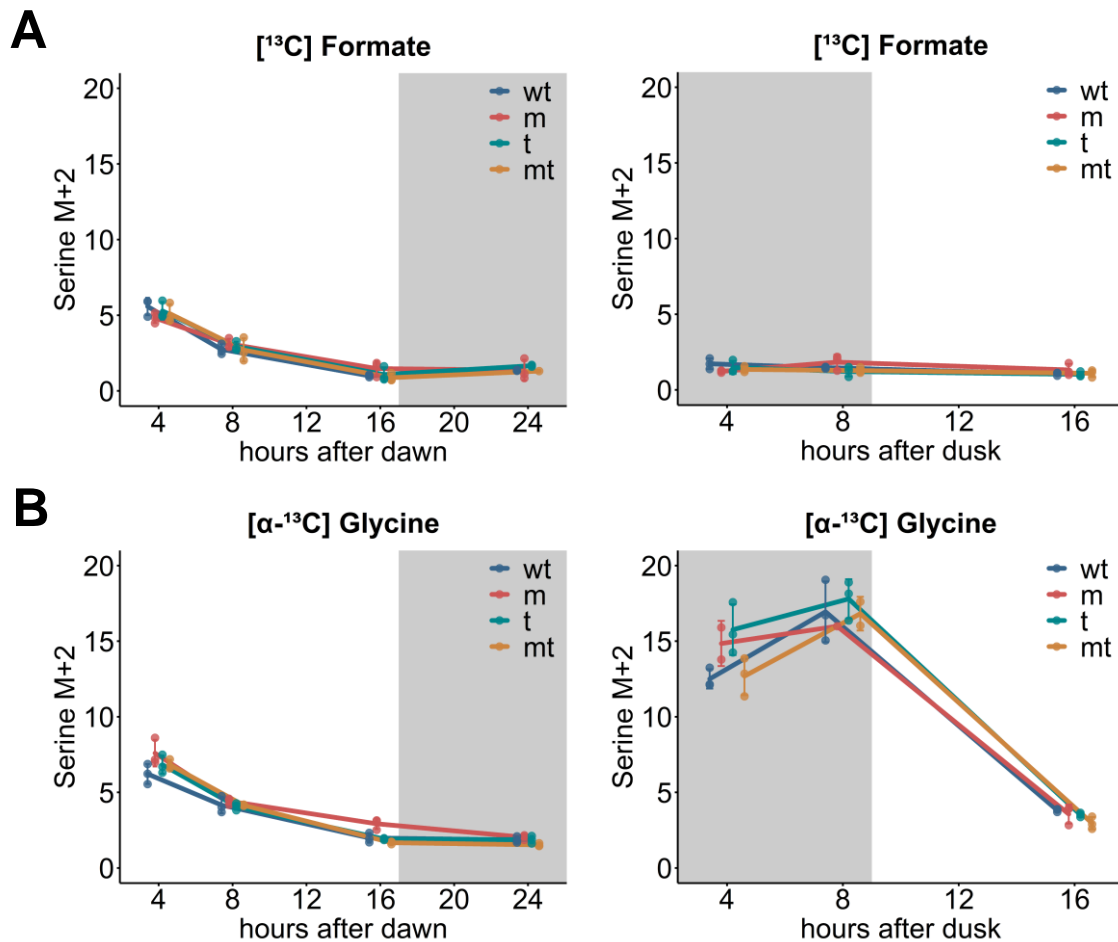


Figure 31. One-carbon flow through the GDC-SHMT complex is not reduced in *mthfd1-1*.

¹³C label enrichment in the M+2 fraction of serine derived from [¹³C] formate (A) and [α -¹³C] glycine (B). Labeled substrates were added aligned to the start of the light period and harvested after 4, 8, 16 and 24 hours after dawn (left plots) or aligned to the dark period with harvest points at 4, 8 and 16 hours after dusk (right plots). Mean values \pm s.d. ($n = 2-3$) are shown. Adjusted P values indicating statistical differences between genotypes at each timepoint (One-way ANOVA followed by post-hoc Tukey test, $P < 0.05$) can be found in **Supplementary Figure 11**.

2.3.3 Formate is a major one-carbon source for methionine synthesis

Label incorporation into methionine was used as a measure of one-carbon supply for Hcy remethylation. The subsequent methionine dependent synthesis of SAM in the cytosol is a major sink of methionine catabolism with 75 % of flux from methionine into SAM (Giovaneli *et al*, 1985; Sauter *et al*, 2013). Conclusively, steady supply of folate-mediated one-carbon units is crucial. [¹³C] formate-derived one-carbon strongly accumulated in methionine in wild type compared to the mutant genotypes after the labeled substrate was added (**Figure 32 A**). Additionally, there was a day-time dependent effect of label incorporation: the label doubled from 4 to 8 hours after dawn in wild type (**Figure 32 A** left plot), while the incorporation rate between 4 and 8 hours after dusk increased only ~1.3 fold (**Figure 32 A** right plot). *mthfd1-1* plants showed higher label enrichment compared to *thfs* and *mthfd1-1 x thfs* in both setups, when labeled formate was supplied aligned to the start of the light or dark period. This highlights that the point mutation in *MTHFD1* still allowed for higher flow of formate-derived one-carbon than the *thfs* mutant background that harbored a T-DNA insertion in *THFS*. Supposedly, residual flow through mutants of *THFS* to methionine was most likely the result of one-carbon transfer from formate to glycine as shown before (**Figure 29 A**), which was then introduced into the cytosolic folate metabolism. This was confirmed by [α -¹³C] glycine-derived one-carbon incorporation into methionine (**Figure 32 B**). Astonishingly, in *thfs* and *mthfd1-1 x thfs*, ¹³C label in methionine was more pronounced at 24 hours after dawn and 16 hours after dusk compared to wild type and *mthfd1-1* (**Figure 32 B**). Thereby, lack of formate-derived one-carbon could have been compensated through SHMT-mediated one-carbon incorporation from labeled glycine in *thfs* and *mthfd1-1 x thfs*.

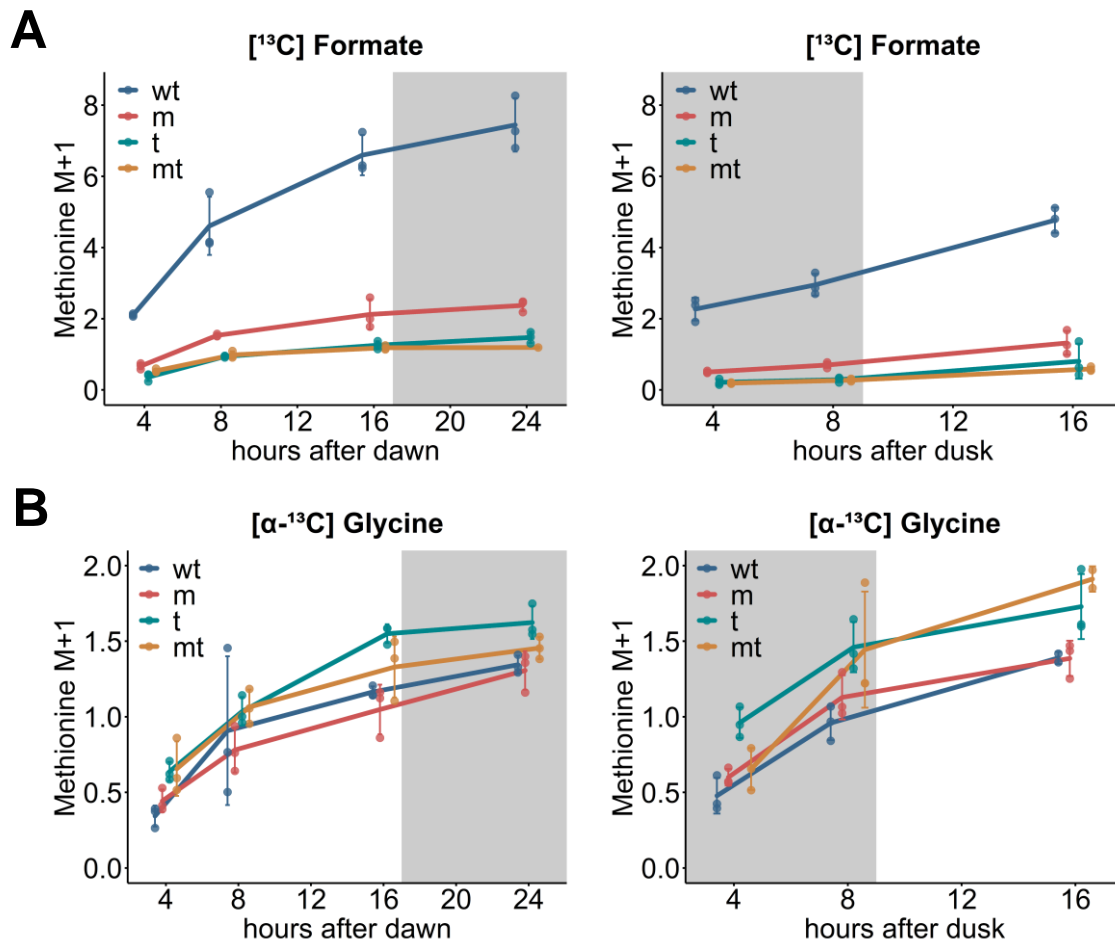


Figure 32. Formate is a major one-carbon source for Hcy remethylation.

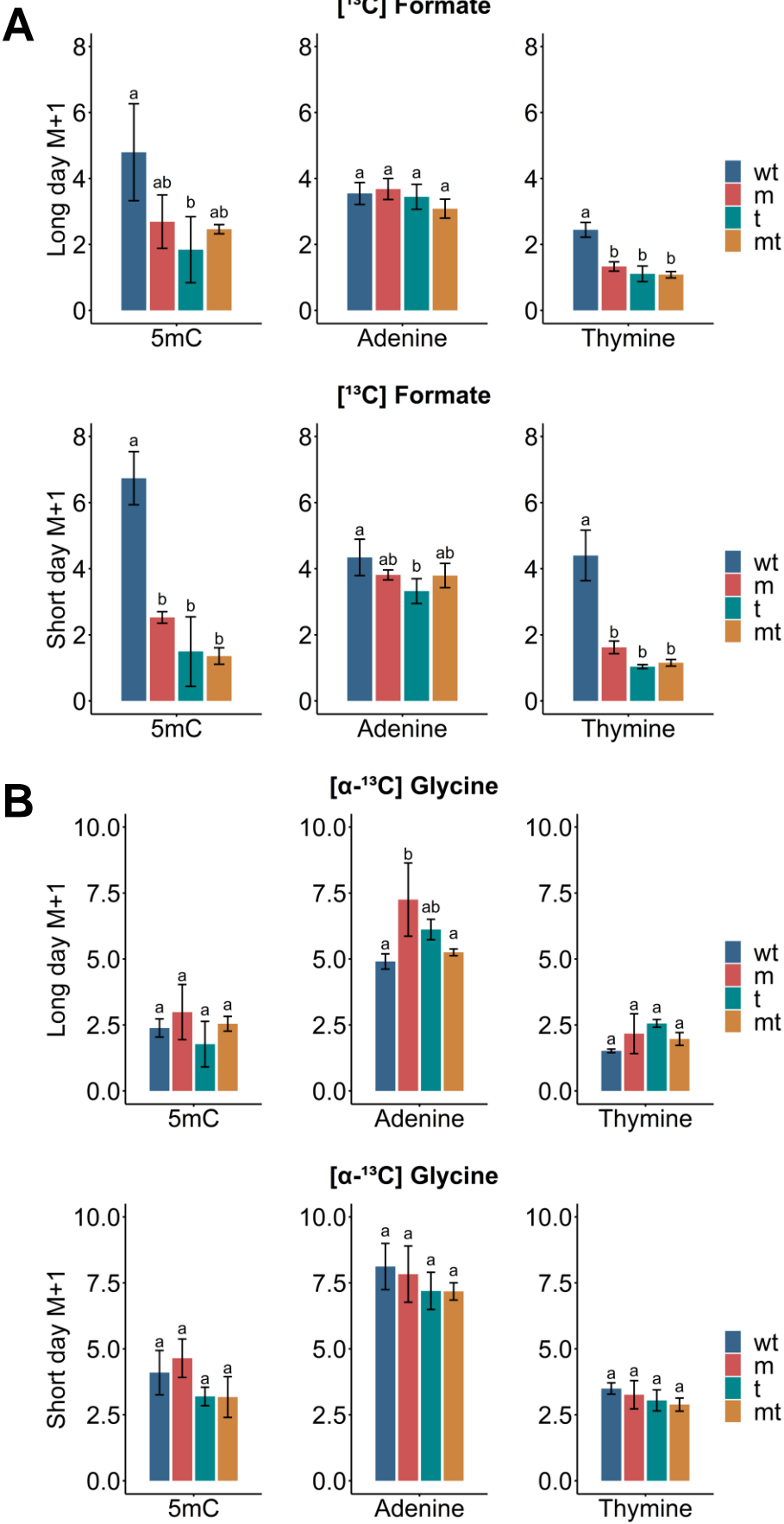
¹³C label enrichment in the M+1 fraction of methionine derived from [¹³C] formate (A) and [α-¹³C] glycine (B). Labeled substrates were added aligned to the start of the light period and harvested after 4, 8, 16 and 24 hours after dawn (left plots) or aligned to the dark period with harvest points at 4, 8 and 16 hours after dusk (right plots). Mean values ± s.d. ($n = 2-3$ except for mt fed with [¹³C] formate at 24 hours after dawn where $n = 1$) are shown. Adjusted P values indicating statistical differences between genotypes at each timepoint (One-way ANOVA followed by post-hoc Tukey test, $P < 0.05$) can be found in **Supplementary Table 10**.

2.3.4 Formate is a major source of one-carbon for DNA methylation

The contribution of the formate-dependent pathway as well as glycine-derived flow of one-carbon for DNA methylation, purine and thymidylate synthesis was assessed by label enrichment analyses in 5-methylcytosine, adenine and thymine, respectively. Labeled substrates were provided one week prior to harvest at midday for LD and SD grown plants. After DNA isolation and subsequent hydrolysis into nucleobases, [^{13}C] formate and [$\alpha\text{-}^{13}\text{C}$] glycine-derived label enrichment was found in all targets under LD and SD conditions (**Figure 33**). Notably, accumulation of [^{13}C] formate-derived one-carbon in 5-methylcytosine and thymine under both LD and SD growth was more pronounced in the wild type compared to the mutant genotypes (**Figure 33 A**). Interestingly, label enrichment in 5-methylcytosine and thymine was higher under SD conditions compared to LD in the wild type. Especially under SD growth, 5-methylcytosine and thymine displayed similar patterns as formate-derived label enrichment in methionine: significantly higher ^{13}C label in wild type, reduced levels in *methfd1-1* and lowest in *thfs* and *methfd1-1 x thfs*. No differences in formate-derived ^{13}C enrichment could be observed in adenine between genotypes when grown under LD conditions (**Figure 33 A**). SD grown plants however, showed reduced formate-derived one-carbon enrichment in *thfs*. [$\alpha\text{-}^{13}\text{C}$] glycine-derived one-carbon was enriched in all target compounds in all genotypes under both growth environments, LD and SD (**Figure 33 B**). However, only LD grown *methfd1-1* plants showed increased label in adenine compared to wild type. Additionally, the strongest enrichment between targets was detected in adenine with a twofold increase compared to 5-methylcytosine and thymine which displayed similar patterns and a similar degree of label enrichment between genotypes and photoperiod length (**Figure 33**).

Figure 33. Formate is a main source for cytosine methylation and thymine synthesis.

^{13}C label enrichment derived from [^{13}C] formate (A) and [$\alpha\text{-}^{13}\text{C}$] glycine (B) in the M+1 fractions of nucleobases 5-methylcytosine (5mC), adenine and thymine. Plants were grown under LD and SD conditions. Labeled substrates were added 1 week before plant material was harvested at midday, 6 hours after dawn. Mean values \pm s.d. ($n = 2\text{-}3$) are shown. Lowercase letters represent statistical differences between genotypes for each nucleobase target (One-way ANOVA followed by post-hoc Tukey test, $P < 0.05$).



3 Discussion

In the past three decades, a multitude of studies characterized the targeting mechanisms that faithfully regulate and catalyze cytosine methylation (Law & Jacobsen, 2010; Du *et al*, 2015; Lloyd & Lister, 2022). In this study, a novel mechanism of regulation is presented: the one-carbon metabolic network that provides methyl groups for DNA methylation. The concept that gene expression is regulated by the metabolism dates back to the experiments of Jacob and Monod in *E. coli* in which they outlined the regulation of the so called *lactose (lac)* operon by the availability of substrates in the surrounding growth environment (JACOB & MONOD, 1961; Schvartzman *et al*, 2018). That was the first gene regulatory mechanism that was fully understood – one that is under the control of the nutrient environment. Nevertheless, epigenetic regulation in eukaryotes is far more complex. It is the result of the combined actions of chromatin remodeling complexes, modifying enzymes that add or remove chromatin marks including DNA methylation as well as the resulting transcriptional activation or repression (Schvartzman *et al*, 2018). DNA methylation is controlled by the cellular Methylation Index (MI) which is sustained through the diurnal supply of one-carbon for SAM synthesis and removal of SAH. Perturbations of this dynamic supply can reduce the MI and therefore alter DNA methylation levels.

Plants are photoautotrophic organisms that use photosynthesis for the formation of carbohydrates that fuel cellular processes. A cellular network of metabolic reactions serves to convert these carbohydrates to intermediates which are further partitioned to function as substrates and cofactors for enzymatic reactions (Dai *et al*, 2020). In this context, the role of the cytosolic, formate-dependent pathway was elucidated for Hcy remethylation and SAM synthesis. Here, it is demonstrated that the flow of one-carbon depends on the daytime and day length, bridging the environment-dependent metabolic status and DNA methylation mediated regulation of gene expression.

3.1 The universal methyl group donor SAM is just not universal

The cytosolic folate cycle is unparalleled within the cellular one-carbon metabolism due to its functional link to the activated methyl cycle (AMC), the sole source of SAM. But it would be dubious to focus only on SAM and to neglect the role of SAH and the associated reactions of the AMC. SAHH, which processes SAH to adenosine and Hcy, thermodynamically favors the formation of SAH (La Haba & Cantoni, 1959). Under cellular conditions however, SAHH activity leads to the formation of Hcy if adenosine and Hcy are effectively removed (Green *et al*, 1988;

Herbig *et al*, 2002; Moffatt *et al*, 2002). This was not the case in LD grown *methfd1-1* plants, which showed diurnal oscillation of SAH and Hcy with significantly higher concentrations during the day compared to night and in wild type (**Figure 14 A**). In contrast to SAH, SAM never deviated from wild type levels in *methfd1-1* throughout the day and was even higher during the dark period. Thus, the resulting decrease in DNA methylation was not caused by deficiency of SAM but rather its efficacy for DNA methyltransferases and the causal, underlying reduction of the MI (**Figure 14 B**). As mentioned before, mutation of *SAHH1* in *Arabidopsis* results in SAH accumulation (Furner *et al*, 1998; Rocha *et al*, 2005; Mull *et al*, 2006; Ouyang *et al*, 2012). In this study, non-mutational *SAHH1* showed higher relative gene expression in *methfd1-1* compared to wild type during the day (**Figure 13 B**). Still, higher expression was not reflected in higher metabolism of SAH but rather enforced an equilibrium between SAH and Hcy during the day that disrupted the cyclic flow of the AMC. Nevertheless, this metabolic block of the AMC was not static but resolved at dusk in the dark period when SAH and Hcy levels started to decline, and methionine and SAM increased. It is likely that the direction of the *SAHH1*-catalyzed, reversible reaction had shifted towards the formation of Hcy at night, breaking the equilibrium between Hcy and SAH during the day. Conversely, the increase of the MI in *methfd1-1* at night reversed inhibition of DNA methylation by SAH, resulting in decreased expression of *SDC* as the locus was likely sufficiently remethylated (**Figure 14 B**).

Additionally, SD growth of *methfd1-1* prevented accumulation of SAH and Hcy (**Figure 16 A**). These results indicated that Hcy remethylation strongly depends on functional MTHFD1 activity and that the phenotype associated with impaired MTHFD1 activity is conditional: under LD growth, *methfd1-1* showed strong defects associated with deregulation of one-carbon metabolism while SD growth complemented adverse effects almost entirely including Hcy remethylation, which led to the reduction of SAH. Furthermore, it was shown that knockout of *THFS* in *methfd1-1* also complemented the phenotype. These findings were astonishing as both enzymes are part of the same cytosolic formate-dependent pathway that appears to control the MI. And since the MI as well as Hcy remethylation showed diurnal oscillation in *methfd1-1*, it became obvious that the flow of one-carbon through the formate-dependent pathway plays an essential role in the preservation of the MI for DNA methylation reactions, especially during the day.

3.2 A stable metabolome ensures a functional epigenome

It appears plausible that deregulation of metabolic pathways along the course of the 24 h of the day might impact cellular processes and developmental responses to the surrounding

environment. As such, the pleiotropic phenotype of *mthfd1-1* is most probably not caused by reduced DNA methylation but due to the time-of-day-dependent disruption of the one-carbon metabolism. This is supported by the fact that epigenetic mutants in *Arabidopsis* such as *drm1 drm2 cmt3* show reduction in DNA methylation but weak phenotypic defects compared to *mthfd1-1* (Chan *et al*, 2006; Groth *et al*, 2016). Nonetheless, alterations of the cellular metabolism, such as the folate cycle in *mthfd1-1*, can have a drastic impact on the epigenome and its regulation (Groth *et al*, 2016; Lindermayr *et al*, 2020; Lu *et al*, 2023). Whole genome bisulfite sequencing was used to assess genome-wide DNA methylation levels in wild type, *mthfd1-1*, *thfs* and *mthfd1-1 x thfs*. As previously reported (Groth *et al*, 2016), *mthfd1-1* showed genome-wide loss of DNA methylation, especially in the CHG sequence context. In contrast, *thfs* single and *mthfd1-1 x thfs* double mutants showed wild type like DNA methylation for CHG hypo-DMRs (**Figure 7**). This was possible because the MIs of *thfs* and *mthfd1-1 x thfs* were not reduced and showed wild type-like levels (**Figure 14 B**). Accordingly, TEs remained silent in *thfs* and *mthfd1-1 x thfs* under both LD and SD growth compared to *mthfd1-1* (**Figure 12 C**). However, because of the reduced SAH and Hcy levels, SD grown *mthfd1-1* plants also exhibited lower expression of TEs compared to plants that were shifted from SD to LD. As already mentioned, losses and gains of DNA methylation are often caused by genetic variation (Dubin *et al*, 2015; Kawakatsu *et al*, 2016). This also applies to the mutation in *mthfd1-1*. The difference, however, is that the changes in DNA methylation in *mthfd1-1* depend on the growth regime. Different lengths of light and dark periods during the day were recreated as they also occur in seasonal day lengths of the natural environment. But plants are exposed to greater variation and fluctuations in their natural habitat that would ultimately define their phenotype – in the case of *mthfd1-1*, the pleiotropic phenotype was induced under LD growth while it was suppressed under SD conditions.

Nevertheless, changes in the epigenome are often more subtle. Similar to genetic variation, epigenetic mutations, so called epimutations can appear instantaneously and be passed on to subsequent generations (Denkena *et al*, 2021). Strikingly, these epimutations can arise independently of genetic variation (Schmitz *et al*, 2011; Becker *et al*, 2011), while the focus is often set on stochastic epimutations of CG methylation and the rate of their appearance (Hazarika *et al*, 2022; Goedel & Johannes, 2023). It has been proposed that epimutations emerge as a byproduct of imprecise maintenance fidelity of DNA methylation pathways (Hofmeister *et al*, 2020; Shahryary *et al*, 2020; Denkena *et al*, 2021). As mentioned before, disruption of the MI can affect the fidelity of DNA methyltransferases, and in this study, it was shown that the MI needs to be sustained by a diurnal supply of one-carbon. In contrast to the controlled conditions in greenhouses, natural environments are fluctuating noticeably, which

affects the cellular metabolism and thus also the stability of the MI. This is all the more serious because folates, methionine and SAM, among others, belong to the most damage-prone metabolites that tend to spontaneous chemical reactions such as elimination, oxidation or hydrolysis (Lerma-Ortiz *et al*, 2016). It is therefore feasible that a fluctuating growth environment with challenging abiotic and biotic stressors translates into a cellular metabolome that can inflict epimutations, just because the folate-mediated one-carbon metabolism does not meet the substrate requirements for DNA methylation. This is supported by the fact that folate metabolic enzymes and chromatin remodelers were shown to interact in a spatio-temporal manner. For example, mammalian bromodomain-containing protein 4 (BRD4), a regulator of chromatin structure and transcription interacts with and recruits MTHFD1 to distinct genomic loci – a mechanism that suggests direct involvement of MTHFD1 in nuclear metabolism and the control of gene expression (Sdelci *et al*, 2019). Also in mammals, ADENOSYLHOMOCYSTEINASE (AHCY), the mammalian counterpart of SAHH, was shown to cyclically associate with the circadian clock regulator complex CLOCK-BMAL1 at distinct loci to regulate circadian gene expression (Greco *et al*, 2020). Interestingly, pharmacological inhibition of AHCY resulted in time-dependent reduction of H3K4 methylation at genes related to circadian rhythm and thus leading to changes in gene expression (Greco *et al*, 2020). Additionally, it was shown that enzymes of one-carbon metabolism translocate to nuclei of mammals during the S-phase of the cell cycle to support DNA replication (Field *et al*, 2018). It is obvious that one-carbon metabolism not only supports DNA replication and repair mechanisms but could also contribute to the maintenance of DNA methylation during cell division (Field *et al*, 2018). Nuclear targeting of SAHH has also been described in *Arabidopsis* (Lee *et al*, 2012). Additionally, it was shown that transcript and protein levels of SAHH fluctuate similarly to enzyme activities to meet the higher demand for SAM supply and removal of SAH in rapidly dividing cells (Pereira *et al*, 2007). Logically, one-carbon is required for this, the provision of which depends strictly on the growth environment.

3.3 Supply of one-carbon methylation reactions: when and where is it coming from?

Photosynthesis and more generally the transition from daily light and dark periods imply an environment-dependent pattern of metabolism (Lindermayr *et al*, 2020). This was also the case for the partitioning of one-carbon in the shape of formate, serine and glycine for the various reactions supported by folate species.

3.3.1 Formate is an important but neglected source of one-carbon

Towards the AMC, it was thus observed that more one-carbon was provided by formate for the remethylation of Hcy during the day than during the night. More one-carbon from [¹³C] formate was incorporated into methionine in wild type at 4 and 8 hours after dawn compared to dusk (**Figure 32**). Subsequently, this led to higher ¹³C label incorporation into 5-methylcytosine which derived from the newly synthesized SAM and methionine from Hcy remethylation in wild type (**Figure 33 A**). Not only 5-methylcytosine but also thymine showed an increase in one-carbon derived from [¹³C] formate in wild type compared to the other genotypes (**Figure 33 A**). Similar ¹³C label distributions in 5-methylcytosine, thymine and methionine between genotypes suggested a common pool of 5,10-methylene-THF that constitutes a hub for the synthesis of thymine, remethylation of Hcy to methionine and the subsequent transmethylation of cytosine to 5-methylcytosine. This formate-derived pool of 5,10-methylene-THF is sustained through the same series of enzymes in the cytosol: THFS and MTHFD1.

In the case of purines, specifically adenines, there are several genes of precursor synthesis that are localized to plastids, including 10-formyl-THF-dependent enzymes GAR TRANSFORMYLASE (GART) and AICAR TRANSFORMYLASE (ATIC) (Zrenner *et al*, 2006). Consistently, mutation of cytosolic *THFS* and *MTHFD1* did not affect 10-formyl-THF bioavailability for purine synthesis in the organelle, as ATP concentrations were not reduced in the mutant genotypes compared to wild type (**Figure 23**) and one-carbon incorporation into adenine was mostly uniform between genotypes (**Figure 33**). These results are in line with previously reported stable isotope labeling experiments in *MTHFD1*-deficient patient fibroblasts (Field *et al*, 2015). Mutation of the dehydrogenase motif of the human, trifunctional *MTHFD1* did not affect purine *de novo* biosynthesis, but led to reduced thymidylate and thus thymine synthesis as well as impaired Hcy remethylation (Field *et al*, 2015). Interestingly, one-carbon was directed towards thymidylate synthesis at the expense of Hcy remethylation. In this study it was the other way around: a slight increase of formate-derived one-carbon towards Hcy remethylation which was reflected by higher label incorporation into 5-methylcytosine could be observed at the expense of thymidylate, respectively thymine synthesis (**Figure 33 A**).

Still, it is not entirely conclusive how [¹³C] formate-derived one-carbon was fed into the plastic purine synthesis pathway in the *mthfd1-1*, *thfs* and *mthfd1-1 x thfs* mutant plants. The obvious reason for the lower incorporation of [¹³C] formate-derived one-carbon into thymine and 5-methylcytosine as well as methionine was the mutation in *MTHFD1* and *THFS*, which limited

formate-derived one-carbon for these reactions (**Figure 28 A**). Yet the double mutant *mthfd1-1 x thfs*, which showed reduced levels of 10-formyl-FA (**Figure 15 B**), and thus 10-formyl-THF as well as impaired enzymatic activity of THFS (**Figure 25 B**), the enzyme that introduces one-carbon from formate into the folate cycle, showed no difference in label incorporation into adenine compared to wild type (**Figure 33 A**). In general, the formate metabolism is enigmatic in mammals and plants and often neglected for one-carbon metabolism (Brosnan & Brosnan, 2016). It is therefore difficult to say from which metabolic pathway and compartment it arises. However, a study by Collakova *et al* (2008) has shown that the activity of 10-FDF leads to the production of formate in mitochondria and that this reaction is essential for photorespiration. Since photorespiration is directly linked to photosynthesis, formate could be introduced into the cytosolic folate cycle from the mitochondria during the day, which would explain the higher flow rate of [¹³C] formate-derived one-carbon into methionine during the day compared to nighttime in wild type (**Figure 32 A**). Furthermore, this path would explain the origin of formate as well as its dismantling in contrast to previous stable isotope labeling studies which suggested that formate is primarily degraded to CO₂ via FORMATE DEHYDROGENASE (FDH) (Li *et al*, 2003).

3.3.2 Glycine and serine interconversion is an additional source of one-carbon

One-carbon metabolism is adapted to specific needs of yeast, plants and mammals (Christensen & MacKenzie, 2006). In plants, glycine and serine are important intermediates of photorespiration, the context of which they were most studied (Igamberdiev & Kleczkowski, 2018). Photorespiration is a process linked to photosynthesis, that starts with the oxygenase instead of carboxylase activity of RIBULOSE-1,5-BISPHOSPHAT-CARBOXYLASE/OXYGENASE (RuBisCO) (Mouillon *et al*, 1999; Bauwe *et al*, 2010). Thereby, a two-carbon molecule, 2-phosphoglycolate is recycled into a three-carbon metabolite, 3-phosphoglycerate that is reintroduced into the Calvin-Benson cycle to produce glucose (Mouillon *et al*, 1999; Bauwe *et al*, 2010). During photorespiration, glycine is produced which is further metabolized via the mitochondrial GDC-SHMT complex, where serine is synthesized from two molecules of glycine (Mouillon *et al*, 1999). However, it was shown that glycine is not completely used for the synthesis of serine (Abadie *et al*, 2016; Abadie *et al*, 2018), which opened two ways to introduce [α -¹³C] glycine into the one-carbon metabolism. Either through GDC, that led to the formation of [¹³C] 5,10-methylene-THF which could be further synthesized to [¹³C] 5-methyl-THF via MTHFR in the cytosol and ultimately to [¹³C] methionine through Hcy remethylation (**Figure 28 A, B**). Alternatively, ¹³C-labeled 5,10-methylene-THF formed from [α -¹³C] glycine by GDC was converted to [β -¹³C] serine through SHMT or [α - β -¹³C] serine if another molecule

Discussion

of [α - ^{13}C] glycine instead of unlabeled glycine was used (**Figure 28 A, B**). [β - ^{13}C] serine or [α - β - ^{13}C] serine then served as one-carbon source through SHMT in the cytosol (Bauwe *et al*, 2010). While both options are possible, the second one is more feasible as previous studies showed that the combined activities of the mitochondrial GDC-SHMT complex are the major pathway of serine formation (Prabhu *et al*, 1996; Wingler *et al*, 1999; Bauwe *et al*, 2010).

Glycine is *per se* not a one-carbon donor but was used instead of labeled serine which was used in preliminary experiments where no label enrichment could be retrieved in any of the amino acid or nucleobase targets. Glycine-derived ^{13}C label enrichment in the different isotopologues of serine was uniform between genotypes (**Figure 30 & Figure 31**) and reflected the equal distribution and enrichment in nucleobases (**Figure 33**). Since it appeared that the conversion of glycine and serine through SHMT was not affected in any genotype, an inhibitory effect of 5-formyl-THF could also be ruled out. It even seemed that due to the increased total daily activity of SHMT in *thfs* and *methfd1-1 x thfs* (**Figure 26 A** right plot), more [β - ^{13}C] serine and [α - β - ^{13}C] serine was introduced into the cytosolic folate cycle. This then led to increased glycine-derived ^{13}C label in methionine (**Figure 32 B**) and could explain how *thfs* and *methfd1-1 x thfs* compensated for the hindered formate-dependent pathway.

Serine is a metabolic signal, and as such, its accumulation leads to down-regulation of the expression of genes encoding enzymes of photorespiratory metabolism (Timm *et al*, 2013; Timm *et al*, 2016). Furthermore, it was shown that even slightly impaired photorespiration as seen in the mutant of peroxisomal *HYDROXYPYRUVATE REDUCTASE 1* (*HPR1*) leads to glycine accumulation during the day (Timm *et al*, 2021). In *hpr1*, this effect was more pronounced under SD growth compared to LD which indicated a reduction and slowdown of flux through the GDC-SHMT complex (Timm *et al*, 2021). In *methfd1-1*, glycine did not accumulate under SD or LD conditions. In contrast, serine accumulated strongly (**Figure 15 A**), but this did not seem to have any influence on photorespiration in *methfd1-1*, at least at the level of the GDC-SHMT complex where [α - ^{13}C] glycine was readily converted to ^{13}C labeled serine (**Figure 30 B & Figure 31 B**). Interestingly, the GDC-SHMT complex was shown to be a major site of glycine catabolism in non-photosynthetic cell cultures of higher plants coupled to serine synthesis (Mouillon *et al*, 1999). The authors proposed an important role of GDC-SHMT-mediated glycine catabolism in all plant tissues, not only photosynthetically active foliage (Mouillon *et al*, 1999). This could explain why [α - ^{13}C] glycine-derived one-carbon was incorporated into fractions M+1 and M+2 of serine during the night while [^{13}C] formate-derived one-carbon in serine was almost absent (**Figure 30 B & Figure 31 B**).

3.3.3 Distribution and compartmentalization of folate metabolism controls one-carbon partitioning

While the biochemical pathways of formate and its function are still not fully understood in plants (Igamberdiev, 1999; Igamberdiev & Kleczkowski, 2018), recent studies have shown that formate is a hallmark of cancer-specific one-carbon metabolism in mammals (Meiser *et al*, 2016; Meiser *et al*, 2018; Green *et al*, 2023). Green *et al* (2023) could show that mitochondria-derived formate leads to accumulation of 10-formyl-THF in the cytosol if the cyclohydrolase and dehydrogenase activities of MTHFD1 are pharmacologically inhibited. The trapping of folate as 10-formyl-THF was proposed to deplete folates for biosynthetic pathways (Green *et al*, 2023). In *mthfd1-1*, a similar mechanism might have depleted one-carbon in the form of 5-formyl-THF under LD growth: formate derived from mitochondria entered the cytosolic folate cycle through THFS which catalyzed the formation of 10-formyl-THF. Subsequently, the cyclohydrolase activity of MTHFD1 which was still functional compared to the dehydrogenase activity (**Figure 25 A**), led to the formation of 5,10-methenyl-THF in *mthfd1-1*. SHM4 catalyzed formation of 5-formyl-THF from 5,10-methenyl-THF might have prevented the accumulation of 5,10-methenyl-THF and led to strong accumulation of 5-formyl-THF in *mthfd1-1* (**Figure 15 B**). The isotopic labeling data and enzyme activity measurements suggested that accumulation of 5-formyl-THF was most likely not causing inhibition of SHMT in *mthfd1-1* but similar to the study of Green *et al* (2023), it might act as a 'folate trap'. Depletion of one-carbon as 5-formyl-THF would conclusively lead to reduced levels of other folate species. Although the stable isotope dilution assay (SIDA) using LC-MS/MS that was used to measure folates in this study is state of the art for folate analysis (Striegel *et al*, 2018), it is important to acknowledge what cannot be measured through this approach: 5,10-methenyl-THF and 5,10-methylene-THF (**Figure 3 B & Figure 5**). As a result, 5-formyl-THF could have had an indirect influence on the flow of one-carbon by potentially minimizing the pool of 5,10-methenyl-THF and 5,10-methylene-THF.

Cytosolic MTHFR catalyzes the reduction of 5,10-methylene-THF to 5-methyl-THF and thus maintains steady supply of 5-methyl-THF for Hcy remethylation to methionine in the AMC (**Figure 5**). In mammals, MTHFR activity is irreversible and regulated by allosteric inhibition through SAM binding (Froese *et al*, 2018). This feedback inhibition is considered to regulate and avoid depletion of the 5,10-methylene-THF pool for other biosynthetic pathways (Roje *et al*, 2002a). Activity of plant MTHFR is NADH-dependent and was proposed to be reversible and insensitive to SAM (Roje *et al*, 1999; Roje *et al*, 2002a). Wu *et al* (2018) could show that down-regulation of MTHFR in maize leads to a decrease in 5-methyl-THF accompanied by increased levels of 5,10-methylene-THF. While this down-regulation did not affect SAM levels,

SAH rose and led to a decreased MI, inhibiting methyltransferases of lignin biosynthesis (Wu *et al*, 2018). Interestingly, CAFFEYL COA O-METHYLTRANSFERASE (CCOAMT) was more sensitive to SAH inhibition than CAFFEIC ACID O-METHYLTRANSFERASE (COMT), highlighting another potential form of transmethylation regulation through substrate specificity of methyltransferases (Wu *et al*, 2018). No differences were discovered in the diurnal MTHFR activity between wild type, *mthfd1-1*, *thfs* and *mthfd1-1 x thfs* (**Figure 26 B**). Also, diurnal levels of 5-methyl-THF and NADH were mostly uniform between genotypes, at least between wild type and *mthfd1-1* (**Figure 15 & Figure 23**). Accordingly, there was seemingly no lack of one-carbon for Hcy remethylation and no lack of SAM for transmethylation reactions.

As mentioned before, previous studies in *Lemna* could show that 75 % of the methionine pool are associated with SAM synthesis in the AMC, highlighting the importance of methionine for DNA methylation (Giovanelli *et al*, 1985; Amir, 2010). Since methionine *de novo* synthesis also depends on Hcy methylation, which is impaired in the *mthfd1-1* phenotype, complementation of reduced methionine could not be anticipated. On the contrary, more HserP might have been targeted towards threonine formation which led to higher levels in *mthfd1-1* (**Figure 19**). Increased levels of MTA in *mthfd1-1* suggested that methionine scavenging was also impaired and could therefore not sustain methionine concentrations. In the mutants *thfs* and *mthfd1-1 x thfs* on the other hand, reduced levels of MTA might indicate higher rates of metabolization towards methionine which could have further compensated the formate-dependent pathway (**Figure 20**).

Furthermore, it is not clear why 5-formyl-THF was not fed back into the folate cycle in *mthfd1-1*. It has been proposed that 5-formyl-THF is a storage form of folates that is also capable to rescue mutants of folate metabolic enzymes such as *fpgs1* (Srivastava *et al*, 2011; Zhou *et al*, 2013). This is all the more interesting since *fpgs1* mutant plants exhibited upregulation of SAH and reduction of DNA methylation, similar to *mthfd1-1* (Zhou *et al*, 2013). In contrast to *fpgs1*, *mthfd1-1* and *mthfd1-1 x thfs* mutant plants were not rescued by exogenous application of 5-formyl-THF – on the contrary, it had a detrimental effect on the phenotype, although this defect was independent of DNA methylation (**Figure 17**). Until now, only mitochondrial 5-FCL has been described to reintroduce 5-formyl-THF back into the folate cycle (**Figure 5**). In *mthfd1-1*, 5-formyl-THF showed stable, elevated concentrations throughout the day suggesting that accumulation was confined to the cytosol and not imported into mitochondria. In this study, only cellular levels of metabolites were measured, which is why the subcellular distribution of individual metabolites could not be traced.

Discussion

It was also shown that polyglutamylation led to subcellular compartmentation and increased stability of folates (Mehrshahi *et al*, 2010). Several studies investigated the impact of mono- and polyglutamylated folates on enzyme activities – polyglutamylation of folates enhances folate affinity and reduces K_m values of folate substrates (Rebeille *et al*, 1994). In *methfd1-1*, glutamate, which is the substrate for FPGS catalyzed polyglutamylation of folates was reduced compared to wild type and the other genotypes under LD conditions (**Figure 22 A**). This suggests that, although folates could be present in wild type like concentrations, they might not be readily available or compartmentalized in *methfd1-1* due to reduced glutamylation.

The time-of-day-dependent equilibrium between SAH and Hcy is certainly a benchmark for functional DNA methylation, but it is not the only example in which fluctuating metabolite levels alter the thermodynamic characteristics of enzymes. For instance, studies have shown that steady-state kinetic parameters of SHMT isoforms in plants and mammals strongly dependent on factors, such as pH, substrate and product concentrations (Tramonti *et al*, 2018; Nogués *et al*, 2022). Accordingly, K_m values can change noticeably and increase the demand for the supply of substrates and removal of products to sustain enzyme reaction rates. The metabolic build-up in *methfd1-1* might have led to altered enzyme reaction rates that could redirect the flow or change the pace of intermediates.

As it is already known in the case of serine, metabolites can also serve as signals that regulate the expression of genes (Timm *et al*, 2013). This might also be true for intermediates of one-carbon metabolism. *SHM4* (AT4G13930) and *SAHH1* (AT4G13940) share the same location on chromosome 4 of the *Arabidopsis thaliana* genome and are only separated by 4500 bp which suggests that both genes are targeted synergistically by a common regulatory pathway. In the case of *methfd1-1*, higher expression of *SHM4* and *SAHH1* (**Figure 13 B**) might be induced to remediate for metabolic homeostasis. The expression of genes encoding metabolic enzymes is also tightly regulated throughout the day by the circadian clock. Early studies could show that especially genes from metabolic and light responsive pathways are circadian-regulated (Harmer *et al*, 2000). More recent studies could show how epigenetic modifications of mRNA regulate genes of the circadian clock (Wang *et al*, 2021). Light-induced methylation of adenosine at position N⁶ (N⁶-methyladenosine, m⁶A) of core components of the circadian clock such as *CCA1* stabilizes the circadian transcriptome and ensures circadian rhythms in plants. Like DNA methylation, modifications of the epitranscriptome depend on the spatio-temporal supply of substrates. This might explain why diurnal gene expression patterns of main clock components including *CCA1* were deregulated in *methfd1-1* grown under LD conditions

(**Figure 11 & Figure 13**). In order to ensure these dynamic reactions, a stable, diurnal flow of one-carbon is necessary.

3.4 Energy and redox metabolism are not affected in *mthfd1-1*

Reduction of MTHFD1-mediated NADPH/NADP⁺ content was proposed to disrupt the cellular redox balance (Farquharson, 2017; Gorelova *et al*, 2017a). In *mthfd1-1*, reduced MTHFD1 activity (**Figure 25 A**) actually led to decreased levels of NADPH (**Figure 24 A, B**), which is needed for reduction of glutathione. However, this did not result in reduction of GSH, the reduced form of glutathione (**Figure 24 A, B**). Using *in vivo* imaging of redox-sensitive roGFP, *mthfd1-1* showed the same glutathione redox balance (E_{GSH}) as wild type after treatment with reducing and oxidizing agents DTT and H₂O₂, respectively (**Figure 24 C, D**). In the double mutant *mthfd1-1* x *thfs*, GSH concentrations were even increased compared to wild type and the other mutants (**Figure 24 A, B**). Glutathione consists of glutamate, glycine and cysteine (Taiz *et al*, 2018), three compounds that are linked to sulfur and one-carbon metabolism. Although *mthfd1-1* showed reduced levels of glutamate, this did not affect the formation of glutathione or its redox balance E_{GSH} . Furthermore, previous studies proposed an alternative, GDC-independent pathway of photorespiration where glyoxylate is converted to formate in a nonenzymatic, H₂O₂-dependent decomposition coupled to THFS, MTHFC, MTHFD and SHMT activities that lead to the formation of serine (**Figure 28 B**) (Prabhu *et al*, 1996; Wingler *et al*, 1999; Engel *et al*, 2007). Since the redox balance was not affected in *mthfd1-1*, this mechanism was likely not an option.

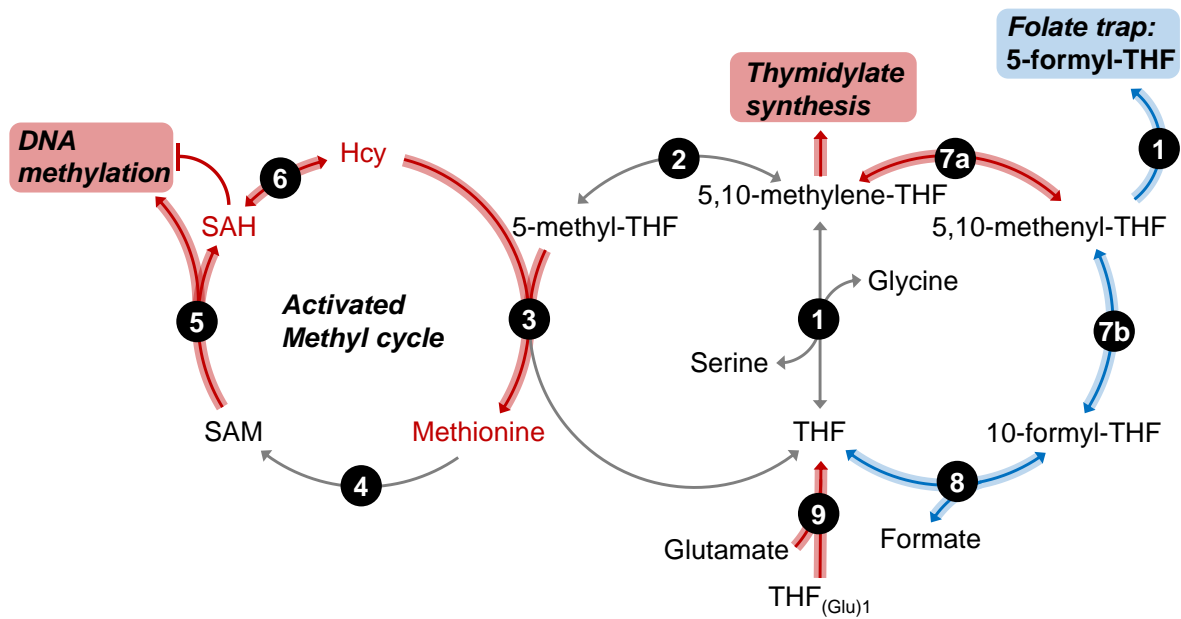
3.5 Either both or none: MTHFD1 and THFS control DNA methylation

Apparently, *MTHFD1* and *THFS* are intimately linked and important for proper DNA methylation – but only if both genes are active or silent. The reason for the strong phenotype of *mthfd1-1* is very complex and involves several aspects in the folate-mediated one-carbon cycle (**Figure 34 A**). Mutation of the MTHFD1 dehydrogenase activity diverted the flow of formate-derived one-carbon into the production of 5-formyl-THF, which most likely acts as a folate trap that sequesters one-carbon rather than an inhibitor of enzyme activity. Although there was no lack of one-carbon in the form of 5-methyl-THF for Hcy remethylation, SAH and Hcy accumulated and led to a reduced Methylation Index (MI) resulting in DNA hypomethylation (Groth *et al*, 2016). Also, it cannot be ruled out that reduction of glutamate affected the bioavailability of folates in *mthfd1-1* which would further exacerbate the bioavailability of one-carbon. In *mthfd1-1* x *thfs* mutant plants, formate is not directed towards

Discussion

the synthesis of 5-formyl-THF since the entry point with THFS is not functional (**Figure 34 B**). Instead, a slightly higher flow of serine derived one-carbon into the cytosolic folate cycle compensates for the absence of the formate-dependent pathway, which ultimately leads to the recovery of Hcy remethylation in *methf1-1 x thfs* and proper DNA methylation patterns. These results could show that THFS plays an important role in the regulation of one-carbon dynamics in the cytosol and that a stable diurnal flow of one-carbon is needed for DNA methylation.

A



B

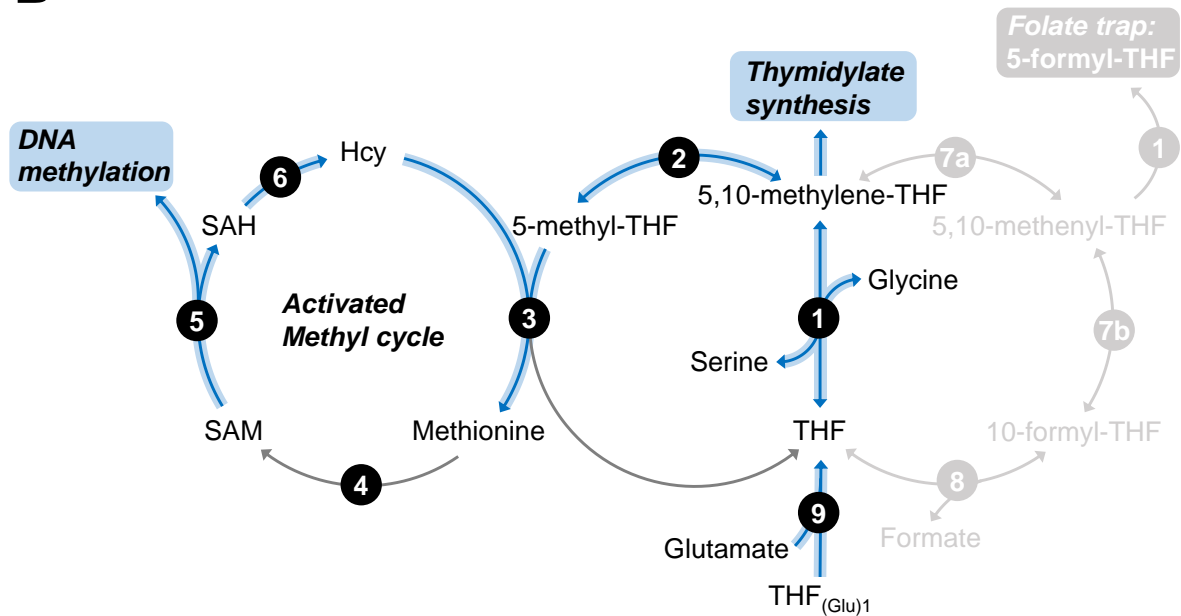


Figure 34. MTHFD1 and THFS regulate the flow of one-carbon.

The flow of one-carbon for Hcy remethylation in *mthfd1-1* (A) and *mthfd1-1 x thfs* (B). Impaired directions of one-carbon indicated in red and preferred directions in blue. (1) SERINE HYDROXYMETHYLTRANSFERASE (SHMT), (2) METHYLENETETRAHYDROFOLATE REDUCTASE (MTHFR), (3) METHIONINE SYNTHASE (MS), (4) S-ADENOSYLMETHIONINE SYNTHETASE (SAMS), (5) methyltransferases including DNA and histone methyltransferases, (6) S-ADENOSYLHOMOCYSTEINE HYDROLASE (SAHH), (7a) METHYLENETETRAHYDROFOLATE DEHYDROGENASE & (7b) METHENYLTETRAHYDROFOLATE CYCLOHYDROLASE (MTHFD), (8) 10-FORMYLTETRAHYDROFOLATE SYNTHETASE (THFS), (9) FOLYLPOLYGLUTAMATE SYNTHETASE (FPGS), THF and THF_{(Glu)1} are abbreviations for poly- and monoglutamylated tetrahydrofolate, respectively. Adapted figure (Lindermayr *et al*, 2020).

3.6 Conclusions and future perspective

The different branches and diversions of the cellular one-carbon metabolism are most likely complementing rather than competing or exclusive for specific biosynthetic pathways. Yet, the results of this study could show that the cytosolic folate-mediated one-carbon metabolism is important to sustain the MI for transmethylation reactions, especially DNA methylation and how it supports the biosynthesis of nucleotides. The flow of one-carbon depending on day length and daytime as well as the resulting dynamic concentrations of folate cycle intermediates constitute a network of metabolites that has self-regulatory properties and thereby controls DNA methylation (**Figure 35**).

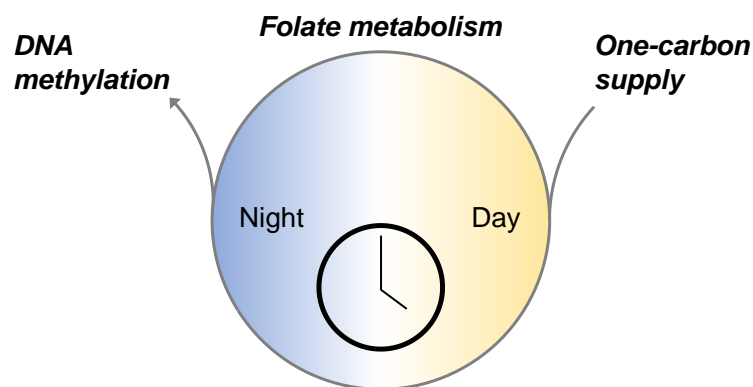


Figure 35. Diurnal regulation and supply of one-carbon control DNA methylation.

This work helped to understand how metabolism changes dynamically and together with genetic and epigenetic changes, determines the phenotype. In future, this understanding could help model phenotypic plasticity depending on the growth environment of plants. And it might also explain how epigenetic variation arises depending on metabolic factors that influence and affect epigenetic regulation. However, further research is needed to elucidate the complex cellular network of metabolic pathways and their crosstalk with epigenetic regulation. Indeed, it was shown in this study how one-carbon dynamics emerge depending on the day length and daytime, but only on a cellular level. Studies on compartmentalized one-carbon metabolism might help understand how it supports epigenetic regulation, specifically DNA methylation, depending on the molecular function it stems from such as photorespiration in mitochondria.

Discussion

This is even more important as the changing global climate affects plant carbon metabolism. In particular, increased atmospheric CO₂ concentrations and rising temperatures have a profound impact on photosynthesis and photorespiration (Dusenge *et al*, 2019). It is therefore no coincidence that recent studies have shown that increased CO₂ concentrations lead to changes in DNA methylation patterns (Panda *et al*, 2023). This underscores why epigenetic and metabolic adaptation to changing environmental conditions should be studied together.

Additionally, this work provided new insights into the complex system of one-carbon regulation. This could also help with other aspects, such as human health and nutrition. Certain metabolites and compounds called vitamins are essential for human health, including folates. Therefore, extensive efforts are made to enhance folate contents in crop plants by metabolic engineering to counteract micronutrient malnutrition (DellaPenna, 2007; Blancquaert *et al*, 2014; Strobbe & van der Straeten, 2017; La Díaz de Garza *et al*, 2019). Mammalian and plant one-carbon metabolism share great similarity in their biochemical pathways. Concepts and conclusions from studies in plants could therefore also be valid and useful in humans – especially when it comes to health (Ducker & Rabinowitz, 2017). In this context, resolving the complex system of folate synthesis, its intrinsic and environment-dependent regulatory mechanisms as well as compartmentalization are worthwhile in an holistic approach towards a One Health perspective.

4 Material and Methods

4.1 Material

4.1.1 Chemicals

5,10-methylene-THF ((6R,S)-5,10-methylene-5,6,7,8-tetrahydrofolic acid, calcium salt; product number: 16.226), THF ((6S)-5,6,7,8-tetrahydrofolic acid trihydrochloride; 16.208), 5-formyl-THF ((6R,S)-5-formyl-5,6,7,8-tetrahydrofolic acid, calcium salt; 16.220) and 5-methyl-THF ((6R,S)-5-methyl-5,6,7,8-tetrahydrofolic acid, calcium salt; 16.235) were purchased from Schircks Laboratories. 5,10-methenyl-THF ((6R,S)-5,10-methenyl-5,6,7,8-tetrahydrofolic acid) was synthesized and provided by the research group of Prof. Dr. Michael Rychlik (Technical University of Munich, Chair of Analytical Food Chemistry,). [α - ^{13}C] glycine (glycine (2- ^{13}C , 99%); product number: CLM-136-PK) and [^{13}C] formate (sodium formate (^{13}C , 99%; CLM-583-PK) were obtained from Cambridge Isotope Laboratories. BSTFA (N,O-Bis-(trimethylsilyl)-trifluoroacetamid) containing 1% TMCS (trimethylchlorosilane) and MTBSTFA (N-tert-Butyldimethylsilyl-N-methyltrifluoroacetamide) containing 1% TMCS (trimethylchlorosilane) from Sigma Aldrich were used as derivatization reagents.

4.1.2 Media

For bacterial growth of *Escherichia coli*, lysogeny broth (LB) medium containing 10 g l⁻¹ sodium chloride (NaCl), 10 g l⁻¹ tryptone, 5 g l⁻¹ yeast extract (Duchefa), adjusted to pH 7.0 using sodium hydroxide (NaOH), solidified with 20 g l⁻¹ agar (Duchefa), was used. NaCl was reduced to 5 g l⁻¹ in low-salt LB medium. Super optimal medium with catabolic repressor (SOC) medium was purchased from Invitrogen. Transformation medium for *Arabidopsis thaliana* transformation with *Agrobacterium tumefaciens* was composed of 50 g l⁻¹ sucrose, 2.13 g l⁻¹ 2-(N-morpholino)ethanesulfonic acid (MES) adjusted to pH 5.7 using potassium hydroxide (KOH), 0.5 ml Silwet L-77, 1 ml 200 mM acetosyringone (dissolved in dimethylsulfoxide (DMSO), Sigma Aldrich). For experiments where plants did not grow on soil, half- or full-strength Murashige and Skoog basal salt medium (MS, Duchefa) was used: full-strength MS: 4.4 g l⁻¹ MS basal salt, 0.5 g l⁻¹ MES hydrate (Sigma Aldrich), adjusted to pH 5.7 using KOH, solidified with 10 g l⁻¹ Gelrite (Duchefa). Half-strength MS medium was reduced to 2.2 g l⁻¹ MS basal salt. For liquid MS medium, Gelrite was omitted.

4.1.3 Vectors

Shuttle vectors for CRISPR-Cas9-mediated mutagenesis of *THFS*, pDGE332, pDGE333, pDGE335, pDGE337 and recipient vector pDGE347 for the multiplex construct generation were provided by PD Dr. Anton Schäffner (Helmholtz Munich, Institute of Biochemical Plant Pathology). *THFS*-GFP fusion constructs were generated via directional Gateway cloning into a pENTR /D-TOPO entry vector (Thermo Fisher Scientific) and ligation into the destination vector pMDC107 provided by Dr. Martin Groth (Helmholtz Munich, Institute of Functional Epigenetics).

4.1.4 Bacterial strains

Escherichia coli strains DH5 α and DB3.1 as well as *Agrobacterium tumefaciens* strain pGV3101/pMP90 were used in this study and provided by PD Dr. Anton Schäffner (Helmholtz Munich, Institute of Biochemical Plant Pathology).

4.1.5 Primers used in this study

Primers and oligonucleotides used in this study are listed in Tables 1-5.

Table 1. List of primers used for genotyping.

Gene/construct	AGI code	Primer	Sequence (5'-3')
<i>THFS</i>	AT1G50480	forward 1 forward 2 reverse	ATTTTGCCGATTTTCGGAAC TCGAATTGGTTTCGATCAAAC TCATCTGCTGTTATCGGATCC
<i>MTHFD1</i>	AT3G12290	forward 1 forward 2 forward 3 reverse 1 reverse 2	CAACGAGCAGTTGTTGTAGGCC ACAATGTCAGCTTCCCGTATG ATTTTGCCGATTTTCGGAAC TGGTGTGAGAATGTACAGTTGTG GCGGTCTATCTGAGAAACACG
<i>SDC_{pro}-GFP</i>	-	forward reverse 1 reverse 2	GTGTCAAGTTGGTGTGGGAC ACGGTACTGCTACTCTGGGA GGTTTCGCTCATGTGTTGA

Table 2. List of primers and oligonucleotides used for CRISPR-Cas9-mediated mutation of *THFS*.

Gene	AGI code	Primer	Sequence (5'-3')
<i>THFS</i>	AT1G50480	forward 1	GATGGATACTATGTTGTTG
		forward 2	CTTGCTTTCATTTATTAGC
		reverse 1	CTGAACATAATGTCACTGAA
		reverse 2	CTAAGCAACAACACTTCAC
		JS1132	AACGCTCTTTTCTCTTAGGT
		sgRNA 111 forward	ATTGGGCAAGAGTACTACCACTGT
		sgRNA 111 reverse	AAACACAGTGGTAGTACTCTTGCC
		sgRNA 243 forward	ATTGCTGTGCCCTCCGAATAAAGA
		sgRNA 243 reverse	AAACTCTTTATTCGGAGGGCACAG
		sgRNA 125 forward	ATTGTAGGCGCTTACCTCGATAAG
		sgRNA 125 reverse	AAACCTTATCGAGGTAAGCGCCTA
		sgRNA 18 forward	ATTGACCGTCACAAGGACCCACCT
sgRNA 18 reverse	AAACAGGTGGGTCCTTGTGACGGT		

Table 3. List of primers used for generating the *THFS*-GFP fusion construct.

Gene	AGI code	Primer	Sequence (5'-3')
<i>THFS</i>	AT1G50480	amplification forward	CACCGGTTTTCTTCTAGAATGG
		amplification reverse	AGAAAGGCCACGAACTTTTCC
		forward	GACTAGAGAAACTGGTTTTG
		M13 forward	GTA AACGACGGCCAG
		M13 reverse	CAGGAAACAGCTATGAC

Table 4. List of primers used for RT-qPCR.

Sequences of forward and reverse primers for *ATCOPIA28*, *SDC* and *SADHU3* were taken from previous publications (Moissiard *et al*, 2014; Groth *et al*, 2016; Yang *et al*, 2020).

Gene	AGI code	Primer	Sequence (5'-3')
<i>GI</i>	AT1G22770	forward reverse	TCTGCGGGCAACTGATGGAATG TTGCCGTGGCTTCAAGTAGCTC
<i>FKF1</i>	AT1G68050	forward reverse	TGAAGTTCTTGGTCGTAACGTGCG AATGGGTGACGCCTTTGAGC
<i>FT</i>	AT1G65480	forward reverse	GCTACAACCTGGAACAACCTTTGGC ACTGTTTGCTGCCAAGCTGTC
<i>ATCOPIA28</i>	-	forward reverse	AGTCCTTTTGGTTGCTGAACA CCGGATGTAGCAACATTCAC
<i>SDC</i>	-	forward reverse	AAAGATCTGCACAGGCCAAAGC TTGACCAATCACCCATTTCTCTCC
<i>SADHU3</i>	-	forward reverse	TATGTTTGCAGGTGGGTGCTGTG ACAGCCTAAACCCACCAATCCG
<i>CCA1</i>	AT2G46830	forward reverse	TCGAAAGACGGGAAGTGAACG GTCGATCTTCATTGGCCATCTCAG
<i>PRR5</i>	AT5G24470	forward reverse	CAGCTTTCACACGGTACGTTTAC TTGGAGGCGGTTTCAGATGTATTG
<i>THFS</i>	AT1G50480	forward reverse	AAGTCATATGGAGCCAGTGGTGT CATCTCAATCTGTTTCTCTGCCTGG
<i>MTHFD1</i>	AT3G12290	forward reverse	ATCTGAGAAACACGGCAAGGTC TCTGGTAGGCCACGTCAAATG
<i>SHM4</i>	AT4G13930	forward reverse	AAAGCCAATGCTGTTGCCCTTG CAGAGCTTCTCAACCTTGTTC
<i>SAHH1</i>	AT4G13940	forward reverse	GACTCTGTCACCAAGAGCAAGTTC AGACCATCAGGGAGTGAGTGAC
<i>PP2A</i>	AT1G13320	forward reverse	TATCGGATGACGATTCTTCGTGCAG GCTTGGTCGACTATCGGAATGAGAG

Table 5. Primers used for McrBC-qPCR.

Locus	AGI code	Primer	Sequence (5'-3')
<i>MG5</i>	-	forward reverse	TGACGACGACTATGGTGAACCTCC ATGCCAACGGTGACAGAGAG

4.2 Methods

4.2.1 Plant material

Arabidopsis thaliana plants used in this study were of the Columbia-0 ecotype. The *mthfd1-1* mutant of *MTHFD1* (AT3G12290) and wild type transgenic lines have been characterized previously (Groth *et al*, 2016). T-DNA insertion mutants of *THFS* (AT1G50480) *thfs* (SALK_067510) and *MTHFD1 mthfd1-3* (SALK_015165) were obtained from the *Arabidopsis* Biological Research Center (Ohio State University). *thfs* mutants were crossed with wt plants carrying *SDC_{pro}-GFP*. The *mthfd1-1* x *thfs* complemented double mutant was crossed by Dr.

Martin Groth. *methf1-3* was crossed with *thfs*. Segregation analyses of mutations with wild type, hetero- or homozygous alleles was achieved with gene-specific primers (**Table 1**).

4.2.2 Plant growth and harvest

Plants were grown under two regimes in growth chambers (Weiss Technik & Vötsch): long day (LD) growth with a light/dark cycle of 16/8 h at 23/20 °C, 65 % relative humidity and a light intensity of 100 $\mu\text{mol m}^{-2} \text{s}^{-1}$ as well as short day (SD) growth with the same configuration as LD except for a light/dark cycle of 10/14 h. Time course harvests of plant material was conducted after 3 weeks for LD and 4 weeks of growth for SD at four timepoints, if not indicated otherwise: 0, 6, 12 and 18 h after dawn. Rosette leaves were collected in liquid nitrogen and pulverized in a bead mill (Retsch TissueLyser, Qiagen) using two 2 mm steel beads. If not stated otherwise, plants were grown on soil, a mixture of 4 parts multiplication substrate (Floragard) and 1 part quartz sand.

4.2.3 Transformation of *Escherichia coli* cells

Plasmid DNA was transformed into *E. coli* cells (DH5 α for cloning reactions and DB3.1 for plasmid DNA propagation) using heat shock. For this purpose, 1 μl of plasmid DNA (50 – 100 ng after cloning reactions, 1 – 10 ng for plasmid DNA propagation) was gently mixed with 50 μl of competent *E. coli* cells and incubated on ice for 15 min. After heat shock at 42 °C for 30 s, the cell suspension was transferred back onto ice. 250 μl of SOC medium without antibiotics was added. The mixture was incubated at 300 rpm and 37 °C for 1 h before it was spread on solid LB plates with antibiotics specific for plasmid resistances and continued to grow at 37 °C ON.

4.2.4 Transformation of *Agrobacterium tumefaciens* cells

Isolated plasmid DNA was used for transformation of competent *Agrobacterium tumefaciens* cells (strain: pGV3101/pMP90) via electroporation. 100 ng plasmid DNA was dissolved in 50 μl competent cells and transferred to a Gene Pulser Electroporation Cuvette with a 0.1 cm electrode gap (Bio-Rad). Electroporation was performed on a Gene Pulser Electroporator (Bio-Rad) with the following settings: capacitance: 25 μF , resistance: 400 ohm, voltage: 1.25 kV. Afterwards, 500 μl of SOC medium without antibiotics were added and the suspension was transferred to a sterile reaction tube and incubated for 2 h at 28 °C with gentle agitation. 50 μl of bacterial suspension were transferred to solid LB plates with appropriate antibiotics: 100 μg

ml⁻¹ rifampicin and 25 µg ml⁻¹ gentamycin for *Agrobacterium tumefaciens* and antibiotics specific for plasmid resistances.

4.2.5 Transformation of *Arabidopsis* with *Agrobacterium tumefaciens* cells

Arabidopsis plants were grown for 4 weeks under LD conditions until flowers started to develop. A single colony of transformed *Agrobacterium tumefaciens* was inoculated in 2 ml of liquid LB medium with appropriate antibiotics and grown ON at 28 °C and 200 rpm. This starter culture was transferred to a 1 l Erlenmeyer flask containing 250 ml low-salt LB medium with antibiotics and was grown ON at 28 °C and 200 rpm. Cells were pelleted at 6000 rpm and RT for 10 min and resuspended in *Arabidopsis* transformation medium. After incubation at 28 °C and 200 rpm for 1.5 h, plants were dipped into the bacterial suspension for 5 min. Plants were covered for 24 h and kept at low light before they returned to grow under initial LD conditions for 3 – 4 more weeks before seeds were harvested.

4.2.6 Isolation of genomic DNA from plant material

Per sample, 100 mg of pulverized material were dissolved in 800 µl cetyltrimethylammonium bromide (CTAB) buffer (2.5 % (w/v) CTAB, 1.42 M NaCl, 20 mM ethylenediaminetetraacetic acid (EDTA), 100 mM tris(hydroxymethyl)aminomethane (Tris) adjusted to pH 8.0 with HCl, 1 % (w/v) polyvinylpyrrolidone with an average molecular weight of 40,000 Dalton, 0.0001 % (v/v) β-mercaptoethanol). After incubation at 65 °C for 20 min, samples were centrifuged at 16,000 rcf and 16 °C for 10 min. 700 µl of clear supernatant were transferred into a new reaction tube and mixed with 550 µl chloroform/isoamylalcohol (24:1) into a turbid emulsion. Samples were incubated at RT for 5 min and subsequently centrifuged at 12,000 rcf and 16 °C for 10 min. 550 µl of the upper, aqueous phase were transferred into a new reaction tube and mixed with 385 µl 100 % isopropanol by inverting the reaction tube ten times. DNA was precipitated ON at -20 °C and collected in a pellet by centrifugation at 16,000 rcf and 4 °C for 10 min. Supernatants were removed and pellets washed with 70 % ice-cold ethanol by inverting the reaction tube three times. Samples were centrifuged at 16,000 rcf and 4 °C for 5 min and supernatants were thoroughly removed afterwards. Finally, pellets were air-dried for 10 min before they were resolved in 50 µl water at 65 °C for 15 min.

4.2.7 Polymerase chain reaction, restriction enzyme digestion, agarose gel electrophoresis, PCR gel extraction and Sanger sequencing

A single polymerase chain reaction (PCR) had a volume of 20 μl and contained 1 μl DNA template, 4 μl 5x reaction buffer (Bioline), 2 μl 2.5 mM deoxyribonucleotide triphosphates (dNTPs), 1 μl 5 μM forward primer, 1 μl 5 μM reverse primer, 1 μl 50 mM magnesium chloride (MgCl_2), 0.2 μl MangoTaq Polymerase (Bioline) and 9.8 μl water. Primers from **Table 1** were used. PCRs were conducted in a T100 Thermal Cycler (Bio-Rad) with the following reaction program: 95 °C for 3 min, followed by 34 cycles of 95 °C for 30 s, 56 °C for 30 s, 72 °C for 30 s kb^{-1} and a final extension at 72 °C for 5 min. For colony PCR of positive transformants after transformation, the DNA template was substituted with a small amount of bacterial cell suspension – for this, a pipette tip was used to pick up bacterial suspension from singled colonies and to transfer them to PCR reactions. PCR products of *MTHFD1/mthfd1-1* genotyping reactions were treated by restriction enzyme digestion. 3 μl PCR product were incubated with 1.7 μl CutSmart buffer (New England Biolabs), 0.4 μl HpaII (New England Biolabs) and 14.9 μl water in total volume of 20 μl for 2 h at 37 °C. After reactions were inactivated at 65 °C for 10 min, digested PCR products were separated by gel electrophoresis using 3 % (w/v) low-melt agarose dissolved in TAE buffer (Tris Acetate-EDTA; 40 mM Tris, 20 mM acetic acid, 1 mM EDTA) containing 0.5 $\mu\text{g ml}^{-1}$ ethidium bromide. Non-digested PCR amplification products were separated by gel electrophoresis using 1 % (w/v) agarose. A Gel Doc2000 system (Bio-Rad) was used to visualize nucleic acids with UV light. PCR products were extracted from agarose gels using QIAquick Gel Extraction Kits (Qiagen) according to the manufacturer's instructions. Sanger sequencing was performed by Eurofins Genomics Germany GmbH. Template, forward and reverse primers were provided in concentrations according to the sequencing service.

4.2.8 *SDC_{pro}-GFP* expression analyses

SDC_{pro}-GFP expression was analyzed by imaging and quantification of GFP fluorescence. Images were captured via confocal microscopy (Leica TCS SP8) with a 40x water immersion objective and sequential scanning at an excitation wavelength of 488 nm and detection at 495 – 525 nm for GFP and 682 – 690 nm for chlorophyll. Images were captured using the Leica Application Suite X software (Leica Microsystems). For each sample, z-stacks with 10 optical slices and constant step size were acquired and combined into maximum projections along the z axis using the Fiji software. Fiji was also used for the quantification of the corrected total cell fluorescence (CTCF).

4.2.9 Subcellular localization of THFS

For the generation of the C-terminally tagged fusion protein THFS-GFP, genomic DNA from *Arabidopsis thaliana* wild type ecotype Col-0 was amplified with Phusion High-Fidelity DNA Polymerase (Thermo Fisher Scientific) and amplification primers (**Table 3**). The reaction mixture of 50 μ l contained 1 μ l DNA template, 10 μ l 5x Phusion High-Fidelity buffer (Thermo Fisher Scientific), 4 μ l 2.5 mM dNTPs, 5 μ l 5 μ M of each amplification primer, 0.5 μ l Phusion Polymerase (Thermo Fisher Scientific) and 24.5 μ l water. The PCR reaction was conducted in a T100 Thermal Cycler (Bio-Rad) with the following reaction program: 98 °C for 1 min, followed by 34 cycles of 98 °C for 10 s, 60 °C for 30 s, 72 °C for 3 min and a final extension at 72 °C for 5 min. The amplified product included 1476 bp ahead of the 5' start codon of *THFS* to retain the native promoter, while the Stop codon was excluded. The product was separated by gel electrophoresis using 1 % (w/v) agarose dissolved in TAE buffer (Tris Acetate-EDTA; 40 mM Tris, 20 mM acetic acid, 1 mM EDTA) containing 0.5 μ g ml⁻¹ ethidium bromide. A Gel Doc2000 system (Bio-Rad) was used to visualize nucleic acids with UV light. The PCR product was extracted from the agarose gel using a QIAquick Gel Extraction Kit (Qiagen) according to the manufacturer's instructions. Sanger sequencing was performed by Eurofins Genomics Germany GmbH. Template, M13 forward and M13 reverse primers (**Table 3**) were provided in concentrations according to the sequencing service. Directional Gateway cloning of the PCR product into the pENTR /D-TOPO entry vector (Thermo Fisher Scientific) was performed according to the manufacturer's manual. After transformation of the pENTR /D-TOPO entry vector containing *THFS* coding and promoter region into DH5 α *E. coli* cells, colony PCR using Mango *Taq* Polymerase (Bioline) and primer pair genotyping forward/M13 reverse was used to identify positive transformants. After plasmids of positive transformants were isolated using a QIAprep Spin Miniprep Kit (Qiagen) according to the manufacturer's manual, Gateway LR Clonase II Enzyme-Mix (Thermo Fisher Scientific) was used for recombination between the entry vector and the destination vector pMDC107 according to the manual. The destination vector containing *THFS* and the native promoter fused to GFP was transformed into *Agrobacterium tumefaciens* cells and subsequently into *Arabidopsis thaliana*. Positive transformants were identified by selection on solidified half-strength MS plates containing 40 μ g ml⁻¹ hygromycin. THFS-GFP expression was analyzed with the same settings for confocal microscopy used for the analysis of SDC_{pro}-GFP fluorescence.

4.2.10 CRISPR-Cas9-mediated mutation of *THFS*

Complementation of *methfd1-1* x *thfs* was verified using CRISPR-Cas9-mediated gene editing of *THFS* in the *methfd1-1* genetic background utilizing Cas9 multiplexing vector systems (Ordon

et al, 2017; Stuttmann *et al*, 2021). Designing sgRNAs, generation of shuttle vectors containing sgRNAs and ligation into the destination vector was performed by Dr. Inonge Gross (Helmholtz Munich, Institute of Biochemical Plant Pathology). Specific sgRNA sequences targeting exon 2 and 3 were selected using CRISPOR (**Table 2**) (Jean-Paul Concordet & Maximilian Haeussler) and verified using Sanger sequencing. Pairs of hybridized sgRNAs were inserted into shuttle vectors: oligonucleotides sgRNA 111 forward/reverse into shuttle vector pDGE332, sgRNA 243 forward/reverse into pDGE333, sgRNA 125 forward/reverse into pDGE335 and sgRNA 18 forward/reverse into pDGE337 using Golden Gate transformation. For this, pairs of complementary sgRNAs of 10 μ M were denatured at 98 °C for 5 min, before they were diluted to 50 fM. Hybridized sgRNAs were introduced into vectors in a 10 μ l reaction volume containing 50 fM complementary sgRNAs, 20 fM shuttle vector, 1x Ligation buffer (Thermo Fisher Scientific), 0.1 mg ml⁻¹ Bovine Serum Albumin (BSA), 5 U Bpil and 0.5 U T4 DNA Ligase (Thermo Fisher Scientific) with following reaction cycles: 15 cycles alternating 2 min at 37 °C and 5 min at 16 °C followed by two final steps at 50 °C and 80 °C for 10 min each, performed in a T100 Thermal Cycler (Bio-Rad). After transformation of whole 10 μ l reactions into DH5 α *E. coli* cells and incubation at 37 °C ON, shuttle vectors containing sgRNAs were isolated using a QIAprep Spin Miniprep Kit (Qiagen) according to the manufacturer's manual. Insertion of sgRNAs was verified using restriction enzyme digestion of the plasmid DNA using PvuII (Thermo Fisher Scientific) according to the manufacturer's manual. Afterwards, shuttle vectors were assembled in the recipient vector pDGE437 in a 20 μ l reaction volume containing 4 fM recipient vector, 15 fM shuttle vectors, 1x Ligation buffer (Thermo Fisher Scientific), 0.1 mg ml⁻¹ BSA, 10 U Bsal and 1 U T4 DNA Ligase (Thermo Fisher Scientific) with same cycling conditions as sgRNA cloning into shuttle vectors. Reactions were transformed into DH5 α *E. coli* cells and incubated at 37 °C ON. After isolation of the multiplex construct containing sgRNAs, the vector was sequenced using Sanger sequencing with the genotyping primer JS1132 (**Table 2**). Afterwards, the vector was transformed into *Agrobacterium tumefaciens* cells and subsequently into *Arabidopsis thaliana*. Positive transformants were selected by RFP expression in seed coats.

4.2.11 Whole genome bisulfite sequencing

Genomic DNA was isolated from 3-week-old rosette leaves or 2-week-old seedlings. DNA concentrations were determined using a Qubit dsDNA High Sensitivity Assay Kit (Thermo Fisher Scientific) and a Qubit 2.0 Fluorometer (Thermo Fisher Scientific). DNA methylation analysis of 3-week-old LD grown wild type, *mthfd1-1*, *thfs* and *mthfd1-1* x *thfs* plants was conducted by the whole genome bisulfite sequencing service of BGI Genomics. This included

library preparation including DNA fragmentation, bisulfite treatment and sequencing at 100 bp length. DMRs were defined as previously reported (Groth *et al*, 2016). Genome-wide DNA methylation levels of 3-week-old CRISPR-Cas9 mutant lines *thfs-20* and *thfs-23* as well as 2-week-old *thfs* and *mthfd1-1 x thfs* seedlings from exogenous folate application were analyzed using the whole genome bisulfite sequencing service from Novogene. Again, the sequencing service included DNA fragmentation, bisulfite conversion and sequencing at 100 bp length. However, samples analyzed by Novogene were sequenced with an average coverage of approximately 2X to assess global DNA methylation levels. Bioinformatic analyses of sequencing results were conducted by Dr. Martin Groth (Helmholtz Munich, Institute of Functional Epigenetics).

4.2.12 Gene expression analyses

100 mg of *Arabidopsis thaliana* rosette leaves were used per sample for total RNA extraction using a RNeasy Plant Mini Kit (Qiagen) with on-column DNA digestion using a RNase-Free DNase Set (Qiagen) according to the manufacturer's guidelines. RNA integrity and concentration analyses were carried out with a Nanodrop ND-1000 spectrophotometer (Kisker-biotech) by measuring absorptions at 260 nm and 280 nm. 4 µg of total RNA were used for cDNA synthesis using SuperScript II Reverse Transcriptase (Invitrogen) together with Random Hexamer Primer (Invitrogen) and RNase inhibitor RNaseOut (Invitrogen) according to the manufacturer's instructions. Real-time PCR quantification was performed using Power SYBR Green Master Mix (Applied Biosystems) and a 7500 real-time PCR system (Applied Biosystems). To amplify transcripts, 2 µl of 1:2 diluted cDNA were added to a 8 µl reaction mix containing 1x Power SYBR Green Master Mix (Applied Biosystems) and 5 µM of each primer (**Table 4**) with following reaction cycles: 2 min at 50 °C before initial denaturation for 10 min at 95 °C, 40 cycles with 15 s at 95 °C, 60 s at 60 °C. Relative expression was normalized to the reference gene *PP2A* and timepoint 0.

4.2.13 Enzymatic activity analyses.

Spectrophotometric MTHFD and THFS activity measurements were adapted from previous methods (Vickers *et al*, 2009; Appling & Rabinowitz, 1985). Assays of THFS activity were performed by Jisha Suresh Kumar (Helmholtz Munich, Institute of Biochemical Plant Pathology). 30 mg of plant material were resuspended in 700 µl extraction buffer (25 mM Gomori pH 7.5 (mixture of 81.2 % (v/v) 25 mM dipotassium hydrogen orthophosphate (K₂HPO₄) and 18.8 % (v/v) 25 mM potassium dihydrogenphosphate (KH₂PO₄)), 10 mM potassium chloride (KCl), 1mM phenylmethylsulfonyl fluoride (PMSF), 1mM benzamidine and

Material and Methods

10 mM β -mercaptoethanol), incubated at 1400 rpm and 4 °C for 5 min and subsequently centrifuged at 15,000 rcf and 4 °C for 15 min to isolate total soluble proteins. 50 μ l of clear lysate were incubated with 75 μ l reaction buffer (for MTHFD: 25 mM Gomori pH 7.5, 10 mM β -mercaptoethanol, 100 mM KCl, 0.6 mM NADP⁺, 1.5 mM 5,10-methylene-THF; for THFS: 25 mM Gomori pH 7.5, 10 mM β -mercaptoethanol, 100 mM KCl, 10 mM magnesium sulfate (MgSO₄), 5 mM ATP, 1 mM THF, 200 mM sodium formate) at 30 °C in a microplate reader (TECAN Infinite M+1000 Pro microplate reader). THF was dissolved in 250 mM triethanolamine adjusted to pH 7.0 with HCl, 40 mM β -mercaptoethanol (Vickers *et al*, 2009) and 5,10-methylene-THF was dissolved in desalted water in an ultrasonication bath right before the reactions were initiated. Reactions were stopped after 0, 5 and 10 min through addition of 25 μ l 2 M HCl. Absorbance of the reaction product 5,10-methenyl-THF was measured at 350 nm with an extinction coefficient of 12 720 M⁻¹ cm⁻¹.

LC-MS based MTHFR and SHMT activity measurements were adapted from methods previously described (Zhang *et al*, 2008; Roje *et al*, 1999) and performed in cooperation with Birgit Lange who operated LC-MS and quantified metabolites from chromatograms (Helmholtz Munich, Institute of Biochemical Plant Pathology). Total soluble proteins were isolated from 30 mg of plant material by addition of 300 μ l extraction buffer (for MTHFR: 200 mM 3-(N-morpholino)propanesulfonic acid (MOPS) adjusted to pH 7.5 with NaOH, 10 % glycerol, 10 mM EDTA, 10 mM β -mercaptoethanol, 1 mM PMSF, 1mM benzamidine; for SHMT: 200 mM MOPS adjusted to pH 7.5 with NaOH, 10 % glycerol, 10 mM EDTA, 10 mM tris(hydroxypropyl)phosphine, 100 μ M pyridoxal-5-phosphate (PLP), 1 mM PMSF, 1 mM benzamidine) and incubation at 1400 rpm and 4 °C for 5 min in a vortex mixer. The cell debris was collected by dual centrifugation at 15,000 rcf and 4 °C for 15 min. 50 μ l of clear supernatant was incubated with 50 μ l reaction buffer (for MTHFR: 50 mM MOPS adjusted to pH 7.5 with NaOH, 1 mM 5,10-methylene-THF, 0.1 mM NADPH, 0.1 mM glucose-6-phosphate, 0.1 U of glucose-6-phosphate dehydrogenase (Sigma Aldrich), 4 mM β -mercaptoethanol; for SHMT: 50 mM MOPS adjusted to pH 7.5 with NaOH, 1 mM THF, 2 mM serine, 4 mM tris(hydroxypropyl)phosphine, 0.5 μ M PLP) at 30 °C for 20 min. Reactions were quenched with 25 μ l 100 mM DTT. For SHMT activity measurement, 50 μ l of freshly prepared 100 mM sodium borohydride (NaBH₄) were added to reactions and incubated for 15 min at 37 °C to drive the formation of 5-methyl-THF. For both enzymes, reactions were boiled at 95 °C for 3 min before 25 μ l 0.6 M DTT were added to avoid product decomposition (Zhang *et al*, 2008). Denatured protein was pelleted and supernatants containing the reaction product 5-methyl-THF were analyzed by Ultra Performance Liquid Chromatography (UPLC) Ultra-High Resolution (UHR) tandem quadrupole/Time-Of-Flight (QqToF) Mass Spectrometry (MS) on an UltiMate 3000RS

Material and Methods

UPLC system (Thermo Fisher Scientific) coupled to an Impact II with Apollo II ESI source (Bruker Daltonics) Chromatographic separation was performed on a BEH C18 reverse-phase column (150 x 2.1 mm, 1.7 μm particles, Waters Technologies) with eluents A (LC-MS grade water with 0.1 % formic acid) and B (100 % acetonitrile). Gradient elution started with an isocratic hold with 5 % B for 9 min, followed by 40 % B until 11 min, 95 % B until 13 min, decreasing to 40 % B until 14 min and finally 5 % B until 17 min. To measure 5-methyl-THF, 3 μl per sample were injected and separated at a flow rate of 0.3 ml min⁻¹ and a constant column temperature of 30 °C. Analytes were charged in negative-ionization mode with following settings: nebulizer pressure set to 2 bar, dry gas flow at 10 l min⁻¹, dry gas temperature at 220 °C and end plate offset at 500 V. Mass spectra were acquired in a mass-to-charge (m/z) range of 50 – 1300. 5-methyl-THF and 5-formyl-THF were identified using pure standards and normalized to the internal standard 10-camphorsulfonic acid (Sigma Aldrich) with the following m/z ratios and Retention Times (RT): 5-methyl-THF: m/z 456.1626 and RT: 6.3 min, 5-formyl-THF: m/z 470.1418 and RT: 11.8 min, 10-camphorsulfonic acid: m/z 231.0695 and RT: 12.3 min.

Desalted extracts for SHMT inhibition measurements were prepared similarly with small changes: 100 mg of plant material were dissolved in 500 μl extraction buffer (same composition as used for non-desalted extracts above). After dual centrifugation, clear supernatants were desalted with PD-10 Desalting Columns according to the manufacturer's guidelines (GE Healthcare). PD-10 columns were equilibrated with equilibration buffer (50 mM MOPS adjusted to pH 7.5 with NaOH, 10 % glycerol, 5 mM tris(hydroxypropyl)phosphine, 100 μM PLP), before protein extracts were added. Enzyme reactions, chemical conversion and measurements via LC-MS were carried out as described above.

4.2.14 Folate quantification

Plants were grown on soil under LD and SD conditions for 3 and 4 weeks, respectively, and harvested in liquid nitrogen at timepoints 0, 6, 12 and 18 hours after dawn. Quantification of folates was performed by Lisa Obermaier and Prof. Dr. Michael Rychlik (Technical University of Munich, Chair of Analytical Food Chemistry,).

4.2.15 Analyses of DNA methylation level

DNA methylation levels were analyzed using McrBC-qPCR (Bond & Baulcombe, 2015), performed by Gabriele Barthel (Helmholtz Munich, Institute of Biochemical Plant Pathology). DNA concentrations were determined using a Qubit dsDNA High Sensitivity Assay Kit (Thermo

Material and Methods

Fisher Scientific) and a Qubit 2.0 Fluorometer (Thermo Fisher Scientific). A 100 µl reaction volume contained 100 ng DNA, 1x NEBuffer 2 (50 mM NaCl, 10 mM Tris pH 7.9 adjusted with HCl, 10 mM MgCl₂, 1 mM DTT, New England Biolabs), 20 µg Recombinant Albumin and 1 mM GTP. The reaction was split into two: one was subjected to DNA digestion using 10 U McrBC (New England Biolabs) while the other one was treated as control with 1 µl of 50 % (v/v) glycerol. Both were incubated at 37 °C for 6 h. Reactions were stopped by heat inactivation at 65 °C for 20 min. For quantitative PCR (qPCR), 2 µl of control-treated or digested DNA were added to 18 µl containing 5 µM of each Primer (**Table 5**) and 1x Power SYBR Green Master Mix (Applied Biosystems). The qPCR was carried out in a 7500 real-time PCR system (Applied Biosystems) with following cycling conditions: 2 min at 50 °C before initial denaturation at 95 °C for 10 min, 40 cycles each at 95 °C for 15 s and 60 s at 60 °C. Results were calculated as percentage of methylation $[(\{1/2^{-Ct_{\text{digested}}}\}/\{1/2^{-Ct_{\text{undigested}}}\}) \times 100]$.

4.2.16 Quantification of thiols, amino acids, and adenosine nucleotides

Plants were grown on soil under LD and SD conditions for 3 and 4 weeks, respectively, and harvested in liquid nitrogen at timepoints 0, 6, 12 and 18 hours after dawn. Quantification of metabolites was carried out as previously reported (Groth *et al*, 2016) by Dr. Gernot Poschet, Dr. Markus Wirtz and Prof. Dr. Rüdiger Hell (Heidelberg University, Centre for Organismal Studies).

4.2.17 roGFP measurement

Monitoring and quantification of redox-sensitive GRX1-roGFP2 expression was performed by Dr. José Manuel Ugalde and Prof. Dr. Andreas Meyer (University of Bonn, Institute of Crop Science and Resource Conservation). Wild type and *mthfd1-1* plants harboring the GRX1-roGFP2 construct were generated by Dr. Martin Groth (Helmholtz Munich, Institute of Functional Epigenetics).

4.2.18 Isotopic labeling analyses

Arabidopsis thaliana seeds were surface sterilized with 40 % (v/v) commercial bleach at 1500 rpm for 10 min and washed six times with sterile water afterwards. Seeds were stratified for two days at 4 °C before they were grown under SD or LD conditions on a shaker at 100 rpm. Approximately 30 seeds were provided per well in six-well dishes containing 2.5 ml half-strength MS basal salt medium with 0.5 % sucrose adjusted to pH 5.7 using KOH. After nine days of growth, plants had grown upright and growth media were replaced: short-term, free

Material and Methods

amino acid labeling samples continued to grow in half-strength MS medium without sucrose adjusted to pH 5.7 using KOH, while growth media for long-term nucleobase labeling samples were supplemented with either 1 mM of labeled [α - ^{13}C] glycine or [^{13}C] formate or 1 mM unlabeled glycine or formate used for correction of naturally occurring isotopes. After 11 and 13 days, renewal of growth media supplemented with labeled/unlabeled substrates was repeated for long-term nucleobase labeling samples. Plant material was harvested after 15 days of growth by washing seedlings thoroughly with desalted water to remove residual growth media, drying material carefully with tissues and flash freezing whole seedlings in liquid nitrogen without roots. Growth medium with labeled/unlabeled substrates was provided to short-term free amino acid labeling samples 13 days after growth in two setups: aligned to the start of the light period or aligned to the beginning of the dark period. Plant material was harvested like long-term labeling samples but at timepoints 4, 8 and 16 hours after the labeling media were supplied and additionally after 24 hours in samples aligned to the light period. Seedlings were ground in a bead mill in liquid nitrogen (Retsch TissueLyser, Qiagen).

Per sample, 100 mg pulverized plant material were used for genomic DNA isolation. DNA was dissolved in ultrapure water using ultrasonication for 10 min, transferred to 2 ml amber glass vials with a 11 mm crimp top (Thermo Fisher Scientific) and dried under a constant stream of gaseous nitrogen for 30 min. For the hydrolysis of DNA into nucleobases, 100 μl of neat formic acid were added to samples. Vials were briefly flushed with gaseous nitrogen and wiped with dust-free Kimwipes (Kimtech) before they were tightly closed with 11 mm crimp caps with PTFE/silicone septa (Agilent). After incubation at 150 $^{\circ}\text{C}$ for 6 h, samples were dried under a constant stream of gaseous nitrogen. Nucleobases were derivatized as followed: 50 μl acetonitrile and 50 μl BSTFA were added to samples which were then briefly flushed with gaseous nitrogen, wiped with dust-free Kimwipes (Kimtech) and tightly closed with 11 mm crimp caps with PTFE/silicone septa (Agilent). Samples were briefly mixed and incubated at 150 $^{\circ}\text{C}$ for 60 min. The derivatized nucleobases were transferred to 250 μl glass inserts (Merck) using glass pipettes and placed back into the 2 ml amber glass vials. Free amino acid extraction was adapted from previous methods (Pérez-Palacios *et al*, 2015). 100 mg of pulverized plant material were dissolved in 1 ml 1 M HCl by incubation at 60 $^{\circ}\text{C}$ and 500 rpm for 30 min. After centrifugation at 10,000 rpm and 4 $^{\circ}\text{C}$ for 15 min, 800 μl of the supernatant were transferred to a new reaction tube. Centrifugation was repeated, thereafter 250 μl of clear supernatant were added to 2 ml amber vials and dried under a constant stream of gaseous nitrogen for 60 min. Free amino acids were derivatized like nucleobases with following changes: BSTFA was substituted with MTBSTFA, and derivatization lasted for 90 min at 60 $^{\circ}\text{C}$.

Material and Methods

Stable isotope enrichment in derivatized nucleobases and free amino acid samples was determined by Thermal Desorption Gas Chromatography Mass Spectrometry (TD-GC-MS; thermal desorption unit (TDU), Gerstel; GC: 7890A; MS: 5975C, both Agilent Technologies) together with Dr. Andrea Ghirardo, Baris Weber and Prof. Dr. Jörg-Peter Schnitzler (Helmholtz Munich, Research Unit Environmental Simulation). Dr. Andrea Ghirardo developed and optimized the separation method and Baris Weber helped with the preparation of samples. 1 μl per sample was injected into the TDU and vaporized by increasing the temperature from 40 $^{\circ}\text{C}$ to 280 $^{\circ}\text{C}$ at a rate of 360 $^{\circ}\text{C min}^{-1}$ and a hold for 2.5 min. Vaporized compounds were concentrated by cryofocusing using a Cooled Injection System (CIS, Gerstel) at -50 $^{\circ}\text{C}$ before desorption in splitless mode to 280 $^{\circ}\text{C}$ at 6 $^{\circ}\text{C s}^{-1}$ and holding for 2.5 min. Compounds were separated on a J&W 122-5562G_1- DB-5MS + 10m DG column (Agilent Technologies, 70 m x 250 μm x 0.25 μm) with a 1 ml min^{-1} constant flow rate of helium as carrier gas. Separation of compounds lasted for 31.5 min and started at 90 $^{\circ}\text{C}$ followed by a ramp up to 150 $^{\circ}\text{C}$ at a rate of 30 $^{\circ}\text{C min}^{-1}$. Afterwards, temperature rose to 260 $^{\circ}\text{C}$ at a rate of 5 $^{\circ}\text{C min}^{-1}$ and eventually to 310 $^{\circ}\text{C}$ at 100 $^{\circ}\text{C min}^{-1}$ with a final hold of 7 min. Target compounds were unambiguously identified by mass spectra and retention time comparison with pure standards. Mass spectral peaks of target compounds were acquired from Total Ion Chromatogram (TIC) and Selected Ion Monitoring (SIM) mode. In order to obtain label enrichment in target compounds, SIM parameters were set in groups with mass-to-charge ratios (m/z) as followed for amino acids: glycine: start time: 12.1 min; ions: M+0: m/z 246.0, M+1: m/z 247.0, M+2: m/z 248.0, M+3: m/z 249.0; dwell time each: 10 ms, methionine: start time: 19.1 min; ions: M+0: m/z 320.0, M+1: m/z 321.0, M+2: m/z 322.0, M+3: m/z 323.0; dwell time each: 5 ms, serine: start time: 19.9 min; ions: M+0: m/z 390.0, M+1: m/z 391.0, M+2: m/z 392.0, M+3: m/z 393.0; dwell time each: 10 ms, and as followed for nucleobases: 5-methylcytosine: start time: 11.78 min; ions: M+0: m/z 254.0, M+1: m/z 255.0, M+2: m/z 256.0, M+3: m/z 257.0; dwell time each: 5 ms, adenine: start time: 17.3 min; ions: M+0: m/z 264.0, M+1: m/z 265.0, M+2: m/z 266.0, M+3: m/z 267.0; dwell time each: 10 ms, thymine: start time: 8.5 min; ions: M+0: m/z 255.0, M+1: m/z 256.0, M+2: m/z 257.0, M+3: m/z 258.0; dwell time each: 5 ms.

4.2.19 Automated plant phenotyping

Automated phenotyping of *Arabidopsis thaliana* plants was carried out on a PlantScreen platform (Photon Systems Instruments, abbreviated PSI) under SD and LD growth conditions. In a controlled growth environment, plants grew on a mixture of 4 parts multiplication substrate (Florigard) and 1 part quartz sand with 60 % relative humidity and a light intensity of 110 μmol

$\text{m}^{-2} \text{s}^{-1}$. A built-in balance kept pots at an equal weight while RGB pictures were taken for plant morphology analysis of foliage.

4.2.20 Root growth analysis

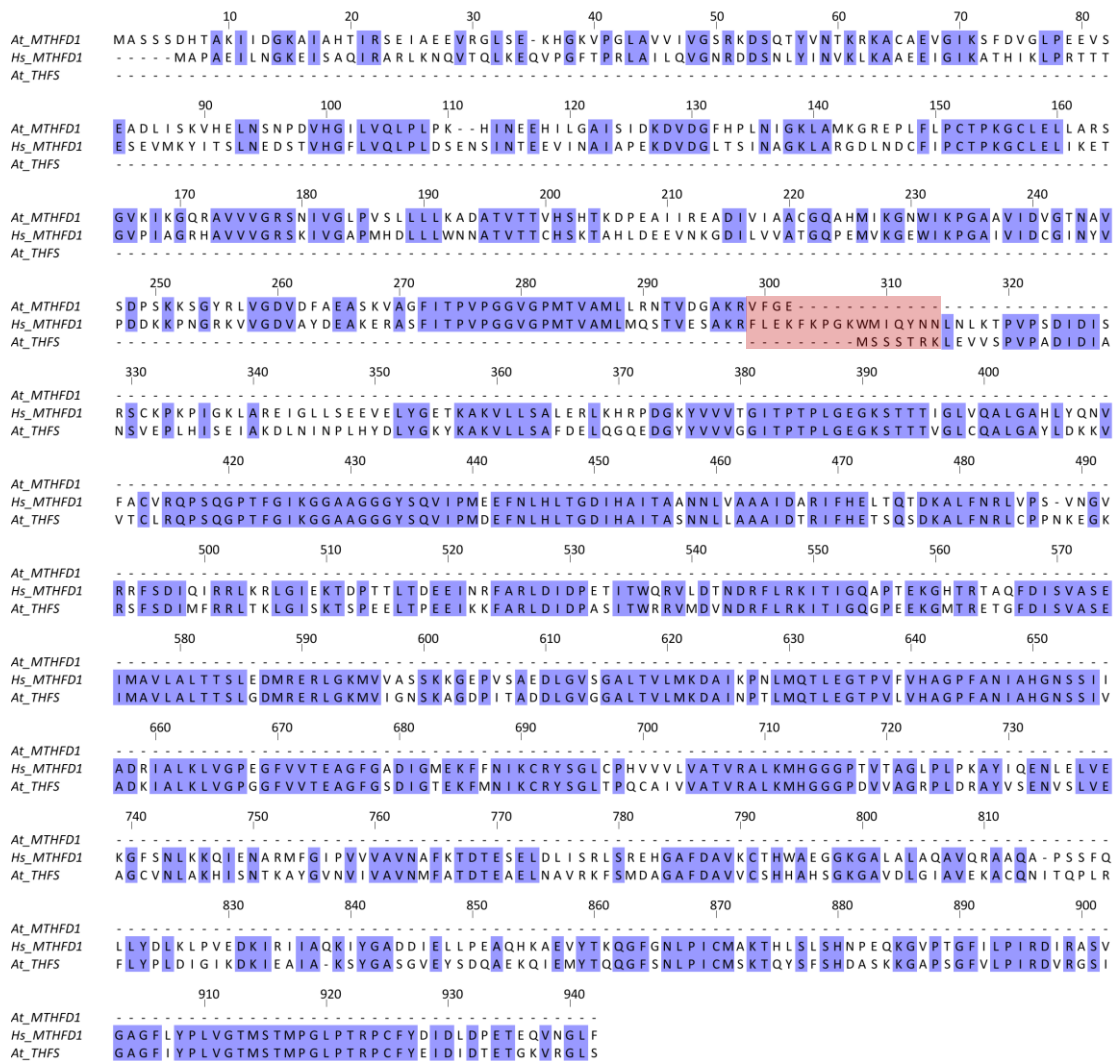
Seeds were surface sterilized with 40 % (v/v) commercial bleach at 1500 rpm for 10 min and washed six times with sterile water. Afterwards, seeds were stratified for two days at 4 °C before they were placed on rectangular full-strength MS plates and grown vertically under LD conditions for 5 days to germinate. Thereafter, seedlings were transferred to rectangular full-strength MS plates supplemented with the following chemicals: 500 μM 5-methyl-THF, 500 μM 5-formyl-THF and 25 μM sulfanilamide. Chemicals were dissolved in water by ultrasonication and sterile filtered – plates containing no chemicals were used as controls. Pictures of plates were taken before plants were grown vertically for 9 days. 1 ml of 500 μM 5-methyl-THF was resupplied directly to roots every second day. After 14 days of growth, pictures were taken again, and plants were harvested without roots in liquid nitrogen. Root length was analyzed and calculated comparing pictures before and after growth with chemicals for 9 days, using Fiji.

4.2.21 Computational analysis and tools

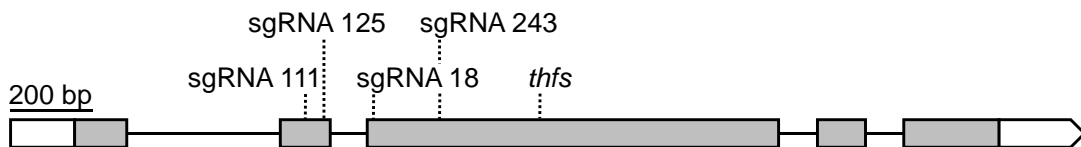
Statistical analysis was performed using R version 4.2.1 (The R Project). Details of sample size, statistical tests and error bars are indicated in figure legends. Statistical significances are indicated by *P* values, where * or letter code = $P < 0.05$ or can be found in Supplementary Tables to preserve readability and comprehensibility of figures. No data were excluded from analysis, however, measurements below detection limits were included as *Not Available (NA)*. Multiple sequence alignments were generated using the Clustal Omega web tool from the European Bioinformatics Institute (Goujon *et al*, 2010; Sievers *et al*, 2011; McWilliam *et al*, 2013). Isotope label enrichment and peak integration was performed with ChemStation (Agilent). Primer design and Sanger sequencing analysis were made with CLC Genomics (Qiagen) and Vector NTI (Thermo Fisher Scientific). Images from confocal microscopy were captured using the Leica Application Suite X (Leica Microsystems) and quantified using Fiji version 1.53t (ImageJ). Primer for RT-qPCR were designed with QuantPrime (Arvidsson *et al*, 2008).

Supplementary Figures

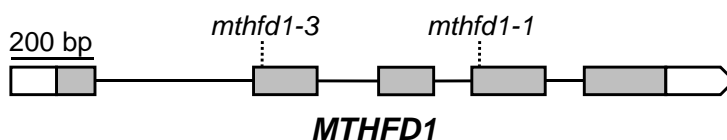
A



B

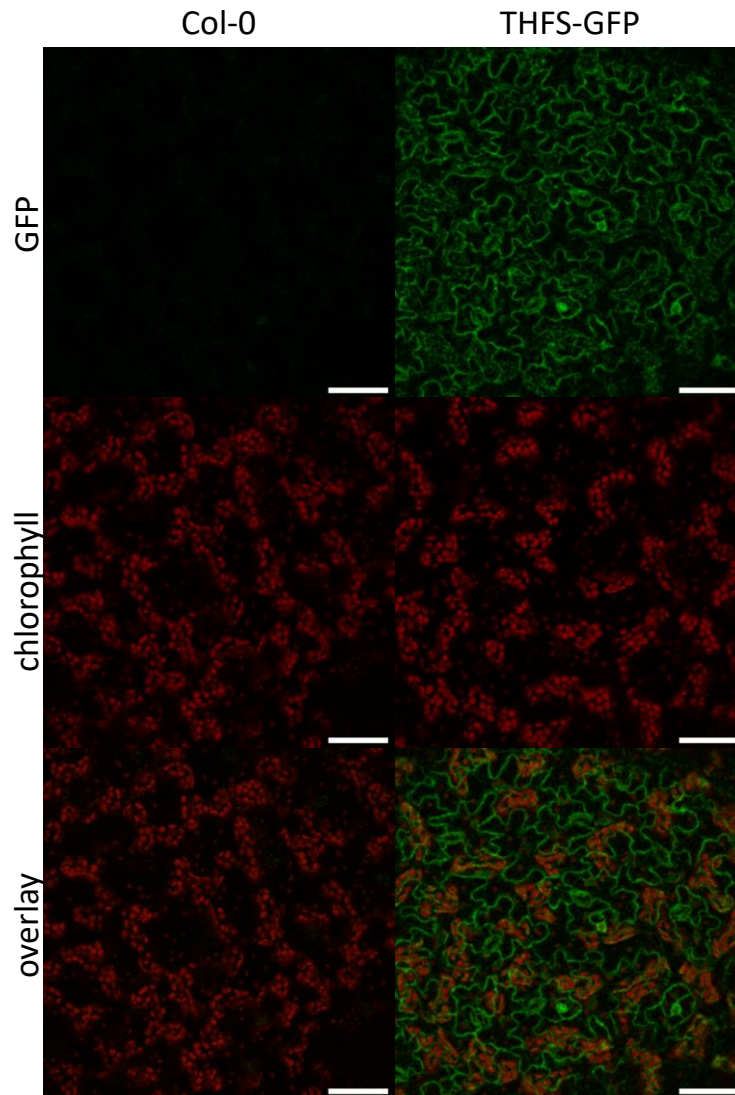


C



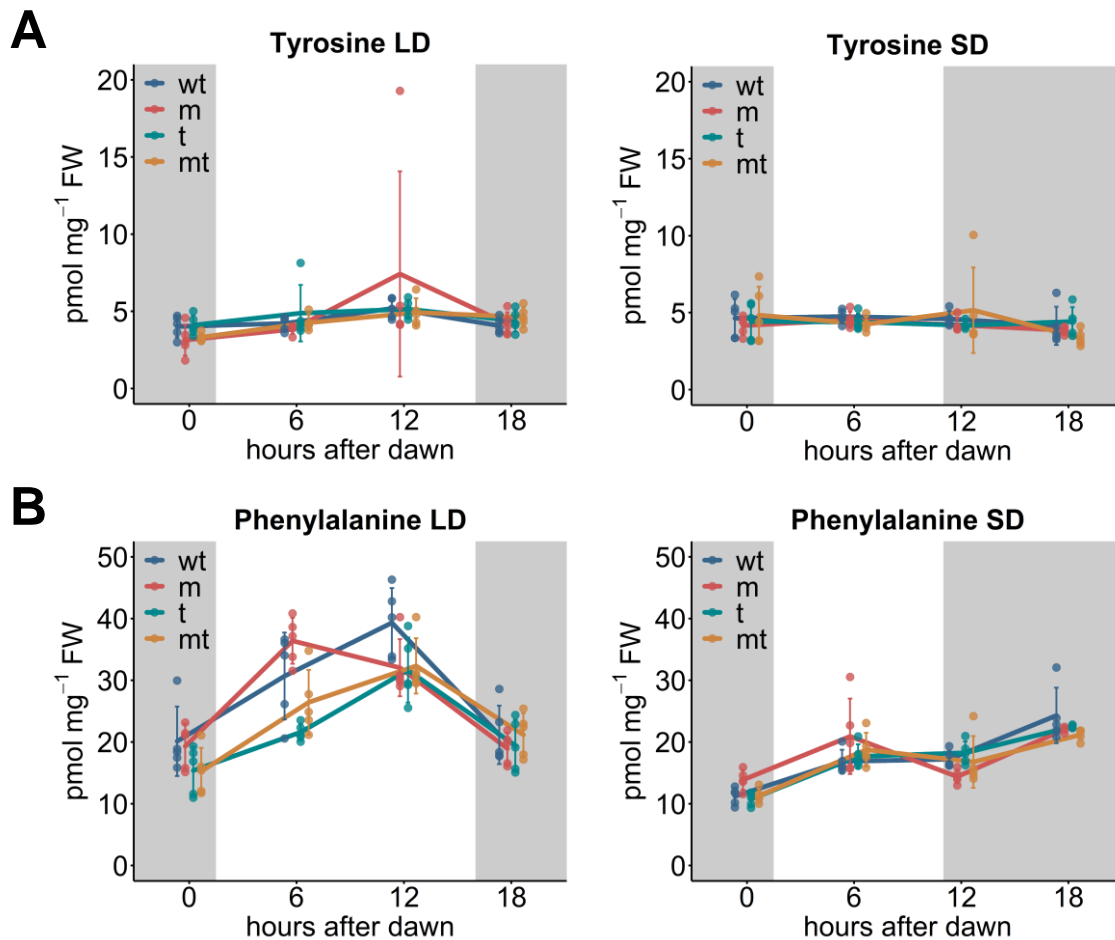
Supplementary Figure 1. Plant *MTHFD1* and *THFS* genes share conserved sequences with mammalian *MTHFD1* which combines both gene functions.

(A) Sequence alignment of *Arabidopsis thaliana* genes *MTHFD1* and *THFS* (*At_MTHFD1*, *At_THFS*, respectively) with the mammalian *MTHFD1* gene from *Homo sapiens* (*Hs_MTHFD1*) using Clustal Omega. Conserved sequences shared between plants and humans are highlighted in blue. The linker sequence that combines motifs of *MTHFD1* and *THFS* gene function in mammalian *MTHFD1* but is missing in *Arabidopsis* is indicated in red. Gene structures of *Arabidopsis thaliana* *THFS* (B) and *MTHFD1* (C) are indicated with positions for sgRNA-mediated targeted mutagenesis of *THFS* using CRISPR-Cas9, positions of T-DNA insertions of *thfs* (SALK_067510), *mthfd1-3* (SALK_015165) mutants and EMS generated mutation in *mthfd1-1* that led to a R175Q substitution.



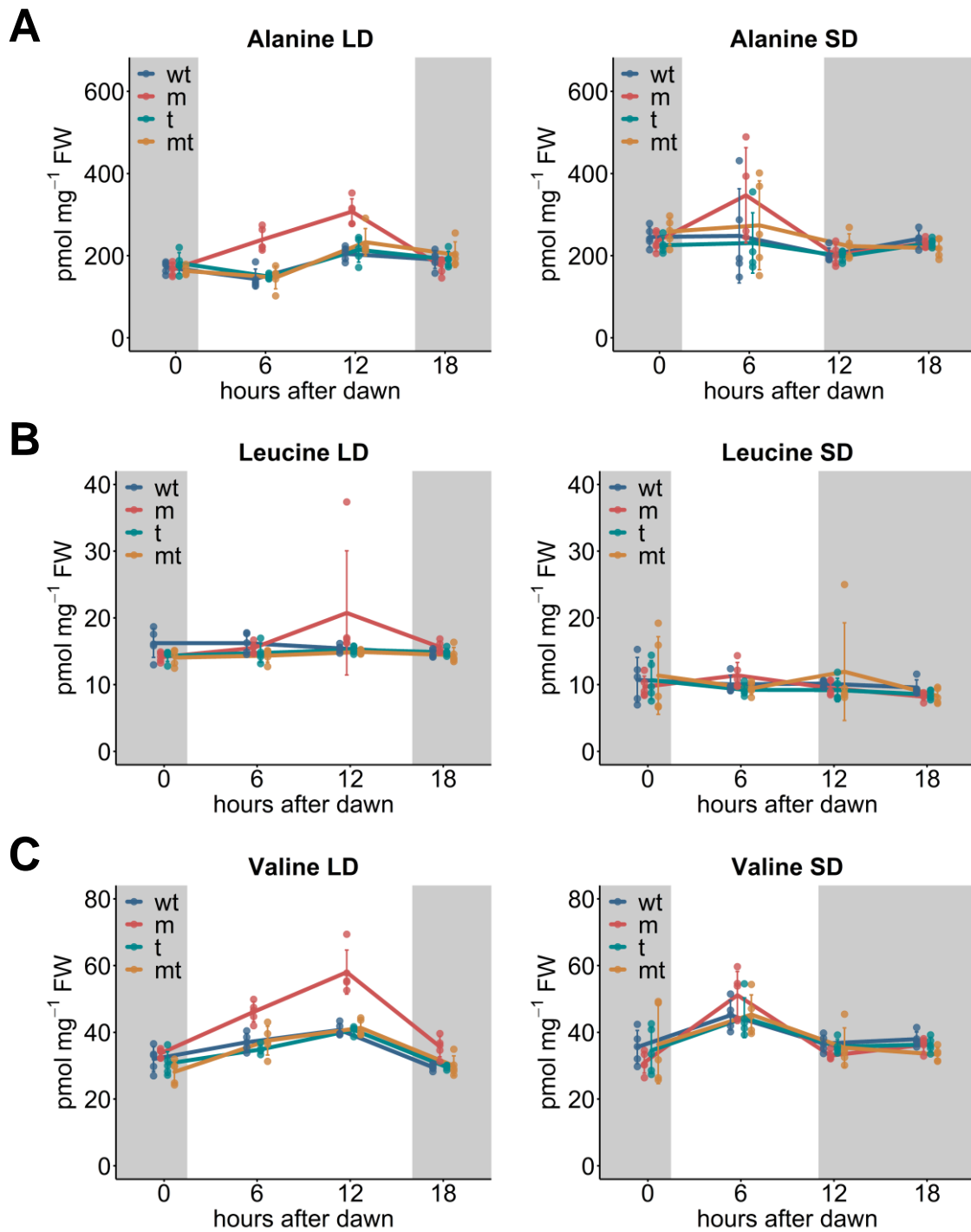
Supplementary Figure 2. *THFS* is localized in the cytosol.

The subcellular localization of *THFS* in the cytosol was confirmed using a fluorescent *THFS*-GFP fusion protein under the control of the native promoter of *THFS*. Maximum projections along the z axis were acquired from confocal laser scanning microscopy of the ventral side of leaves. *THFS*-GFP is visible in the periphery of the cells, while no signal was detected in Col-0 which was used to exclude artificial fluorescent background signals.



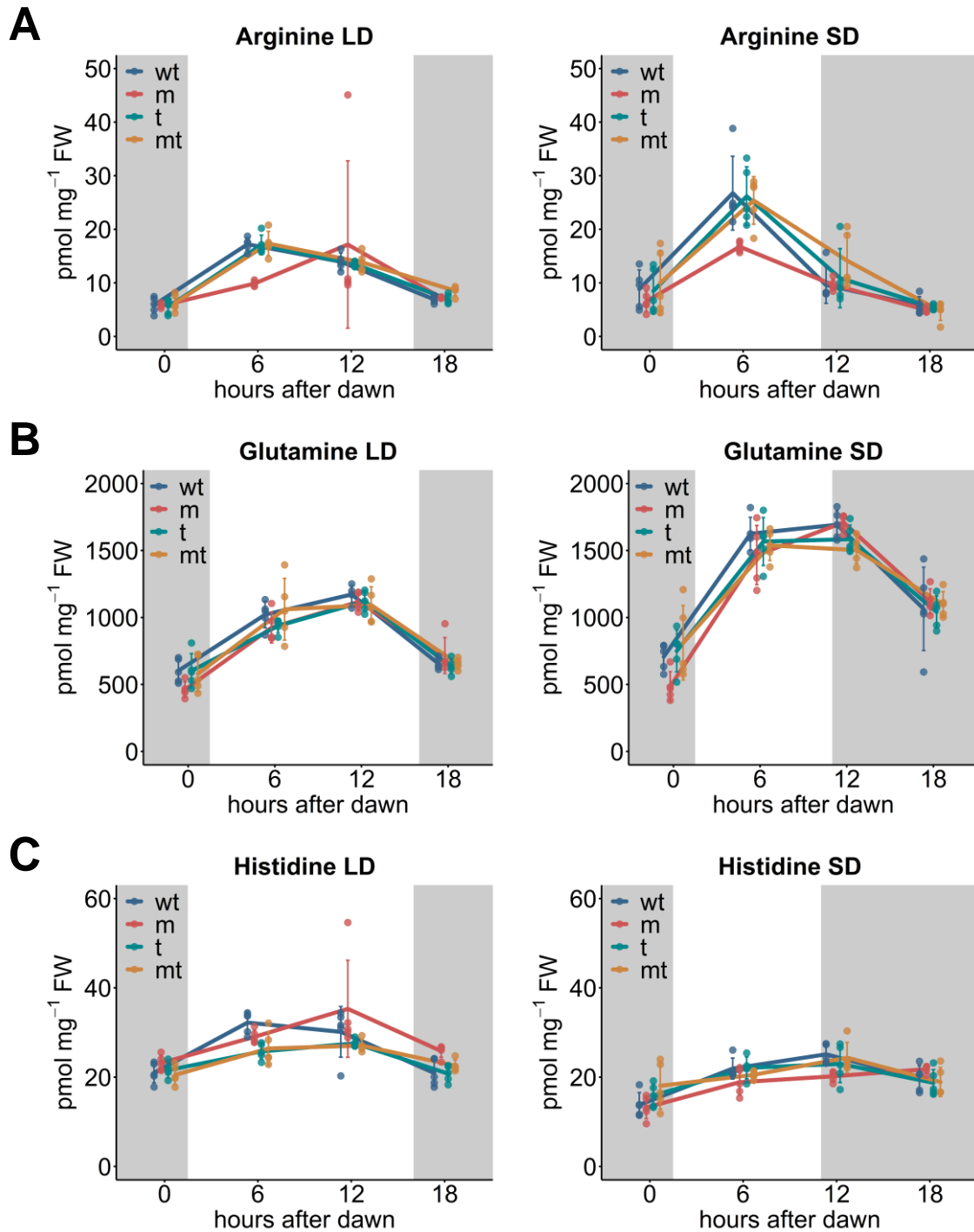
Supplementary Figure 3. Biosynthesis of aromatic amino acids is not impaired in *mthfd1-1*.

Steady-state levels of tyrosine (A) and phenylalanine (B) in leaves of 3 and 4-week-old wild type (wt), *mthfd1-1* (m), *thfs* (t) and *mthfd1-1* x *thfs* (mt) plants grown under LD and SD conditions, respectively. Plant material was harvested at 0, 6, 12 and 18 hours after dawn. Mean values \pm s.d. ($n = 5$) are shown. Adjusted P values indicating statistical differences between genotypes at each timepoint (One-way ANOVA followed by post-hoc Tukey test, $P < 0.05$) can be found in **Supplementary Table 12**.



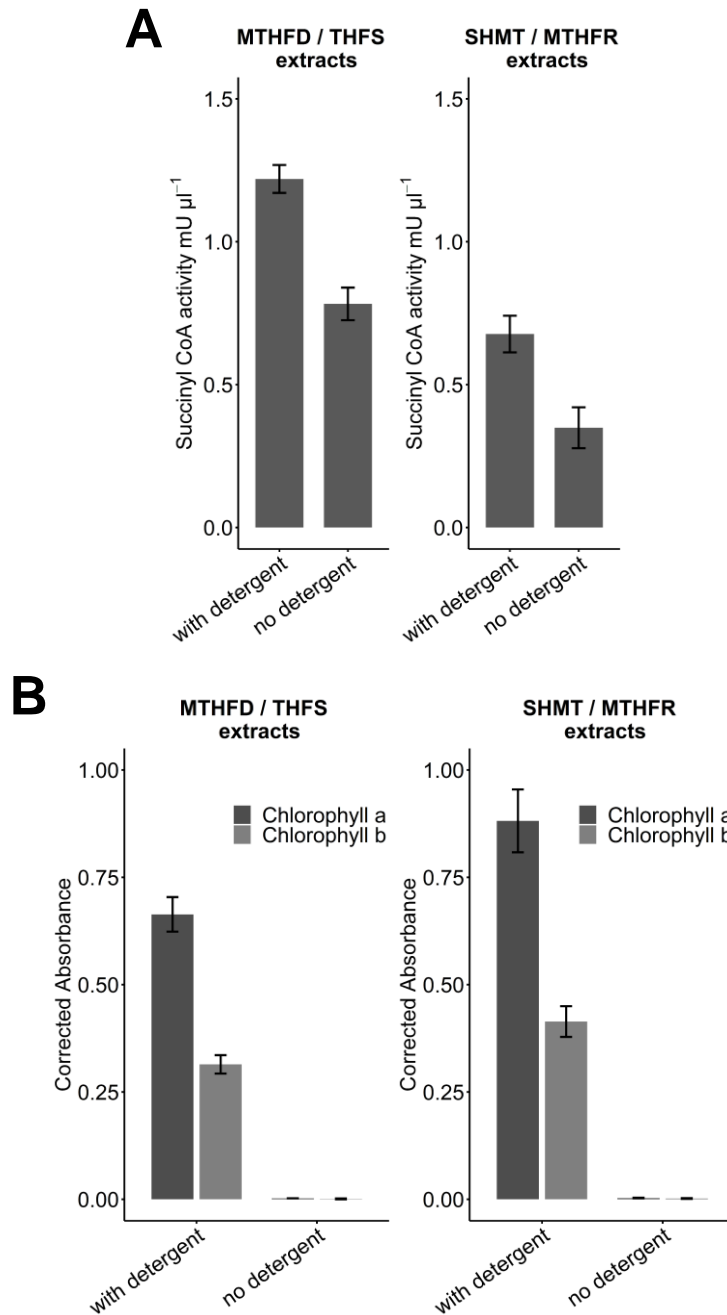
Supplementary Figure 4. *mthfd1-1* shows accumulation of alanine and valine during the day under LD growth.

Steady-state levels of pyruvate-derived amino acids alanine (A) leucine (B) and valine (C) in leaves of 3 and 4-week-old wild type (wt), *mthfd1-1* (m), *thfs* (t) and *mthfd1-1* x *thfs* (mt) plants grown under LD and SD conditions, respectively. Leaves were harvested at 0, 6, 12 and 18 hours after dawn. Mean values \pm s.d. ($n = 5$) are shown. Adjusted P values indicating statistical differences between genotypes at each timepoint (One-way ANOVA followed by post-hoc Tukey test, $P < 0.05$) can be found in **Supplementary Table 12**.



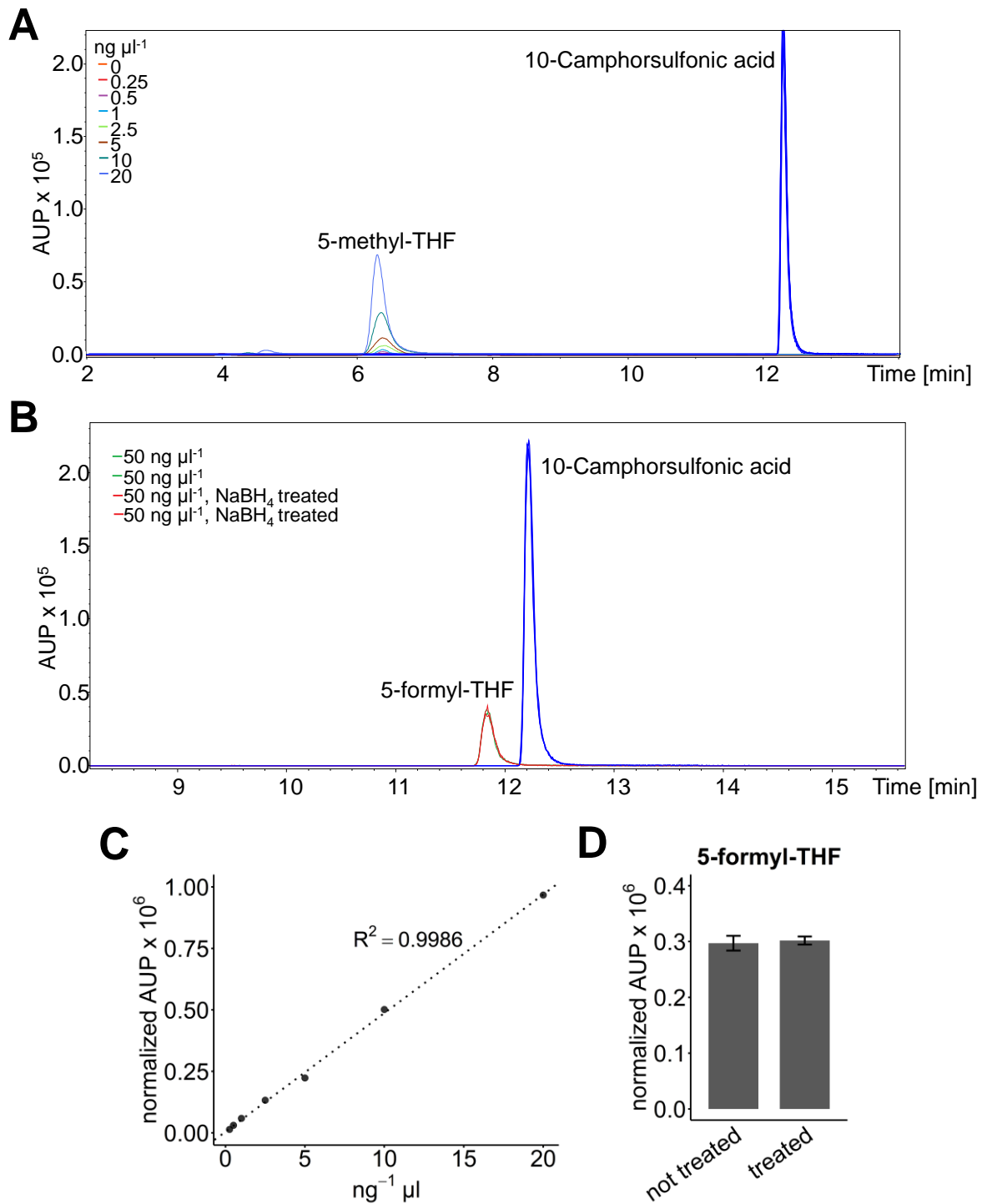
Supplementary Figure 5. Biosynthesis of arginine, glutamine and histidine are mostly unaffected in *mthfd1-1*.

Steady-state levels of amino arginine (A) glutamine (B) and histidine (C) in leaves of 3 and 4-week-old wild type (*wt*), *mthfd1-1* (*m*), *thfs* (*t*) and *mthfd1-1* × *thfs* (*mt*) plants grown under LD and SD conditions, respectively. Leaves were harvested at 0, 6, 12 and 18 hours after dawn. Mean values ± s.d. ($n = 5$) are shown. Adjusted P values indicating statistical differences between genotypes at each timepoint (One-way ANOVA followed by post-hoc Tukey test, $P < 0.05$) can be found in **Supplementary Table 13**.



Supplementary Figure 6. Chloroplastic and mitochondrial fractions of protein extracts for enzyme activity measurements.

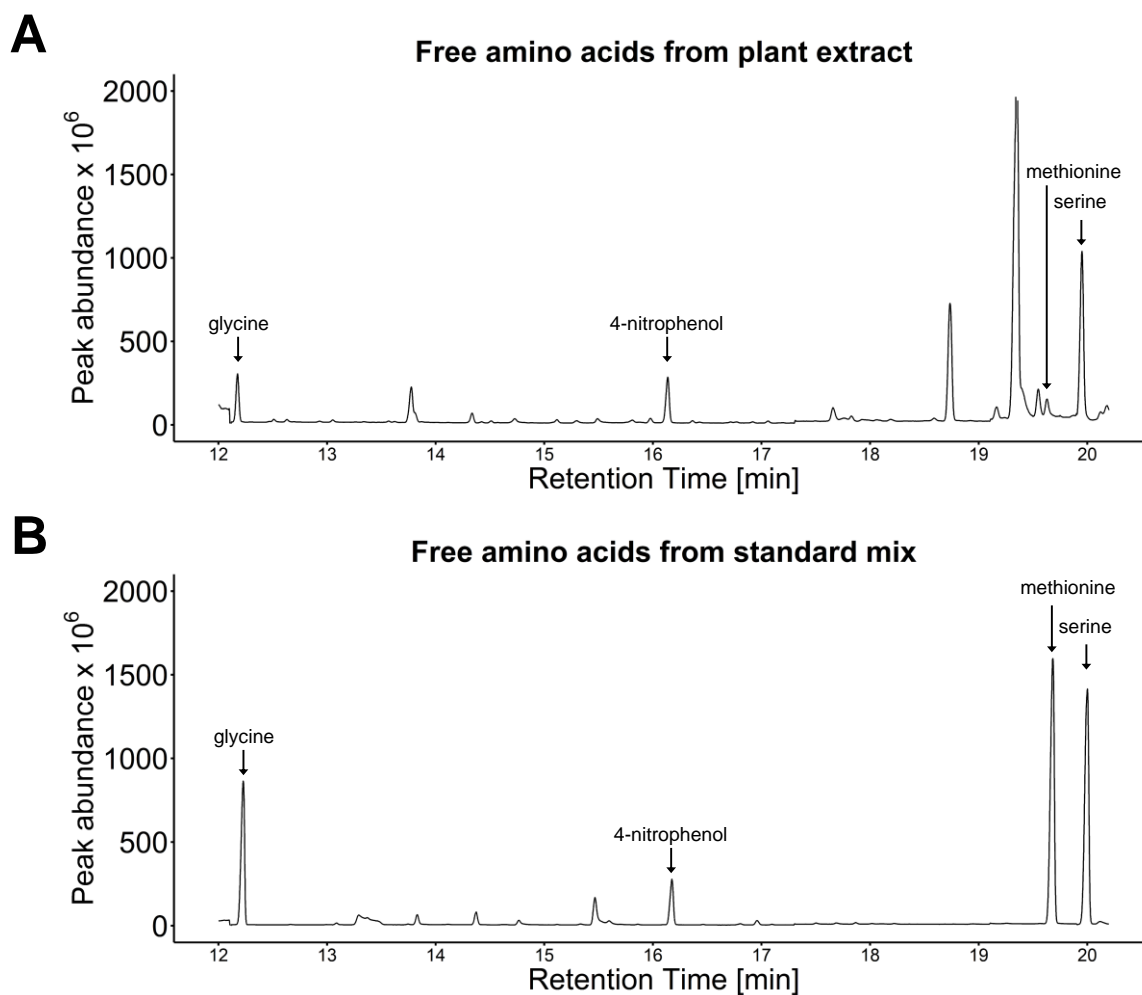
Protein extracts for enzyme activity measurements were extracted without detergents in the extraction buffer to keep organellar membranes from dissolving and to retrieve the cellular soluble proteome. As controls, cellular extracts were isolated with extraction buffers including 0.1 % of the detergent Triton X-100 to resolve total cellular proteins. (A) The mitochondrial fraction was measured by Succinyl CoA activity measurement, a marker enzyme of the mitochondrial Citric acid cycle. (B) The chloroplastic fraction in protein extracts was determined by chlorophyll a and b measurements at 664 and 647 nm, respectively.



Supplementary Figure 7. SHMT activity was measured via the formation of 5-methyl-THF.

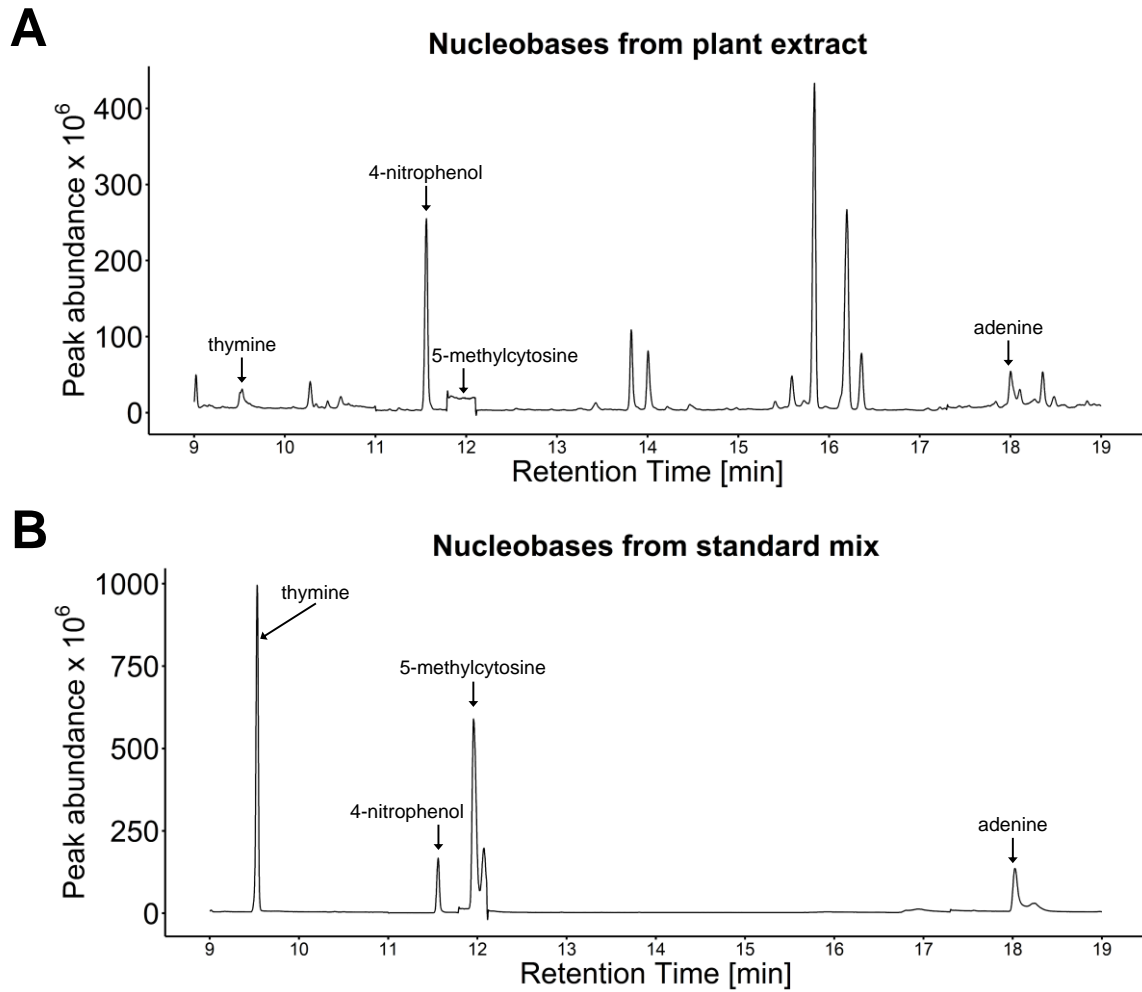
(A) Overlaid chromatograms of a 5-methyl-THF calibration curve with a dilution series of 0, 0.25, 0.5, 1, 2.5, 5, 10, 20 ng μl^{-1} with 1 ng μl^{-1} 10-Camphorsulfonic acid per sample used as internal standard for peak normalization. Reduction of the concentration led to reduction of the Area under the peak (AUP) (C). (B) To test if 5-formyl-THF was also prone for chemical conversion with NaBH₄, 50 ng μl^{-1} of 5-formyl-THF standards were treated with NaBH₄ and compared with 50 ng μl^{-1} non-treated standards.

Again, $1 \text{ ng } \mu\text{l}^{-1}$ 10-Camphorsulfonic acid per sample used as internal standard for peak normalization (D).



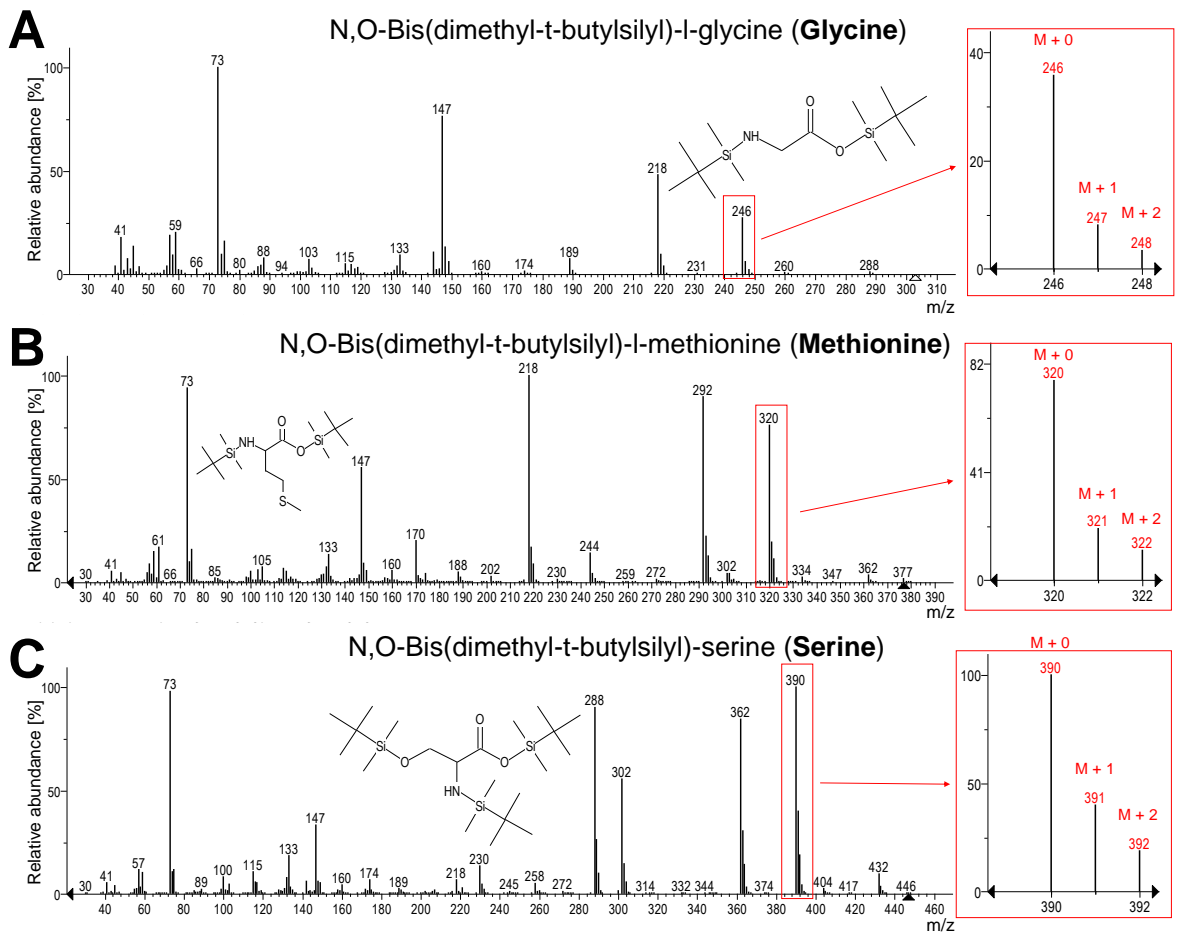
Supplementary Figure 8. TIC chromatograms of free amino acids from plant extract and standard mix.

TIC chromatograms with peaks of free amino acids glycine, methionine, serine, and internal standard 4-nitrophenol with retention times from plant extract (A) and standard mix (B).



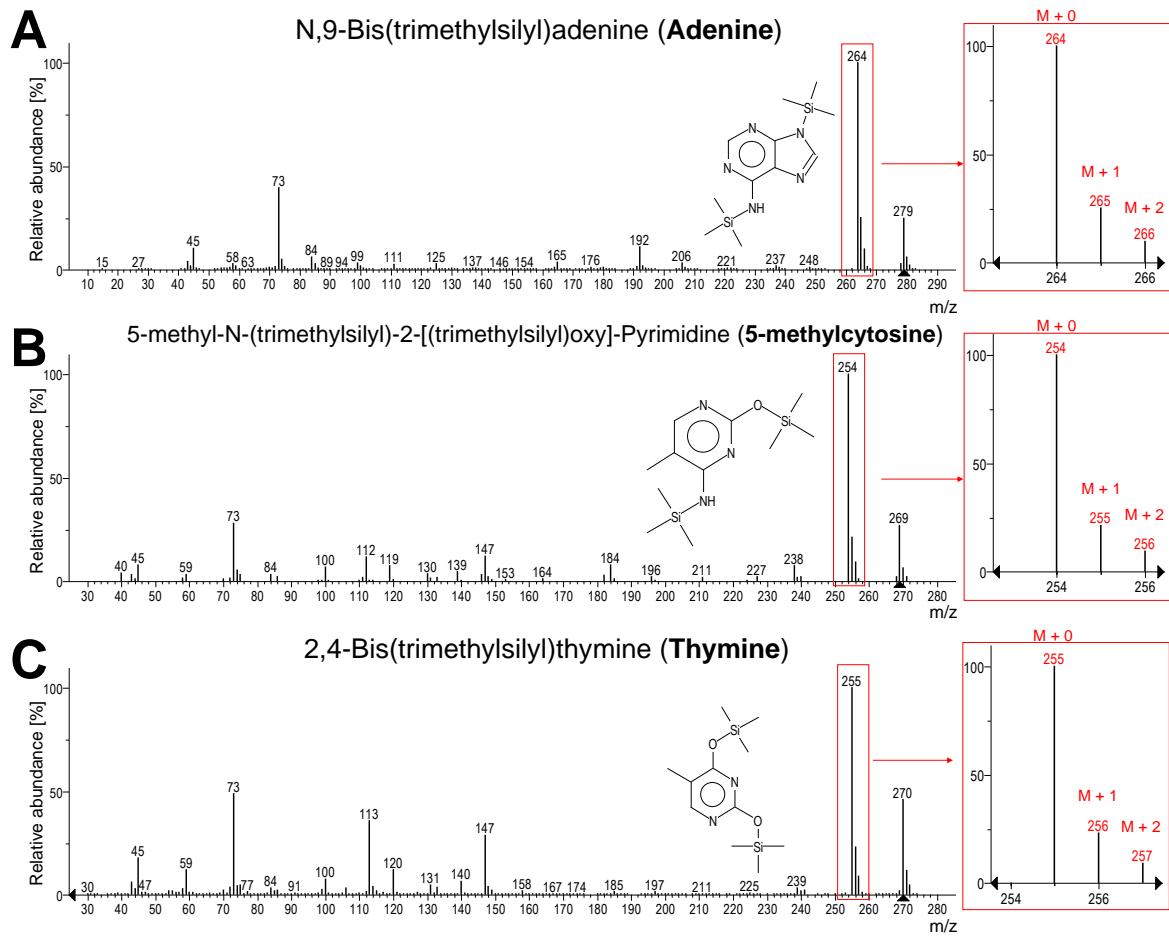
Supplementary Figure 9. TIC chromatograms of nucleobases from plant extract and standard mix.

TIC chromatograms with peaks of nucleobases 5-methylcytosine, adenine, thymine, and internal standard 4-nitrophenol with retention times from plant extract (A) and standard mix (B).



Supplementary Figure 10. Mass spectra of free amino acids glycine, methionine, and serine.

Mass spectra and structural formulas of tert-butyltrimethylsilyl ester derivatives of glycine (A), methionine (B) and serine (C) acquired from TD-GC-MS analysis of 50 ng μl^{-1} standards and compared to reference mass spectral data from the library of the National Institute of Standards and Technology (NIST). Ions used for isotopic label enrichment are highlighted with red boxes: glycine M+0: m/z 246.0, M+1: m/z 247.0, M+2: m/z 248.0; methionine M+0: m/z 320.0, M+1: m/z 321.0, M+2: m/z 322.0 and serine M+0: m/z 390.0, M+1: m/z 391.0, M+2: m/z 392.0.



Supplementary Figure 11. Mass spectra of nucleobases adenine, 5-methylcytosine and thymine.

Mass spectra and structural formulas of trimethylsilyl ester derivatives of adenine (A), 5-methylcytosine (B) and thymine (C) acquired from TD-GC-MS analysis of 50 ng μl^{-1} standards and compared to reference mass spectral data from the library of the National Institute of Standards and Technology (NIST). Ions used for isotopic label enrichment are highlighted with red boxes: adenine M+0: m/z 264.0, M+1: m/z 265.0, M+2: m/z 266.0; 5-methylcytosine M+0: m/z 254.0, M+1: m/z 255.0, M+2: m/z 256.0 and thymine M+0: m/z 255.0, M+1: m/z 256.0, M+2: m/z 257.0.

Supplementary Tables

Supplementary Table 1. Adjusted *P* values corresponding to Figures 11, 13 and 14.
P values < 0.05 are indicated in red.

hours after dawn		<i>GI</i>	<i>FKF1</i>	<i>FT</i>	<i>PRR5</i>	<i>CCA1</i>	<i>THFS</i>	<i>MTHFD1</i>	<i>SHM4</i>	<i>SAHH1</i>	<i>SDC</i>
0	m-wt	0,949	0,001	0,872	0,314	0,051	0,239	0,916	0,229	0,089	0,000
	t-wt	0,946	0,976	0,181	0,986	0,144	0,008	0,516	0,670	0,531	0,990
	mt-wt	0,418	0,794	0,021	0,921	0,794	0,008	0,690	0,707	0,432	0,990
	t-m	1,000	0,001	0,466	0,204	0,002	0,143	0,856	0,777	0,540	0,000
	mt-m	0,704	0,002	0,061	0,136	0,014	0,130	0,962	0,742	0,646	0,000
	mt-t	0,710	0,953	0,464	0,991	0,465	1,000	0,989	1,000	0,997	1,000
6	m-wt	0,178	0,919	0,550	0,183	0,065	0,013	1,000	0,043	0,001	0,000
	t-wt	0,998	0,637	0,720	0,187	0,388	0,000	0,160	0,993	1,000	0,999
	mt-wt	0,424	0,179	0,692	0,010	0,999	0,000	0,689	0,363	1,000	0,999
	t-m	0,224	0,322	0,989	0,008	0,007	0,039	0,162	0,030	0,002	0,000
	mt-m	0,019	0,074	0,138	0,001	0,053	0,037	0,693	0,004	0,001	0,000
	mt-t	0,345	0,711	0,209	0,220	0,459	1,000	0,613	0,489	0,999	1,000
12	m-wt	0,008	0,050	0,370	0,215	0,002	0,978	0,494	0,008	0,089	0,002
	t-wt	0,995	0,999	0,987	1,000	0,987	0,003	0,771	0,987	0,997	1,000
	mt-wt	0,772	0,446	0,828	0,800	0,964	0,001	0,384	0,711	0,811	1,000
	t-m	0,010	0,094	0,312	0,256	0,005	0,004	0,983	0,010	0,102	0,003
	mt-m	0,003	0,377	0,126	0,065	0,003	0,002	0,995	0,005	0,280	0,002
	mt-t	0,919	0,601	0,970	0,885	1,000	0,999	0,939	0,896	0,757	1,000
18	m-wt	0,930	0,362	0,002	0,892	0,015	0,095	0,024	0,005	0,002	0,004
	t-wt	0,038	0,996	0,104	0,778	0,327	0,000	0,843	1,000	0,932	0,983
	mt-wt	0,016	1,000	0,036	0,650	0,149	0,000	0,476	0,984	0,782	0,979
	t-m	0,017	0,279	0,057	0,402	0,197	0,000	0,076	0,005	0,003	0,003
	mt-m	0,007	0,342	0,166	0,302	0,415	0,000	0,198	0,003	0,005	0,003
	mt-t	0,911	0,998	0,871	0,995	0,932	0,647	0,899	0,984	0,983	1,000

Supplementary Table 2. Adjusted *P* values corresponding to Figure 14.
P values < 0.05 are indicated in red.

hours after dawn		<i>SAH LD</i>	<i>Hcy LD</i>	<i>SAM LD</i>	<i>Met LD</i>	<i>MI LD</i>
0	m-wt	7,15E-06	1,72E-07	5,62E-01	4,26E-02	1,18E-02
	t-wt	9,87E-01	9,98E-01	7,51E-01	8,34E-01	5,05E-01
	mt-wt	9,98E-01	6,41E-02	1,62E-03	6,05E-01	5,24E-03
	t-m	4,15E-06	1,36E-07	9,88E-01	1,94E-01	6,66E-04
	mt-m	5,34E-06	1,18E-05	2,36E-02	3,59E-01	6,07E-06
	mt-t	9,99E-01	4,65E-02	1,24E-02	9,76E-01	8,66E-02
6	m-wt	5,44E-09	6,55E-10	9,67E-01	3,41E-06	3,74E-09
	t-wt	1,00E+00	1,00E+00	7,08E-01	2,65E-01	3,15E-01
	mt-wt	9,99E-01	1,00E+00	3,24E-04	1,00E+00	3,18E-05
	t-m	5,31E-09	6,72E-10	9,25E-01	9,47E-05	5,50E-10
	mt-m	6,22E-09	6,77E-10	7,98E-04	3,17E-06	7,70E-12
	mt-t	9,99E-01	1,00E+00	2,77E-03	2,47E-01	9,47E-04
12	m-wt	3,68E-07	4,75E-09	8,36E-04	1,44E-03	3,35E-09
	t-wt	1,00E+00	9,77E-01	1,83E-01	4,99E-01	8,75E-03
	mt-wt	1,00E+00	9,99E-01	6,06E-04	6,79E-01	2,30E-06
	t-m	3,76E-07	7,60E-09	6,08E-02	2,61E-02	7,32E-11
	mt-m	4,04E-07	5,55E-09	9,98E-01	1,42E-02	2,54E-12
	mt-t	1,00E+00	9,93E-01	4,46E-02	9,90E-01	2,10E-03
18	m-wt	1,06E-08	7,57E-08	2,00E-06	2,16E-06	5,19E-03
	t-wt	1,00E+00	9,42E-01	3,91E-01	9,47E-01	6,13E-02
	mt-wt	9,95E-01	5,17E-01	4,24E-02	9,71E-01	6,13E-03
	t-m	1,13E-08	1,63E-07	3,11E-05	9,27E-07	2,54E-05
	mt-m	1,42E-08	5,43E-07	3,66E-04	4,36E-06	3,55E-06
	mt-t	9,98E-01	8,35E-01	5,65E-01	7,63E-01	6,60E-01

Supplementary Table 3. Adjusted *P* values corresponding to Figure 15.
P values < 0.05 are indicated in red.

hours after dawn		Ser LD	Gly LD	THF LD	10-formyl-FA LD	5-methyl-THF LD	5-formyl-THF LD
0	m-wt	9,8E-06	2,6E-01	1,9E-01	6,7E-01	1,8E-01	3,1E-03
	t-wt	7,6E-01	7,9E-02	9,8E-01	1,0E+00	8,0E-01	1,0E+00
	mt-wt	6,1E-01	9,9E-01	4,3E-01	2,0E-01	1,4E-01	4,5E-01
	t-m	1,9E-06	3,1E-01	1,1E-01	5,8E-01	5,5E-01	3,2E-03
	mt-m	1,3E-06	9,2E-01	9,1E-01	3,9E-02	6,4E-03	2,2E-02
	mt-t	9,9E-01	1,0E+00	2,8E-01	2,4E-01	4,0E-02	4,7E-01
	m-wt	2,5E-06	9,8E-01	7,1E-01	1,8E-01	6,0E-01	1,4E-03
6	t-wt	2,1E-01	1,0E+00	4,7E-01	4,6E-01	6,7E-01	1,0E+00
	mt-wt	9,8E-01	4,7E-01	7,7E-01	3,2E-01	9,9E-01	9,3E-01
	t-m	1,2E-07	9,8E-01	4,3E-05	8,7E-01	1,0E+00	2,9E-03
	mt-m	1,3E-06	2,3E-02	4,4E-01	1,4E-02	4,4E-01	2,5E-03
	mt-t	3,9E-01	9,9E-01	9,8E-01	3,8E-02	5,0E-01	9,6E-01
	m-wt	1,5E-11	3,2E-01	1,4E-04	9,9E-01	8,1E-01	2,7E-06
	t-wt	9,8E-01	6,6E-01	5,3E-01	1,0E+00	7,0E-03	8,3E-01
12	mt-wt	1,0E+00	NA	6,9E-01	4,1E-01	4,1E-01	1,0E+00
	t-m	1,1E-11	4,3E-02	6,4E-01	9,7E-01	2,4E-03	1,7E-06
	mt-m	1,6E-11	NA	5,8E-05	2,7E-01	1,3E-01	2,5E-06
	mt-t	9,7E-01	NA	2,7E-01	4,6E-01	6,4E-02	8,8E-01
	m-wt	1,5E-08	6,0E-03	9,4E-01	5,1E-01	9,1E-01	3,9E-05
	t-wt	1,0E+00	NA	NA	4,4E-01	2,6E-02	9,0E-01
	mt-wt	1,0E+00	NA	9,9E-02	7,6E-01	9,4E-02	8,9E-02
18	t-m	1,5E-08	NA	NA	1,0E+00	6,4E-02	6,6E-05
	mt-m	1,5E-08	NA	6,3E-02	1,5E-01	2,3E-01	4,1E-04
	mt-t	1,0E+00	NA	NA	1,2E-01	8,0E-01	2,3E-01

Supplementary Table 4. Adjusted *P* values corresponding to Figure 16.
P values < 0.05 are indicated in red.

hours after dawn		SAH SD	Hcy SD	SAM SD	Met SD	Ser SD	Gly SD	THF SD	10-formyl-FA SD	5-methyl-THF SD	5-formyl-THF SD
0	m-wt	0,64	NA	0,06	0,03	0,51	0,99	NA	NA	NA	NA
	t-wt	1,00	NA	0,03	0,65	0,82	0,99	NA	NA	NA	NA
	mt-wt	0,65	NA	0,96	0,71	0,67	1,00	NA	NA	NA	NA
	t-m	0,56	NA	0,99	0,23	0,14	0,66	NA	NA	NA	NA
	mt-m	0,13	NA	0,14	0,19	0,09	0,10	NA	NA	NA	NA
	mt-t	0,74	NA	0,09	1,00	0,99	0,59	NA	NA	NA	NA
	m-wt	0,08	NA	0,44	0,06	0,02	0,00	1,00	0,00	1,00	0,96
6	t-wt	1,00	NA	0,05	0,64	1,00	0,45	0,88	0,03	1,00	0,99
	mt-wt	0,91	NA	1,00	0,95	0,85	0,24	0,99	0,00	0,04	0,67
	t-m	0,07	NA	0,58	0,42	0,02	1,00	0,86	0,23	1,00	1,00
	mt-m	0,24	NA	0,34	0,15	0,12	1,00	0,96	0,03	0,05	0,33
	mt-t	0,89	NA	0,04	0,90	0,81	0,99	0,76	0,00	0,04	0,41
	m-wt	0,71	NA	0,92	0,15	0,00	0,16	NA	NA	NA	NA
	t-wt	0,25	NA	0,99	0,91	0,51	0,95	NA	NA	NA	NA
12	mt-wt	0,94	NA	0,25	0,97	0,80	0,96	NA	NA	NA	NA
	t-m	0,82	NA	0,80	0,05	0,00	0,00	NA	NA	NA	NA
	mt-m	0,96	NA	0,09	0,30	0,00	0,00	NA	NA	NA	NA
	mt-t	0,54	NA	0,37	0,70	0,95	0,97	NA	NA	NA	NA
	m-wt	0,63	NA	0,83	0,90	0,95	NA	1,00	0,43	0,99	1,00
	t-wt	0,90	NA	0,28	0,98	0,52	NA	0,60	0,69	0,76	0,45
	mt-wt	0,06	NA	0,99	0,32	0,08	NA	0,90	0,03	0,11	0,99
18	t-m	0,27	NA	0,06	0,99	0,83	0,36	0,65	0,10	0,89	0,46
	mt-m	0,01	NA	0,94	0,70	0,20	0,39	0,94	0,00	0,08	0,99
	mt-t	0,20	NA	0,17	0,50	0,60	1,00	0,90	0,14	0,03	0,62

Supplementary Table 5. Adjusted *P* values corresponding to Figures 19 and 20.
P values < 0.05 are indicated in red.

hours after dawn		Asp LD	Asn LD	Cys LD	Lys LD	Thr LD	Ile LD	MTA LD
0	m-wt	0,064	0,962	0,000	0,562	0,000	0,058	0,142
	t-wt	0,576	0,969	0,083	0,805	0,881	0,997	0,701
	mt-wt	0,995	0,999	0,000	1,000	0,628	0,376	0,009
	t-m	0,005	0,791	0,000	0,974	0,000	0,039	0,018
	mt-m	0,041	0,933	0,001	0,517	0,000	0,002	0,000
	mt-t	0,716	0,987	0,000	0,764	0,963	0,486	0,077
6	m-wt	0,031	0,936	0,941	0,002	0,097	0,871	0,005
	t-wt	1,000	0,930	0,999	0,063	0,325	0,400	0,335
	mt-wt	0,622	0,833	0,000	0,262	0,714	0,864	0,004
	t-m	0,027	1,000	0,970	0,000	0,003	0,829	0,000
	mt-m	0,003	0,993	0,000	0,000	0,012	1,000	0,000
	mt-t	0,664	0,995	0,000	0,840	0,896	0,837	0,110
12	m-wt	0,013	0,474	0,038	0,628	0,033	0,004	0,247
	t-wt	1,000	0,156	0,001	0,999	0,491	1,000	0,116
	mt-wt	0,481	0,773	0,001	0,999	0,847	0,958	0,000
	t-m	0,012	0,872	0,308	0,696	0,002	0,004	0,002
	mt-m	0,001	0,955	0,230	0,711	0,007	0,011	0,000
	mt-t	0,509	0,593	0,997	1,000	0,920	0,964	0,053
18	m-wt	0,585	0,005	0,001	0,016	0,000	0,000	0,000
	t-wt	1,000	0,496	0,000	0,939	0,986	0,998	0,031
	mt-wt	0,033	0,281	0,000	0,444	0,810	0,630	0,336
	t-m	0,595	0,091	0,709	0,050	0,000	0,000	0,000
	mt-m	0,314	0,191	0,169	0,001	0,000	0,004	0,000
	mt-t	0,034	0,973	0,689	0,195	0,946	0,728	0,533

Supplementary Table 6. Adjusted *P* values corresponding to Figure 19 and 20.
P values < 0.05 are indicated in red.

hours after dawn		Asp SD	Asn SD	Cys SD	Lys SD	Thr SD	Ile SD	MTA SD
0	m-wt	1,00	0,97	0,56	0,75	0,00	0,96	0,10
	t-wt	1,00	0,90	1,00	0,99	0,98	1,00	0,09
	mt-wt	0,98	0,30	1,00	0,67	1,00	0,94	0,65
	t-m	1,00	1,00	0,47	0,90	0,00	0,99	1,00
	mt-m	0,96	0,53	0,69	0,18	0,00	0,71	0,57
	mt-t	0,94	0,67	0,98	0,49	0,97	0,85	0,54
6	m-wt	0,04	0,88	0,73	0,86	0,18	0,64	0,00
	t-wt	0,58	0,87	0,28	0,32	0,99	0,87	0,21
	mt-wt	0,97	0,97	0,70	0,94	0,78	1,00	0,27
	t-m	0,34	0,46	0,84	0,09	0,10	0,25	0,06
	mt-m	0,08	0,64	1,00	0,55	0,63	0,73	0,04
	mt-t	0,82	0,99	0,86	0,62	0,59	0,80	1,00
12	m-wt	0,98	0,14	0,00	0,95	0,00	0,90	0,00
	t-wt	0,90	0,74	0,67	0,60	0,70	1,00	0,09
	mt-wt	0,86	0,85	1,00	0,19	0,36	0,89	0,00
	t-m	0,99	0,59	0,00	0,31	0,00	0,87	0,00
	mt-m	0,65	0,46	0,00	0,07	0,00	1,00	0,00
	mt-t	0,47	1,00	0,69	0,83	0,93	0,86	0,13
18	m-wt	0,00	0,02	0,24	0,50	0,00	0,39	0,15
	t-wt	0,83	0,58	0,80	0,51	0,09	1,00	0,92
	mt-wt	0,20	0,78	0,72	0,51	0,05	0,98	1,00
	t-m	0,02	0,20	0,05	1,00	0,00	0,43	0,05
	mt-m	0,17	0,11	0,04	1,00	0,00	0,22	0,13
	mt-t	0,61	0,99	1,00	1,00	0,99	0,96	0,94

Supplementary Table 7. Adjusted *P* values corresponding to Figure 22.
P values < 0.05 are indicated in red.

hours after dawn		Glu LD	Pro LD	Glu SD	Pro SD
0	m-wt	0,016	0,000	0,942	0,001
	t-wt	1,000	0,967	1,000	1,000
	mt-wt	0,629	0,913	0,999	0,994
	t-m	0,015	0,000	0,952	0,001
	mt-m	0,158	0,000	0,890	0,001
	mt-t	0,614	0,997	0,998	0,995
	m-wt	0,004	0,000	0,009	0,002
6	t-wt	0,520	0,945	0,735	0,994
	mt-wt	1,000	0,946	0,675	0,968
	t-m	0,061	0,000	0,069	0,001
	mt-m	0,003	0,000	0,084	0,005
	mt-t	0,463	1,000	1,000	0,890
	m-wt	0,009	0,000	0,003	0,000
	t-wt	0,762	0,933	0,999	0,496
12	mt-wt	0,997	0,997	0,236	0,201
	t-m	0,061	0,000	0,004	0,000
	mt-m	0,006	0,000	0,145	0,000
	mt-t	0,649	0,978	0,292	0,916
	m-wt	0,003	0,000	0,999	0,000
	t-wt	0,998	1,000	0,976	0,578
	mt-wt	0,928	0,998	0,926	0,192
18	t-m	0,002	0,000	0,949	0,000
	mt-m	0,001	0,000	0,880	0,000
	mt-t	0,970	1,000	0,997	0,847

Supplementary Table 8. Adjusted *P* values corresponding to Figures 23 and 24.
P values < 0.05 are indicated in red.

hours after dawn		NADH LD	ATP LD	NADH SD	ATP SD	NADPH LD	GSH LD	NADPH SD	GSH SD
0	m-wt	0,995	0,510	0,000	0,553	0,004	0,000	0,649	0,003
	t-wt	0,256	0,183	0,000	1,000	0,961	0,521	0,956	0,063
	mt-wt	0,000	0,993	0,224	0,938	0,597	0,000	0,999	0,368
	t-m	0,362	0,885	0,495	0,615	0,012	0,000	0,914	0,402
	mt-m	0,001	0,364	0,005	0,261	0,000	0,002	0,675	0,071
	mt-t	0,023	0,115	0,000	0,903	0,332	0,000	0,976	0,714
	m-wt	0,619	1,000	0,001	0,949	0,099	0,896	0,893	0,222
6	t-wt	0,382	0,887	0,004	0,998	0,995	0,851	0,984	0,992
	mt-wt	0,065	0,223	0,484	0,999	0,315	0,000	0,993	0,748
	t-m	0,049	0,924	0,882	0,892	0,064	0,458	0,984	0,139
	mt-m	0,006	0,189	0,019	0,979	0,003	0,000	0,768	0,744
	mt-t	0,709	0,063	0,080	0,989	0,434	0,000	0,926	0,583
	m-wt	0,637	0,763	0,000	0,022	0,215	0,033	0,365	0,002
	t-wt	0,031	0,950	0,370	0,997	0,084	0,001	0,575	0,944
12	mt-wt	0,000	0,383	0,002	0,103	0,327	0,000	0,999	0,985
	t-m	0,266	0,454	0,000	0,033	0,001	0,391	0,994	0,006
	mt-m	0,000	0,078	0,101	0,853	0,008	0,015	0,314	0,004
	mt-t	0,005	0,686	0,050	0,147	0,843	0,286	0,514	0,997
	m-wt	0,030	0,344	0,507	0,255	0,219	0,000	0,914	0,001
	t-wt	0,000	0,998	0,360	0,955	0,864	0,000	0,991	1,000
	mt-wt	0,000	0,455	0,905	0,983	0,242	0,000	1,000	0,941
18	t-m	0,095	0,430	0,031	0,108	0,056	0,242	0,991	0,001
	mt-m	0,096	0,024	0,878	0,424	0,005	0,006	0,925	0,000
	mt-t	1,000	0,366	0,124	0,816	0,643	0,235	0,993	0,955

Supplementary Table 9. Adjusted *P* values corresponding to Figures 25, 26 and 27.
P values < 0.05 are indicated in red.

hours after dawn		MTHFD1	THFS	SHMT LD	MTHFR	SHMT SD
0	m-wt	0,000	0,968	0,477	1,000	0,187
	t-wt	0,492	0,000	0,703	0,984	0,256
	mt-wt	0,000	0,000	0,999	0,982	0,998
	t-m	0,000	0,000	0,117	0,976	0,995
	mt-m	0,093	0,000	0,406	0,989	0,145
	mt-t	0,000	0,897	0,781	0,887	0,200
6	m-wt	0,000	0,973	0,963	0,984	1,000
	t-wt	0,802	0,000	0,466	0,983	0,962
	mt-wt	0,000	0,000	0,070	0,999	0,850
	t-m	0,000	0,000	0,724	1,000	0,954
	mt-m	0,035	0,000	0,137	0,966	0,834
	mt-t	0,000	0,984	0,515	0,964	0,987
12	m-wt	0,000	0,698	0,296	0,901	NA
	t-wt	0,889	0,000	0,279	0,580	NA
	mt-wt	0,000	0,000	0,053	0,997	NA
	t-m	0,000	0,000	1,000	0,919	NA
	mt-m	0,533	0,000	0,618	0,960	NA
	mt-t	0,000	1,000	0,644	0,688	NA
18	m-wt	0,005	0,459	0,883	0,409	NA
	t-wt	0,991	0,000	0,889	0,980	NA
	mt-wt	0,005	0,000	0,653	0,559	NA
	t-m	0,004	0,000	1,000	0,608	NA
	mt-m	1,000	0,001	0,966	0,991	NA
	mt-t	0,004	0,707	0,963	0,768	NA

Supplementary Table 10. Adjusted *P* values corresponding to Figures 29 and 32.
P values < 0.05 are indicated in red.

hours after dawn	Glycine M+1		Methionine M+1		hours after dusk	Glycine M+1		Methionine M+1			
	[13C] Formate	[α-13C] Glycine	[13C] Formate	[α-13C] Glycine		[13C] Formate	[α-13C] Glycine	[13C] Formate	[α-13C] Glycine		
4	m-wt	0,972	0,100	0,000	0,681	4	m-wt	0,616	0,201	0,000	0,539
	t-wt	0,708	0,998	0,000	0,042		t-wt	0,961	0,968	0,000	0,003
	mt-wt	0,872	0,974	0,000	0,031		mt-wt	1,000	1,000	0,000	0,261
	t-m	0,910	0,127	0,005	0,204		t-m	0,867	0,357	0,226	0,015
	mt-m	0,987	0,178	0,231	0,153		mt-m	0,647	0,180	0,178	0,922
	mt-t	0,987	0,994	0,085	0,996		mt-t	0,972	0,950	0,998	0,034
8	m-wt	0,350	0,540	0,000	0,934	8	m-wt	0,998	0,638	0,000	0,803
	t-wt	0,676	0,643	0,000	0,934		t-wt	0,972	0,999	0,000	0,104
	mt-wt	0,998	0,912	0,000	0,888		mt-wt	0,804	0,909	0,000	0,118
	t-m	0,918	0,119	0,354	0,663		t-m	0,933	0,703	0,058	0,349
	mt-m	0,424	0,251	0,415	0,588		mt-m	0,720	0,944	0,052	0,388
	mt-t	0,766	0,945	0,999	0,999		mt-t	0,962	0,946	1,000	1,000
16	m-wt	0,174	0,278	0,000	0,729	16	m-wt	0,674	0,371	0,000	1,000
	t-wt	1,000	0,519	0,000	0,033		t-wt	0,994	0,238	0,000	0,113
	mt-wt	0,999	0,766	0,000	0,480		mt-wt	0,995	0,303	0,000	0,013
	t-m	0,190	0,039	0,071	0,008		t-m	0,805	0,984	0,338	0,072
	mt-m	0,148	0,073	0,051	0,126		mt-m	0,801	0,998	0,122	0,007
	mt-t	0,998	0,968	0,995	0,263		mt-t	1,000	0,997	0,868	0,316
24	m-wt	0,310	0,001	0,000	0,961						
	t-wt	0,657	0,656	0,000	0,031						
	mt-wt	1,000	0,884	0,000	0,529						
	t-m	0,878	0,004	0,169	0,016						
	mt-m	0,567	0,001	0,208	0,304						
	mt-t	0,839	0,298	0,946	0,218						

Supplementary Table 11. Adjusted *P* values corresponding to Figures 30 and 31.
P values < 0.05 are indicated in red.

hours after dawn		Serine M+1		Serine M+2		hours after dusk		Serine M+1		Serine M+2	
		[13C] Formate	[α-13C] Glycine	[13C] Formate	[α-13C] Glycine			[13C] Formate	[α-13C] Glycine	[13C] Formate	[α-13C] Glycine
4	m-wt	0.109	0,045	0,384	0,118	4	m-wt	0,215	0,911	0,238	0,126
	t-wt	0,816	0,210	0,910	0,669		t-wt	0,727	0,999	0,745	0,274
	mt-wt	0,622	0,235	0,717	0,666		mt-wt	0,498	0,696	0,471	0,999
	t-m	0,352	0,699	0,733	0,512		t-m	0,696	0,854	0,720	0,937
	mt-m	0,527	0,652	0,920	0,515		mt-m	0,898	0,356	0,940	0,147
8	mt-t	0,983	1,000	0,975	1,000	mt-t	0,974	0,773	0,957	0,316	
	m-wt	0,853	0,813	0,777	0,754	8	m-wt	0,689	0,787	0,522	0,576
	t-wt	0,871	0,995	0,955	0,983	t-wt	0,815	0,929	0,767	0,982	
	mt-wt	1,000	0,806	0,999	1,000	mt-wt	0,929	0,989	0,876	0,824	
	t-m	1,000	0,911	0,968	0,554	t-m	0,264	0,461	0,155	0,776	
16	mt-m	0,844	1,000	0,718	0,723	mt-m	0,374	0,618	0,212	0,966	
	mt-t	0,862	0,906	0,923	0,990	mt-t	0,992	0,991	0,995	0,958	
	m-wt	0,388	0,002	0,436	0,007	16	m-wt	0,613	0,998	0,615	0,851
	t-wt	0,983	0,937	0,991	0,986	t-wt	0,986	0,834	0,998	0,779	
	mt-wt	0,993	0,990	0,976	0,450	mt-wt	0,991	0,980	0,999	0,099	
24	t-m	0,570	0,003	0,586	0,004	t-m	0,794	0,905	0,527	0,999	
	mt-m	0,278	0,001	0,267	0,001	mt-m	0,771	0,944	0,700	0,294	
	mt-t	0,920	0,819	0,899	0,629	mt-t	1,000	0,633	0,989	0,353	
	m-wt	0,999	0,931	1,000	0,680						
	t-wt	0,730	0,886	0,794	1,000						
24	mt-wt	0,999	0,558	0,999	0,208						
	t-m	0,807	0,999	0,802	0,724						
	mt-m	0,993	0,282	0,999	0,043						
	mt-t	0,809	0,240	0,864	0,186						

Supplementary Table 12. Adjusted *P* values corresponding to Supplementary Figures 3 and 4.
P values < 0.05 are indicated in red.

hours after dawn		Tyr LD	Phe LD	Ala LD	Leu LD	Val LD	Tyr SD	Phe SD	Ala SD	Leu SD	Val SD
0	m-wt	0,234	0,991	0,962	0,106	0,824	0,936	0,025	0,895	0,972	0,764
	t-wt	0,998	0,336	0,786	0,162	0,908	0,994	0,938	0,591	1,000	0,996
	mt-wt	0,426	0,315	0,851	0,091	0,262	0,995	1,000	0,842	0,992	0,998
	t-m	0,176	0,488	0,506	0,995	0,443	0,987	0,008	0,938	0,974	0,870
	mt-m	0,973	0,462	0,988	1,000	0,059	0,843	0,030	0,446	0,891	0,667
6	mt-t	0,338	1,000	0,335	0,987	0,609	0,959	0,908	0,195	0,991	0,980
	m-wt	0,928	0,277	0,000	0,791	0,001	0,901	0,319	0,201	0,408	0,400
	t-wt	0,719	0,039	0,981	0,257	0,669	0,677	0,984	0,996	0,763	0,997
	mt-wt	1,000	0,518	0,997	0,112	0,994	0,406	0,838	0,987	0,880	1,000
	t-m	0,372	0,001	0,000	0,754	0,000	0,970	0,504	0,138	0,086	0,305
12	mt-m	0,902	0,022	0,000	0,463	0,002	0,798	0,782	0,333	0,132	0,433
	mt-t	0,760	0,413	0,998	0,958	0,521	0,964	0,963	0,943	0,995	0,994
	m-wt	0,728	0,142	0,000	0,311	0,000	0,972	0,299	1,000	0,992	0,371
	t-wt	1,000	0,115	0,948	1,000	1,000	0,965	0,905	0,996	0,978	0,971
	mt-wt	0,999	0,166	0,420	0,998	0,992	0,925	0,992	0,441	0,880	0,938
18	t-m	0,716	0,999	0,000	0,279	0,000	1,000	0,099	0,998	0,999	0,617
	mt-m	0,656	1,000	0,004	0,237	0,000	0,724	0,439	0,415	0,740	0,698
	mt-t	1,000	0,996	0,733	1,000	0,993	0,704	0,774	0,331	0,672	0,999
	m-wt	0,993	0,798	0,688	0,296	0,002	0,949	0,432	0,773	0,129	0,601
	t-wt	0,876	0,890	1,000	0,987	1,000	0,945	0,614	0,820	0,279	0,625
18	mt-wt	0,548	1,000	0,859	0,964	0,991	0,465	0,184	0,200	0,177	0,016
	t-m	0,961	0,997	0,677	0,461	0,002	0,702	0,989	1,000	0,964	1,000
	mt-m	0,703	0,792	0,267	0,139	0,004	0,776	0,936	0,680	0,998	0,173
	mt-t	0,930	0,886	0,866	0,852	0,995	0,214	0,806	0,627	0,991	0,162

Supplementary Table 13. Adjusted *P* values corresponding to Supplementary Figure 5.
P values < 0.05 are indicated in red.

hours after dawn		Arg LD	Gln LD	His LD	Arg SD	Gln SD	His SD
0	m-wt	0,998	0,198	0,334	0,825	0,229	0,993
	t-wt	0,972	1,000	0,964	0,999	0,980	0,776
	mt-wt	0,959	0,987	0,980	0,969	0,790	0,244
	t-m	0,994	0,204	0,591	0,885	0,121	0,624
	mt-m	0,906	0,326	0,185	0,572	0,044	0,160
	mt-t	0,792	0,989	0,826	0,936	0,947	0,750
	m-wt	0,000	0,698	0,233	0,027	0,444	0,196
6	t-wt	1,000	0,780	0,005	0,998	0,942	1,000
	mt-wt	0,999	0,970	0,012	0,972	0,836	0,779
	t-m	0,000	0,999	0,221	0,038	0,768	0,165
	mt-m	0,000	0,438	0,401	0,062	0,899	0,666
	mt-t	0,996	0,521	0,975	0,994	0,992	0,722
	m-wt	0,917	0,772	0,565	1,000	0,992	0,077
	t-wt	1,000	0,805	0,911	0,961	0,307	0,668
12	mt-wt	1,000	0,527	0,859	0,344	0,028	0,976
	t-m	0,881	1,000	0,237	0,963	0,198	0,468
	mt-m	0,909	0,974	0,193	0,350	0,016	0,159
	mt-t	1,000	0,962	0,999	0,614	0,544	0,881
	m-wt	0,903	0,631	0,007	0,704	0,961	0,602
	t-wt	1,000	0,969	0,999	0,977	0,997	0,941
	mt-wt	0,011	1,000	0,594	0,566	0,991	0,969
18	t-m	0,921	0,378	0,005	0,903	0,898	0,301
	mt-m	0,041	0,607	0,082	0,995	0,997	0,353
	mt-t	0,012	0,976	0,512	0,799	0,959	0,999

Supplementary Table 14. Preliminary control reactions of MTHFR and SHMT.

Preliminary control reactions for enzyme activities of MTHFR (A) and SHMT (B) were performed in wild type to assess the effect of background formation of 5-methyl-THF, the product of both. Omitting either NADPH (A, reaction b) or 5,10-methylene-THF (A, reaction c) led to strong reduction in 5-methyl-THF formation (A). Omitting Serine (B, reaction b) also strongly reduced the SHMT-mediated formation of 5,10-methylene-THF, which was chemically converted to 5-methyl-THF.

A

MTHFR enzyme activity			
	5,10-methylene-THF	NADPH	Area under the peak
a	0.5 mM	0.1 mM	18880,4 ± 8157,2
b	0.5 mM		4930,2 ± 1464,7
c		0.1 mM	372,9 ± 415,0

B

SHMT enzyme activity			
	THF	Serine	Area under the peak
a	1 mM	2 mM	487755, 7 ± 45411,7
b	1 mM		27999, 0 ± 4239,8

References

- Abadie C, Bathellier C, Tcherkez G (2018) Carbon allocation to major metabolites in illuminated leaves is not just proportional to photosynthesis when gaseous conditions (CO₂ and O₂) vary. *New Phytol* 218: 94–106
- Abadie C, Boex-Fontvieille ERA, Carroll AJ, Tcherkez G (2016) In vivo stoichiometry of photorespiratory metabolism. *Nat Plants* 2: 15220
- Akhtar TA, Orsomando G, Mehrshahi P, Lara-Núñez A, Bennett MJ, Gregory JF, Hanson AD (2010) A central role for gamma-glutamyl hydrolases in plant folate homeostasis. *Plant J* 64: 256–266
- Amir R (2010) Current understanding of the factors regulating methionine content in vegetative tissues of higher plants. *Amino Acids* 39: 917–931
- Amir R, Hacham Y, Galili G (2002) Cystathionine gamma-synthase and threonine synthase operate in concert to regulate carbon flow towards methionine in plants. *Trends Plant Sci* 7: 153–156
- Andrés F, Coupland G (2012) The genetic basis of flowering responses to seasonal cues. *Nat Rev Genet* 13: 627–639
- Appling DR (1991) Compartmentation of folate-mediated one-carbon metabolism in eukaryotes. *FASEB J* 5: 2645–2651
- Appling DR, Rabinowitz JC (1985) Regulation of expression of the ADE3 gene for yeast C1-tetrahydrofolate synthase, a trifunctional enzyme involved in one-carbon metabolism. *Journal of Biological Chemistry* 260: 1248–1256
- Arvidsson S, Kwasniewski M, Riaño-Pachón DM, Mueller-Roeber B (2008) QuantPrime--a flexible tool for reliable high-throughput primer design for quantitative PCR. *BMC Bioinformatics* 9: 465
- Auge G, Hankofer V, Groth M, Antoniou-Kourouniotti R, Ratikainen I, Lampei C (2023) Plant environmental memory: implications, mechanisms and opportunities for plant scientists and beyond. *AoB Plants* 15: plad032
- Basset G, Quinlivan EP, Ziemak MJ, La Diaz De Garza R, Fischer M, Schiffmann S, Bacher A, Gregory JF, Hanson AD (2002) Folate synthesis in plants: the first step of the pterin branch is mediated by a unique bimodular GTP cyclohydrolase I. *Proc Natl Acad Sci U S A* 99: 12489–12494
- Basset GJC, Quinlivan EP, Ravanel S, Rébeillé F, Nichols BP, Shinozaki K, Seki M, Adams-Phillips LC, Giovannoni JJ, Gregory JF et al (2004a) Folate synthesis in plants: the p-aminobenzoate branch is initiated by a bifunctional PabA-PabB protein that is targeted to plastids. *Proc Natl Acad Sci U S A* 101: 1496–1501
- Basset GJC, Ravanel S, Quinlivan EP, White R, Giovannoni JJ, Rébeillé F, Nichols BP, Shinozaki K, Seki M, Gregory JF et al (2004b) Folate synthesis in plants: the last step of the p-aminobenzoate branch is catalyzed by a plastidial aminodeoxychorismate lyase. *The Plant Journal* 40: 453–461

- Bauwe H, Hagemann M, Fernie AR (2010) Photorespiration: players, partners and origin. *Trends Plant Sci* 15: 330–336
- Becker C, Hagemann J, Müller J, Koenig D, Stegle O, Borgwardt K, Weigel D (2011) Spontaneous epigenetic variation in the *Arabidopsis thaliana* methylome. *Nature* 480: 245–249
- Berger SL, Kouzarides T, Shiekhattar R, Shilatifard A (2009) An operational definition of epigenetics. *Genes Dev* 23: 781–783
- Bernatavichute YV, Zhang X, Cokus S, Pellegrini M, Jacobsen SE (2008) Genome-wide association of histone H3 lysine nine methylation with CHG DNA methylation in *Arabidopsis thaliana*. *PLoS One* 3: e3156
- Besson V, Rebeille F, Neuburger M, Douce R, Cossins EA (1993) Effects of tetrahydrofolate polyglutamates on the kinetic parameters of serine hydroxymethyltransferase and glycine decarboxylase from pea leaf mitochondria. *Biochem J* 292 (Pt 2): 425–430
- Blancquaert D, Steur H de, Gellynck X, van der Straeten D (2014) Present and future of folate biofortification of crop plants. *J Exp Bot* 65: 895–906
- Boldt R, Zrenner R (2003) Purine and pyrimidine biosynthesis in higher plants. *Physiol Plant* 117: 297–304
- Bond DM, Baulcombe DC (2015) Epigenetic transitions leading to heritable, RNA-mediated de novo silencing in *Arabidopsis thaliana*. *Proc Natl Acad Sci U S A* 112: 917–922
- Braun H-P (2020) The Oxidative Phosphorylation system of the mitochondria in plants. *Mitochondrion* 53: 66–75
- Brosnan ME, Brosnan JT (2016) Formate: The Neglected Member of One-Carbon Metabolism. *Annu Rev Nutr* 36: 369–388
- Cantoni GL (1975) Biological methylation: selected aspects. *Annu Rev Biochem* 44: 435–451
- Cervela-Cardona L, Alary B, Mas P (2021) The *Arabidopsis* Circadian Clock and Metabolic Energy: A Question of Time. *Front Plant Sci* 12: 804468
- Chan SW-L, Henderson IR, Zhang X, Shah G, Chien JS-C, Jacobsen SE (2006) RNAi, DRD1, and histone methylation actively target developmentally important non-CG DNA methylation in *Arabidopsis*. *PLOS Genetics* 2: e83
- Chen L, Nargang FE, Cossin EA (1999) Isolation and Sequencing of a Plant cDNA Encoding a Bifunctional Methylene tetrahydrofolate Dehydrogenase : Methenyl tetrahydrofolate Cyclohydrolase Protein. *Pteridines* 10: 171–177
- Choi J, Lyons DB, Kim MY, Moore JD, Zilberman D (2020) DNA Methylation and Histone H1 Jointly Repress Transposable Elements and Aberrant Intragenic Transcripts. *Mol Cell* 77: 310-323.e7
- Christensen KE, MacKenzie RE (2006) Mitochondrial one-carbon metabolism is adapted to the specific needs of yeast, plants and mammals. *Bioessays* 28: 595–605

- Christensen KE, Patel H, Kuzmanov U, Mejia NR, MacKenzie RE (2005) Disruption of the *mthfd1* gene reveals a monofunctional 10-formyltetrahydrofolate synthetase in mammalian mitochondria. *Journal of Biological Chemistry* 280: 7597–7602
- Collakova E, Goyer A, Naponelli V, Krassovskaya I, Gregory JF, Hanson AD, Shachar-Hill Y (2008) Arabidopsis 10-formyl tetrahydrofolate deformylases are essential for photorespiration. *Plant Cell* 20: 1818–1832
- Coxon KM, Chakauya E, Ottenhof HH, Whitney HM, Blundell TL, Abell C, Smith AG (2005) Pantothenate biosynthesis in higher plants. *Biochem Soc Trans* 33: 743–746
- Czeizel AE, Dudás I (1992) Prevention of the first occurrence of neural-tube defects by periconceptional vitamin supplementation. *N Engl J Med* 327: 1832–1835
- Dai Z, Ramesh V, Locasale JW (2020) The evolving metabolic landscape of chromatin biology and epigenetics. *Nat Rev Genet* 21: 737–753
- DellaPenna D (2007) Biofortification of plant-based food: enhancing folate levels by metabolic engineering. *Proc Natl Acad Sci U S A* 104: 3675–3676
- Denkena J, Johannes F, Colomé-Tatché M (2021) Region-level epimutation rates in *Arabidopsis thaliana*. *Heredity (Edinb)* 127: 190–202
- Dominguez-Salas P, Moore SE, Baker MS, Bergen AW, Cox SE, Dyer RA, Fulford AJ, Guan Y, Laritsky E, Silver MJ et al (2014) Maternal nutrition at conception modulates DNA methylation of human metastable epialleles. *Nat Commun* 5: 3746
- Dorion S, Ouellet JC, Rivoal J (2021) Glutathione Metabolism in Plants under Stress: Beyond Reactive Oxygen Species Detoxification. *Metabolites* 11
- Du J, Johnson LM, Jacobsen SE, Patel DJ (2015) DNA methylation pathways and their crosstalk with histone methylation. *Nat Rev Mol Cell Biol* 16: 519–532
- Du J, Zhong X, Bernatavichute YV, Stroud H, Feng S, Caro E, Vashisht AA, Terragni J, Chin HG, Tu A et al (2012) Dual binding of chromomethylase domains to H3K9me2-containing nucleosomes directs DNA methylation in plants. *Cell* 151: 167–180
- Dubin MJ, Zhang P, Meng D, Remigereau M-S, Osborne EJ, Paolo Casale F, Drewe P, Kahles A, Jean G, Vilhjálmsson B et al (2015) DNA methylation in *Arabidopsis* has a genetic basis and shows evidence of local adaptation. *Elife* 4: e05255
- Ducker GS, Rabinowitz JD (2017) One-Carbon Metabolism in Health and Disease. *Cell Metab* 25: 27–42
- Dusenge ME, Duarte AG, Way DA (2019) Plant carbon metabolism and climate change: elevated CO₂ and temperature impacts on photosynthesis, photorespiration and respiration. *New Phytol* 221: 32–49
- Ebbs ML, Bender J (2006) Locus-specific control of DNA methylation by the *Arabidopsis* SUVH5 histone methyltransferase. *Plant Cell* 18: 1166–1176
- Engel N, van den Daele K, Kolukisaoglu U, Morgenthal K, Weckwerth W, Pärnik T, Keerbergh O, Bauwe H (2007) Deletion of glycine decarboxylase in *Arabidopsis* is lethal under nonphotorespiratory conditions. *Plant Physiol* 144: 1328–1335

- Eriksson MC, Szukala A, Tian B, Paun O (2020) Current research frontiers in plant epigenetics: an introduction to a Virtual Issue. *New Phytol* 226: 285–288
- Fan J, Ye J, Kamphorst JJ, Shlomi T, Thompson CB, Rabinowitz JD (2014) Quantitative flux analysis reveals folate-dependent NADPH production. *Nature* 510: 298–302
- Farquharson KL (2017) Folate Metabolism Linked to Redox Balance in Arabidopsis. *Plant Cell* 29: 2682
- Fedoroff NV (2012) Presidential address. Transposable elements, epigenetics, and genome evolution. *Science* 338: 758–767
- Fernie AR, Carrari F, Sweetlove LJ (2004) Respiratory metabolism: glycolysis, the TCA cycle and mitochondrial electron transport. *Curr Opin Plant Biol* 7: 254–261
- Field MS, Kamynina E, Chon J, Stover PJ (2018) Nuclear Folate Metabolism. *Annu Rev Nutr* 38: 219–243
- Field MS, Kamynina E, Watkins D, Rosenblatt DS, Stover PJ (2015) Human mutations in methylenetetrahydrofolate dehydrogenase 1 impair nuclear de novo thymidylate biosynthesis. *Proc Natl Acad Sci U S A* 112: 400–405
- Froese DS, Kopec J, Rembeza E, Bezerra GA, Oberholzer AE, Suormala T, Lutz S, Chalk R, Borkowska O, Baumgartner MR et al (2018) Structural basis for the regulation of human 5,10-methylenetetrahydrofolate reductase by phosphorylation and S-adenosylmethionine inhibition. *Nat Commun* 9: 2261
- Furner IJ, Sheikh MA, Collett CE (1998) Gene silencing and homology-dependent gene silencing in Arabidopsis: genetic modifiers and DNA methylation. *Genetics* 149: 651–662
- Gehring M (2013) Genomic imprinting: insights from plants. *Annu Rev Genet* 47: 187–208
- Gehring M, Huh JH, Hsieh T-F, Penterman J, Choi Y, Harada JJ, Goldberg RB, Fischer RL (2006) DEMETER DNA glycosylase establishes MEDEA polycomb gene self-imprinting by allele-specific demethylation. *Cell* 124: 495–506
- Giovanelli J, Mudd SH, Datko AH (1985) In vivo regulation of de novo methionine biosynthesis in a higher plant (lemna). *Plant Physiol* 77: 450–455
- Goeldel C, Johannes F (2023) Stochasticity in gene body methylation. *Curr Opin Plant Biol* 75: 102436
- Gong Z, Morales-Ruiz T, Ariza RR, Roldán-Arjona T, David L, Zhu JK (2002) ROS1, a repressor of transcriptional gene silencing in Arabidopsis, encodes a DNA glycosylase/lyase. *Cell* 111: 803–814
- Gorelova V, Ambach L, Rébeillé F, Stove C, van der Straeten D (2017a) Foliates in Plants: Research Advances and Progress in Crop Biofortification. *Front Chem* 5: 21
- Gorelova V, Bastien O, Clerck O de, Lespinats S, Rébeillé F, van der Straeten D (2019) Evolution of folate biosynthesis and metabolism across algae and land plant lineages. *Sci Rep* 9: 5731
- Gorelova V, Lepeleire J de, van Daele J, Pluim D, Meï C, Cuypers A, Leroux O, Rébeillé F, Schellens JHM, Blancquaert D et al (2017b) Dihydrofolate Reductase/Thymidylate Synthase

Fine-Tunes the Folate Status and Controls Redox Homeostasis in Plants. *Plant Cell* 29: 2831–2853

Goujon M, McWilliam H, Li W, Valentin F, Squizzato S, Paern J, Lopez R (2010) A new bioinformatics analysis tools framework at EMBL-EBI. *Nucleic Acids Res* 38: W695-9

Goyer A, Collakova E, La Díaz de Garza R, Quinlivan EP, Williamson J, Gregory JF, Shachar-Hill Y, Hanson AD (2005) 5-Formyltetrahydrofolate is an inhibitory but well tolerated metabolite in Arabidopsis leaves. *J Biol Chem* 280: 26137–26142

Goyer A, Illarionova V, Roje S, Fischer M, Bacher A, Hanson AD (2004) Folate biosynthesis in higher plants. cDNA cloning, heterologous expression, and characterization of dihydroneopterin aldolases. *Plant Physiol* 135: 103–111

Greco CM, Cervantes M, Fustin J-M, Ito K, Ceglia N, Samad M, Shi J, Koronowski KB, Forne I, Ranjit S et al (2020) S-adenosyl-L-homocysteine hydrolase links methionine metabolism to the circadian clock and chromatin remodeling. *Sci Adv* 6

Green AC, Marttila P, Kiweler N, Chalkiadaki C, Wiita E, Cookson V, Lesur A, Eiden K, Bernardin F, Vallin KSA et al (2023) Formate overflow drives toxic folate trapping in MTHFD1 inhibited cancer cells. *Nat Metab* 5: 642–659

Green JM, MacKenzie RE, Matthews RG (1988) Substrate flux through methylenetetrahydrofolate dehydrogenase: predicted effects of the concentration of methylenetetrahydrofolate on its partitioning into pathways leading to nucleotide biosynthesis or methionine regeneration. *Biochemistry* 27: 8014–8022

Greenham K, McClung CR (2015) Integrating circadian dynamics with physiological processes in plants. *Nat Rev Genet* 16: 598–610

Groth M, Moissiard G, Wirtz M, Wang H, Garcia-Salinas C, Ramos-Parra PA, Bischof S, Feng S, Cokus SJ, John A et al (2016) MTHFD1 controls DNA methylation in Arabidopsis. *Nat Commun* 7: 11640

Halter T, Wang J, Amesefe D, Lastrucci E, Charvin M, Singla Rastogi M, Navarro L (2021) The Arabidopsis active demethylase ROS1 cis-regulates defence genes by erasing DNA methylation at promoter-regulatory regions. *Elife* 10

Hancock AM, Brachi B, Faure N, Horton MW, Jarymowycz LB, Sperone FG, Toomajian C, Roux F, Bergelson J (2011) Adaptation to climate across the Arabidopsis thaliana genome. *Science* 334: 83–86

Hanson AD, Gage DA, Shachar-Hill Y (2000) Plant one-carbon metabolism and its engineering. *Trends Plant Sci* 5: 206–213

Hanson AD, Gregory JF (2011) Folate biosynthesis, turnover, and transport in plants. *Annu Rev Plant Biol* 62: 105–125

Hanson AD, Roje S (2001) ONE-CARBON METABOLISM IN HIGHER PLANTS. *Annual Review of Plant Physiology and Plant Molecular Biology* 52: 119–137

Harmer SL, Hogenesch JB, Straume M, Chang HS, Han B, Zhu T, Wang X, Kreps JA, Kay SA (2000) Orchestrated transcription of key pathways in Arabidopsis by the circadian clock. *Science* 290: 2110–2113

Harris CJ, Scheibe M, Wongpalee SP, Liu W, Cornett EM, Vaughan RM, Li X, Chen W, Xue Y, Zhong Z et al (2018) A DNA methylation reader complex that enhances gene transcription. *Science* 362: 1182–1186

Hashemi S, Laitinen R, Nikoloski Z (2023) Models and molecular mechanisms for trade-offs in the context of metabolism. *Mol Ecol*

Hazarika RR, Serra M, Zhang Z, Zhang Y, Schmitz RJ, Johannes F (2022) Molecular properties of epimutation hotspots. *Nat Plants* 8: 146–156

Heard E, Martienssen RA (2014) Transgenerational epigenetic inheritance: myths and mechanisms. *Cell* 157: 95–109

Henderson IR, Jacobsen SE (2008) Tandem repeats upstream of the Arabidopsis endogene SDC recruit non-CG DNA methylation and initiate siRNA spreading. *Genes Dev* 22: 1597–1606

Henikoff S, Greally JM (2016) Epigenetics, cellular memory and gene regulation. *Curr Biol* 26: R644-8

Herbig K, Chiang E-P, Lee L-R, Hills J, Shane B, Stover PJ (2002) Cytoplasmic serine hydroxymethyltransferase mediates competition between folate-dependent deoxyribonucleotide and S-adenosylmethionine biosyntheses. *J Biol Chem* 277: 38381–38389

Hjortmo S, Patring J, Andlid T (2008) Growth rate and medium composition strongly affect folate content in *Saccharomyces cerevisiae*. *Int J Food Microbiol* 123: 93–100

Hofmeister BT, Denkena J, Colomé-Tatché M, Shahryary Y, Hazarika R, Grimwood J, Mamidi S, Jenkins J, Grabowski PP, Sreedasyam A et al (2020) A genome assembly and the somatic genetic and epigenetic mutation rate in a wild long-lived perennial *Populus trichocarpa*. *Genome Biol* 21: 259

Hooper C, Millar H, Black K, Castleden I, Aryamanesh N, Grasso S (2022) *Subcellular Localisation database for Arabidopsis proteins version 5*: The University of Western Australia

Hooper CM, Castleden IR, Tanz SK, Aryamanesh N, Millar AH (2017) SUBA4: the interactive data analysis centre for Arabidopsis subcellular protein locations. *Nucleic Acids Res* 45: D1064-D1074

Hossain T, Rosenberg I, Selhub J, Kishore G, Beachy R, Schubert K (2004) Enhancement of folates in plants through metabolic engineering. *Proc Natl Acad Sci U S A* 101: 5158–5163

Huang X-Y, Chao D-Y, Koprivova A, Danku J, Wirtz M, Müller S, Sandoval FJ, Bauwe H, Roje S, Dilkes B et al (2016) Nuclear Localised MORE SULPHUR ACCUMULATION1 Epigenetically Regulates Sulphur Homeostasis in *Arabidopsis thaliana*. *PLoS Genet* 12: e1006298

Huang X-Y, Li M, Luo R, Zhao F-J, Salt DE (2019) Epigenetic regulation of sulfur homeostasis in plants. *J Exp Bot* 70: 4171–4182

Hum DW, Bell AW, Rozen R, MacKenzie RE (1988) Primary structure of a human trifunctional enzyme. Isolation of a cDNA encoding methylenetetrahydrofolate dehydrogenase-methenyltetrahydrofolate cyclohydrolase-formyltetrahydrofolate synthetase. *Journal of Biological Chemistry* 263: 15946–15950

Ichino L, Boone BA, Strauskulage L, Harris CJ, Kaur G, Gladstone MA, Tan M, Feng S, Jami-Alahmadi Y, Duttke SH et al (2021) MBD5 and MBD6 couple DNA methylation to gene silencing through the J-domain protein SILENZIO. *Science*

Igamberdiev A (1999) Origins and metabolism of formate in higher plants. *Plant Physiology and Biochemistry* 37: 503–513

Igamberdiev AU, Kleczkowski LA (2018) The Glycerate and Phosphorylated Pathways of Serine Synthesis in Plants: The Branches of Plant Glycolysis Linking Carbon and Nitrogen Metabolism. *Front Plant Sci* 9: 318

Jackson JP, Johnson L, Jasencakova Z, Zhang X, PerezBurgos L, Singh PB, Cheng X, Schubert I, Jenuwein T, Jacobsen SE (2004) Dimethylation of histone H3 lysine 9 is a critical mark for DNA methylation and gene silencing in *Arabidopsis thaliana*. *Chromosoma* 112: 308–315

Jackson JP, Lindroth AM, Cao X, Jacobsen SE (2002) Control of CpNpG DNA methylation by the KRYPTONITE histone H3 methyltransferase. *Nature* 416: 556–560

JACOB F, MONOD J (1961) Genetic regulatory mechanisms in the synthesis of proteins. *J Mol Biol* 3: 318–356

Jander G, Joshi V (2009) Aspartate-Derived Amino Acid Biosynthesis in *Arabidopsis thaliana*. *Arabidopsis Book* 7: e0121

Jang C, Chen L, Rabinowitz JD (2018) Metabolomics and Isotope Tracing. *Cell* 173: 822–837

Jean-Paul Concordet, Maximilian Haeussler CRISPOR: intuitive guide selection for CRISPR/Cas9 genome editing experiments and screens

Johnson LM, Du J, Hale CJ, Bischof S, Feng S, Chodavarapu RK, Zhong X, Marson G, Pellegrini M, Segal DJ et al (2014) SRA- and SET-domain-containing proteins link RNA polymerase V occupancy to DNA methylation. *Nature* 507: 124–128

Kawakatsu T, Huang S-SC, Jupe F, Sasaki E, Schmitz RJ, Urich MA, Castanon R, Nery JR, Barragan C, He Y et al (2016) Epigenomic Diversity in a Global Collection of *Arabidopsis thaliana* Accessions. *Cell* 166: 492–505

Kirk CD, Chen L, Imeson HC, Cossins EA (1995) A 5,10-methylenetetrahydrofolate dehydrogenase: 5,10-methenyltetrahydrofolate cyclohydrolase protein from *Pisum sativum*. *Phytochemistry* 39: 1309–1317

Kirk CD, Imeson HC, Zheng L-L, Cossins EA (1994) The affinity of pea cotyledon 10-formyltetrahydrofolate synthetase for polyglutamate substrates. *Phytochemistry* 35: 291–296

Kirma M, Araújo WL, Fernie AR, Galili G (2012) The multifaceted role of aspartate-family amino acids in plant metabolism. *J Exp Bot* 63: 4995–5001

Kleessen S, Antonio C, Sulpice R, Laitinen R, Fernie AR, Stitt M, Nikoloski Z (2012) Structured patterns in geographic variability of metabolic phenotypes in *Arabidopsis thaliana*. *Nat Commun* 3: 1319

Köhler C, Weinhofer-Molisch I (2010) Mechanisms and evolution of genomic imprinting in plants. *Heredity (Edinb)* 105: 57–63

- Kolton A, Długosz-Grochowska O, Wojciechowska R, Czaja M (2022) Biosynthesis Regulation of Folates and Phenols in Plants. *Scientia Horticulturae* 291: 110561
- Koornneef M, Alonso-Blanco C, Vreugdenhil D (2004) Naturally occurring genetic variation in *Arabidopsis thaliana*. *Annu Rev Plant Biol* 55: 141–172
- Koornneef M, Hanhart CJ, van der Veen JH (1991) A genetic and physiological analysis of late flowering mutants in *Arabidopsis thaliana*. *Mol Gen Genet* 229: 57–66
- La Díaz de Garza RI, Ramos-Parra PA, Vidal-Limon HR (2019) Biofortification of Crops with Folates: From Plant Metabolism to Table. In *Nutritional quality improvement in plants*, Jaiwal PK, Chhillar AK, Chaudhary D, Jaiwal R (eds) pp. 137–175. Cham, Switzerland: Springer
- La Haba G de, Cantoni GL (1959) The Enzymatic Synthesis of S-Adenosyl-L-homocysteine from Adenosine and Homocysteine. *Journal of Biological Chemistry* 234: 603–608
- Lamers J, van der Meer T, Testerink C (2020) How Plants Sense and Respond to Stressful Environments. *Plant Physiol* 182: 1624–1635
- Lämke J, Bäurle I (2017) Epigenetic and chromatin-based mechanisms in environmental stress adaptation and stress memory in plants. *Genome Biol* 18: 124
- Law JA, Du J, Hale CJ, Feng S, Krajewski K, Palanca AMS, Strahl BD, Patel DJ, Jacobsen SE (2013) Polymerase IV occupancy at RNA-directed DNA methylation sites requires SHH1. *Nature* 498: 385–389
- Law JA, Jacobsen SE (2010) Establishing, maintaining and modifying DNA methylation patterns in plants and animals. *Nat Rev Genet* 11: 204–220
- Lee J, Jang H, Shin H, Choi WL, Mok YG, Huh JH (2014) AP endonucleases process 5-methylcytosine excision intermediates during active DNA demethylation in *Arabidopsis*. *Nucleic Acids Res* 42: 11408–11418
- Lee S, Doxey AC, McConkey BJ, Moffatt BA (2012) Nuclear targeting of methyl-recycling enzymes in *Arabidopsis thaliana* is mediated by specific protein interactions. *Mol Plant* 5: 231–248
- Lerma-Ortiz C, Jeffryes JG, Cooper AJL, Niehaus TD, Thamm AMK, Frelin O, Aunins T, Fiehn O, Crécy-Lagard V de, Henry CS et al (2016) 'Nothing of chemistry disappears in biology': the Top 30 damage-prone endogenous metabolites. *Biochem Soc Trans* 44: 961–971
- Lesk C, Anderson W, Rigden A, Coast O, Jägermeyr J, McDermid S, Davis KF, Konar M (2022) Compound heat and moisture extreme impacts on global crop yields under climate change. *Nat Rev Earth Environ* 3: 872–889
- Li R, Moore M, King J (2003) Investigating the regulation of one-carbon metabolism in *Arabidopsis thaliana*. *Plant Cell Physiol* 44: 233–241
- Li W, Liang Q, Mishra RC, Sanchez-Mu Oz R, Wang H, Chen X, van der Straeten D, Zhang C, Xiao Y (2021) The 5-formyl-tetrahydrofolate proteome links folates with C/N metabolism and reveals feedback regulation of folate biosynthesis. *Plant Cell* 33: 3367–3385
- Li Y, Córdoba-Cañero D, Qian W, Zhu X, Tang K, Zhang H, Ariza RR, Roldán-Arjona T, Zhu J-K (2015) An AP endonuclease functions in active DNA demethylation and gene imprinting in *Arabidopsis* corrected. *PLOS Genetics* 11: e1004905

- Lindermayr C, Rudolf EE, Durner J, Groth M (2020) Interactions between metabolism and chromatin in plant models. *Mol Metab* 38: 100951
- Lindroth AM, Cao X, Jackson JP, Zilberman D, McCallum CM, Henikoff S, Jacobsen SE (2001) Requirement of CHROMOMETHYLASE3 for maintenance of CpXpG methylation. *Science* 292: 2077–2080
- Lister R, O'Malley RC, Tonti-Filippini J, Gregory BD, Berry CC, Millar AH, Ecker JR (2008) Highly integrated single-base resolution maps of the epigenome in Arabidopsis. *Cell* 133: 523–536
- Liu Q, Bischof S, Harris CJ, Zhong Z, Zhan L, Nguyen C, Rashoff A, Barshop WD, Sun F, Feng S et al (2020) The characterization of Mediator 12 and 13 as conditional positive gene regulators in Arabidopsis. *Nat Commun* 11: 2798
- Liu Z-W, Shao C-R, Zhang C-J, Zhou J-X, Zhang S-W, Li L, Chen S, Huang H-W, Cai T, He X-J (2014) The SET domain proteins SUVH2 and SUVH9 are required for Pol V occupancy at RNA-directed DNA methylation loci. *PLoS Genet* 10: e1003948
- Lloyd JPB, Lister R (2022) Epigenome plasticity in plants. *Nat Rev Genet* 23: 55–68
- Lu C, Thompson CB (2012) Metabolic regulation of epigenetics. *Cell Metab* 16: 9–17
- Lu Y, Bu Q, Chuan M, Cui X, Zhao Y, Zhou D-X (2023) Metabolic regulation of the plant epigenome. *Plant J*
- Lyko F (2018) The DNA methyltransferase family: a versatile toolkit for epigenetic regulation. *Nat Rev Genet* 19: 81–92
- Malagnac F, Bartee L, Bender J (2002) An Arabidopsis SET domain protein required for maintenance but not establishment of DNA methylation. *EMBO J* 21: 6842–6852
- Martha S. Field, Elena Kamynina, James Chon, Patrick J. Stover Nuclear Folate Metabolism
- Martínez-Macías MI, Qian W, Miki D, Pontes O, Liu Y, Tang K, Liu R, Morales-Ruiz T, Ariza RR, Roldán-Arjona T et al (2012) A DNA 3' phosphatase functions in active DNA demethylation in Arabidopsis. *Mol Cell* 45: 357–370
- Mas-Droux C, Biou V, Dumas R (2006) Allosteric threonine synthase. Reorganization of the pyridoxal phosphate site upon asymmetric activation through S-adenosylmethionine binding to a novel site. *Journal of Biological Chemistry* 281: 5188–5196
- Mattioli R, Costantino P, Trovato M (2009) Proline accumulation in plants: not only stress. *Plant Signal Behav* 4: 1016–1018
- Matzke MA, Mosher RA (2014) RNA-directed DNA methylation: an epigenetic pathway of increasing complexity. *Nat Rev Genet* 15: 394–408
- McNeil JB, Bogner AL, Pearlman RE (1996) In vivo analysis of folate coenzymes and their compartmentation in *Saccharomyces cerevisiae*. *Genetics* 142: 371–381
- McWilliam H, Li W, Uludag M, Squizzato S, Park YM, Buso N, Cowley AP, Lopez R (2013) Analysis Tool Web Services from the EMBL-EBI. *Nucleic Acids Res* 41: W597–600

- Mehrshahi P, Gonzalez-Jorge S, Akhtar TA, Ward JL, Santoyo-Castelazo A, Marcus SE, Lara-Núñez A, Ravanel S, Hawkins ND, Beale MH et al (2010) Functional analysis of folate polyglutamylolation and its essential role in plant metabolism and development. *Plant J* 64: 267–279
- Meiser J, Schuster A, Pietzke M, Vande Voorde J, Athineos D, Oizel K, Burgos-Barragan G, Wit N, Dhayade S, Morton JP et al (2018) Increased formate overflow is a hallmark of oxidative cancer. *Nat Commun* 9: 1368
- Meiser J, Tumanov S, Maddocks O, Labuschagne CF, Athineos D, van den Broek N, Mackay GM, Gottlieb E, Blyth K, Vousden K et al (2016) Serine one-carbon catabolism with formate overflow. *Sci Adv* 2: e1601273
- Meng J, Wang L, Wang J, Zhao X, Cheng J, Yu W, Jin D, Li Q, Gong Z (2018) METHIONINE ADENOSYLTRANSFERASE4 Mediates DNA and Histone Methylation. *Plant Physiol* 177: 652–670
- Meyer AJ (2008) The integration of glutathione homeostasis and redox signaling. *Journal of Plant Physiology* 165: 1390–1403
- Meyer AJ, Brach T, Marty L, Kreye S, Rouhier N, Jacquot J-P, Hell R (2007) Redox-sensitive GFP in *Arabidopsis thaliana* is a quantitative biosensor for the redox potential of the cellular glutathione redox buffer. *The Plant Journal* 52: 973–986
- Moffatt BA, Stevens YY, Allen MS, Snider JD, Pereira LA, Todorova MI, Summers PS, Weretilnyk EA, Martin-McCaffrey L, Wagner C (2002) Adenosine kinase deficiency is associated with developmental abnormalities and reduced transmethylation. *Plant Physiol* 128: 812–821
- Moffatt BA, Weretilnyk EA (2001) Sustaining S-adenosyl-L-methionine-dependent methyltransferase activity in plant cells. *Physiol Plant* 113: 435–442
- Moissiard G, Bischof S, Husmann D, Pastor WA, Hale CJ, Yen L, Stroud H, Papikian A, Vashisht AA, Wohlschlegel JA et al (2014) Transcriptional gene silencing by *Arabidopsis* microorchidia homologues involves the formation of heteromers. *Proceedings of the National Academy of Sciences* 111: 7474–7479
- Moissiard G, Cokus SJ, Cary J, Feng S, Billi AC, Stroud H, Husmann D, Zhan Y, Lajoie BR, McCord RP et al (2012) MORC family ATPases required for heterochromatin condensation and gene silencing. *Science* 336: 1448–1451
- Mouillon JM, Aubert S, Bourguignon J, Gout E, Douce R, Rébeillé F (1999) Glycine and serine catabolism in non-photosynthetic higher plant cells: their role in C1 metabolism. *Plant J* 20: 197–205
- Mouillon J-M, Ravanel S, Douce R, Rébeillé F (2002) Folate synthesis in higher-plant mitochondria: coupling between the dihydropterin pyrophosphokinase and the dihydropterolate synthase activities. *Biochemical Journal* 363: 313–319
- Mull L, Ebbs ML, Bender J (2006) A histone methylation-dependent DNA methylation pathway is uniquely impaired by deficiency in *Arabidopsis* S-adenosylhomocysteine hydrolase. *Genetics* 174: 1161–1171

- Nakamichi N (2020) The Transcriptional Network in the Arabidopsis Circadian Clock System. *Genes (Basel)* 11
- Neuburger M, Rébeillé F, Jourdain A, Nakamura S, Douce R (1996) Mitochondria are a major site for folate and thymidylate synthesis in plants. *Journal of Biological Chemistry* 271: 9466–9472
- Nieborak A, Schneider R (2018) Metabolic intermediates - Cellular messengers talking to chromatin modifiers. *Mol Metab* 14: 39–52
- Nogués I, Sekula B, Angelaccio S, Grzechowiak M, Tramonti A, Contestabile R, Ruszkowski M (2022) Arabidopsis thaliana serine hydroxymethyltransferases: functions, structures, and perspectives. *Plant Physiol Biochem* 187: 37–49
- Onouchi H, Nagami Y, Haraguchi Y, Nakamoto M, Nishimura Y, Sakurai R, Nagao N, Kawasaki D, Kadokura Y, Naito S (2005) Nascent peptide-mediated translation elongation arrest coupled with mRNA degradation in the CGS1 gene of Arabidopsis. *Genes Dev* 19: 1799–1810
- Onoue N, Yamashita Y, Nagao N, Goto DB, Onouchi H, Naito S (2011) S-adenosyl-L-methionine induces compaction of nascent peptide chain inside the ribosomal exit tunnel upon translation arrest in the Arabidopsis CGS1 gene. *J Biol Chem* 286: 14903–14912
- Ordon J, Gantner J, Kemna J, Schwalgun L, Reschke M, Streubel J, Boch J, Stuttmann J (2017) Generation of chromosomal deletions in dicotyledonous plants employing a user-friendly genome editing toolkit. *Plant J* 89: 155–168
- Orsomando G, La Garza RD de, Green BJ, Peng M, Rea PA, Ryan TJ, Gregory JF, Hanson AD (2005) Plant gamma-glutamyl hydrolases and folate polyglutamates: characterization, compartmentation, and co-occurrence in vacuoles. *J Biol Chem* 280: 28877–28884
- Ortega-Galisteo AP, Morales-Ruiz T, Ariza RR, Roldán-Arjona T (2008) Arabidopsis DEMETER-LIKE proteins DML2 and DML3 are required for appropriate distribution of DNA methylation marks. *Plant Mol Biol* 67: 671–681
- Ouyang B, Fei Z, Joung J-G, Kolenovsky A, Koh C, Nowak J, Caplan A, Keller WA, Cui Y, Cutler AJ et al (2012) Transcriptome profiling and methyl homeostasis of an Arabidopsis mutant deficient in S-adenosylhomocysteine hydrolase1 (SAHH1). *Plant Mol Biol* 79: 315–331
- Panda K, Mohanasundaram B, Gutierrez J, McLain L, Castillo SE, Sheng H, Casto A, Gratacós G, Chakrabarti A, Fahlgren N et al (2023) The plant response to high CO₂ levels is heritable and orchestrated by DNA methylation. *New Phytol* 238: 2427–2439
- Park DH, Somers DE, Kim YS, Choy YH, Lim HK, Soh MS, Kim HJ, Kay SA, Nam HG (1999) Control of circadian rhythms and photoperiodic flowering by the Arabidopsis GIGANTEA gene. *Science* 285: 1579–1582
- Penterman J, Zilberman D, Huh JH, Ballinger T, Henikoff S, Fischer RL (2007) DNA demethylation in the Arabidopsis genome. *Proc Natl Acad Sci U S A* 104: 6752–6757
- Pereira LAR, Todorova M, Cai X, Makaroff CA, Emery RJN, Moffatt BA (2007) Methyl recycling activities are co-ordinately regulated during plant development. *J Exp Bot* 58: 1083–1098

- Pérez-Palacios T, Barroso MA, Ruiz J, Antequera T (2015) A Rapid and Accurate Extraction Procedure for Analysing Free Amino Acids in Meat Samples by GC-MS. *Int J Anal Chem* 2015: 209214
- Peri KG, Belanger C, MacKenzie RE (1989) Nucleotide sequence of the human NAD-dependent methylene tetrahydrofolate dehydrogenase-cyclohydrolase. *Nucleic Acids Res* 17: 8853
- Pikaard CS, Haag JR, Pontes OMF, Blevins T, Cocklin R (2012) A transcription fork model for Pol IV and Pol V-dependent RNA-directed DNA methylation. *Cold Spring Harb Symp Quant Biol* 77: 205–212
- Prabhu V, Chatson KB, Abrams GD, King J (1996) ¹³C nuclear magnetic resonance detection of interactions of serine hydroxymethyltransferase with C1-tetrahydrofolate synthase and glycine decarboxylase complex activities in Arabidopsis. *Plant Physiol* 112: 207–216
- Prabhu V, Chatson KB, Lui H, Abrams GD, King J (1998) Effects of sulfanilamide and methotrexate on ¹³C fluxes through the glycine decarboxylase/serine hydroxymethyltransferase enzyme system in arabidopsis. *Plant Physiol* 116: 137–144
- Quesneville H (2020) Twenty years of transposable element analysis in the Arabidopsis thaliana genome. *Mob DNA* 11: 28
- Quinlivan EP, Roje S, Basset G, Shachar-Hill Y, Gregory JF, Hanson AD (2003) The folate precursor p-aminobenzoate is reversibly converted to its glucose ester in the plant cytosol. *Journal of Biological Chemistry* 278: 20731–20737
- Rahikainen M, Alegre S, Trotta A, Pascual J, Kangasjärvi S (2018) Trans-methylation reactions in plants: focus on the activated methyl cycle. *Physiol Plant* 162: 162–176
- Rangwala SH, Richards EJ (2010) The structure, organization and radiation of Sadhu non-long terminal repeat retroelements in Arabidopsis species. *Mob DNA* 1: 10
- Ravanel S, Block MA, Rippert P, Jabrin S, Curien G, Rébeillé F, Douce R (2004) Methionine metabolism in plants: chloroplasts are autonomous for de novo methionine synthesis and can import S-adenosylmethionine from the cytosol. *J Biol Chem* 279: 22548–22557
- Ravanel S, Cherest H, Jabrin S, Grunwald D, Surdin-Kerjan Y, Douce R, Rébeillé F (2001) Tetrahydrofolate biosynthesis in plants: molecular and functional characterization of dihydrofolate synthetase and three isoforms of folylpolyglutamate synthetase in Arabidopsis thaliana. *Proc Natl Acad Sci U S A* 98: 15360–15365
- Rebeille F, Neuburger M, Douce R (1994) Interaction between glycine decarboxylase, serine hydroxymethyltransferase and tetrahydrofolate polyglutamates in pea leaf mitochondria. *Biochem J* 302 (Pt 1): 223–228
- Rébeillé F, Macherel D, Mouillon JM, Garin J, Douce R (1997) Folate biosynthesis in higher plants: purification and molecular cloning of a bifunctional 6-hydroxymethyl-7,8-dihydropterin pyrophosphokinase/7,8-dihydropteroyl synthase localized in mitochondria. *EMBO J* 16: 947–957
- Rita Zrenner, Mark Stitt, Uwe Sonnewald, Ralf Boldt PYRIMIDINE AND PURINE BIOSYNTHESIS AND DEGRADATION IN PLANTS

Rocha PSCF, Sheikh M, Melchiorre R, Fagard M, Boutet S, Loach R, Moffatt B, Wagner C, Vaucheret H, Furner I (2005) The Arabidopsis HOMOLOGY-DEPENDENT GENE SILENCING1 gene codes for an S-adenosyl-L-homocysteine hydrolase required for DNA methylation-dependent gene silencing. *Plant Cell* 17: 404–417

Roje S (2006) S-Adenosyl-L-methionine: beyond the universal methyl group donor. *Phytochemistry* 67: 1686–1698

Roje S, Chan SY, Kaplan F, Raymond RK, Horne DW, Appling DR, Hanson AD (2002a) Metabolic engineering in yeast demonstrates that S-adenosylmethionine controls flux through the methylenetetrahydrofolate reductase reaction in vivo. *J Biol Chem* 277: 4056–4061

Roje S, Janave MT, Ziemak MJ, Hanson AD (2002b) Cloning and characterization of mitochondrial 5-formyltetrahydrofolate cycloligase from higher plants. *J Biol Chem* 277: 42748–42754

Roje S, Wang H, McNeil SD, Raymond RK, Appling DR, Shachar-Hill Y, Bohnert HJ, Hanson AD (1999) Isolation, characterization, and functional expression of cDNAs encoding NADH-dependent methylenetetrahydrofolate reductase from higher plants. *J Biol Chem* 274: 36089–36096

Ruszkowski M, Sekula B, Ruszkowska A, Dauter Z (2018) Chloroplastic Serine Hydroxymethyltransferase From *Medicago truncatula*: A Structural Characterization. *Front Plant Sci* 9: 584

Sanchez SE, Kay SA (2016) The Plant Circadian Clock: From a Simple Timekeeper to a Complex Developmental Manager. *Cold Spring Harb Perspect Biol* 8

Sanchez SE, Rugnone ML, Kay SA (2020) Light Perception: A Matter of Time. *Mol Plant* 13: 363–385

Sato H, Köhler C (2022) Genomic imprinting regulates establishment and release of seed dormancy. *Curr Opin Plant Biol* 69: 102264

Sauter M, Moffatt B, Saechao MC, Hell R, Wirtz M (2013) Methionine salvage and S-adenosylmethionine: essential links between sulfur, ethylene and polyamine biosynthesis. *Biochem J* 451: 145–154

Schmitz RJ, Schultz MD, Lewsey MG, O'Malley RC, Urich MA, Libiger O, Schork NJ, Ecker JR (2011) Transgenerational epigenetic instability is a source of novel methylation variants. *Science* 334: 369–373

Schmitz RJ, Schultz MD, Urich MA, Nery JR, Pelizzola M, Libiger O, Alix A, McCosh RB, Chen H, Schork NJ et al (2013) Patterns of population epigenomic diversity. *Nature* 495: 193–198

Schvartzman JM, Thompson CB, Finley LWS (2018) Metabolic regulation of chromatin modifications and gene expression. *J Cell Biol* 217: 2247–2259

Sdelci S, Rendeiro AF, Rathert P, You W, Lin J-MG, Ringler A, Hofstätter G, Moll HP, Gürtl B, Farlik M et al (2019) MTHFD1 interaction with BRD4 links folate metabolism to transcriptional regulation. *Nat Genet* 51: 990–998

- Sekula B, Ruszkowski M, Dauter Z (2020) S-adenosylmethionine synthases in plants: Structural characterization of type I and II isoenzymes from *Arabidopsis thaliana* and *Medicago truncatula*. *Int J Biol Macromol* 151: 554–565
- Shahryary Y, Symeonidi A, Hazarika RR, Denkena J, Mubeen T, Hofmeister B, van Gurp T, Colomé-Tatché M, Verhoeven KJF, Tuskan G et al (2020) AlphaBeta: computational inference of epimutation rates and spectra from high-throughput DNA methylation data in plants. *Genome Biol* 21: 260
- Shane B (1989) Folylpolyglutamate synthesis and role in the regulation of one-carbon metabolism. *Vitam Horm* 45: 263–335
- Sievers F, Wilm A, Dineen D, Gibson TJ, Karplus K, Li W, Lopez R, McWilliam H, Remmert M, Söding J et al (2011) Fast, scalable generation of high-quality protein multiple sequence alignments using Clustal Omega. *Mol Syst Biol* 7: 539
- Smith LM, Pontes O, Searle I, Yelina N, Yousafzai FK, Herr AJ, Pikaard CS, Baulcombe DC (2007) An SNF2 protein associated with nuclear RNA silencing and the spread of a silencing signal between cells in *Arabidopsis*. *Plant Cell* 19: 1507–1521
- Smithells RW, Sheppard S, Schorah CJ (1976) Vitamin deficiencies and neural tube defects. *Arch Dis Child* 51: 944–950
- Song YH, Shim JS, Kinmonth-Schultz HA, Imaizumi T (2015) Photoperiodic flowering: time measurement mechanisms in leaves. *Annu Rev Plant Biol* 66: 441–464
- Srivastava AC, Ramos-Parra PA, Bedair M, Robledo-Hernández AL, Tang Y, Sumner LW, La Díaz de Garza RI, Blancaflor EB (2011) The folylpolyglutamate synthetase plastidial isoform is required for postembryonic root development in *Arabidopsis*. *Plant Physiol* 155: 1237–1251
- Striegel L, Chebib S, Netzel ME, Rychlik M (2018) Improved Stable Isotope Dilution Assay for Dietary Folates Using LC-MS/MS and Its Application to Strawberries. *Front Chem* 6: 11
- Strobbe S, van der Straeten D (2017) Folate biofortification in food crops. *Curr Opin Biotechnol* 44: 202–211
- Stroud H, Do T, Du J, Zhong X, Feng S, Johnson L, Patel DJ, Jacobsen SE (2014) Non-CG methylation patterns shape the epigenetic landscape in *Arabidopsis*. *Nat Struct Mol Biol* 21: 64–72
- Stroud H, Greenberg MVC, Feng S, Bernatavichute YV, Jacobsen SE (2013) Comprehensive analysis of silencing mutants reveals complex regulation of the *Arabidopsis* methylome. *Cell* 152: 352–364
- Stuttman J, Barthel K, Martin P, Ordon J, Erickson JL, Herr R, Ferik F, Kretschmer C, Berner T, Keilwagen J et al (2021) Highly efficient multiplex editing: one-shot generation of 8x *Nicotiana benthamiana* and 12x *Arabidopsis* mutants. *Plant J* 106: 8–22
- Taiz L, Zeiger E, Møller IM, Murphy AS (eds) (2018) *Plant physiology and development*. Sunderland, Massachusetts, New York, NY: Sinauer Associates; Oxford Univeristy Press
- Takou M, Wieters B, Kopriva S, Coupland G, Linstädter A, Meaux J de (2019) Linking genes with ecological strategies in *Arabidopsis thaliana*. *J Exp Bot* 70: 1141–1151

- Tang K, Lang Z, Zhang H, Zhu J-K (2016) The DNA demethylase ROS1 targets genomic regions with distinct chromatin modifications. *Nat Plants* 2: 16169
- Tibbetts AS, Appling DR (2010) Compartmentalization of Mammalian folate-mediated one-carbon metabolism. *Annu Rev Nutr* 30: 57–81
- Timm S, Florian A, Fernie AR, Bauwe H (2016) The regulatory interplay between photorespiration and photosynthesis. *J Exp Bot* 67: 2923–2929
- Timm S, Florian A, Wittmiß M, Jahnke K, Hagemann M, Fernie AR, Bauwe H (2013) Serine acts as a metabolic signal for the transcriptional control of photorespiration-related genes in Arabidopsis. *Plant Physiol* 162: 379–389
- Timm S, Nunes-Nesi A, Florian A, Eisenhut M, Morgenthal K, Wirtz M, Hell R, Weckwerth W, Hagemann M, Fernie AR et al (2021) Metabolite Profiling in Arabidopsis thaliana with Moderately Impaired Photorespiration Reveals Novel Metabolic Links and Compensatory Mechanisms of Photorespiration. *Metabolites* 11
- Tong H, Laitinen RAE, Nikoloski Z (2023) Predicting plasticity of rosette growth and metabolic fluxes in Arabidopsis thaliana. *New Phytol*
- Tramonti A, Paiardini A, Paone A, Bouzidi A, Giardina G, Guiducci G, Magnifico MC, Rinaldo S, McDermott L, Menendez JA et al (2018) Differential inhibitory effect of a pyrazolopyran compound on human serine hydroxymethyltransferase-amino acid complexes. *Arch Biochem Biophys* 653: 71–79
- Trovato M, Funck D, Forlani G, Okumoto S, Amir R (2021) Editorial: Amino Acids in Plants: Regulation and Functions in Development and Stress Defense. *Front Plant Sci* 12: 772810
- Turck F, Fornara F, Coupland G (2008) Regulation and identity of florigen: FLOWERING LOCUS T moves center stage. *Annu Rev Plant Biol* 59: 573–594
- Turner SR, Ireland R, Morgan C, Rawsthorne S (1992) Identification and localization of multiple forms of serine hydroxymethyltransferase in pea (*Pisum sativum*) and characterization of a cDNA encoding a mitochondrial isoform. *Journal of Biological Chemistry* 267: 13528–13534
- Ugalde JM, Fecker L, Schwarzländer M, Müller-Schüssele SJ, Meyer AJ (2020) Live monitoring of ROS-induced cytosolic redox changes with roGFP2-based sensors in plants
- Vickers TJ, Murta SMF, Mandell MA, Beverley SM (2009) The enzymes of the 10-formyl-tetrahydrofolate synthetic pathway are found exclusively in the cytosol of the trypanosomatid parasite *Leishmania major*. *Mol Biochem Parasitol* 166: 142–152
- Vriet C, Hennig L, Laloi C (2015) Stress-induced chromatin changes in plants: of memories, metabolites and crop improvement. *Cell Mol Life Sci* 72: 1261–1273
- Wang X, Jiang B, Gu L, Chen Y, Mora M, Zhu M, Noory E, Wang Q, Lin C (2021) A photoregulatory mechanism of the circadian clock in Arabidopsis. *Nat Plants* 7: 1397–1408
- Watanabe M, Chiba Y, Hirai MY (2021) Metabolism and Regulatory Functions of O-Acetylserine, S-Adenosylmethionine, Homocysteine, and Serine in Plant Development and Environmental Responses. *Front Plant Sci* 12: 643403

- Weiszmann J, Walther D, Clauw P, Back G, Gunis J, Reichardt I, Koemeda S, Jez J, Nordborg M, Schwarzerova J et al (2023) Metabolome plasticity in 241 *Arabidopsis thaliana* accessions reveals evolutionary cold adaptation processes. *Plant Physiol*
- West MG, Barlowe CK, Appling DR (1993) Cloning and characterization of the *Saccharomyces cerevisiae* gene encoding NAD-dependent 5,10-methylenetetrahydrofolate dehydrogenase. *Journal of Biological Chemistry* 268: 153–160
- West MG, Horne DW, Appling DR (1996) Metabolic role of cytoplasmic isozymes of 5,10-methylenetetrahydrofolate dehydrogenase in *Saccharomyces cerevisiae*. *Biochemistry* 35: 3122–3132
- Wibowo A, Becker C, Marconi G, Durr J, Price J, Hagmann J, Papareddy R, Putra H, Kageyama J, Becker J et al (2016) Hyperosmotic stress memory in *Arabidopsis* is mediated by distinct epigenetically labile sites in the genome and is restricted in the male germline by DNA glycosylase activity. *Elife* 5
- Williams BP, Bechen LL, Pohlmann DA, Gehring M (2022) Somatic DNA demethylation generates tissue-specific methylation states and impacts flowering time. *Plant Cell* 34: 1189–1206
- Wingler A, Lea PJ, Leegood RC (1999) Photorespiratory metabolism of glyoxylate and formate in glycine-accumulating mutants of barley and *Amaranthus edulis*. *Planta* 207: 518–526
- Wu Z, Ren H, Xiong W, Roje S, Liu Y, Su K, Fu C (2018) Methylenetetrahydrofolate reductase modulates methyl metabolism and lignin monomer methylation in maize. *J Exp Bot* 69: 3963–3973
- Yang R, He L, Huang H, Zhu J-K, Lozano-Duran R, Zhang H (2020) RNA-directed DNA methylation has an important developmental function in *Arabidopsis* that is masked by the chromatin remodeler PICKLE. *J Integr Plant Biol* 62: 1647–1652
- Yang XM, MacKenzie RE (1993) NAD-dependent methylenetetrahydrofolate dehydrogenase-methenyltetrahydrofolate cyclohydrolase is the mammalian homolog of the mitochondrial enzyme encoded by the yeast MIS1 gene. *Biochemistry* 32: 11118–11123
- Zemach A, Kim MY, Hsieh P-H, Coleman-Derr D, Eshed-Williams L, Thao K, Harmer SL, Zilberman D (2013) The *Arabidopsis* nucleosome remodeler DDM1 allows DNA methyltransferases to access H1-containing heterochromatin. *Cell* 153: 193–205
- Zhang H, Lang Z, Zhu J-K (2018) Dynamics and function of DNA methylation in plants. *Nat Rev Mol Cell Biol* 19: 489–506
- Zhang H, Ma Z-Y, Zeng L, Tanaka K, Zhang C-J, Ma J, Bai G, Wang P, Zhang S-W, Liu Z-W et al (2013) DTF1 is a core component of RNA-directed DNA methylation and may assist in the recruitment of Pol IV. *Proceedings of the National Academy of Sciences* 110: 8290–8295
- Zhang H, Tang K, Qian W, Duan C-G, Wang B, Zhang H, Wang P, Zhu X, Lang Z, Yang Y et al (2014) An Rrp6-like protein positively regulates noncoding RNA levels and DNA methylation in *Arabidopsis*. *Mol Cell* 54: 418–430
- Zhang Y, Sun K, Roje S (2008) An HPLC-based fluorometric assay for serine hydroxymethyltransferase. *Anal Biochem* 375: 367–369

Zhang Y, Sun K, Sandoval FJ, Santiago K, Roje S (2010) One-carbon metabolism in plants: characterization of a plastid serine hydroxymethyltransferase. *Biochem J* 430: 97–105

Zhao C, Liu B, Piao S, Wang X, Lobell DB, Huang Y, Huang M, Yao Y, Bassu S, Ciais P et al (2017) Temperature increase reduces global yields of major crops in four independent estimates. *Proceedings of the National Academy of Sciences* 114: 9326–9331

Zhou H-R, Zhang F-F, Ma Z-Y, Huang H-W, Jiang L, Cai T, Zhu J-K, Zhang C, He X-J (2013) Folate polyglutamylation is involved in chromatin silencing by maintaining global DNA methylation and histone H3K9 dimethylation in Arabidopsis. *Plant Cell* 25: 2545–2559

Zhou M, Coruh C, Xu G, Martins LM, Bourbousse C, Lambolez A, Law JA (2022) The CLASSY family controls tissue-specific DNA methylation patterns in Arabidopsis. *Nat Commun* 13: 244

Zhou M, Palanca AMS, Law JA (2018) Locus-specific control of the de novo DNA methylation pathway in Arabidopsis by the CLASSY family. *Nat Genet* 50: 865–873

Acknowledgment

An dieser Stelle möchte ich allen danken, die zum Erfolg dieser Arbeit beigetragen haben.

Ein großes Dankeschön gilt meinem Betreuer und Mentor Dr. Martin Groth. Lieber Martin, danke für die Möglichkeit an diesem spannenden Thema arbeiten zu dürfen. Danke für die hervorragende Betreuung, deine Förderung, und ganz besonders für deine Motivation als die Zeiten schwieriger wurden.

Außerdem möchte ich meinem Doktorvater Prof. Dr. Jörg Durner für seine unermüdliche Unterstützung, auch aus dem Ruhestand heraus danken – das rechne ich Ihnen hoch an!

Vielen Dank an Prof. Dr. Frank Johannes für seine Beiträge als externer Experte meines Thesis Advisory Committee.

Vielen Dank an den Vorsitz und die Mitglieder der Prüfungskommission.

Ich danke vielmals all meinen Kooperationspartnerinnen und -partnern ohne die diese Arbeit in dieser Form nicht möglich gewesen wäre: Dr. Gernot Poschet, Dr. Markus Wirtz und Prof. Dr. Rüdiger Hell von der Universität Heidelberg, Lisa Obermaier und Prof. Dr. Michael Rychlik von der Technischen Universität München sowie Dr. José Ugalde und Prof. Dr. Andreas Meyer von der Universität Bonn. Für die Kooperation am Helmholtz Zentrum München bedanke ich mich sehr bei: Dr. Andrea Ghirardo, Baris Weber, Prof. Dr. Jörg-Peter Schnitzler sowie Birgit Lange, PD Dr. Anton Schäffner als auch bei Dr. Andrey Tvardovskiy und Prof. Dr. Robert Schneider.

Weiterhin möchte ich mich herzlich bei allen Kolleginnen und Kollegen am Institut für Biochemische Pflanzenpathologie bedanken und im besonderem bei: Dr. Sibylle Bauer, Marko Bertić, Birgit Geist, Georg Gerl, Lucia Gößl, Dr. Inonge Gross, Komal Jhala, Peter Kary, Claudia Knappe, Monika Kugelman, PD Dr. Christian Lindermayr, Diana Lochner, Elke Mattes, Mustafa Özden, Armin Richter, Thayssa Rabelo Schley, Prof. Dr. Corina Vlot-Schuster, Karoline Stoll, Dr. Uta von Rad, Marion Wenig, Dr. Barbro Winkler, Ping Xu, Ting Zhu und Ina Zimmer.

Ein besonderer Dank gilt auch allen Studentinnen und Studenten, die ich betreuen durfte oder die Mitglieder der AG Groth waren: Jerina Hoxha, Mark Klöpfer, Jisha Suresh Kumar, Katarzyna Terlecka und Nandini Terway.

Lieben Dank an Gabriele Barthel, Birgit Lange und Christoph Wurm für die Hilfe bei kleinen und großen Problemen, die Kaffeepausen und das Grantln zwischendurch. Gabi, danke für deine exzellente Unterstützung im Labor und die morgendlichen Leberkäsemmeln!

Zuletzt möchte ich meiner Familie und Freunden für ihren Rückhalt danken. Im besonderem meiner Mutter Evelyn, meinem Bruder Kilian und vor allem meiner Partnerin Larisa.

